Aspects of Flavor Leptogenesis in Particle Physics and Cosmology

Arghyajit Datta

A thesis
submitted for the degree of

Doctor of Philosophy

Supervisor

Prof. Arunansu Sil

Department of Physics
Indian Institute of Technology Guwahati
Guwahati - 781039, Assam, India

Aspects of Flavor Leptogenesis in Particle Physics and Cosmology

A thesis submitted by

Arghyajit Datta

to

Indian Institute of Technology Guwahati
in partial fulfillment of the requirements
for the award of the degree of
Doctor of Philosophy in Physics

Supervisor

Prof. Arunansu Sil

Department of Physics
Indian Institute of Technology Guwahati
Guwahati - 781039, Assam, India

This thesis is dedicated to
my late Boro Mama.

Declaration

Arghyajit Datta
Roll No. 176121017
Department of Physics
IIT Guwahati
Guwahati, India

I hereby declare that works presented in the thesis entitled "**Aspects of Flavor Leptogenesis in Particle Physics and Cosmology**" has been carried out by me under the supervision of Prof. Arunansu Sil at the Department of Physics, Indian Institute of Technology Guwahati, India. The thesis has not been submitted anywhere else for any degree. Works presented in the thesis are all my own unless referenced to the contrary in the thesis.

Arghyajit Datta
Arghyajit Datta

Date: 23/05/2023

Certificate

Dr. Arunansu Sil
Professor
Department of Physics
Indian Institute of Technology Guwahati
Guwahati, India
email:asil@iitg.ac.in

It is certified that the work contained in the thesis entitled "**Aspects of Flavor Leptogenesis in Particle Physics and Cosmology**" by Mr. Arghyajit Datta (Roll No - 176121017), a Ph.D. student in the Department of Physics, Indian Institute of Technology Guwahati is carried out under my supervision and has not been submitted elsewhere for the award of any other degree.

Dr. Arunansu Sil

Date : 23/05/2023

Acknowledgements

First and foremost, I would like to express my deepest gratitude towards my supervisor Prof. Arunansu Sil for all the guidance, stimulation and support he has given to me during my PhD. Most importantly, his expertise, insights, and constructive criticism have been invaluable in shaping my work and helping me overcome obstacles. I feel extremely privileged and grateful for his guardianship, mentoring help and encouragement which I received during the course of my PhD. I have learned a great deal from him not just about how to be a good researcher or an eloquent speaker, but also to be patient, honest and diligent. It was indeed a great learning experience for me altogether.

I am grateful to my doctoral committee members Dr. Soumitra Nandi, Dr. Subhaditya Bhattacharya and Dr. Debasish Borah for their insightful comments and suggestions whenever needed. I thank my seniors and collaborators: Dr. Biswajit Karmakar, Dr. Rishav Roshan. It was because of them that I got the opportunity to work on various problems and in the process acquired a great extent of knowledge and experience. I would like to express my deepest respect and gratitude to my other seniors Dr. Abhijit Kumar Saha, Dr. Amit Dutta Banik and Dr. Basabendu Barman. I am especially thankful to my other seniors: Dr. Dibyendu Nanda, Dr. Lopamudra Mukherjee, Dr. Kajol Samanta , my colleagues cum friends: Samit, Pronoy, Riajul, Surojit, Ipsita, Madhurima, Devabrat, Rakesh, Rajesh, Sayan Da my juniors: Prantik, Sumit, Sahabub, Suruj, Soumen, Dipendu and Swarup for having exciting academic as well non-academic discussions.

The list of acknowledgments would be incomplete without mentioning the professors from my past and present institutes Dr. Tapas Mitra, Prof. Subhradip Ghosh, Dr. Subhaditya Bhattacharya, Dr. Soumitra Nandi to whom I am indebted. It is for them that now not only have I improved as a physics student, but I have also grown as an individual.

Last, but not the least, I would like to convey a very special thanks to my parents for their unconditional love as well as their invaluable support and understanding throughout my academic career. Finally, I want to express my heartfelt appreciation to Sayantani, my partner in crime for her selfless affection and care.

Abstract

The dynamical generation of the baryon asymmetry of the Universe is one of the leading problems in the field of particle physics and cosmology, which the Standard Model of particle physics can not explain. In this thesis, we have analyzed in detail the generation of baryon asymmetry by out-of-equilibrium decay of heavy particle states responsible for neutrino mass generation. The relevant mechanism is known as *baryogenesis via leptogenesis*. In this process, heavy particle states (such as right handed neutrinos) decay out-of-equilibrium to produce lepton asymmetry, which is then converted to baryon asymmetry by sphaleron processes before they decouple. It is shown in the literature that the individual charged lepton Yukawa interactions of different flavors could influence the lepton asymmetry generation when they become dominant over the expansion of the Universe, known as flavor leptogenesis. In this thesis, we have investigated some beyond the Standard Model scenarios which can influence such *flavor leptogenesis* setups. Firstly, we have investigated the impact of an additional flavor symmetry on charged lepton, neutrino Yukawa, and Majorana right handed neutrino sectors. This eventually leads to interesting results not only in the neutrino sector but also in terms of the *flavor leptogenesis*. The scenario favors the normal hierarchical masses of light neutrinos in the neutrino mass and falsifies the leptonic sector's maximal CP asymmetry. On top of that, a successful low scale leptogenesis scenario is achieved. Then, we propose two scenarios which not only explain the existence of dark matter, baryon asymmetry, and neutrino mass simultaneously but also provide a platform where the early universe dynamics of dark matter, either in terms of its production mechanism or its involvement in leptogenesis, can impact the baryon asymmetry of the Universe. Here, individual lepton flavors have played an important role in determining the correct amount of asymmetry in all these scenarios. Finally, we have studied the impact of prolonged reheating in the post-inflationary era of the Universe on the charged lepton equilibration temperatures that eventually affect the so-called individual lepton flavor regimes of *flavor leptogenesis* setup. As a result, allowed parameter space significantly gets altered if leptogenesis occurs during the reheating period.

A. Publications included in the thesis :

1. Flavored leptogenesis and neutrino mass with A_4 symmetry, **JHEP 12 (2021) 051**.
   Authors: **Arghyajit Datta**, Biswajit Karmakar, Arunansu Sil.

2. Imprint of the Seesaw Mechanism on Feebly Interacting Dark Matter and the Baryon Asymmetry, **Phys.Rev.Lett. 127 (2021) 23, 231801**.
   Authors: **Arghyajit Datta**, Rishav Roshan, Arunansu Sil.

3. Scalar triplet flavor leptogenesis with dark matter, **Phys.Rev.D 105 (2022) 9, 095032**.
   Authors: **Arghyajit Datta**, Rishav Roshan, Arunansu Sil.

4. Effects of Reheating on Charged Lepton Yukawa Equilibration and Leptogenesis, **arXiv:2206.10650 (Under Review)**.
   Authors: **Arghyajit Datta**, Rishav Roshan, Arunansu Sil.

5. Flavor Leptogenesis During Reheating Era, **arXiv: 2301.10791 (Under Review)**
   Authors: **Arghyajit Datta**, Rishav Roshan, Arunansu Sil.

Contents

1 Introduction **4**

1.1 The Standard Model of Particle Physics . . . 4
1.1.1 Basic Building Blocks . . . 4
1.1.2 Lagrangian . . . 5
1.1.3 Generation of Mass . . . 6
1.1.4 Need for physics beyond the SM . . . 8
1.2 Early Universe Cosmology . . . 9
1.2.1 Dynamics of Universe . . . 9
1.2.2 Thermodynamics of Early Universe . . . 11
1.2.2.1 Equilibrium Dynamics . . . 12
1.2.2.2 Non-equilibrium Dynamics . . . 12
1.2.3 Different Phases of Early Universe . . . 14
1.2.4 Shortcoming of Standard Big Bang Cosmology . . . 14
1.2.4.1 Possible resolution via inflation . . . 15
1.3 Neutrino Mass . . . 16
1.3.1 Type-I seesaw mechanism . . . 17
1.3.2 Type-II seesaw mechanism . . . 18
1.4 Dark Matter . . . 19
1.4.1 Production of Dark Matter . . . 20
1.4.1.1 Freeze-out Mechanism . . . 20
1.4.1.2 Freeze-in Mechanism . . . 23
1.5 Baryon asymmetry of the Universe . . . 24
1.5.1 Antimatter search and constraint on baryon asymmetry . . . 24
1.5.2 Generation of baryon asymmetry . . . 26
1.5.2.1 Sakharov Condition . . . 27
1.6 Baryogenesis via Leptogenesis . . . 28
1.6.1 Unflavored thermal leptogenesis . . . 28
1.6.2 Charged lepton equilibration and flavored leptogenesis . . . 31
1.6.2.1 Evaluation of equilibration temperature of charged lepton Yukawa . . . 32
1.6.2.2 Formation of Boltzmann equation . . . 33

1.6.2.3 Different temperature regimes and flavor structure of Boltzmann equation . . . 35
1.7 Objective and outline of the thesis . . . 37

2 Flavor Origin of Flavor Leptogenesis **39**
2.1 Introduction . . . 39
2.2 Structure of The Model . . . 41
2.3 Neutrino phenomenology . . . 46
2.3.1 Constraining the parameter space . . . 46
2.3.2 Implications for light neutrino masses and low energy phase . . . 48
2.3.3 Neutrinoless Double beta decay . . . 49
2.3.4 Lepton flavor violation . . . 50
2.4 Leptogenesis . . . 50
2.4.1 Generation of mass splitting and CP asymmetry . . . 51
2.4.1.1 Lifting the mass degeneracy . . . 52
2.4.1.2 Estimating CP asymmetry . . . 54
2.4.2 Solution of Boltzmann equation . . . 55
2.5 Summary . . . 58

3 Connecting Dark Matter with Flavor Leptogenesis **60**
3.1 Introduction . . . 60
3.2 Imprint of Seesaw on FIMP Dark Matter and Flavor Leptogenesis . . . 60
3.2.1 Setup . . . 61
3.2.2 Production of DM . . . 62
3.2.3 Decay of dark matter . . . 65
3.2.4 Lepton asymmetry generation . . . 66
3.2.5 Summary . . . 67
3.3 Scalar triplet flavor leptogenesis with dark matter . . . 68
3.3.1 The Model . . . 69
3.3.2 Neutrino Mass . . . 71
3.3.3 Dark Matter Phenomenology . . . 73
3.3.3.1 Relic Density . . . 73
3.3.3.2 Direct and Indirect Detection . . . 75
3.3.4 Leptogenesis . . . 75
3.3.4.1 CP asymmetry generation . . . 76
3.3.4.2 Evolution of $B - L$ asymmetry . . . 77
3.3.4.3 Results . . . 80
3.3.5 Summary . . . 83

4 Effect of Post-inflationary epoch in Flavor Leptogenesis **85**
4.1 Introduction . . . 85
4.2 Setup a: inflaton couples to SM fermions . . . 86
4.2.1 Reheating Process . . . 87
4.2.2 Change in equilibration temperature of charged Yukawa interactions . . . 88

4.2.3 Lepton asymmetry generation 89
4.2.4 summary 92
4.3 Setup b: inflaton couples to lightest RHN and SM fermions 93
4.3.1 Setup and Boltzmann equation 93
4.3.2 Results 96
4.3.3 Summary 104

5 Summary and conclusion **106**

A Appendix related to chapter 2 **109**
A.1 A_4 Multiplication Rules: 109

Chapter 1

Introduction

1.1 The Standard Model of Particle Physics

1.1.1 Basic Building Blocks

One of the past century's most notable accomplishments in particle physics has been the development of a unified theory of strong, weak, and electromagnetic interactions, also known as the Standard Model (SM)[1–7] of Particle physics. The fundamental principle underlying the SM is the gauge invariance, which unites elementary matter particles and their interactions, and incorporates the gauge bosons as a mediator of these interactions. The gauge group $SU(3)_c \times SU(2)_L \times U(1)_Y$ serves as the mathematical construction for the SM, where c stands for color, while L and Y represent left-handed chirality, and weak hypercharge respectively. Here, $SU(2)_L \times U(1)_Y$ describes the electroweak interactions, mediated by 4 gauge bosons $(W_\mu^{i=1,2,3}, B_\mu)$, while the remaining symmetry $SU(3)_c$ denotes the strong interaction mediated by the 8 gluons $(G_\mu^{a=1,2..8})$. Altogether, 12 mediators are present in SM, which are spin-1 bosonic fields. Table 1.1 shows the field content and corresponding quantum number with respect to $(w.r.t.)$ the SM gauge group. As seen from the table, the matter field spectrum of the SM is composed of three generations of spin$-\frac{1}{2}$ fermions, with two helicity states, namely left and right of each charged fermion, transforming differently under the $SU(2)_L$ group. Left-handed components transform as doublets, while right-handed ones are singlets. The fermion sector includes quarks, leptons, and their antiparticles. The Quark sector comprises of 3 generations of up [namely up (u), charm (c), and top (t)] and down [namely down (d), strange(s), and bottom (b)] type quarks. All the fermions are combined to form doublets and singlets of $SU(2)_L$ as:

$$Q_{L_\alpha} \equiv \begin{bmatrix} u \\ d \end{bmatrix}_L \; ; \quad \begin{bmatrix} c \\ s \end{bmatrix}_L \; ; \quad \begin{bmatrix} t \\ b \end{bmatrix}_L , \quad U_{R_\alpha} \equiv u_R; c_R; t_R \, , \quad D_{R_\alpha} \equiv d_R; s_R; b_R \, ,$$

Where Q_L is the left-handed quark doublet state, constructed by taking one up type and one down type quark from each generation, and U_R and D_R are the right-handed singlet states, respectively. Index α represents the number of generations. On the other hand, left-handed

Field			$SU(3)_c \times SU(2)_L \times U(1)_Y$
Spin	Nature	Particle	
$\frac{1}{2}$	Quarks	Q_{L_α}	$(3, 2, 1/6)$
		$U_{R_\alpha}, D_{R_\alpha}$	$(3, 1, 2/3),\ (3, 1, 1/3)$
	Leptons	ℓ_{L_α}	$(1, 2, -1/2)$
		E_{R_α}	$(1, 1, -1)$
1	Gauge Bosons	G^a_μ	$(8, 1, 0)$
		W^i_μ, B_μ	$(1, 3, 0), (1, 1, 0)$
0	Scalar	H	$(1, 2, 1/2)$

Table 1.1: Particle spectrum and their charges under Standard Model gauge symmetry.

doublet and right-handed singlet states in the leptonic sector are constructed as:

$$\ell_{L_\alpha} \equiv \begin{bmatrix} \nu_e \\ e^- \end{bmatrix}_L ; \quad \begin{bmatrix} \nu_\mu \\ \mu^- \end{bmatrix}_L ; \quad \begin{bmatrix} \nu_\tau \\ \tau^- \end{bmatrix}_L , \quad E_{R_\alpha} \equiv e_R; \mu_R; \tau_R \,,$$

where $\nu_e,\ \nu_\mu,\ \nu_\tau$ are the neutrinos of different flavors. The charged leptons are denoted by $e^-,\ \mu^-,\ \tau^-$. It is important to note that the neutrinos in SM do not have any right-handed partners. There is only one $SU(2)_L$ doublet in the scalar sector, known as the Higgs, a spin-0 boson represented by $H = \begin{pmatrix} H^+ & H^0 \end{pmatrix}^T$. Here, H^0 and H^+ represent the neutral and charged components of the Higgs field.

1.1.2 Lagrangian

Using gauge invariance of the SM gauge group, the entire Lagrangian can be written which is discussed below for each of the sectors consisting of gauge bosons, fermions and scalar.

I. **Electroweak Gauge Bosons**
The following Lagrangian can express kinetic terms associated with gauge bosons:

$$-\mathcal{L}_G = \frac{1}{4} G^a_{\mu\nu} G^{\mu\nu,a} + \frac{1}{4} W^i_{\mu\nu} W^{\mu\nu,i} + \frac{1}{4} B_{\mu\nu} B^{\mu\nu} \tag{1.1}$$

where $G^a_{\mu\nu}$, $W^i_{\mu\nu}$ and $B_{\mu\nu}$ are the field tensors associated with the $SU(3)_c$, $SU(2)_L$ and $U(1)_Y$ gauge groups respectively. They can be expressed as follows:

$$G^a_{\mu\nu} = \partial_\mu G^a_\nu - \partial_\nu G^a_\mu - g_3 f^{abc} G^b_\mu G^c_\nu, \tag{1.2}$$
$$W^i_{\mu\nu} = \partial_\mu W^i_\nu - \partial_\nu W^a_\mu - g_2 \epsilon^{ijk} W^j_\mu W^k_\nu, \tag{1.3}$$
$$B_{\mu\nu} = \partial_\mu B_\nu - \partial_\nu B_\mu \tag{1.4}$$

with g_3 (g_2) and f^{abc} (ϵ^{ijk}) representing the gauge coupling constants and structure constants for $SU(3)_c$ ($SU(2)_L$) symmetry respectively.

II. **Fermion fields**

Quarks and leptons, being fermion fields, will have a similar form of Lagrangian. Expressing both quarks and leptons as $\psi = \psi_L + \psi_R$, the Lagrangian will look like:

$$-\mathcal{L}_F = \overline{\psi}_L \not{D} \psi_L + \overline{\psi}_R \not{D} \psi_R \tag{1.5}$$

where $\not{D} = \gamma^\mu . D_\mu$ denotes the Lorentzian inner product of gamma matrices γ_μ and covariant derivative operator D_μ. The covariant derivative D_μ is expressed in terms of SM gauge bosons as:

$$D_\mu \equiv \partial_\mu - ig_1 Y B_\mu - ig_2 \frac{\tau^i}{2} W^i_\mu - ig_3 \frac{\lambda^a}{2} G^a_\mu. \tag{1.6}$$

where g_1 is the gauge coupling for $U(1)_Y$ symmetry. Y, $\frac{\tau^{i=1,2,3}}{2}$, and $\frac{\lambda^{a=1,2,..8}}{2}$ rare the generators of gauged $U(1)_Y$, $SU(2)_L$, and $SU(3)_c$ symmetry respectively with τ^i denoting three 2×2 Pauli spin matrices, while λ^a represents 3×3 Gell-Mann matrices.

III. **Scalar field and its interaction with fermions**

Finally, the most general Lagrangian involving Higgs and its interaction with the fermion fields consistent with the SM gauge group, is given by:

$$\mathcal{L}_H = (D_\mu H)^\dagger (D^\mu H) - V(H)\,, \tag{1.7}$$

$$-\mathcal{L}_Y = (Y_u)_{\alpha\beta} \overline{Q}_{L_\alpha} \widetilde{H} U_{R_\beta} + (Y_d)_{\alpha\beta} \overline{Q}_{L_\alpha} H D_{R_\beta} + (Y_\ell)_{\alpha\beta} \bar{\ell}_{L_\alpha} H E_{R_\beta} + h.c, \tag{1.8}$$

where α, β are the generation indices and $V(H)$ represents the Higgs potential which can be expressed as:

$$V(H) = \mu^2 H^\dagger H + \lambda (H^\dagger H)^2, \tag{1.9}$$

with μ^2 and λ are the quadratic and quartic couplings respectively.To make the $\mathcal{L}_Y$ invariant under the SM gauge group, a doublet with $Y = -1/2$ is introduced with the notation: $\widetilde{H} = i\sigma_2 H^*$, σ_2 is the second Pauli matrix.

1.1.3 Generation of Mass

The most effective way to generate the mass for all particles within SM is to spontaneously break the SM gauge symmetry, which the Lagrangian preserves, but the system's ground state does not. The mechanism is known as *Spontaneous Symmetry Breaking* (SSB)[8–10], and the generation of mass using SSB is accomplished with the help of Eq (1.7)-(1.9), which is discussed below.

Following Eq. (1.9), with $\mu^2 < 0$ and $\lambda > 0$, it can lead to non-zero minima of the

potential. Choosing a specific minimum such as

$$\langle H \rangle = \begin{pmatrix} 0 \\ \frac{v}{\sqrt{2}} \end{pmatrix}, \tag{1.10}$$

with $v = \sqrt{-\mu^2/\lambda}$, known as the vacuum expectation value (vev) would break the $SU(2)_L \times U(1)_Y$ gauge group down to $U(1)_{EM}$. As a result, gauge fields corresponding to the three broken generators become massive, which are identified as $W^{\pm}_{\mu}$ and Z_{μ} bosons having masses $M_{W^{\pm}} = g_2 v/2$ and $M_z = \frac{g_2 v}{2\cos\theta_w}$ respectively. On the other hand, the gauge field corresponding to the unbroken $U(1)_{EM}$ symmetry nothing but the photon field: A_{μ}. One can define these massive and massless bosonic states in terms of previously defined bosonic mediators:

$$W^{\pm}_{\mu} = \frac{1}{\sqrt{2}} \left(W^1_{\mu} \mp i W^2_{\mu} \right), \tag{1.11}$$

$$Z_{\mu} = \cos\theta_w W^3_{\mu} - \sin\theta_w B_{\mu}, \tag{1.12}$$

$$A_{\mu} = \sin\theta_w W^3_{\mu} + \cos\theta_w B_{\mu}, \tag{1.13}$$

with $\theta_w = \tan^{-1}\left(\frac{g_1}{g_2}\right)$ known as the Weinberg angle. Finally, eight massless generators of $SU(3)_c$ are known as $gluons$.With respect to this new ground state, the Higgs field can be developed as (in the unitary gauge):

$$H = \frac{1}{\sqrt{2}} \begin{pmatrix} 0 \\ v + h \end{pmatrix}, \tag{1.14}$$

where h is the physical Higgs field having mass $m_h = \sqrt{2\lambda} v$.

The SM fermion masses arise from the Yukawa interactions denoted by the Lagrangian in Eq: (1.8) after the Higgs gets a vev. Using Eq. (1.14), the mass matrices from SM quarks and charged leptons are obtained as:

$$(m_u)_{\alpha\beta} = \frac{v}{\sqrt{2}} (Y_u)_{\alpha\beta}\,, \quad (m_d)_{\alpha\beta} = \frac{v}{\sqrt{2}} (Y_d)_{\alpha\beta}\,, \quad (m_\ell)_{\alpha\beta} = \frac{v}{\sqrt{2}} (Y_\ell)_{\alpha\beta} \tag{1.15}$$

In general these matrices are nondiagonal. Then in the quark sector, diagonalization of m_u and m_d mass matrices can be done via bi-unitary transformations, which will eventually connect the flavor basis of quark states (with subscript α) to mass diagonal basis (with subscript i) as:

$$\begin{aligned} (u_L)_\alpha &= (U_u)_{\alpha i} (u'_L)_i, \; (d_L)_\alpha = (U_d)_{\alpha i} (d'_L)_i, \\ (U_R)_\alpha &= (V_u)_{\alpha i} (U'_R)_i, \; (D_R)_\alpha = (V_d)_{\alpha i} (D'_R)_i. \end{aligned} \tag{1.16}$$

Following this, the charged current interaction takes the form, in this mass diagonal basis,

$$-\mathcal{L}^{q}_{cc} = \frac{g_2}{\sqrt{2}} \sum_{i,j} (\overline{u}'_L)_i \gamma^\mu W^+_\mu (U^\dagger_u U_d)_{ij} (d'_L)_j + h.c., \tag{1.17}$$

which indicates the mixing between the quarks where i, j run for 1 to 3 (no. of generations). The mixing matrix $U^\dagger_u U_d$ is known as $Cabibo-Kobayashi-Maskawa$ (CKM) matrix [11, 12].

Similar to the quark sector, the diagonalization of the charged lepton mass matrix m_e involves a rotation connecting the leptonic flavor eigenstates to the mass eigenstates. On the other hand, the absence of any right-handed neutrinos results massless neutrinos. Hence, It is always possible to make the mass eigenstates of charged lepton and neutrinos coincide with their corresponding flavor states. As a result, there would not be any CKM-like mixing in lepton sector of the SM.

1.1.4 Need for physics beyond the SM

The experimental findings and the theoretical predictions of SM agree remarkably well. Furthermore, the discovery of the Higgs boson at the LHC completes the particle spectrum of the Standard Model. Despite being so successful, there are several issues in particle physics and cosmology which SM fails to explain. Here let us look at some of these fascinating issues.

- **Neutrino Mass:** According to the SM, neutrinos are the only massless fermions. However, various neutrino experiments conducted since Ray Davis' Homestake experiment in the 1960s have estimated deficit of observed neutrinos as compared to the predicted ones. These anomalies eventually lead to the postulate of oscillating neutrinos where neutrinos of different flavor can oscillate among each other, which requires neutrinos to have non-zero mass.
- **Dark Matter:** There are various astrophysical evidences, such as the galactic rotation curve of galaxies[13], gravitational lensing effects[14], and so on, which point towards the presence of non-luminous matter in the Universe, popularly known as dark matter (DM)[15, 16]. Furthermore, if one believes that DM is made up of fundamental particles, then the SM particle spectrum alone cannot explain the nature of DM. This encourages one to look beyond the SM (BSM).
- **Baryon Asymmetry of the Universe:** Another critical issue SM fails to address is the dominance of baryonic matter over antibaryon in our visible Universe[17, 18]. Dynamical generation of baryon asymmetry requires beyond SM degrees of freedom. The current thesis revolves primarily around the study of baryon asymmetry generation, which will be discussed in greater depth in the following sections.

Apart from the problems mentioned above, there are problems like the stability of the EW vaccum[19, 20], hierarchy problem[21], strong CP problem[22, 23] in the theoretical frontier of SM which are worthy of addressing. In the context of BSM physics, the mechanism of baryon asymmetry generation in the form of leptogenesis can be intertwined with many such issues which will be addressed in this thesis having a particular emphasis on flavor

aspect of it. Since some of these issues are intricately connected with the dynamics of the early Universe, in the next section we will look into the relevant concepts associated with the early Universe cosmology. Then in the following sections, we will elaborate on some of the connected issues relevant to the current thesis as well as the background of lepton asymmetry generation in the Leptogenesis mechanism.

1.2 Early Universe Cosmology

Similar to the SM of particle physics, there exists a cosmological model that describes our Universe's structure and evolution on the grandest scale. In this section, we will briefly review the essential features and drawbacks of this model to set the stage for the thesis.

1.2.1 Dynamics of Universe

The theory, also known as Standard Cosmological Model, is predicated on the notion that the Universe, on a large scale, is homogeneous and isotropic[24–27]. With such assumptions, the metric adopts the typical Friedmann-Lemaître-Robertson-Walker (FLRW) form[24]:

$$ds^2 = g_{\mu\nu}dx^\mu dx^\nu = -dt^2 + a^2(t)\left[\frac{dr^2}{1-kr^2} + r^2\left(d\theta^2 + \sin^2\theta\, d\phi^2\right)\right], \tag{1.18}$$

where t is the physical time, with (r, θ, ϕ) representing the spatial comoving coordinates. The parameter k denotes the spatial curvature, with $k = 0$ corresponding to a flat Universe and $k > 0$, $(k < 0)$ leading to a closed (open) Universe respectively. Parameter $a(t)$ is known as the scale factor, representing the size of the Universe. The physical distances $\mathcal{R}$ are weighted by the scale factor as:

$$\mathcal{R} = a(t)\int_0^r \frac{dr}{(1-kr^2)^{\frac{1}{2}}}, \tag{1.19}$$

and hence increase with time in an expanding Universe. Another important quantity that denotes the evolution of the Universe is the expansion rate, also known as the Hubble parameter. It is defined as:

$$\mathcal{H} \equiv \frac{1}{a}\frac{da}{dt} \tag{1.20}$$

It has a dimension of inverse time and is positive for expanding Universe (negative for a collapsing Universe). The current value of this parameter is generally expressed as:

$$\mathcal{H}_0 = 100\ \mathrm{h\ km\ s^{-1}\ MPc^{-1}}, \tag{1.21}$$

where h is the dimensionless parameter and currently known to be $\mathrm{h} \sim 0.7$.

Knowing the metric, one can look for the dynamics of the Universe, which is entirely encoded in the time-dependent scale factor $a(t)$. The evolution of $a(t)$ is determined by the Einstein equations:

$$G_{\mu\nu} = 8\pi G T_{\mu\nu} - \Lambda\, g_{\mu\nu} \tag{1.22}$$

Λ is the Einstein cosmological constant and $G_{\mu\nu}$ is known as Einstein tensor and denoted as:

$$G_{\mu\nu} = R_{\mu\nu} - \frac{1}{2} g_{\mu\nu} R, \tag{1.23}$$

with the Ricci scalar R and the Ricci tensor $R_{\mu\nu}$ defined as:

$$R = g^{\mu\nu} R_{\mu\nu}\,, \qquad R_{\mu\nu} = \Gamma^{\alpha}_{\beta\alpha}\Gamma^{\beta}_{\mu\nu} - \Gamma^{\alpha}_{\beta\nu}\Gamma^{\beta}_{\mu\alpha} + \Gamma^{\alpha}_{\mu\nu,\alpha} - \Gamma^{\alpha}_{\mu\alpha,\nu}\,. \tag{1.24}$$

Here, $\Gamma^{\mu}_{\alpha\beta}$ are the Christoffel symbols and are related to the first derivative of the metric as:

$$\Gamma^{\mu}_{\alpha\beta} = \frac{g^{\mu\nu}}{2}\left[\frac{\partial g_{\alpha\nu}}{\partial x^{\beta}} + \frac{\partial g_{\beta\nu}}{\partial x^{\alpha}} - \frac{\partial g_{\alpha\beta}}{\partial x^{\nu}}\right]. \tag{1.25}$$

Notation G in Eq. (1.22) is known as Newton's constant and can be expressed as: $G = 8\pi/M_p^2$, where $M_{Pl} \simeq 1.22 \times 10^{19}$ GeV is the Plack mass. Finally, $T_{\mu\nu}$ denotes the stress-energy tensor of all the matter species in the Universe.

Comparing the matter element of the Universe with a perfect fluid having no viscosity, one can deduce the Friedmann equations:

$$\mathcal{H}^2 = \frac{8\pi G}{3}\rho - \frac{k}{a^2} + \frac{\Lambda}{3}, \tag{1.26}$$

$$\frac{d\mathcal{H}}{dt} + \mathcal{H}^2 = \frac{4\pi G}{3}(\rho + 3\mathcal{P}) + \frac{\Lambda}{3}, \tag{1.27}$$

where ρ and $\mathcal{P}$ denote the energy density and pressure of all the elements of the Universe such as relativistic matter (denoted as $radiation$), the non-relativistic matter (represented by $matter$), and the cosmological constant. Furthermore, the covariance conservation of stress-energy tensor leads to a continuity equation:

$$\frac{d\rho}{dt} + 3\mathcal{H}(\rho + \mathcal{P}) = 0 \tag{1.28}$$

Knowing the equation of state $\omega = \mathcal{P}/\rho$ for different elements, one can solve the Eq: (1.28), which will eventually lead to the scale factor dependence for energy density of different species.

The first and the second column of Table 1.2 shows the value of ω and behavior of $\rho(a)$ for different components of the Universe. As depicted by the the second column, at the early time, Universe was dominated by the radiation matter (RD). Subsequently, non-relativistic matter elements dominated (MD) the energy density of the Universe. Finally, Universe is dominated by the cosmological constant. To know the dynamics of $a(t)$ during such MD, RD and cosmological constant dominated Universe (having fixed ω), one need to solve the Eq: (1.26). Eventually the evolution of $a(t)$ takes different forms, which is mentioned in the

last column of Table 1.2. The present Observations of the cosmic microwave background

Species	$\omega = \mathcal{P}/\rho$	$\rho(a)$	$a(t)$
Matter	0	a^{-3}	$t^{2/3}$
Radiation	$\frac{1}{3}$	a^{-4}	$t^{1/2}$
Λ	-1	a^0	e^{Ht}

Table 1.2

(CMB) [17] and large-scale structure (LSS) can predict the present day energy density of a species i, which is parametrized by:

$$\Omega_i^0 \equiv \frac{\rho_{i_0}}{\rho^0_{\text{crit.}}} \tag{1.29}$$

where $\rho^0_{\text{crit.}} = \frac{3\mathcal{H}_0^2}{8\pi G}$ is the energy density required to halt the expansion of the Universe, also known as $critical\ energy\ density$. According to these experiments, currently, our Universe is a flat $i.e.\ k = 0$. Furthermore, it is composed of only 4% baryons, 26% non-relativistic (cold) DM and 68% dark energy (DE) as a form of Λ having $\omega_\Lambda = -1$:

$$\Omega_B^0 = 0.04, \quad \Omega_{DM}^0 = 0.119, \quad \Omega_\Lambda^0 = 0.72. \tag{1.30}$$

1.2.2 Thermodynamics of Early Universe

To learn about the macroscopic properties of various elements in the Universe, one must first determine whether the elements remain in thermodynamic equilibrium during the Universe's evolution. Different number-conserving scatterings generally establish kinetic equilibrium. In contrast, interactions that reduce the number of particles of a given species, such as pair annihilation, enforce chemical equilibrium among different species. As the Universe expands, a species stays in equilibrium if the rate of its interactions is higher than the expansion rate H. Considering the case of two body processes of the form $a + b \to c + d$, the thermally averaged interaction rate can be denoted by

$$\langle \Gamma_a \rangle = n_b \langle \sigma v \rangle, \tag{1.31}$$

Here, $\langle \sigma v \rangle$ denotes the thermal average of σv, where σ is the cross-section of the process, and v is the relative velocity of $a\ w.r.t.\ b$. Furthermore, n_b represents the number density of the target material b. The equilibrium will be maintained if :

$$\frac{\langle \Gamma_a \rangle}{\mathcal{H}} >> 1 \tag{1.32}$$

while, the same species a will become decoupled, when $\langle \Gamma_a \rangle << \mathcal{H}$.

1.2.2.1 Equilibrium Dynamics

When a species stays in equilibrium, its macroscopic properties can be easily evaluated starting from the distribution function of particles in phase space:

$$f(\vec{p}) = [exp\{(E-\mu)/T\} \pm 1]^{-1} \tag{1.33}$$

where $E(=\sqrt{|\vec{p}|^2+m^2})$, μ are the energy and chemical potential of the species respectively, while T representing the temperature of the heat bath it shares as it is in equilibrium. $+1$, -1 correspond to the Fermi-Dirac and Bose-Einstein distribution respectively. For a relativistic and non-relativistic particle, the number density (n), energy density (ρ), and the pressure density (p) take the form as depicted in table 1.3.

Nature	Species	n	ρ	p
Relativistic $(T >> m, \mu)$	Boson	$\zeta(3)gT^3/\pi^2$	$\pi^2 gT^4/30$	$\rho/3$
	Fermion	$(3/4)\zeta(3)gT^3/\pi^2$	$(7/8)\pi^2 gT^4/30$	$\rho/3$
Non-Relativistic $(m >> T)$	Boson & Fermion	$g(\frac{mT}{2\pi})^{3/2}exp[-(m-\mu)/T]$	mn	nT

Table 1.3

Looking at the energy density of non-relativistic particles, one can easily see that its contribution towards the total energy density is exponentially suppressed compared to the relativistic counterpart. Consequently, it is convenient to include only the relativistic species while calculating the total energy density of the Universe during the RD phase:

$$\rho_{tot.} = \rho_R = \frac{\pi^2}{30} g_* T^4, \tag{1.34}$$

where g_* is the total massless degrees of freedom and is denoted as:

$$g_* = \frac{7}{8} \sum_{a(\text{fermions})} g_a \left(\frac{T_a}{T}\right)^4 + \sum_{a(\text{bosons})} g_a \left(\frac{T_a}{T}\right)^4, \tag{1.35}$$

where T_a is the temperature of the species a. Entropy density of the Universe is the another macroscopic variable which is important to look for. Similar to the energy density, entropy density is again mostly influenced by the relativistic particle and can be evaluated as:

$$s = \frac{2\pi^2}{45} g_*^s T^3. \tag{1.36}$$

1.2.2.2 Non-equilibrium Dynamics

However, due to the expansion of the Universe, a species may not remain in equilibrium indefinitely. In this case, kinetic theory is the most useful tool to learn about the evolu-

tion of the system in time. The method involves determining the time evolution of the particle distribution function as a solution to an integrodifferential Equation known as the $Boltzmann\ equation$ which is discussed below.

Assuming the particle distribution function as $f(x^\mu, P^\mu)$, one can construct the Boltzmann equation as:

$$\hat{\mathbf{L}}[f(x^\mu, P^\mu)] = \mathbf{C}[f(x^\mu, P^\mu)] \tag{1.37}$$

where $\hat{\mathbf{L}}$ is the Liouville operator which, in a flat homogeneous and isotropic Universe, leads to :

$$\hat{\mathbf{L}}[f(x^\mu, P^\mu)] = \left[E\frac{\partial}{\partial t} - \mathcal{H}E^2\frac{\partial}{\partial E}\right] f(t, E). \tag{1.38}$$

Here $\mathbf{C}$ denotes the collision operator which indicates the presence of particle scattering, annihilation, decay etc. For a species a, having interactions $a + b \leftrightarrow c + d$, the collision operator takes the form:

$$\begin{aligned}\mathbf{C}(f_a; f_b, f_c, f_d) = \int \frac{d^3p_b}{(2\pi)^3 2E_b}\frac{d^3p_c}{(2\pi)^3 2E_c}\frac{d^3p_d}{(2\pi)^3 2E_d}(2\pi)^4\delta^{(4)}(P_a + P_b - P_c - P_d) \\ \times \Big[|\mathcal{M}_{cd\to ab}|^2 f_c f_d(1 \pm f_a)(1 \pm f_b) - |\mathcal{M}_{ab\to cd}|^2 f_a f_b(1 \pm f_c)(1 \pm f_d)\Big],\end{aligned} \tag{1.39}$$

where $\mathcal{M}_{ab\to cd}$ ($\mathcal{M}_{cd\to ab}$) is the invarient Feynman amplitude square for the process $a+b \to c+d$ ($c+d \to a+b$). The functions $(1 \overset{+}{(-)} f)$ represent the Bose enhancement (Pauli blocking) effect for final state fermion (boson) particle. The $4-$ dimension delta function denotes the energy-momentum conservation for the process. Finally, to learn about the time evolution of number density of the specific particle a, one need to integrate both side of Eq: (1.37) with the factor $\int \frac{d^3p_a}{(2\pi)^3}$ which will eventually results in the following form of the Boltzmann equation (BE):

$$\frac{dn_a}{dt} + 3\mathcal{H}n_a = \int \frac{d^3p_a}{(2\pi)^3 E_a}\mathbf{C}(f_a; f_b, f_c, f_d). \tag{1.40}$$

Here first term in the left side indicates the change in the number density of species a $w.r.t.$ time, while second term represents the dilution of number density of a due to expansion of the Universe.

We will see throughout this thesis that the above-mentioned out-of-equilibrium phenomena played a crucial role in a variety of important events during the early Universe, such as i) the production of DM, ii) the production of baryon asymmetry, and so on. In the later part of the thesis, we will again come back to discuss it in greater detail while investigating the DM and baryon asymmetry generation process.

1.2.3 Different Phases of Early Universe

Shortly after the big bang, Universe was filled with massless relativistic elements, and radiation domination was attained. The first significant change in the Universe occurred around $t \sim 10^{-10}$ sec. ($T \sim 100$ GeV) when sponteneus electroweak symmetry breaking took place. As a result, all the particles attained mass. As the Universe continued to expand, its temperature decreases. At about $t \sim 10^{-4}$ sec. ($T \sim 100$ MeV) quarks and gluons started to combine themselves and formed hadronic bound states. Subsequently, around $t \sim 3$ min. ($T \sim 0.1$ MeV), temperature became so small that protons and neutrons started to form nuclear bound states. The phenomenon is commonly referred to as $Big\ Bang\ Neucleosyntesis$ (BBN). Matter energy density began to dominate over radiation energy density around $t \sim 10^4$ yrs. ($T \sim 1$ eV). Then around $t \sim 10^5$ yrs. ($T \sim 0.1$ eV), the energy of the photon became so low that it could freely stream through the Universe and eventually being detected as the cosmic microwave background (CMB) radiation.

1.2.4 Shortcoming of Standard Big Bang Cosmology

Despite its success, there are still a few intriguing observations that cannot be explained by the standard big bang cosmology. Here we briefly review few such problems:

- Horizon Problem: The CMB spectrum reveals that the Universe is amazingly isotropic, with an average temperature of $T_0 = 2.7255 \pm 0.01$ K [17]. Therefore, it is anticipated that the CMB photons we observe today from different directions of the Universe were in causal contact at the time of decoupling. However, one can predict whether the photons were in a causal connection at the time of decoupling using the tools available in the standard cosmological model. To learn about it, one need to know about the maximum distance traveled by the photon or calculate the comoving particle horizon, which is denoted as:

$$\tau_H \equiv \int_0^a d(\ln a) \left(\frac{1}{a\mathcal{H}}\right), \tag{1.41}$$

  where $1/(a\mathcal{H})$ is known as comoving Hubble radius, which depends on the the equation of state ω of the species that dominates the Universe as:

$$\frac{1}{a\mathcal{H}} = \frac{1}{\mathcal{H}_0} a^{\frac{1}{2}(1+3\omega)}. \tag{1.42}$$

  Eventually, using the above relation, one can find :

$$\tau_H \propto \begin{cases} a & \text{Radiation domiantion} \\ a^{1/2} & \text{Matter domination,} \end{cases} \tag{1.43}$$

  This indicates that the comoving particle horizon grew monotonically with time which implies that there should be a large amount of regions outside the horizon at CMB decoupling. In fact, it can be shown that there were almost 10^4 number of disconnected

patches during CMB decoupling[28]. Because of such obvious contradiction between theory and experimental results, the question of why two apparently causally disconnected regions appear similar in CMB arises. This is known as the $Horizon\ Problem$[29, 30].

- Flatness Problem: To understand this issue, we must return to the Friedmann equation in Eq: (1.26) and rewrite it as follows:

$$\frac{\rho(a)}{\rho_{\text{crit.}}} - 1 = \Omega(a) - 1 = \frac{k}{(a\mathcal{H})^2}. \tag{1.44}$$

As measured by the CMB, the solution to this equation should result in a spatially flat Universe today, $i.e.$, $\Omega(\text{today}) - 1 = \pm 0.02$[17]. Furthermore, we have learned from Eq. (1.42) that the comoving Hubble radius $1/(a\mathcal{H})$ increases monotonically $w.r.t.$ scale factor. Using this information, one can find the solution of Eq. (1.44) at a very early Universe (say at Planck scale) as[31]:

$$\Omega(\text{Planck scale}) - 1 \lesssim \mathcal{O}(10^{-61}) \tag{1.45}$$

Accordingly, the spatial curvature of the early Universe must be extremely finetuned to 0 in order to achieve an almost flat Universe today, known as the $Flatness\ Problem$[29, 30].

1.2.4.1 Possible resolution via inflation

To resolve the issues mentioned above the idea of inflation was introduced by Alan Guth around 1980 [32]. The basic assumption behind inflaton was to introduce an exponentially accelerated phase before the conventional RD era of the Universe, which can be explained by:

$$\ddot{a} > 0 \rightarrow \frac{d}{dt}(a\mathcal{H})^{-1} < 0 \tag{1.46}$$

Due to such exponential expansion, comoving Hubble radius $1/(a\mathcal{H})$ decreases during inflation. Owing to such outcome, it can be assumed that the whole observable Universe was inside the comoving Hubble radius at the onset of inflation. Then as the Universe expanded exponentially, some causally connected regions went outside the comoving Hubble radius. After the end of inflation, as the Universe started to deaccelarate, $1/(a\mathcal{H})$ started to increase. As a result, those regions which were earlier causally disconnected again started to come inside the comoving Hubble radius. Thus one can trace back the apparently causally disconnected regions during the CMB decoupling phase to the causally connected regions at the beginning of the inflation and resolve the $Horizon\ Problem$.

Inflation can also solve the $Flatness\ Problem$. Due to the decreasing property of $1/(a\mathcal{H})$ during inflation, solving Eq. (1.44) with any arbitrary initial condition on $\Omega - 1$ at the start of inflation will result in a spatially flat Universe after inflation. As a result, it can explain the early flatness of the Universe.

However, to solve both problems, inflationary models that can sustain inflation for an extended period of time need to be developed. Several interesting models are already present

in the literature. In the context of our analysis, the post-inflationary epoch remains interesting as we will talk about it later.

1.3 Neutrino Mass

Neutrinos are special particles playing an important role in the expanding Universe. They are the only fermion in the SM which are electrically neutral and do not have right handed counterparts. As a result, neutrinos were assumed to be massless. However, since 1998, starting from the Super-Kamiokande (SK) collaboration[33], various different neutrino oscillation experiments such as K2K[34], KamLand[35] have observed neutrino deficits (with respect to the expected flux) in different types of neutrino flux coming from different sources. For example, SK was the first experiment that observed a flux asymmetry in upward-going and downward-going atmospheric μ-neutrino flux. The ratio of upward-going and downward-going ν_μ flux was found to be of order ~ 0.55 [36], which indicates almost 50% deficit. On the other hand, with the solar neutrinos sector, almost all the experiments observed significantly smaller amounts of solar ν_e than the amount predicted by the standard solar model[37]. Similar deficits of neutrino flux have also been observed for reactor neutrinos[35] as well. All these anomalies can be resolved if one incorporates the three-flavor oscillation framework of neutrinos, which requires the existence of negligible but non-zero neutrino mass along with definite mixing among different flavors of neutrino. The presence of such non-zero mass and mixing induces an additional rotation, hence leading to a lepton mixing matrix analogous to CKM mixing in the quark sector. There are a large number of neutrino mass mechanism models present in the literature generating light neutrino mass. One can now relate the flavor and mass eigenstates in the lepton sector as:

$$(e_L)_\alpha = (U_e)_{\alpha i}(e'_L)_i\,, \quad (E_R)_\alpha = (V_e)_{\alpha i}(E'_R)_i\,, \text{ and, } \quad (\nu_L)_\alpha = (U_\nu)_{\alpha i}(\nu'_L)_i, \tag{1.47}$$

which finally leads to a lepton mixing angle $U = U_e^\dagger U_\nu$ explicitly present in the charged current interaction for leptons as:

$$-\mathcal{L}_{cc}^{lep.} = \frac{g_2}{\sqrt{2}}\sum_{i,j}(\overline{e}'_L)_i\gamma^\mu W_\mu^+(U_e^\dagger U_\nu)_{ij}(\nu'_L)_j + h.c.. \tag{1.48}$$

This U matrix is known as Pentecorvo-Maki-Nakagawa-Sakata (PMNS) matrix and it follows the relation $U^\dagger U = 1$ ($i.e.$ U is unitary in nature). Consequently, for three generations of neutrinos it has nine independent real parameters out of which three denote mixing angles and six represent phases. Some of these six phases can be rotated away depending on the nature of the neutrinos and only few will remain as the physical phase. For Dirac type neutrino one can show that only one physical phase is relevant, which is known as Dirac phase δ. On the other hand, if neutrino possesses Majorana property, three physical phases remain out of which one in δ and the other two are denoted as Majorana phases. The PDG parametrization of the PMNS matrix is given by:

$$U = \begin{pmatrix} c_{12}c_{13} & s_{12}c_{13} & s_{13}e^{-i\delta} \\ -s_{12}c_{23} - c_{12}s_{13}s_{23}e^{-i\delta} & c_{12}c_{23} - s_{12}s_{13}s_{23}e^{-i\delta} & c_{13}s_{23} \\ s_{12}s_{23} - c_{12}s_{13}c_{23}e^{i\delta} & c_{12}s_{23} - s_{12}s_{13}c_{23}e_{i\delta} & c_{13}c_{23} \end{pmatrix} U_m \tag{1.49}$$

where, $c_{ij} = \cos\theta_{ij}$ and $s_{ij} = \sin\theta_{ij}$, while δ represents the Dirac phase. Here, matrix $U_m = diag(1, e^{\alpha_{21}/2}, e^{\alpha_{31}/2})$ contains the Majorana phases α_{21} and α_{31}.

Neutrino oscillation experiments provide estimates on neutrino mixing and mass square differences. The constraint on absolute values of neutrino mass comes as a form of the sum of neutrino mass $\sum_i m_{\nu_i} < 0.12$ eV from the observation of CMB[17]. On the other hand, direct detection experiments measuring beta decay like KATRIN[38] provide an upper limit on effective mass $m_\beta = \sqrt{\sum_i |(U)_{ei}|^2 m_i^2} < 1.1$ eV, while neutrinoless double beta decay experiment like CUPID [39] gives the best limit on a different parameter $m_{\beta\beta} \propto \sum_i U_{ei}^2 m_i < 0.2 - 0.5$ eV.

All these experimental results indicate that neutrinos should have mass. In the literature, there exist different variants of seesaw mechanisms such as Type-I seesaw[40–46], Type-II seesaw[46–50], Type-III seesaw[51], inverse seesaw [52, 53] etc., radiative neutrino mass models such as Zee-Wolfenstein Model[54], Zee-Babu Model[55, 56], Ma-Model[57] and so on, which provide novel setup for generation of neutrino mass. Below we provide detailed discussion on type-I and II scenarios, which are particularly important for this thesis.

1.3.1 Type-I seesaw mechanism

The most simple and attractive mechanism, which can explain the smallness of neutrino mass is the Type-I seesaw mechanism. In this setup, the particle content of the SM can be extended by three electrically neutral gauge singlet right handed neutrinos (RHNs), N_{R_i} with $i = 1, 2, 3$, which are Majorana fields in nature. Consequently, utilizing these RHNs following Lagrangian is constructed on top of the SM lagrangian:

$$-\mathcal{L}_{type-I} = (Y_\nu)_{\alpha i} \bar{l}_{L_\alpha} \widetilde{H} N_{R_i} + \frac{1}{2}(M_R)_{ij} \overline{(N_{R_i})^c} N_{R_j} + h.c., \tag{1.50}$$

where the first term denotes the Yukawa interaction involving left handed lepton doublet, Higgs doublet and RHNs similar to the SM Yukawa interactions. The second term represents the bare Majorana mass term for the RHNs. As a result of which, such SM gauge invariant bare Majorana mass term can be introduced in the Lagrangian (though the term breaks the lepton number symmetry by two units). After SSB, the Lagrangian denoting the neutrino mass terms can be expressed as:

$$\mathcal{L}_{mass} = \frac{1}{2} \begin{pmatrix} \overline{\nu_L} & \overline{N_R^c} \end{pmatrix} \begin{pmatrix} 0 & m_D \\ (m_D)^T & M_R \end{pmatrix} \begin{pmatrix} \nu_L^c \\ N_R \end{pmatrix} + h.c., \tag{1.51}$$

where $m_D = Y_\nu v/\sqrt{2}$ is the Dirac mass matrix generated after SSB while the matrix in the middle is identified as seesaw mass matrix m_{seesaw}. For three added RHNs, m_D and M_R would have 3×3 matrix structure, with M_R being symmetric in nature. Subsequently, m_{seesaw} will be a 6×6 symmetric matrix. Under the assumption $m_D << M_R$, the block diagonalisation of m_{seesaw} yields two non-zero eigenvalues in the form of 3×3 matrices:

$$m_\nu^I \simeq -m_D M_R^{-1} m_D^T \tag{1.52}$$

$$M_N \simeq M_R. \tag{1.53}$$

To generate the mass of the light neutrinos, one need to diagonalize the light neutrino mass m_ν^I as:

$$U_\nu^\dagger m_\nu^I U_\nu^* = diag(m_1, m_2, m_3) = D_m, \tag{1.54}$$

where U_ν is the PMNS matrix defined in Eq. (1.48) if one assumes the charged lepton mass matrix to be diagonal. Finally, for the mass of the heavy RHNs, one again diagonalizes the symmetric matrix M_N by orthogonal transformation with a Unitary matrix V_N:

$$V_N^\dagger M_N V_N^* = diag(M_1, M_2, M_3) = D_M. \tag{1.55}$$

1.3.2 Type-II seesaw mechanism

In type-II seesaw setup, one new scalar field $\mathbf{\Delta} = (\Delta_1, \quad \Delta_2, \quad \Delta_3)$ is added into the SM. The new scalar Δ being triplet under the SM gauge group can be expressed as:

$$\Delta = \frac{\tau_i}{\sqrt{2}}\Delta_i = \frac{1}{\sqrt{2}} \begin{pmatrix} \Delta^+/\sqrt{2} & \Delta^{++} \\ \Delta^0 & -\Delta^+/\sqrt{2} \end{pmatrix}, \tag{1.56}$$

where $\Delta^+ = \Delta_3$, $\Delta^0 = \frac{\Delta_1 + i\Delta_2}{\sqrt{2}}$ and $\Delta^{++} = \frac{\Delta_1 - i\Delta_2}{\sqrt{2}}$. Here, τ_i represents the Pauli spin matrices with $i = 1, 2, 3$. Using this representation, one can construct the new interaction terms responsible for neutrino mass[1] as:

$$-\mathcal{L}_{type-II} = (Y_\Delta)_{\alpha\beta} \overline{\ell_{L_\alpha}^c} (i\tau_2 \Delta) \ell_{L_\beta} + \mu_1 H^T (i\tau_2 \Delta^\dagger) H + h.c.\,. \tag{1.57}$$

After SSB, the vev of the Higgs doublet field induces a non-zero vev for the neutral component of the triplet $\langle \Delta^0 \rangle = v_\Delta$, which can be calculated by minimizing the scalar potential as:

$$\langle \Delta^0 \rangle = v_\Delta = \frac{\mu_1 v^2}{2M_\Delta^2} \tag{1.58}$$

[1]Furthermore, one needs to introduce the kinetic and potential terms relevant for the new triplet in the Lagrangian.

This leads to the Majorana mass term for light neutrinos :

$$(m_\nu^{II})_{ij} \simeq 2v_\Delta (Y_\Delta)_{ij}. \tag{1.59}$$

Finally, diagonalizing m_ν^{II} results in the light neutrino masses.

1.4 Dark Matter

With the development of cosmological research over the last few decades, our understanding of the elements that make up our Universe has steadily increased. One of such study, based on high-precision measurements of the CMB temperature by WMAP [58]and PLANCK [59] collaboration, has revealed that Dark Energy (DE), which accounts for the accelerated expansion of the Universe, makes up the majority (about 70%) of the energy density of the Universe, while rest of the Universe appears to be made up of mostly DM (almost 26%). Finally, visible matter (also known as "baryonic" matter) accounts for only 4% of the total energy density of the Universe. Although the DM has not yet been directly detected, and its characteristics are still mostly unknown, astronomical experiments have provided a wealth of indirect evidence in the form of its gravitational effects that have motivated us to believe in its existence.

The most prominent and earliest evidence of the presence of DM came from the observation of the rotational velocity of galaxies and galaxy clusters. Pioneered by Fritz Zwicky in 1933[60], and later by Vera Ruben in 1970[61], extensive study of the rotational curves of different galaxies were performed. As a result of which, an unique behavior of rotational velocity of galaxies and galaxy clusters (similar to Fig. 1.1) was discovered. Fig. 1.1 shows the variation of rotational velocity of the hydrogen gas clouds around the galaxy NGC 6503 $w.r.t.$ the distance from the center of the galaxy. As seen from the plot, the rotational velocity V_c increases linearly for small distance from center r. Further increasing r leads to a saturation of the V_c till the end of the galaxy. Theoretical calculation using Newtonian mechanics, however, results in a completely different behavior of $V_c \propto r^{-1/2}$ for a larger value of r, which indicates that the rotational velocity should decrease $w.r.t.$ distance r for larger distances. This discrepancy can be eliminated by introducing DM halo on top of visible matter as the galaxy's constituents, which results in the observed V_c.

Another distinct tool to study the presence of DM is searching for gravitational lensing in the sky. According to the Einstein's general relativity, light can bend in presence of bulk of matter. One can utilize this fact to estimate the density profile of the matter content of an intermediate galaxy which acts as a lens for light coming from distant galaxies. As the light comes through this intermediate galaxy, bending of light occurs due to the gravitational effect of the constituents of the galaxy. Consequently, a distorted pattern of light rays is observed in the detectors. Looking at the amount of distortion, one can distinguish the amount of DM from the visible matter in the intermediate galaxy. One such astonishing outcome was presented by Bergmann, Petrosian by looking at the leansing effects of several clusters. A more recent study on Bullet cluster[14, 62] together with various other galaxy survey experiments also have provided important signatures of DM. We can get some clues about some of the microscopic nature of DM from the experimental evidences discussed

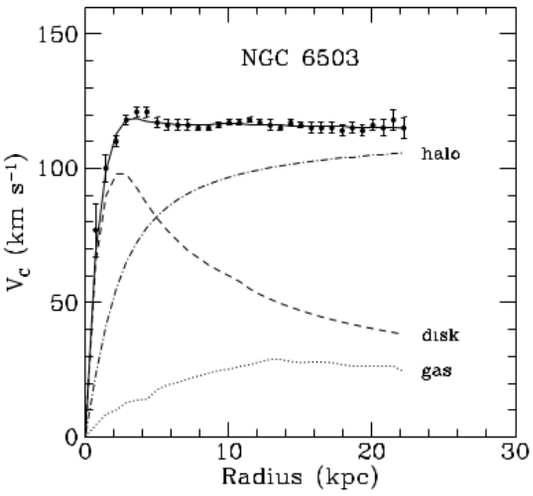

Figure 1.1: Rotation velocities V_c of different constituents of galaxy NGC 6503 [13]. Different lines depict the contribution of the three major components towards V_c . As seen from the plot, Dark matter, dubbed *"halo"* makes the most significant contribution at long distances.

above. The Existence of DM's gravitational interaction is one of them, while the nonexistence of electromagnetic charge is another important property of DM. Furthermore, DM should be a stable object or at least its lifetime should not be smaller than the age of the Universe. Despite this knowledge, we still do not know many things about DM, the most important of them is whether or not DM is a particle. Going one step further, if one assumes that the DM is a fundamental particle, many more questions start to arise whose answers are still unknown to us, such as, what is the spin of DM? How strong is DM's interaction with other fundamental particles? How were they produced in the early Universe? and so on. Answering such questions is one of the main tasks of the beyond SM model builders as SM fails to provide any particle DM candidate.

In the present thesis, we will devote one whole chapter to discuss the influence of possible DM candidates on the matter-antimatter asymmetry generation process. Hence, our goal for the rest of this section will be to discuss elaborately some of the possible production mechanisms of DM, more importantly, "Freeze-out" and "Freeze-in" mechanisms.

1.4.1 Production of Dark Matter

There are primarily two mutually exclusive mechanisms available in the literature that can be used to produce the required amount of stable DM. One is known as "Freeze-out" mechanism while the other is known as "Freeze-in". Let us discuss them one by one.

1.4.1.1 Freeze-out Mechanism

In this setup, the DM particle is assumed to have weak coupling with SM fields. Such DMs are popularly known as *Weakly interacting massive particle* (WIMP)[63–69]. As a result, the DMs are in thermal equilibrium in the early Universe. Hence it can be produced from the thermal bath. Subsequently, it decouples from the bath when this equilibrium ceases to exist. Depending on the nature of DM at the time of decoupling, DM can be further classified

as i) hot DM (HDM)- the DM which stays ultra-relativistic during decoupling, ii) warm DM (WDM)- it decouples when it becomes relativistic, and, iii) cold DM (CDM)- the DM which becomes completely nonrelativistic at the time of decoupling. The easiest way to evaluate the decoupling temperature of such DMs is by comparing the DM annihilation rate (more specifically, the thermal average of annihilation rate $\langle\Gamma\rangle$) with the expansion rate of the Universe $\mathcal{H}$. As described in Eq. (1.31) and (1.32), when $\langle\Gamma\rangle < \mathcal{H}$, the interactions of the DM freeze out and DM decouples from the thermal bath. As a result, DM can have a significant abundance surviving till now.

A more rigorous and accurate way to learn about the decoupling temperature as well as the relic abundance of DM particle (say ψ) today is by solving the Boltzmann equation (BE) for DM particle (say ψ) as presented in Eq. (1.40), where n_a will be now replaced by n_ψ and collision term in the right side will represent all the number changing processes for ψ. To see how it works, let us assume that the ψ particle only annihilates to SM particle-antiparticle pairs ($X, \bar{X}$ and inverse processes) $\psi\bar{\psi} \leftrightarrow X\bar{X}$. As a result of which, the right side of the BE can be expressed as:

$$\mathbf{C}(f_\psi; f_{\bar{\psi}}, f_X, f_{\bar{X}}) = \int \frac{d^3p_{\bar{\psi}}}{(2\pi)^3 2E_{\bar{\psi}}} \frac{d^3p_X}{(2\pi)^3 2E_X} \frac{d^3p_{\bar{X}}}{(2\pi)^3 2E_{\bar{X}}} (2\pi)^4 \delta^{(4)}(P_\psi + P_{\bar{\psi}} - P_X - P_{\bar{X}}) \times \Big[|\mathcal{M}_{X\bar{X}\to\psi\bar{\psi}}|^2 f_X f_{\bar{X}} (1 \pm f_\psi)(1 \pm f_{\bar{\psi}}) - |\mathcal{M}_{\psi\bar{\psi}\to X\bar{X}}|^2 f_\psi f_{\bar{\psi}} (1 \pm f_X)(1 \pm f_{\bar{X}}) \Big]. \tag{1.60}$$

One can simplify the above expression with the following approximations: (i) there is no CP violation within the interaction processes. As a result of which, owing to the CPT theorem, one can denote

$$|\mathcal{M}_{\psi\bar{\psi}\to X\bar{X}}|^2 = |\mathcal{M}_{X\bar{X}\to\psi\bar{\psi}}|^2. \tag{1.61}$$

(ii) One can safely neglect the Pauli blocking/ Bose condensation effect in the early Universe. Consequently, $1 \pm f_a \sim 1$ holds. Furthermore, since the SM particles are in thermal equilibrium, $f_X(f_{\bar{X}})$ can be expressed as:

$$f_X = f_X^{eq} = Exp(-E_X/T), \qquad f_{\bar{X}} = f_{\bar{X}}^{eq} = Exp(-E_{\bar{X}}/T). \tag{1.62}$$

Finally, along with the above approximations (i) and (ii), the delta function for energy conservation $E_\psi + E_{\bar{\psi}} = E_X + E_{\bar{X}}$ leads to the following form of the collision term:

$$\mathbf{C}(f_\psi; f_{\bar{\psi}}, f_X, f_{\bar{X}}) = \int \frac{d^3p_{\bar{\psi}}}{(2\pi)^3 2E_{\bar{\psi}}} \frac{d^3p_X}{(2\pi)^3 2E_X} \frac{d^3p_{\bar{X}}}{(2\pi)^3 2E_{\bar{X}}} (2\pi)^4 \delta^{(4)}(P_\psi + P_{\bar{\psi}} - P_X - P_{\bar{X}}) \times |\mathcal{M}_{\psi\bar{\psi}\to X\bar{X}}|^2 \Big(f_\psi^{eq} f_{\bar{\psi}}^{eq} - f_\psi f_{\bar{\psi}} \Big). \tag{1.63}$$

Incorporating the left side of Eq. (1.40), the BE for DM looks like:

$$\frac{dn_\psi}{dt} + 3\mathcal{H} n_\psi = \langle\sigma v\rangle_{\psi\bar{\psi}\to X\bar{X}} \Big[(n_\psi^{eq})^2 - n_\psi^2 \Big] \tag{1.64}$$

where n_ψ^{eq} denotes the equilibrium number density of DM:

$$n_\psi^{eq} = \frac{g_{eff}T^3}{2\pi^2}\left(\frac{m_\psi}{T}\right)^2 K_2(m_\psi/T), \tag{1.65}$$

with $g_{eff} = g$ $(3g/4)$ for bosonic (fermionic) DM, while m_ψ representing the mass of the DM. Here $\langle\sigma v\rangle_{\psi\bar{\psi}\to X\bar{X}}$ is the thermal average of scattering cross section times the relative velocity of DM and can be expressed as [70–72]:

$$\begin{aligned}\langle\sigma v\rangle_{\psi\bar{\psi}\to X\bar{X}} =& \frac{1}{(n_\psi^{eq})^2}\int \frac{d^3p_\psi}{(2\pi)^3 2E_\psi}\frac{d^3p_{\bar{\psi}}}{(2\pi)^3 2E_{\bar{\psi}}}\frac{d^3p_X}{(2\pi)^3 2E_X}\frac{d^3p_{\bar{X}}}{(2\pi)^3 2E_{\bar{X}}}(2\pi)^4 \\ &\times \delta^{(4)}(P_\psi + P_{\bar{\psi}} - P_X - P_{\bar{X}})|\mathcal{M}_{\psi\bar{\psi}\to X\bar{X}}|^2 Exp(-E_\psi/T)Exp(-E_{\bar{\psi}}/T).\end{aligned} \tag{1.66}$$

In terms of center of mass energy S of the colliding DMs $\langle\sigma v\rangle_{\psi\bar{\psi}\to X\bar{X}}$ can be evaluated as:

$$\langle\sigma v\rangle_{\psi\bar{\psi}\to X\bar{X}} = \frac{1}{8Tm_\psi^4 K_2^2\,(m_\psi/T)}\int_{4m_\psi^2}^{\infty} dS\sqrt{S}(S-4m_\psi^2)K_1(\sqrt{S}/T)\sigma_{\psi\bar{\psi}\to X\bar{X}}. \tag{1.67}$$

where K_1 and K_2 are the modified Bessel functions respectively.

It is always useful to transform the BE in such a way that the effect of the expansion of the Universe can be scaled out. For that purpose, one can define the new dimensionless variable $Y_\psi = n_\psi/s$, with s being entropy density presented in Eq. (1.36). Consequently, the BE in Eq. (1.64) will look like:

$$\frac{dY_\psi}{dt} = \langle\sigma v\rangle_{\psi\bar{\psi}\to X\bar{X}}\left[(Y_\psi^{eq})^2 - Y_\psi^2\right]. \tag{1.68}$$

Furthermore, since the thermal average of cross section times velocity depends on the temperature of bath T rather than time, it is convenient to solve the BE as a function of temperature or, more specifically dimensionless parameter $z = m_\psi/T$. Thus, assuming a RD Universe, the relation between time and variable z [24]

$$t = \frac{0.301}{\sqrt{g_*}}\frac{M_p}{T^2} = \frac{0.301}{\sqrt{g_*}}\frac{M_p}{m_\psi^2}z^2, \tag{1.69}$$

leads to the following form of BE

$$\frac{dY_\psi}{dz} = \frac{zs\langle\sigma v\rangle}{\mathcal{H}(T=m_\psi)}\left[(Y_\psi^{eq})^2 - Y_\psi^2\right], \tag{1.70}$$

where $\mathcal{H}(T=m_\psi) = 1.66g_*^{1/2}m_\psi^2/M_P = \mathcal{H}(T)z^2$. One can solve this simple form of BE to learn how a DM evolves with the evolution of the Universe. The yield at the decoupling period Y_{fo} can now be easily estimated from the solution of BE. Since there will be no number changing processes available after freeze out, Y_{fo} will remain constant after the decoupling till now. Consequently, the current relic abundance of the DM can be estimated using the

relation:

$$\Omega^0_{DM} = \frac{\rho^0_{DM}}{\rho^0_{\text{crit.}}} = \frac{s_0 Y_{fo} m_\psi}{\rho^0_{\text{crit.}}}, \tag{1.71}$$

where $s_0 = 2970\ \text{cm}^{-3}$ is the entropy density of the Universe today.

There exists a large amount of WIMP DM models in the literature which relies on such freeze-out mechanism. It is interesting to point out that if one assumes a DM having mass of the order of weak scale, which has weak interaction mediated annihilation processes, the estimated relic abundance of such DM comes out as the observed value in CMB. This is known as $WIMP\ miracle$. Due to the weak coupling, these DMs can produce signals at the LHC. There are other direct and indirect detection experiments available for WIMP type DMs, some of which we will discuss in a later chapter.

1.4.1.2 Freeze-in Mechanism

This is another well studied mechanism, which was pioneered by L.J. Hall[73] in 2009. In this setup, DM is assumed to have very feeble interaction strength with other particles. As a result of which, the DM never attains thermal equilibrium during its evolution. Due to the feeble nature of its interactions, this type of DM is popularly known as the *Feebly interacting massive particle* (FIMP)[73–77]. These particles can be produced from the decay or annihilation of heavier particles.

To learn about the evolution of this type of DM over time, one again needs to solve the BE presented in Eq. (1.40). However, the final form of the equation becomes pretty simple for this type of DM due to its feeble coupling. For example, let us analyze a simple scenario where DM (say ψ) is assumed to be produced only from the decay of heavier particles (say X) from the bath: $X \to \psi\psi$. This is a good assumption since the annihilation of particles to the DM will be highly suppressed compared to their decay processes due to the associated feeble coupling. In addition, in this case, one can assume that the initial abundance of DM was negligibly small due to its very weak coupling. As a result of which, the collision term in Eq. (1.39) will look like:

$$\mathbf{C}(f_\psi; f_\psi, f_X) = \int \frac{d^3p_\psi}{(2\pi)^3 2E_\psi} \frac{d^3p_X}{(2\pi)^3 2E_X} (2\pi)^4 \delta^{(4)}(P_X - 2P_\psi) \Big[|\mathcal{M}_{X\to\psi\psi}|^2 f_X (1 \pm f_\psi)^2 \Big] \tag{1.72}$$

Assuming $1 \pm f_\psi \sim 1$ and $f_X = f_X^{eq}$, and finally representing the Eq. (1.40) in terms of $Y_\psi = n_\psi/s$, one can generate the final form of the BE as:

$$\frac{dY_\psi}{dz'} = \frac{1}{\mathcal{H} z'} Y_X^{eq} \langle \Gamma_{X\to\psi\psi} \rangle, \tag{1.73}$$

which provides the evolution of FIMP DM yeild Y_ψ $w.r.t.$ the dimensionless variable $z' = M_X/T$ where M_X is the mass of the X particle. Here $\langle \Gamma_{X\to\psi\psi} \rangle = \Gamma_{X\to\psi\psi} K_1(z)/K_2(z)$ denotes the thermal average of decay width $\Gamma_{X\to\psi\psi}$ of X particle. Here contrary to the WIMP scenario, DM with zero abundance in the early Universe is gradually produced from the

decay of X particles till the X particle becomes nonrelativistic and its abundance drops exponentially. As a result, the abundance of DM practically freezes in and remains constant till now. We will study in detail a simple DM candidate produced from a such freeze-in mechanism and its indirect impact on the lepton asymmetry generation in a later chapter.

1.5 Baryon asymmetry of the Universe

In particle physics and cosmology, the imbalance between matter and antimatter in the observable Universe remains a significant enigma that is yet to be fully understood. Although the standard model of cosmology is capable of predicting CMB radiation and the primordial quantities of light elements, it falls short of explaining why antibaryon abundance $n_{\bar{B}}$ is almost absent in our visible Universe, more precisely why the baryonic abundance $Y_B = (n_B - n_{\bar{B}})/s$ is of the order of 8.7×10^{-11}[17]. We will begin this section by presenting experimental evidence that confirms our Universe has more baryons than antibaryons. Then, we will discuss the necessary conditions to create such asymmetry through dynamic processes. One such process, called the leptogenesis mechanism, is the most promising baryon asymmetry generation mechanism as it is inherently tied to the origin of neutrino mass generation from the seesaw mechanism. In the next section, we will discuss the specifics of this mechanism and provide a broad overview.

1.5.1 Antimatter search and constraint on baryon asymmetry

Due to the almost identical nature of fundamental interactions of particles as well as antiparticles, it is natural to believe that the Universe should be symmetric in matter and antimatter. However, to verify such speculation, it is necessary to search for and detect an equivalent amount of antimatter (antibaryon) to the matter (baryonic) already observed in our Universe. There are two ways one can look for antimatter in the Universe: (i) direct search for antinuclei or (ii) search for the diffused gamma rays generated due to a possible annihilation of the matter and antimatter if both are present.

To start with, one can search for antimatter on the Earth. However, no antimatter is found. The solar system is the next closest source where antimatter can be searched. The presence of antimatter in the solar system would result in a strong photon signal due to its interaction with solar winds[78]. However, the absence of such signals has ruled out the possibility of antimatter in the solar system. Another compelling evidence of the absence of antimatter in our solar system and our galaxy comes from the direct observation of cosmic rays. PAMELA and FERMI space observatories are extensively studying these cosmic rays. Recently they have discovered some traces of positrons and antiprotons. However, the antiproton to proton flux is only found to be of $\mathcal{O}(10^{-4})$. Such small antiprotons are generated by the interaction of cosmic ray protons via $p + p \to \bar{p} + 3p$ process. This again indicates that no antimatter structure in the form of stars is present in our solar system or our galaxy.

The presence of antimatter in the remaining part of the Universe can be heavily constrained by the indirect detection process. In that case, One can think of two fundamentally different types of regions in the Universe: (a) regions where matter and antimatter are mixed homogeneously similar to the environment at intergalactic medium or interstellar medium,

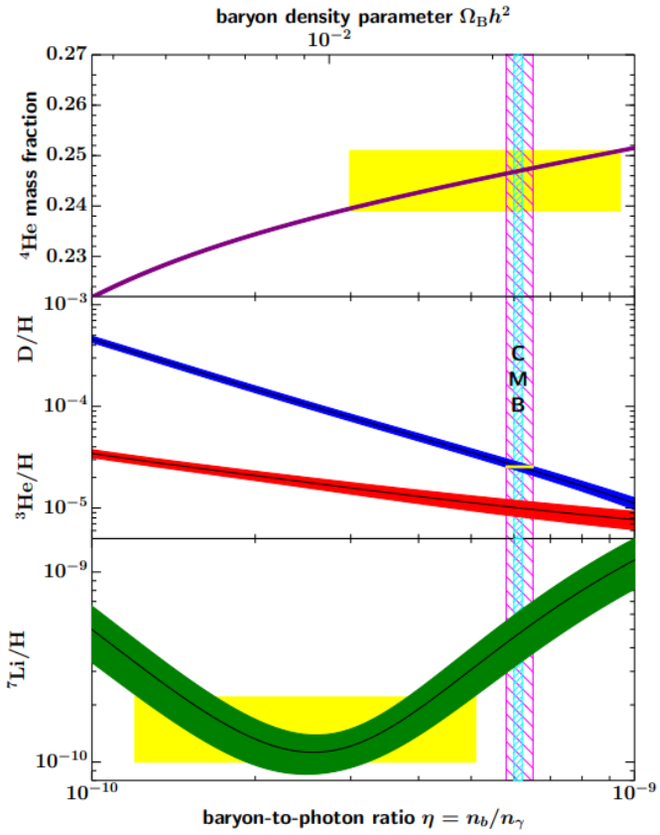

Figure 1.2: The primordial abundances of ^{4}He, D, ^{3}He, and^{7}Li as a function of cosmic baryon density predicted by the standard model of Big-Bang nucleosynthesis. The bands indicate the 95% CL range[18], while yellow boxes denote the observed light element abundances. The narrow blue vertical band is the CMB measure of the cosmic baryon density, while the wider magenta band indicates the D+4He BBN concordance range (at 95% CL). Credit to [79].

where along with matter, a certain amount of antimatter can be found, and (b) large patches of regions consist of only matter or antimatter.

The majority of the baryons in galaxy clusters are found in the warm, intracluster gaseous medium that emits X-rays. These X-rays are produced due to thermal bremsstrahlung emission from the two-body collisions. However, If a fraction of this gas (say f) were to consist of antibaryons, matter-antimatter annihilation would produce high-energy gamma rays, which are related to the observed X-ray flux. Non-observance of these gamma-ray flux provides an upper limit on the fraction f[80]:

$$f \leq 3 \times 10^{-11} \frac{T}{\text{keV}} \frac{F_\gamma}{F_X}, \tag{1.74}$$

where T is the temperature of the gas, while F_X and F_γ represent the flux for X-ray and gamma-rays respectively. EGRET experiment searches for these gamma photons. It has surveyed 55 galaxy clusters[81] and has provided an upper bound on the gamma-ray flux for each cluster of galaxies. Using these upper bounds, fraction f is constrained in [82]. The largest bound on f is found to be $f < 10^{-6}$, which indicates that these clusters are almost entirely made up of matters. On the other hand, if there were large regions consisting of only matter or antimatter, a large amount of matter-antimatter annihilation would occur at the boundary between the two patches. Non-observation of such annihilation signal as a form

of photons generally provides a bound on the size of such individual patches. In [83], the authors provide an estimate of the size of such domains, which is found to be of the order of the observable Universe.

All these observations discussed till now indicate a baryon asymmetric Universe. There are two ways one can quantify such baryon asymmetry: i) by taking a ratio of baryon density and photon density of the Universe: $\eta_B = (n_B - n_{\bar{B}})/n_\gamma$, or ii) by taking the ratio of baryon density and entropy density: $Y_B = (n_B - n_{\bar{B}})/s$, with $n_{\bar{B}} = 0$ holds today as discussed above. Analyzing the acoustic peaks in the angular power spectrum of the CMB, one can provide a bound on η_B (or Y_B) of the present day (indicated by η_B^0 or Y_B^0) with a good degree of accuracy as[17]:

$$\eta_B^0 = (6.12 \pm 0.04) \times 10^{-10} \text{ or } \quad Y_B^0 = (8.7 \pm 0.06) \times 10^{-11}. \tag{1.75}$$

On the other hand, the measurement of the abundance of the primordial light elements during the big bang nucleosynthesis (BBN) period also provides an estimate of η_B^0 (or Y_B^0) as[18]:

$$\eta_B^0 = (5.7 - 6.5) \times 10^{-10}, \quad Y_B^0 = (8.2 - 8.8) \times 10^{-11} \quad (95\% \text{ CL}). \tag{1.76}$$

Fig 1.2 shows the variation of the primordial fraction abundances of ^{4}He, D, ^{3}He, and ^{7}Li $w.r.t.$ the baryon density as predicted by the standard model of Big Bang nucleosynthesis. Here, the CMB measurement of the cosmic baryon density (as presented in Eq. (1.75)) is denoted by the narrow blue vertical band, while the observation from BBN [18](at 95% CL) is indicated by the wider magenta band. The overlap between these two bands indicates that both CMB and BBN observations of cosmic baryon density are consistent with each other. It should be noted that the time for BBN formation differs significantly from that of CMB formation. Nonetheless, the similar amount of baryon asymmetry obtained from these two epochs is quite intriguing.

1.5.2 Generation of baryon asymmetry

To explain such observed baryon asymmetry, the simplest solution would be to assume the baryon number asymmetry as the initial condition from the beginning of the Universe. However, in that case, one would require 6000001 baryons for every 6000000 antibaryon leading to a highly fine-tuned initial situation. A state with such fine tuning seems quite unlikely. More importantly, we have compelling evidence from CMB that inflation occurred in the early Universe. As a result, any primordial baryon asymmetry would have been erased by the exponential expansion of the Universe during the inflation era. Hence a dynamical generation mechanism of baryon asymmetry from a baryon-antibaryon symmetric Universe is necessary, which is popularly known as $baryogenesis$. Let us now discuss the conditions necessary for baryogenesis and search for the conditions within the SM of particle physics.

1.5.2.1 Sakharov Condition

The three ingredients required to dynamically generate a baryon asymmetry were proposed by Sakharov in 1967[84]. They are summarized as follows:

1. Baryon number violation: It would be obvious that the Universe with an initial condition $B = 0$ can not gain any baryon number excess if all fundamental interactions maintain the baryon number. So, one needs baryon number violating interactions in the system. Within the SM of particle physics, both baryon number and lepton number are conserved at the classical level. However, due to the axial anomaly and nontrivial vacuum states of the non-abelian gauge symmetries of SM, these accidental symmetries of SM are broken at the quantum level. Hence, at the nonperturbative level, baryon number violating interaction, called the sphaleron process, is present within SM.
2. Charge-conjugate (C) and Charge-conjugate-Parity (CP) violation: C or CP symmetry indicates that the interaction rate for a process and its charge conjugate or CP-conjugate process are equal. As a result, the C or CP-conjugate process of a baryon number violating interaction would produce an equal and opposite amount of baryon asymmetry leading to a system having vanishing net baryon number. So, C and CP violation is essential for baryon asymmetry generation. The weak interactions within the SM violate C maximally, and the CKM matrix related to quark mixing violates CP. Therefore SM itself satisfies Sakharov's second condition. However, the amount of CP violation present within the CKM matrix is so small that it is impossible to generate baryon asymmetry of the order $\eta_B \sim 10^{-10}$ with such a small CP violation.
3. Departure from equilibrium: Baryon asymmetry produced from processes satisfying the above two conditions would evolve with the temperature of the Universe. If during this whole process, the system stays in thermal equilibrium, an equal amount of interaction and its inverse process would occur, erasing the whole baryon asymmetry. Hence, a system must go out of equilibrium for the survival of the produced baryon asymmetry. Within the SM, the electroweak phase transition process (EWPT) is present, which may provide such out of equilibrium phase for the process generating baryon asymmetry. However, for this purpose, the EWPT has to be of first order[85, 86] which is currently inconsistent within the Higgs boson's mass $\sim$ 125 GeV[87–89]. As a result, the out-of-equilibrium condition is not satisfied within SM.

All these indicate that to generate the required amount of baryon asymmetry, one should search for new physics scenarios beyond the SM, which can provide not only a new source of CP violation but it should also introduce new out-of-equilibrium dynamics. There are many interesting scenarios present in the literature which can dynamically produce the baryon asymmetry successfully, such as GUT baryogenesis[90–92], Affleck-Dine baryogenesis[93, 94], baryogenesis via leptogenesis[95–97], etc. However, we will not go into the detail of these mechanisms; rather, we will discuss the baryogenesis via leptogenesis mechanism in the next section elaborately, followed by a discussion on the importance of individual charged lepton flavors on leptogenesis mechanism as its understanding is crucial in view of the present thesis.

1.6 Baryogenesis via Leptogenesis

One of the most attractive mechanisms for the dynamical generation of baryon asymmetry is leptogenesis due to its close proximity with the seesaw variant of neutrino mass mechanisms. As discussed earlier, within a seesaw framework, the SM is generally extended with heavy degrees of freedom. Consequently, the smallness of the light neutrino masses is explained by the large masses of newly added fields. Among all such seesaw setups, the type-I setup is most attractive[2] as, in this case, the inclusion of heavy RHNs is enough for the generation of light neutrino mass. Given that the decays of these seesaw-related heavy RHNs generally satisfy all the conditions necessary for generating a lepton asymmetry, such a canonical seesaw framework can accommodate the leptogenesis mechanism naturally. For example, (i) complex Yukawa couplings present in the Yukawa interaction associated with such RHNs can be the source of CP violation, (ii) due to the Majorana nature, the mass term of the RHNs violates lepton number; (ii) the decay process of the RHNs at $T \lesssim M_1$ can go out of equilibrium as a result of the expansion of the Universe. Hence, a finite amount of lepton asymmetry can be generated, which is then partially converted into a baryon asymmetry through anomalous $B + L$ violating electroweak sphaleron interactions. In the remaining section, we will mainly discuss in detail the leptogenesis mechanism and the importance of individual charged lepton flavors on lepton asymmetry generation within the type-I seesaw framework.

1.6.1 Unflavored thermal leptogenesis

The relevant Lagrangian, which can explain the leptogenesis naturally within the type-I seesaw framework is presented in Eq. (1.50). In this setup, due to the existence of Yukawa interaction as well as the Majorana mass term, the RHNs would be produced from the thermal bath in the early Universe ($T >> M_i$) by means of inverse decay ($\ell_{L_\alpha} + H \to N_i$ and $\bar{\ell}_{L_\alpha} + \bar{H} \to N_i$) as well as $2 - 2$ scatterings mediated via Higgs boson. Typically, it is considered that the interaction rates of these processes were fast enough in the early Universe to keep the RHNs in thermal equilibrium. Subsequently, as the temperature of the Universe dropped below the mass of the individual RHNs, the decay of respective heavy field N_i would become active via $N_i \to \ell_{L_\alpha} + H$ and $N_i \to \bar{\ell}_{L_\alpha} + \bar{H}$, which would produce a finite amount of CP asymmetry in the individual lepton flavor direction. One can parametrize such CP asymmetry as:

$$\varepsilon_i^\alpha = \frac{\Gamma(N_i \to \ell_{L_\alpha} + H) - \Gamma(N_i \to \bar{\ell}_{L_\alpha} + \bar{H})}{\sum_\alpha \left\{\Gamma(N_i \to \ell_{L_\alpha} + H) + \Gamma(N_i \to \bar{\ell}_{L_\alpha} + \bar{H})\right\}}, \tag{1.77}$$

where $\Gamma(N_i \to \ell_{L_\alpha} + H)$ and $\Gamma(N_i \to \bar{\ell}_{L_\alpha} + \bar{H})$ are the decay width of the decay process $N_i \to \ell_{L_\alpha} + H$ and $N_i \to \bar{\ell_{L_\alpha}} + \bar{H}$ respectively. The denominator represents the total decay

[2]The original leptogenesis setup provided by Fukugita and Yanagida also incorporated the type-I seesaw framework.

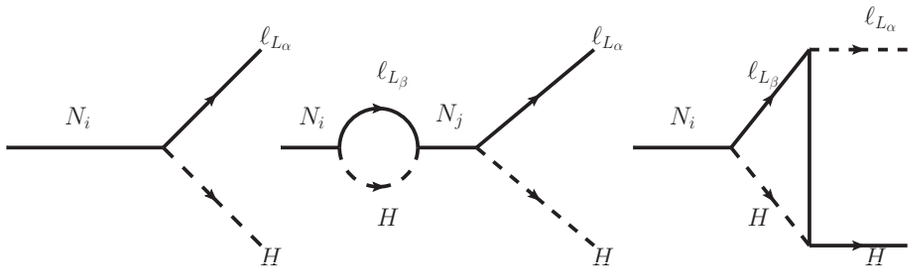

Figure 1.3: Tree and one-loop Feynman diagrams for the decay of the RHNs.

width of N_i and can be easily estimated at the tree level to be

$$\sum_\alpha \left\{\Gamma(N_i \to \ell_{L_\alpha} + H) + \Gamma(N_i \to \bar{\ell}_{L_\alpha} + \bar{H})\right\} = \frac{(Y_\nu^\dagger Y_\nu)_{ii}}{8\pi} M_i. \tag{1.78}$$

Note that the difference between $\Gamma(N_i \to \ell_{L_\alpha} + H)$ and $\Gamma(N_i \to \bar{\ell}_{L_\alpha} + \bar{H})$ vanishes at the tree level. However, at the one loop level, interference between the tree and one loop decay amplitudes can give rise to a finite amount of CP asymmetry. The relevant Feynman diagrams are shown in Fig.1.3. As can be seen from the diagrams, both the one loop self energy[98, 99] and vertex correction diagram[95, 96] (middle and right diagrams of Fig.1.3 respectively) contribute to the CP asymmetry. Additionally, one needs to have at least two RHNs to have a non-vanishing CP asymmetry. After performing the loop calculations, the individual CP asymmetry ε_i^α can be estimated as:

$$\varepsilon_i^\alpha = \frac{1}{8\pi (Y_\nu^\dagger Y_\nu)_{ii}} \sum_{j\neq i} \Bigg[\mathrm{Im}\left\{(Y_\nu^\dagger)_{i\alpha}(Y_\nu)_{\alpha j}(Y_\nu^\dagger Y_\nu)_{ij}\right\} \mathbb{F}\left(\frac{M_j^2}{M_i^2}\right) + \mathrm{Im}\left\{(Y_\nu^\dagger)_{i\alpha}(Y_\nu)_{\alpha j}(Y_\nu^\dagger Y_\nu)_{ji}\right\} \mathbb{G}\left(\frac{M_j^2}{M_i^2}\right) \Bigg], \tag{1.79}$$

where $\mathbb{F}(x) = \sqrt{x}\left[1 + \frac{1}{1-x} + (1+x)\ln\left(\frac{x}{1+x}\right)\right]$ and $\mathbb{G}(x) = 1/(1-x)$ are the loop functions. Finally, to generate the total CP asymmetry from the decay of N_i, sum over flavor index α needs to be performed so that $\varepsilon_i = \sum_\alpha \varepsilon_i^\alpha = \varepsilon_i^e + \varepsilon_i^\mu + \varepsilon_i^\tau$. Consequently, the total CP asymmetry ε_i (from the decay of i-th RHN) will be given by:

$$\varepsilon_i = \frac{1}{8\pi (Y_\nu^\dagger Y_\nu)_{ii}} \sum_{j\neq i} \mathrm{Im}\left[(Y_\nu^\dagger Y_\nu)_{ij}^2\right] \mathbb{F}\left(\frac{M_j^2}{M_i^2}\right), \tag{1.80}$$

Furthermore, if one assumes a hierarchical RHN scenario, where the masses of the RHNs follow the relation $M_1 << M_2 << M_3$, the lightest RHN might stay in the thermal equilibrium for a much longer period of time compared to the other two RHNs. As a result, the CP-asymmetries generated by N_2 and N_3 are expected to be washed out by the lepton number violating interactions of N_1. This leaves only the CP asymmetry generated by N_1 as the dominant contribution to the process of leptogenesis. Such an asymmetry, however, can further be washed out partially by the lepton number violating $2-2$ scattering interactions. Incorporating all these effects into account, one can approximately estimate the final lepton

asymmetry as:

$$Y_{B-L} = n_{B-L}/s = -\frac{1}{7.04}\frac{3}{4}\varepsilon_1\kappa_f \tag{1.81}$$

where κ_f represents the efficiency factor that accounts for the fraction of lepton asymmetry surviving the washout processes. If N_1 decays strongly out-of-equilibrium, all back reactions can be negligible and one can assume $\kappa_f \sim 1$. On the other hand, if the departure from equilibrium for N_1 is mild, $\kappa_f \sim 10^{-2} - 10^{-3}$ can produce the required amount of lepton asymmetry. An accurate estimate for the efficiency factor κ_f or, in other words, the final asymmetry will however follow if one solves coupled BEs that correlate the abundance of N_1 with the produced $B - L$ asymmetry.

To construct the BE for $B - L$ number asymmetry from Eq. (1.40), one can conveniently construct a new basis, ℓ_i, out of the lepton doublets ℓ_{L_α} as[95, 96, 100]:

$$\ell_i = \frac{(Y_\nu^*)_{\alpha i}}{\sqrt{(Y_\nu^\dagger Y_\nu)_{ii}}}\ell_{L_\alpha}, \tag{1.82}$$

in the unflavor limit, where the asymmetries produced in $\ell_{L_{e,\mu,\tau}}$ can not be distinguished. In terms of new states, the neutrino Yukawa interaction of N_i becomes $\sqrt{(Y_\nu^\dagger Y_\nu)_{ii}}\bar{\ell}_i\widetilde{H}N_i$. If one assumes the hierarchy among RHN masses as $M_1 << M_2 << M_3$, only the following relevant interactions associated with ℓ_1 lepton state will influence the lepton asymmetry:

- Decay process of RHNs: interaction rate density is denoted by $\gamma_D \equiv \gamma(N_1 \to \ell_1 H) + \gamma(N_1 \to \bar{\ell}_1\bar{H})$ while the same for inverse decay processes is denoted by $\gamma(\ell_1 H \to N_1)$ and $\gamma(\bar{\ell}_1\bar{H} \to N_1)$.
- Higgs mediated $\Delta L = 1$, t and s-channel scattering processes: interaction rate densities are $\gamma_{H_t} \equiv \gamma(\ell_1 Q_{L_3} \leftrightarrow N_1 t_R)$ and $\gamma_{H_s} \equiv \gamma(\ell_1 N_1 \leftrightarrow Q_{L_3} t_R)$ respectively.
- The $\Delta L = 2$, N_1 mediated s-channel scattering processes: interaction rate density $\gamma_{N_s} \equiv \gamma(\ell_1 H \leftrightarrow \bar{\ell}_1\bar{H})$.
- The $\Delta L = 2$ N_1 mediated t and u-channel scattering processes: interaction rate density $\gamma_{N_t} \equiv \gamma(\ell_1\ell_1 \leftrightarrow \bar{H}\bar{H})$.

Consequently, constructing the BE for $B - L$ number asymmetry along ℓ_1 direction will be sufficient. Starting from Eq. (1.40) following the steps provided in Eq.(1.60)-(1.62), the following classical coupled equations can be constructed[3], which represent the evolution of

[3]For most general computation, one needs to construct the density matrix for lepton asymmetry and solve for every entry of it.

number density of N_1 and $B-L$ asymmetry:

$$s\mathcal{H}x\frac{dY_{N_1}}{dx} = -\left(\frac{Y_{N_1}}{Y_{N_1}^{\rm eq}} - 1\right)\left(\gamma_D + 2\gamma_{H_s} + 4\gamma_{H_t}\right), \tag{1.83}$$

$$\begin{aligned} s\mathcal{H}x\frac{dY_{B-L}}{dx} &= -sHx\left(\frac{dY_{\ell_1}}{dx} - \frac{dY_{\bar{\ell}_1}}{dx}\right) \\ &= \left(\frac{Y_{N_1}}{Y_{N_1}^{\rm eq}} - 1\right)\varepsilon_1\gamma_D + \frac{Y_{B-L}}{Y_{\ell_1}^{\rm eq}}\left(2\gamma_{N_s} + 2\gamma_{N_t} + 2\gamma_{H_t} + \frac{Y_{N_1}}{Y_{N_1}^{\rm eq}}\gamma_{H_s}\right), \end{aligned} \tag{1.84}$$

where the total CP asymmetry ε_1 originates from the difference between decay rate[4] $N_1 \to \ell_1 + H$ and $N_1 \to \bar{\ell}_1 + \bar{H}$. Following the CPT theorem, this difference can be parametrized as:

$$\begin{aligned} \gamma(N_1 \to \ell_1 + H) = \gamma(\bar{\ell}_1 + \bar{H} \to N_1) = \frac{1}{2}\gamma_D(1+\varepsilon_1), \\ \gamma(N_1 \to \bar{\ell}_1 + \bar{H}) = \gamma(\ell_1 + H \to N_1) = \frac{1}{2}\gamma_D(1-\varepsilon_1). \end{aligned} \tag{1.85}$$

Here $x = M_1/T$ is the dimensionless parameter, while $Y_{N_1}^{\rm eq}$ and $Y_{\ell_1}^{\rm eq}$ represent the equilibrium number density-to-entropy density ratio of lightest RHN N_1 and new lepton doublet state ℓ_1 respectively and can be evaluated using Eq.(1.36) and a relation similar to Eq.(1.65). Finally, solving the BEs in Eq. (1.83) and (1.84) simultaneously will provide a better estimate of final lepton asymmetry compared to the approximated case presented in Eq. (1.81).

At the leptogenesis scale, sphaleron processes were in thermal equilibrium. As a result of which, these processes efficiently can convert the produced lepton asymmetry into baryon asymmetry till the temperature of the Universe drops below 150 GeV, where the sphaleron interaction becomes exponentially suppressed, and no conversion from lepton asymmetry to baryon asymmetry is possible. During this conversion process, the following relation between baryon number asymmetry and $B-L$ number asymmetry can be derived[101]:

$$Y_B = CY_{B-L}, \tag{1.86}$$

where C denotes the conversion factor. If sphalerons decoupled from the thermal bath just before the SSB scale, it follows $C = 28/79$, while if sphalerons remain in equilibrium till slightly below the SSB scale, the relation modifies to $C = 12/37$. After the sphaleron processes decouple, there would be no interaction that could change the baryon asymmetry.

1.6.2 Charged lepton equilibration and flavored leptogenesis

While evaluating the final $B-L$ asymmetry above, it was assumed that all the lepton asymmetry was generated along the ℓ_1 lepton state direction and eventually, a flavor sum was performed. However, this prescription of evaluating the final lepton asymmetry becomes invalid as soon as the charged lepton Yukawa interaction rate (associated with $Y_{\ell_\alpha}\bar{\ell}_{L_\alpha}HE_{R_\alpha}$ where E_{R_α} represents the right-handed charged singlet leptons) becomes non-negligible

[4]The CP asymmetry produced from the scattering processes can be safely neglected as the amount will be much less compared to the CP asymmetry produced from the decay of N_1.

compared to that of $N_1 - \ell_1 H$ interactions.[102] In that case, as the temperature falls below $T = 5 \times 10^{11}$ $(= 10^9)$ GeV (we will derive these temperatures in the later part), τ (μ) Yukawa interactions become dominant as they come into the thermal equilibrium. During the period $5 \times 10^{11} < T < 10^9$ GeV, if RHN decays while staying out-of-equilibrium to produce lepton asymmetry, the produced lepton (anti lepton) doublet states ℓ_1 $(\bar{\ell}_1)$ can not keep their quantum coherence due to the non-negligible interactions of right handed tau-leptons before they get reabsorbed again for inverse decay. As a result, Universe gets populated with an incoherent mixture of mutually orthogonal states ℓ_τ and ℓ_a, where ℓ_τ is the tau eigenstate, and ℓ_a is a coherent superposition of muon and electron eigenstate. Consequently, not only does the produced lepton asymmetry get distributed unevenly to these two flavor states, but the produced asymmetry along individual flavor directions also dilutes differently[103–107]. Below $T < 10^9$ GeV, the quantum coherence of ℓ_1 states breaks down completely. In that case, one needs to look for the evolution of the individual lepton flavor asymmetries by constructing BEs for lepton asymmetries along individual flavors.

1.6.2.1 Evaluation of equilibration temperature of charged lepton Yukawa

In order to learn whether charged lepton Yukawa interactions of a specific flavor α are fast enough or, more specifically, in thermal equilibrium, one needs to compare the associated interaction rate with the expansion rate of the Universe. In the standard scenario, assuming all these phenomena are occurring in the RD Universe, one can calculate the thermally averaged interaction rate associated with the charged lepton Yukawa interactions (more specifically decay rates of Higgs decaying to left-handed lepton doublets and right-handed charged lepton singlets of α flavor) as[108–110]:

$$\langle \Gamma_\alpha \rangle = \int \frac{d^3p}{(2\pi)^3 2E_P} \int \frac{d^3k}{(2\pi)^3 2E_k} \int \frac{d^3k'}{(2\pi)^3 2E_{k'}} (2\pi)^4 \delta^{(4)}(p - k - k') |\mathcal{M}|^2 \frac{f_H}{n_H} \tag{1.87}$$

where p is the 4-momentum of parent particle (Higgs) while k and k' are the 4-momentum of lepton doublet and singlet charged lepton respectively. The thermal distribution function of Higgs f_H and number density n_H can be denoted as:

$$f_H = \frac{1}{e^{E_p/T} - 1}\,, \tag{1.88}$$

$$n_H = \frac{\zeta(3) T^3}{\pi^2}\,. \tag{1.89}$$

Assuming final state particles have negligible mass, squared Feynmann amplitude $|\mathcal{M}|^2$ for these decays would be:

$$|\mathcal{M}|^2 = 2 Y_{\ell_\alpha}^2 k.k' = Y_{\ell_\alpha}^2 M_H^2\,, \quad \alpha = e, \mu, \tau \tag{1.90}$$

Finally, evaluation of integral in Eq. (1.87) for $T >> M_H$ leads to[108]:

$$\langle \Gamma_\alpha \rangle = \frac{Y_{\ell_\alpha}^2 \pi}{192 \zeta(3) T} M_H(T)^2. \tag{1.91}$$

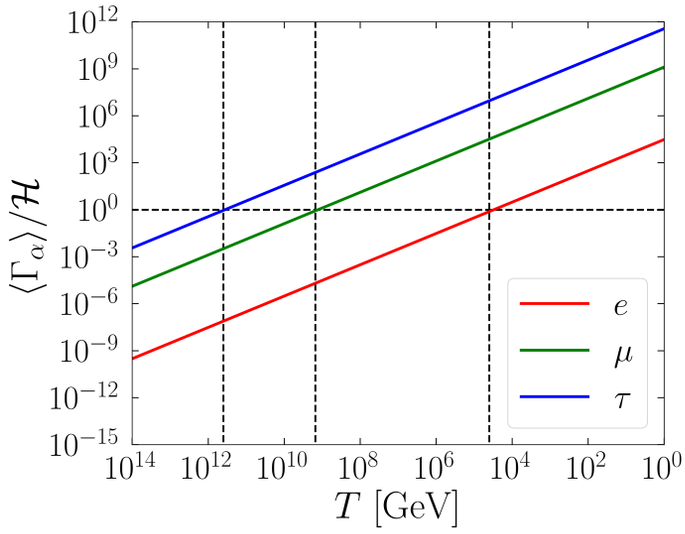

Figure 1.4: Variation of $\langle\Gamma_\alpha\rangle/\mathcal{H}$ *w.r.t.* T in RD phase. The horizontal dashed line denotes $\langle\Gamma_\alpha\rangle/\mathcal{H} = 1$, while the vertical dashed lines indicate the ETs of three charged Yukawa interactions.

where $M_H(T)$ is the thermal mass of Higgs and can be estimated as:

$$M_H(T) \simeq \frac{T}{4}\sqrt{3g_2^2 + g_3^2 + 4y_t^2 + 8\lambda} \tag{1.92}$$

where y_t and λ are the top Yukawa couplings and the Higgs quartic couplings, respectively. With proper numerical values of the relevant couplings, the thermally averaged decay rate of the decay process becomes[111]:

$$\langle\Gamma_\alpha\rangle \simeq 5 \times 10^{-3} Y_{\ell_\alpha}^2 T. \tag{1.93}$$

Comparison between these obtained decay rates with Hubble constant ($\mathcal{H} = 1.66 g_*^{1/2} T^2/M_{\rm Pl}$) will lead to the (ET) of the charged lepton Yukawa interactions. Fig.1.4 shows the variation of $\langle\Gamma_\alpha\rangle/\mathcal{H}$ *w.r.t.* temperature T for different lepton flavors $\alpha = e, \mu, \tau$. As can be seen from the figure, τ Yukawa interaction becomes sizable around $T^*_{0(\tau)} \sim 5 \times 10^{11}$ GeV when $\langle\Gamma_\tau\rangle/\mathcal{H} = 1$, while μ_R and e_R come to thermal equilibrium at $T^*_{0(\mu)} \sim 10^9$ GeV and $T^*_{0(e)} \sim 5 \times 10^4$ GeV[5] respectively. As a result, if the lightest RHN N_1 decays while staying in out of equilibrium in between $5 \times 10^{11} \gtrsim T \gtrsim 10^9$ GeV, quantum coherence of ℓ_1 breaks down and lepton asymmetry along τ lepton direction becomes distinguishable. On the other hand, if leptogenesis occurs at $T < 10^9$ GeV, lepton asymmetry along τ, μ and e directions become distinctive.

1.6.2.2 Formation of Boltzmann equation

To construct the appropriate set of BEs, which can accommodate the evolution of lepton asymmetry along individual flavor directions, one needs to rely on the density operator approach. In that case, to start with, a density matrix ϱ is defined as the difference between the density matrices for the leptons and the antileptons, whose diagonal entries indicate the

[5]Thermal field theory can be used to provide a more accurate estimate of ETs. For example, see [112] for the latest calculation on ET of e_R.

asymmetry along each lepton flavor direction, *i.e.*, $\varrho_{\alpha\alpha} \propto Y_{L_\alpha}$, whereas off-diagonal entries $\varrho_{\alpha\beta}$ with $\alpha \neq \beta$ represent quantum correlations between different lepton flavors. In a most general scenario, one needs to look for the evolution of every element of ϱ to evaluate the final lepton asymmetry further. However, due to some unique properties of the density matrix, the calculation can be simplified. One such feature of ϱ is that whenever charged lepton Yukawa interactions of a specific flavor are strongly in thermal equilibrium, the off-diagonal terms related to that flavor disappear[6]. Consequently, only the diagonal entry of ϱ representing lepton flavor with non-negligible Yukawa interactions survives and evolves with time. Secondly, if the population of lepton flavors that are not in thermal equilibrium is assumed to be negligibly small, using the inequality $|\varrho_{\alpha\beta}|^2 \leq \varrho_{\alpha\alpha}\varrho_{\beta\beta}$, one can also neglect the effect of $\varrho_{\alpha\beta}$ for those lepton states. Due to these characteristics, the general equation for ϱ can be reduced to a subset of equations for the diagonal entries of ϱ matrix. Taking all these informations into account, one can write down the BEs for lepton flavor asymmetries or, more specifically, BEs along individual $\Delta_\alpha \equiv B/3 - L_\alpha$ number direction (as sphaleron conserves Δ_α) as[103, 104]:

$$s\mathcal{H}x\frac{\mathrm{d}Y_{\Delta_\alpha}}{\mathrm{d}x} = -\Bigg\{ \left(\frac{Y_{N_1}}{Y_{N_1}^{eq}} - 1\right) \varepsilon_1^\alpha \, \gamma_D + K_\alpha^0 \sum_\beta \Bigg[\frac{1}{2}\left(C_{\alpha\beta}^\ell + C_\beta^H\right) \gamma_D + \left(\frac{Y_{N_1}}{Y_{N_1}^{eq}} - 1\right) \times \left(C_{\alpha\beta}^\ell \, \gamma_{H_s} + \frac{C_\beta^H}{2} \, \gamma_{H_t} \right) + \left(2\, C_{\alpha\beta}^\ell + C_\beta^H \right) \left(\gamma_{H_t} + \frac{1}{2}\gamma_{H_s} \right) \Bigg] \frac{Y_{\Delta_\beta}}{Y_{\ell_1}^{eq}} \Bigg\}, \quad (1.94)$$

where $\varepsilon_{1\alpha}$ is the CP asymmetry produced along individual lepton flavor from N_1 decay and expressed by Eq. (1.79), while K_α^0 represents the ratio between the tree level total decay width of N_1 to the individual lepton flavor α and the total tree level decay width of N_1 (expressed in Eq (1.78)). Matrices C^ℓ and C^H relate the asymetry in the lepton and Higgs doublets with the asymmetry in Δ_α number according to[104]:

$$y_{\ell_\alpha} = -\sum_\beta C_{\alpha\beta}^\ell \frac{Y_{\Delta_\beta}}{Y_{\ell_1}^{\mathrm{eq}}}, \qquad y_H = -\sum_\beta C_\beta^H \frac{Y_{\Delta_\beta}}{Y_{\ell_1}^{\mathrm{eq}}}, \quad (1.95)$$

where y_x is defined as: $y_x \equiv (n_x - n_{\bar{x}})/n_x^{\mathrm{eq}}$, with $x = \ell_{L_\alpha}, \, H$. The structure of the C^ℓ and C^H matrices can be determined by knowing the constraint equations coming from the chemical equilibration conditions provided by the SM interactions, which are in thermal equilibrium at the relevant temperature regime when the leptogenesis mechanism is active. Few further simplifications were made while constructing the Eq. (1.94):

- Subdominant $\Delta L = 2$ offshell scattering processes and scattering involving gauge bosons have been neglected.
- CP violation in $\Delta L = 1$ scattering processes is ignored, and finite temperature masses and couplings were not included.

[6]However, when a charged lepton Yukawa interaction approaches to the thermal equilibrium, the off-diagonal entries of the ϱ matrix will have finite values. So, during this type of transition period, one needs to solve the whole density matrix to estimate the lepton asymmetry more accurately.

Finally, solving Eq. (1.83) and Eq. (1.94) simultaneously will provide the final lepton asymmetry along individual flavor directions, which is then converted to the baryon asymmetry by sphaleron transition as (assuming sphaleron decouples above SSB):

$$Y_B = \frac{28}{79} \sum_{\alpha} Y_{B/3-L_\alpha}. \tag{1.96}$$

1.6.2.3 Different temperature regimes and flavor structure of Boltzmann equation

Let us now discuss the impact of different SM interactions which are in thermal equilibrium on determining the structure of C^ℓ and C^H matrices and, subsequently the flavor structure of the BEs at various relevant temperature ranges.

At very high temperatures ($T > 10^{15}$ GeV), all SM interactions were out of equilibrium. As temperature decreased, interactions with larger coupling achieved kinetic equilibrium first, followed by chemical equilibrium. As a result of such chemical equilibration, the chemical potential of various particles involved in the reactions became dependent of each other. Since the chemical potential of a particle X is related to the number density asymmetry as:

$$n_X - n_{\bar{X}} = \frac{g_X T^3}{6} \begin{cases} \mu_X/T & \text{fermions}, \\ 2\mu_X/T & \text{bosons}, \end{cases} \tag{1.97}$$

where μ_X represents the chemical potential of X species while g_X is the number of degrees of freedom of X, these chemical equilibration constraints provide a relationship among different particle number asymmetries for particles participating in fast interactions. The constraints on chemical potentials, which are relevant for lepton asymmetry generation are the followings:

1. Since above SSB, the chemical potential of gauge bosons follow $\mu_g = \mu_{W^i} = \mu_B = 0$, the chemical potential of different quark colors as well as two members of $SU(2)_L$ doublets attain equilibrium. This leads to: $\mu_Q \equiv \mu_{u_L} = \mu_{d_L}$, $\mu_\ell \equiv \mu_{e_L} = \mu_{\nu_L}$ and $\mu_H \equiv \mu_{H^+} = \mu_{H^0}$.
2. Irrespective of any temperature, Hypercharge neutrality condition provides:

$$\sum_i (\mu_{Q_i} + 2\mu_{U_i} - \mu_{D_i} - \mu_{\ell_i} - \mu_{E_i}) + 2\mu_H = 0, \tag{1.98}$$

   where μ_{U_i}, μ_{D_i}, μ_{E_i} represent the chemical potential of $SU(2)_L$ singlet fermions of i-th generation.
3. When QCD instanton and electroweak sphaleron interactions reach chemical equilibrium, they enforce the following constraints:

$$\sum_i 2\mu_{Q_i} - \mu_{U_i} - \mu_{D_i} = 0\,, \qquad \sum_i 3\mu_{Q_i} + \mu_{\ell_i} = 0. \tag{1.99}$$

4. Yukawa interactions, when reach thermal equilibrium, provide the following constraints:

$$\mu_{U_i} = \mu_{Q_i} + \mu_H, \quad \text{for Up-type quarks,} \tag{1.100}$$
$$\mu_{D_i} = \mu_{Q_i} - \mu_H, \quad \text{for Down-type quarks,} \tag{1.101}$$
$$\mu_{E_i} = \mu_{\ell_i} - \mu_H, \quad \text{for charged leptons.} \tag{1.102}$$

One can identify four distinctive temperature regimes when different fast reactions along with the charged lepton Yukawa interactions influence the lepton asymmetry production. Those are listed as follows:

- $T > 5 \times 10^{11}$ GeV: In this temperature range top and bottom Yukawa interactions are in equilibrium. Interactions related to the EW sphalerons are also expected to be in equilibrium at $T \sim 10^{12}$ GeV. However, as no charged lepton Yukawa interaction has become fast enough, one can safely use the BE in Eq. (1.84) along with Eq. (1.83) to evaluate the lepton asymmetry of the Universe.
- $5\times10^{11} > T > 10^9$ GeV: Within this temperature window, the lepton doublet states lose their quantum coherence since tau Yukawa interactions come to thermal equilibrium. Consequently, one can define the new lepton flavor basis states as $(\ell_a, \ell_b, \ell_\tau)$ where ℓ_a and ℓ_b are the states made up of different linear combination of ℓ_e and ℓ_μ states. For simplicity one can define ℓ_b state such a way that ℓ_1 is orthogonal to ℓ_b *i.e.* $|\langle\ell_1|\ell_b\rangle|^2 = 0$. As a result of which, one finds $Y_{L_b} = \varrho_{bb} = 0$. This ensures that the off diagonal entries ϱ_{ab} and ϱ_{ba} also vanish. Hence, Eq. (1.94) reduces to only two relevant equations for asymmetry along lepton flavor a and τ directions.
  On the other hand, the equilibration of tau, bottom and top Yukawa interaction leads to the constraints $\mu_t = \mu_{Q_3} + \mu_H$, $\mu_b = \mu_{Q_3} - \mu_H$ and $\mu_\tau = \mu_{\ell_\tau} - \mu_H$. Incorporating these conditions along with the one from Eq. (1.99) for EW sphalerons and Eq. (1.98), following value of C^ℓ and C^H matrices can be constructed[103, 104]:

$$C^\ell = \frac{1}{460}\begin{pmatrix} 196 & -24 \\ -9 & 156 \end{pmatrix}, \quad C^H = \frac{1}{230}\begin{pmatrix} 41 & 56 \end{pmatrix}. \tag{1.103}$$

- $5 \times 10^9 > T > 10^5$ GeV: In this epoch, second generation Yukawa interactions, most importantly, μ charge lepton Yukawa interactions become dominant by entering into the thermal equilibrium. As a result, the quantum coherence of lepton doublet states is completely broken. Consequently, the lepton asymmetries along all the flavor directions become distinguishable. In that case, Eq. (1.94) will be a set of three equations representing evolution of Y_{Δ_e}, Y_{Δ_μ}, and Y_{Δ_τ}.
  To construct the C^ℓ and C^H matrices, one needs to now impose the constraint conditions for third and second generation Yukawa interactions presented in Eq. (1.100),(1.101) and (1.102) in addition to the condition from Eq. (1.99) for EW sphalerons and Eq. (1.98).

Combining all these conditions yields:

$$C^{\ell} = \frac{1}{2148}\begin{pmatrix} 906 & -120 & -120 \\ -75 & 688 & -28 \\ -75 & -28 & 688 \end{pmatrix}, \quad C^{H} = \frac{1}{358}\begin{pmatrix} 37 & 52 & 52 \end{pmatrix}. \tag{1.104}$$

- $T < 10^5$ GeV: In this case, till electroweak symmetry breaking, all the SM interactions are in thermal equilibrium. As a result, all SM particles will gain chemical potential and all the chemical potential conditions presented in Eq. (1.98)-(1.102) for every generation of fermions will be effective. The structure of C^{ℓ} and C^{H} in this regime therefore read:

$$C^{\ell} = \frac{1}{711}\begin{pmatrix} 221 & -16 & -16 \\ -16 & 221 & -16 \\ -16 & -16 & 221 \end{pmatrix}, \quad C^{H} = \frac{8}{79}\begin{pmatrix} 1 & 1 & 1 \end{pmatrix}. \tag{1.105}$$

1.7 Objective and outline of the thesis

The main objective of this thesis is to check the influence of different BSM scenarios, motivated to resolve some of the problems in particle physics and cosmology, which can impact the prediction of leptogenesis, in particular on flavor leptogenesis. As discussed above, flavor leptogenesis is a framework where effects of the individual charge lepton flavors on lepton asymmetry production is analyzed. When a charged lepton Yukawa interaction becomes comparable to the expansion rate of the Universe, the relevant Yukawa interaction may occur rapidly in the Universe. If the out-of-equilibrium decay of any heavy state producing lepton asymmetry happens to be in the era where this charged lepton Yukawa interactions (of one or more flavor) are important enough, the lepton asymmetry along that particular lepton flavor direction (with dominant interactions) gets enhanced or diluted differently compared to the other flavor directions having negligible interaction. This affects the total lepton asymmetry production.

To study the influence of different BSM scenarios on this flavor leptogenesis, we focus our attention on those which address possible resolution to the origin of neutrino mass, dark matter. Although there exists a vast literature that handles these problems independently, in this thesis, we aim to investigate whether some of these can also affect the lepton asymmetry generation process. For example, in chapter 2, we will check if the RHNs responsible for neutrino mass generation become degenerate due to some large scale flavor symmetry, how will it impact the neutrino mass and mixing as well as flavor leptogenesis process. In chapter 3, we will address the DM problem and show that the early Universe evolution of DM can not not only be connected with the lepton asymmetry generation, the same DM may also influence the production of lepton asymmetry directly. In chapter 4, we venture into a new paradigm where in the early Universe, just after inflation, a prolonged reheating

process occurred, and subsequently it impacts the charged lepton Yukawa equilibration and eventually the flavor leptogenesis process. Finally, in chapter 5, we conclude.

Chapter 2

Flavor Origin of Flavor Leptogenesis

2.1 Introduction

Over the last couple of decades, we have witnessed remarkable success in neutrino experiments [35, 113–120] indicating that neutrinos are indeed massive. Furthermore, mixing parameters have been measured with great precision. In fact, two of the three mixing angles namely solar (θ_{12}) and atmospheric (θ_{23}) ones are found to be large while the other one, reactor (θ_{13}) mixing angle, is relatively small. Such a finding clearly shows the distinctive feature associated to the lepton sector in contrast to the quark one where all the three mixing angles are measured to be small. To have a deeper understanding of it, one needs to investigate the origin of the neutrino mass by looking at the neutrino mass matrix as well as the charged lepton sector from a symmetry perspective.

As discussed in Section 1.3, to address the tiny neutrino mass issue, various seesaw mechanisms [40, 43–45, 48, 53, 121, 122] have been proposed by extending the Standard Model (SM) with heavy fermions/scalars. Among these, the type-I seesaw mechanism provides perhaps the simplest explanation of tiny neutrino mass where the SM is extended by three singlet RHNs [40, 43, 44]. Involvement of flavor symmetries within this simple setup is off course an interesting possibility in order to explain the typical mixing pattern in the lepton sector. Non-abelian discrete groups (like $S_3, A_4, S_4, A_5, \Delta(27)$ etc.) in this regard have been extensively used (see reviews [123–130] and references therein).

Among the various discrete groups, A_4 turns out to be the most economical one[1]. It is a group of even permutations of four objects having three inequivalent one-dimensional representations (1, $1'$ and $1''$) as well as one three-dimensional representation (3). Interestingly, the three generations (or flavors) of right-handed charged lepton singlets can naturally fit into these three inequivalent one-dimensional representations of A_4 while the three SM lepton doublets can be accommodated into the triplet representation of A_4 [133–135]. Works along this direction [133, 134, 136, 137] showed that type-I seesaw model with A_4 flavor symmetry in general leads to a typical tri-bimaximal (TBM) lepton mixing ($\sin^2\theta_{12} = 1/3,\ \sin^2\theta_{23} = 1/2$ and $\theta_{13} = 0$) pattern [138, 139] in presence of SM singlet (though charged under A_4) flavon fields. Though such TBM pattern received a great deal of at-

[1] A_4 group was initially proposed as an underlying family symmetry for quark sector by [131, 132].

tention due to its close proximity with experimental observation prior to 2012, it fails to accommodate the recent observation of small, but non-zero θ_{13} [119, 140, 141]. Subsequently, modifications over models based on A_4 (and other discrete groups) are suggested to accommodate non-zero θ_{13} either by considering additional flavon fields or including corrections to vaccuum alignments of the flavons [142, 143] or considering contributions to additional mixing from the charged lepton sector [144].

In this work (based on [145]), we particularly focus on a framework where a non-trivial contribution to lepton mixing is originated from charged lepton sector. We do not consider any additional flavon field apart from those ones incorporated in the original Altarelli-Feruglio (AF) model [133]. While the RHN mass matrix turns out to be diagonal as a result of the flavor symmetry imposed, the structure of the charged lepton mass matrix becomes such that it can be diagonalized by a complex 'magic' matrix [134]. Interestingly, an anti-symmetric contribution to the Dirac neutrino mass matrix, originated from the product of two A_4 triplets, plays a crucial role in generating non-zero θ_{13} [146–149] in our model which was overlooked in an earlier attempt [150]. In doing the analysis, we find the atmospheric mixing angle $\theta_{23} \leq 45^\circ$ *i.e.* to lie in lower octant (LO). We also note that only normal hierarchy (NH) of light neutrino masses are allowed in this model. This turns out to be another salient feature of our construction. These predictions can be tested in ongoing and future neutrino experiments as ambiguities are still present in determining octant for θ_{23} as well as hierarchies of light neutrino masses.

Finally, we discuss the aspects of leptogenesis [95, 96, 99, 151, 152] from the CP-violating decays of RHNs in this A_4 based type-I seesaw scenario in line with observations [153–160]. In doing so, since the involvement of the neutrino Yukawa matrix in the charged-lepton mass diagonal basis is necessary, the specific flavor symmetric construction of it is expected to play an important role. In fact, due to this symmetry, exactly degenerate heavy RHNs result at tree level, thereby indicating the breaking of the perturbative field theory involved in CP asymmetry generation [97]. Following [150], we are able to show that running of the parameters involved in the neutrino sector from the flavor symmetry breaking scale to the RHN mass scale actually eliminates such exact degeneracies and as a result, leptogenesis can indeed be possible. The present study of matter-antimatter asymmetry generation via leptogenesis taking into account the effect of running however differs from that of [150] by two aspects. Firstly, we use less number of flavon fields and secondly, we present a detailed analysis of flavored leptogenesis by solving the relevant Boltzmann equations.

The rest of this chapter is organized as follows. In Section 2.2 we present detail structure of the model including the analysis of the mixing matrices involved. Section 2.3 deals with phenomenology of neutrino mixing. Constrains and predictions on neutrino parameters (including neutrinoless double beta decay) involved are presented here. In Section 2.4 we perform a detailed study on leptogenesis solving flavored Boltzmann equations. Finally in Section 2.5 we summarize the results and make final conclusion.

2.2 Structure of The Model

To realize the canonical type-I seesaw mechanism, we first consider an extension of the SM by including three singlet RHN fields (N_R). Additionally, three flavon fields namely Φ, Ψ, φ and a discrete symmetry $A_4 \times Z_2 \times Z_3$ are also incorporated to probe the typical flavor structure involved in the lepton sector. Note that same fields content was also present in the original AF [123] construction. Here N_R and the flavon fields Φ, Ψ transform as triplet, whereas φ transforms as a singlet under A_4. A judicious choice of additional $Z_2 \times Z_3$ symmetry assists the leptonic mass matrices to take specific forms and hence forbid several unwanted contributions. In Table 2.1, we present transformation properties of all the relevant SM fields, N_R and flavons involved in the analysis.

Fields	ℓ_L	e_R	μ_R	τ_R	N_R	H	φ	Φ	Ψ
SM	$(2, 1/2)$	$(1, 1)$	$(1, 1)$	$(1, 1)$	$(1, 0)$	$(2, -1/2)$	$(1, 0)$	$(1, 0)$	$(1, 0)$
A_4	3	1	$1'$	$1''$	3	1	1	3	3
Z_2	1	1	1	1	-1	1	-1	1	-1
Z_3	ω	1	1	1	1	1	ω	ω	ω

Table 2.1: Representations of the fields under $SU(2)_L \times U(1)_Y \times A_4 \times Z_2 \times Z_3$ symmetry

The relevant effective Lagrangian involving charged leptons and neutrinos can be written as

$$\begin{aligned}\mathcal{L} \supset & \frac{y_1^\ell}{\Lambda}\left(\bar{\ell}_L\,\Phi\right)_{\mathbf{1}} H\, e_R + \frac{y_2^\ell}{\Lambda}\left(\bar{\ell}_L\,\Phi\right)_{\mathbf{1''}} H\,\mu_R + \frac{y_3^\ell}{\Lambda}\left(\bar{\ell}_L\,\Phi\right)_{\mathbf{1'}} H\,\tau_R \\ & + \frac{y_1^\nu}{\Lambda}\left[(\bar{\ell}_L\, N_R)_{\mathbf{s}}\,\Psi\right]_{\mathbf{1}}\widetilde{H} + \frac{y_2^\nu}{\Lambda}\left[(\bar{\ell}_L\, N_R)_{\mathbf{a}}\,\Psi\right]_{\mathbf{1}}\widetilde{H} + \frac{y_3^\nu}{\Lambda}\left(\bar{\ell}_L\, N_R\right)_{\mathbf{1}}\varphi\,\widetilde{H} + \frac{1}{2}M\left(\overline{N_R^c}N_R\right) + \text{h.c.},\end{aligned} \tag{2.1}$$

where $y_{i=1,2,3}^{\ell,\nu}$ are the respective coupling constants, M is the mass parameter of RHNs and Λ is the cut-off scale of the theory. In the first line of Eq. (2.1), terms in the first parentheses represent products of two A_4 triplets forming a one-dimensional representation which further contract with 1, $1'$ and $1''$ of A_4, corresponding to e_R, μ_R and τ_R respectively, to make a true singlet under A_4. On the other hand, in the second line of Eq. (2.1), the subscripts $\mathbf{s}$, $\mathbf{a}$ correspond to symmetric and anti-symmetric parts of triplet products in the S diagonal basis of A_4. The essential multiplication rules of the A_4 group elements are elaborated in appendix A.1.

From Table 2.1 it is evident that the tree level contribution to charged lepton Yukawa interaction, $\bar{\ell}_L\, H E_{R_\alpha}$ (with $\alpha = e, \mu, \tau$), gets forbidden. Instead, such interactions are effectively generated once the flavon Φ gets a vacuum expectation value (vev) via the dimension-5 operators (present in first line of Eq. (2.1)). Similarly in the neutrino sector, the renormalizable Dirac Yukawa coupling is forbidden as the lepton doublet ℓ_L is charged under Z_3 whereas both N_R and H transform trivially under it. However such effective Yukawa coupling is generated from dimension-5 operators involving flavons Ψ and φ, after they obtain

vevs. Presence of Z_2 symmetry is important in identifying Φ from Ψ (both being A_4 triplet) so that they contribute to the charged lepton and Dirac neutrino Yukawa couplings differently.

The flavon fields break the flavor symmetry $A_4 \times Z_3 \times Z_2$ when they acquire vevs along[2]

$$\langle \varphi \rangle = v_\varphi \,, \quad \langle \Phi \rangle = v_\Phi \,(1,1,1) \,, \quad \langle \Psi \rangle = v_\Psi \,(0,1,0) \,, \tag{2.2}$$

as a result of which the part of the Lagrangian contributing to the charged lepton sector can be written as

$$\mathcal{L}_l = \frac{y_1^\ell v_\Phi}{\Lambda}(\bar{\ell}_{L_e}+\bar{\ell}_{L_\mu}+\bar{\ell}_{L_\tau}) H\, e_R + \frac{y_2^\ell v_\Phi}{\Lambda}(\bar{\ell}_{L_e}+\omega\bar{\ell}_{L_\mu}+\omega^2\bar{\ell}_{L_\tau}) H\, \mu_R + \frac{y_3^\ell v_\Phi}{\Lambda}(\bar{\ell}_{L_e}+\omega^2\bar{\ell}_{L_\mu}+\omega\bar{\ell}_{L_\tau}) H\, \tau_R. \tag{2.3}$$

Using the above Lagrangian one obtains the charged lepton mass matrix after the electroweak symmetry breaking as

$$Y_\ell = v' \begin{pmatrix} f_1^\ell & f_2^\ell & f_3^\ell \\ f_1^\ell & \omega\, f_2^\ell & \omega^2\, f_3^\ell \\ f_1^\ell & \omega^2\, f_2^\ell & \omega\, f_3^\ell \end{pmatrix} ; \;\; f_i^\ell = \frac{v_\Phi}{\Lambda}\, y_i^\ell \text{ with } i = 1,2,3, \tag{2.4}$$

where $v' = v/\sqrt{2} = 174$ GeV stands for the vev of the SM Higgs.

In a similar way, the Lagrangian for neutrino sector after breaking of the flavor symmetries can be written as

$$\begin{aligned} \mathcal{L}_\nu =& \frac{y_3^\nu}{\Lambda}\, v_\varphi \left(\bar{\ell_{L_e}}\, N_{1R} + \bar{\ell_{L_\mu}}\, N_{2R} + \bar{\ell_{L_\tau}}\, N_{3R}\right) \widetilde{H} + (y_1^\nu - y_2^\nu)\, \frac{v_\Psi}{\Lambda} \bar{\ell_{L_e}}\, N_{3R}\, \widetilde{H} \\ &+ (y_1^\nu + y_2^\nu)\, \frac{v_\Psi}{\Lambda} \bar{\ell_{L_\tau}}\, N_{1R}\, \widetilde{H} + M \left(\overline{N^c}_{1R} N_{1R} + \overline{N^c}_{2R} N_{2R} + \overline{N^c}_{3R} N_{3R}\right) + \text{h.c.}. \end{aligned} \tag{2.5}$$

This yields the corresponding Dirac and Majorana mass matrices as

$$Y_\nu = \begin{pmatrix} f_3^\nu & 0 & f_1^\nu - f_2^\nu \\ 0 & f_3^\nu & 0 \\ f_1^\nu + f_2^\nu & 0 & f_3^\nu \end{pmatrix}, \tag{2.6}$$

$$M_R = \begin{pmatrix} M & 0 & 0 \\ 0 & M & 0 \\ 0 & 0 & M \end{pmatrix}, \tag{2.7}$$

with $f_i^\nu = \frac{v_\Psi}{\Lambda} y_i^\nu$, $i = 1,2,3$.

[2]Such vev alignments of the flavons is widely used and can be realised in a natural way by minimising the scalar potential following the approach of [123, 146, 150, 161–164].

Let us now discuss the diagonalization of the charged lepton and neutrino mass matrices so as to obtain the lepton mixing matrix. First we note that the charged lepton mass matrix given in Eq. (2.4) can be diagonalized by a bi-unitary transformation

$$Y_\ell = \mathcal{V} d_\ell \mathbb{I}_{3\times 3} \;\text{ with }\; d^\ell = \sqrt{3} v' \,\text{diag}\,(f_1^\ell, f_2^\ell, f_3^\ell), \tag{2.8}$$

where $\mathbb{I}_{3\times 3}$ is a 3×3 identity matrix and

$$\mathcal{V} = \frac{1}{\sqrt{3}} \begin{pmatrix} 1 & 1 & 1 \\ 1 & \omega & \omega^2 \\ 1 & \omega^2 & \omega \end{pmatrix}, \tag{2.9}$$

where ω $(= e^{2i\pi/3})$ is the cube root of unity. From Eq. (2.7), it is evident that the right-handed Majorana neutrino mass matrix M_R is diagonal having degenerate mass eigenvalues (M) to start with.

On the other hand, f_1^ν and f_2^ν appearing in Eq. (2.6) are the symmetric and antisymmetric contributions to the Dirac neutrino Yukawa respectively, originated as products of two A_4 triplets ℓ_L and N_R which further contract with Φ (see the product rules Eq. (A.5) and (A.6)). This antisymmetric part plays an instrumental role[3] in realizing correct neutrino oscillation data.

Here it is worth mentioning that in the vanishing limit of $f_2^\nu \to 0$, (keeping the structure of the charged lepton and Majorana mass matrix intact) one can reproduce the TBM mixing as discussed in [150].

The effective light neutrino mass[4] matrix can be obtained within the type-I seesaw framework as

$$m_\nu = -m_D M_R^{-1} m_D^T, \tag{2.10}$$

where the structure of M_R is given in Eq. (2.7). Now, from Eq. (2.6) and (2.8), in the basis where the charged leptons are diagonal, the Dirac neutrino mass matrix in that basis can be written as,

$$m_D = v' \mathcal{V}^\dagger Y_\nu = v' \mathcal{Y}_\nu. \tag{2.11}$$

Therefore, substituting Eq. (2.11) in the type-I seesaw formula given by Eq. (2.10) one

[3] Earlier the role of such antisymmetric contributions was analyzed in the context of Dirac neutrinos [146–149].

[4] With the symmetries mentioned in Table 2.1 in principle, there will be a contribution to the effective light neutrino mass via a dim-6 operator given by $\frac{y_{eff}}{\Lambda^2}(\ell_L H \ell_L H \Phi)$. However, in the limit $v_\Phi > M$, this additional contribution can be neglected compared to the dominant type-I contribution considered here.

obtains the light neutrino mass matrix as

$$m_\nu = -\,v'^2 \mathcal{V}^\dagger Y_\nu M_R^{-1} {Y_\nu}^T \mathcal{V}^*, \tag{2.12}$$

$$= -\frac{1}{M} \mathcal{V}^\dagger (v'^2 Y_\nu {Y_\nu}^T) \mathcal{V}^*. \tag{2.13}$$

Clearly, to get the mass eigenvalues of light neutrinos we need to diagonalize $Y_\nu {Y_\nu}^T$ where

$$Y_\nu {Y_\nu}^T = \begin{pmatrix} (f_1^\nu - f_2^\nu)^2 + {f_3^\nu}^2 & 0 & 2 f_1^\nu f_3^\nu \\ 0 & {f_3^\nu}^2 & 0 \\ 2 f_1^\nu f_3^\nu & 0 & (f_1^\nu + f_2^\nu)^2 + {f_3^\nu}^2 \end{pmatrix}. \tag{2.14}$$

Though Y^ν is in general a complex matrix, $Y^\nu Y^{\nu T}$ being a complex symmetric matrix can be diagonalized by an orthogonal transformation (in the $(1,3)$ plane) through the relation

$$U_{13}^T (Y_\nu {Y_\nu}^T) U_{13} = d_D^2 = \text{diag}(\lambda_1, \lambda_2, \lambda_3), \tag{2.15}$$

where the rotation matrix U_{13} (parametrised by angle θ and phase ψ) is given by

$$U_{13} = \begin{pmatrix} \cos\theta & 0 & e^{-i\psi}\sin\theta \\ 0 & 1 & 0 \\ -e^{i\psi}\sin\theta & 0 & \cos\theta \end{pmatrix}. \tag{2.16}$$

The complex eigenvalues are given by

$$\lambda_1 = {f_1^\nu}^2 + {f_2^\nu}^2 + {f_3^\nu}^2 - 2\sqrt{{f_1^\nu}^2 ({f_2^\nu}^2 + {f_3^\nu}^2)}, \tag{2.17}$$

$$\lambda_2 = {f_3^\nu}^2, \tag{2.18}$$

$$\lambda_3 = {f_1^\nu}^2 + {f_2^\nu}^2 + {f_3^\nu}^2 + 2\sqrt{{f_1^\nu}^2 ({f_2^\nu}^2 + {f_3^\nu}^2)}. \tag{2.19}$$

Now substituting Eq. (2.15) in Eq. (2.13), we get

$$m_\nu = -\mathcal{V}^\dagger U_{13} \left(\frac{v'^2 d_D^2}{M}\right) U_{13}^T \mathcal{V}^*, \tag{2.20}$$

$$= -\mathcal{V}^\dagger U_{13} \left(d_\nu\right) U_{13}^T \mathcal{V}^*, \tag{2.21}$$

where $d_\nu = v'^2 d_D^2 / M$ is a diagonal matrix having diagonal elements $v'^2 \lambda_i / M$ $(i = 1,2,3)$, representative of three complex light neutrino mass eigenvalues.

In order to extract the real and positive light neutrino mass eigenvalues, we choose the following representations of the parameters $f_{1,2,3}^\nu (= |f_{1,2,3}^\nu| e^{i\phi_{1,2,3}}$ and $\phi_{1,2,3}$ are the three

phases associated) as

$$\frac{f_1^\nu}{f_3^\nu} = \frac{\mid f_1^\nu \mid}{\mid f_3^\nu \mid} e^{i(\phi_1-\phi_3)} = \chi_1 e^{i\gamma_1}, \tag{2.22}$$

$$\frac{f_2^\nu}{f_3^\nu} = \frac{\mid f_2^\nu \mid}{\mid f_3^\nu \mid} e^{i(\phi_2-\phi_3)} = \chi_2 e^{i\gamma_2}, \tag{2.23}$$

where $\chi_1 = |f_1^\nu/f_3^\nu|$, $\chi_2 = |f_2^\nu/f_3^\nu|$ and $(\phi_1 - \phi_3) = \gamma_1$, $(\phi_2 - \phi_3) = \gamma_2$ are the redefined parameters used for the rest of our analysis.

Now we are in a position to define the rotation angle θ and phase ψ of U_{13} matrix (see Eq. (2.16)) as:

$$\tan 2\theta = \frac{2\chi_1}{2\chi_1\chi_2\cos\gamma_2\cos\psi - \left[\chi_1^2\sin\gamma_1 + \chi_2^2\sin(2\gamma_2-\gamma_1) - \sin\gamma_1\right]\sin\psi}, \tag{2.24}$$

$$\tan\psi = \frac{-2\chi_1\chi_2\sin\gamma_2}{\cos\gamma_1 + \chi_2^2\cos(2\gamma_2-\gamma_1) + \chi_1^2\cos\gamma_1}. \tag{2.25}$$

Similarly, the real and positive light neutrino masses can also be expressed in terms of $\chi_{1,2}$ and $\gamma_{1,2}$ after we extract the phases from the complex eigenvalues. To proceed, note that Eq. (2.21) can be rewritten as

$$m_\nu \equiv U\,\mathrm{diag}(m_1, m_2, m_3)U^T, \tag{2.26}$$

with

$$U = \mathcal{V}^\dagger U_{13} e^{i\frac{\pi}{2}} U_p. \tag{2.27}$$

Here U_p stands for a diagonal phase matrix given by $U_p = \mathrm{diag}(1, e^{i\beta_{21}/2}, e^{i\beta_{31}/2})$, and the real positive light neutrino masses are given by:

$$m_1 = \frac{v'^2}{M} \mid f_3^{\nu^2} \mid \sqrt{o_r^2 + o_i^2}, \tag{2.28}$$

$$m_2 = \frac{v'^2}{M} \mid f_3^{\nu^2} \mid, \tag{2.29}$$

$$m_3 = \frac{v'^2}{M} \mid f_3^{\nu^2} \mid \sqrt{n_r^2 + n_i^2}, \tag{2.30}$$

where o_r, o_i, n_r and n_i can be written in terms of the associated parameters (χ_1, χ_2, γ_1 and γ_2) in our model as

$$o_r = \chi_1^2\cos 2\gamma_1 + \chi_2^2\cos 2\gamma_2 + 1 - 2A\chi_1\cos\gamma_1 + 2B\chi_1\sin\gamma_1, \tag{2.31}$$

$$o_i = \chi_1^2\sin 2\gamma_1 + \chi_2^2\sin 2\gamma_2 - 2A\chi\sin\gamma_1 - 2B\chi_1\cos\gamma_1, \tag{2.32}$$

$$n_r = \chi_1^2\cos 2\gamma_1 + \chi_2^2\cos 2\gamma_2 + 1 + 2A\chi_1\cos\gamma_1 - 2B\chi_1\sin\gamma_1, \tag{2.33}$$

$$n_i = \chi_1^2\sin 2\gamma_1 + \chi_2^2\sin 2\gamma_2 + 2A\chi\sin\gamma_1 + 2B\chi_1\cos\gamma_1., \tag{2.34}$$

$$A = \frac{\sqrt{1 + \chi_2^2\cos 2\gamma_2 + \sqrt{1 + \chi_2^4 + 2\chi_2^2\cos 2\gamma_2}}}{\sqrt{2}}, B = \frac{\chi_2^2\sin 2\gamma_2}{2A}. \tag{2.35}$$

parameters	best fit value	3σ range
$\sin^2\theta_{12}$	0.304	$0.269 \to 0.343$
$\sin^2\theta_{23}$	0.573	$0.415 \to 0.616$
$\sin^2\theta_{13}$	0.02219	$0.02032 \to 0.02410$
$\delta_{CP}/^\circ$	197	$120 \to 369$
$\frac{\Delta m^2_{21}}{10^{-5}\ eV^2}$	7.42	$6.82 \to 8.04$
$\frac{\Delta m^2_{31}}{10^{-3}\ eV^2}$	$+2.517$	$+2.435 \to +2.598$

Table 2.2: neutrino oscillation data obtained from NuFIT[165] for NH scenario of light neutrino mass.

The phases $\beta_{21(31)}$ involved in U_p are given by,

$$\beta_{21} = -\tan^{-1}\frac{o_i}{o_r}, \beta_{31} = \tan^{-1}\frac{n_i}{n_r} - \tan^{-1}\frac{o_i}{o_r}. \tag{2.36}$$

Therefore using Eqs. (2.9), (2.16) and (2.27), the final form of the mixing matrix U which diagonalises the effective light neutrino mass matrix (in the charged lepton diagonal basis) can now be written as

$$U = \begin{pmatrix} \frac{\cos\theta - e^{i\psi}\sin\theta}{\sqrt{3}} & \frac{1}{\sqrt{3}} & \frac{\cos\theta + e^{-i\psi}\sin\theta}{\sqrt{3}} \\ \frac{\cos\theta - \omega e^{i\psi}\sin\theta}{\sqrt{3}} & \frac{\omega^2}{\sqrt{3}} & \frac{\omega\cos\theta + e^{-i\psi}\sin\theta}{\sqrt{3}} \\ \frac{\cos\theta - \omega^2 e^{i\psi}\sin\theta}{\sqrt{3}} & \frac{\omega}{\sqrt{3}} & \frac{\omega^2\cos\theta + e^{-i\psi}\sin\theta}{\sqrt{3}} \end{pmatrix} e^{i\pi/2}U_p. \tag{2.37}$$

U is therefore the lepton mixing matrix, called the PMNS matrix (U_{PMNS}), the standard form of which is presented in Eq. (1.49). Comparing above two matrices given in Eq. (2.37) and (1.49) we get the correlation between the neutrino mixing angles (and Dirac CP phase) appearing in U_{PMNS} and the model parameters as [146]

$$|\ s_{13}\ |^2 = \frac{1 + \sin 2\theta\cos\psi}{3}, \quad \tan\delta = \frac{\sin\theta\sin\psi}{\cos\theta + \sin\theta\cos\psi}, \tag{2.38}$$

$$s^2_{12} = \frac{1}{3(1 - |\ s_{13}\ |^2)}, \quad \tan 2\theta_{23}\cos\delta = \frac{1 - 2\,|\ s_{13}\ |^2}{|\ s_{13}\ |\sqrt{2 - 3\,|\ s_{13}\ |^2}}. \tag{2.39}$$

Additionally, the two Majorana phases α_{21} and α_{31} are identified as $\alpha_{21} = \beta_{21}$, and $\alpha_{31} = \beta_{31}$ (ignoring the irrelevant common phase). These correlations given in Eq. (2.38)-(2.39) are the keys to the subsequent analysis of neutrino phenomenology.

2.3 Neutrino phenomenology

2.3.1 Constraining the parameter space

As seen from Eqs. (2.38) and (2.39) in conjugation with Eqs. (2.24) and (2.25), all the mixing angles ($\theta_{13}, \theta_{12}, \theta_{23}$) and the Dirac CP phase (δ) involved in the lepton mixing matrix U_{PMNS} are finally determined by the model parameters χ_1, χ_2, γ_1 and γ_2. Hence, using the

3σ allowed ranges of the three mixing angles $(\theta_{13}, \theta_{12}, \theta_{23})$ from neutrino oscillation data[5] presented in Table 2.2, we can restrict parameter space for $\chi_{1,2}$ and $\gamma_{1,2}$. This parameter space of the current set-up can be further constrained using the 3σ allowed ranges of the mass-squared differences (see Table 2.2). For that purpose, we introduce a dimensionless quantity r, defined as the ratio of solar to atmospheric mass squared difference for normal hierarchy, *i.e.*, $r = \frac{\Delta m^2_{21}}{\Delta m^2_{31}}$ with $\Delta m^2_{21} = m_2^2 - m_1^2$ and $\Delta m^2_{31} = m_3^2 - m_1^2$. Using the three light neutrino mass eigenvalues given in Eq. (2.28)-(2.30), we are able to rewrite it as

$$r = \frac{\Delta m^2_{21}}{\Delta m^2_{31}} = \frac{1 - o_r^2 - o_i^2}{n_r^2 + n_i^2 - o_r^2 - o_i^2}. \tag{2.40}$$

Substituting $o_{r,i}, n_{r,i}$ from Eq. (2.31)-(2.34) into Eq. (2.40), we note that r now becomes function of χ_1, χ_2, γ_1 and γ_2. Apart from the satisfaction of r value obtained from the ratio of the best fit values of mass-squared differences, we must satisfy both the individual mass-squared differences, Δm^2_{21} and Δm^2_{31}, independently within their 3σ allowed ranges using Eqs. (2.28)-(2.30). There also exists a cosmological upper bound on sum of the light neutrinos masses as $\sum_i m_i \leq 0.11$ eV [59, 167] which will also constrain the parameter space. Note that in order to evaluate $\sum_i m_i$, we need to get an estimate of the pre-factor $|f_3^{\nu^2}|v'^2/M$ (see Eqs. (2.28)-(2.30)) which can be obtained by using the relation

$$|f_3^{\nu^2}|v'^2/M = \sqrt{\Delta m^2_{21}/(1 - o_r^2 - o_i^2)}, \tag{2.41}$$

with the known value of Δm^2_{21} from current global analysis [165].

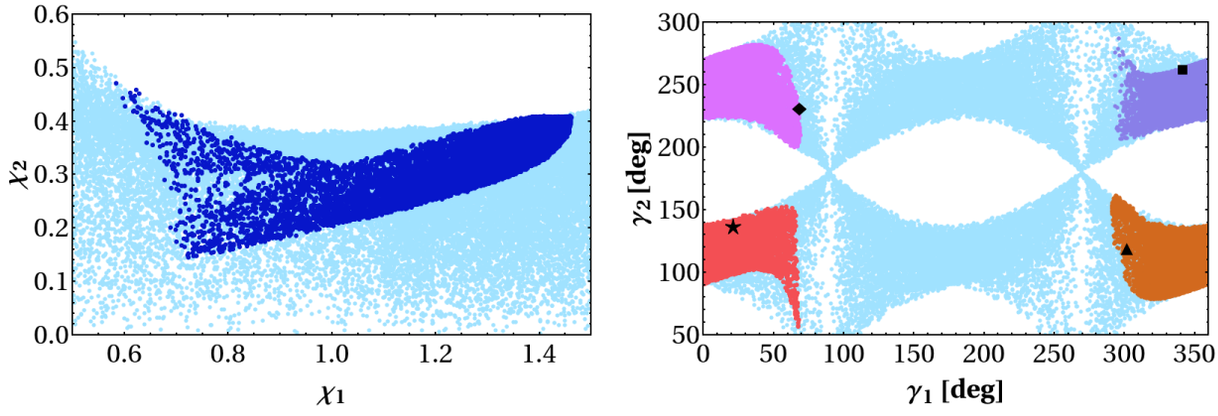

Figure 2.1: Allowed parameter spaces of χ_1-χ_2 (left panel) and γ_1-γ_2 (right panel) using 3σ ranges of neutrino oscillation parameters [165]. The light blue dots in both the panels correspond to 3σ allowed values for the mixing angles while the darker patches in each panel further satisfy constraints coming from the mass-squared differences, their ratio and sum of absolute masses. ★, ▲, ■, ♦ marks of the right panel are indicative of four benchmark points (BP) used in Section 2.4.

Equipped with all these, we provide a range of the allowed parameter space of our model in Fig. 2.1. In the left panel, we first indicate the correlation between two of the parameters $\chi_1 - \chi_2$ while the same for $\gamma_1 - \gamma_2$ is shown in the right panel, indicated by the light blue

[5]The Majorana phases are insensitive to neutrino oscillation experiments. However, they may play an important role in neutrinoless double beta decay [166].

points. The corresponding values of the parameters (light blue points) satisfy the 3σ allowed ranges of the lepton mixing angles, $\theta_{13}, \theta_{12}, \theta_{23}$. In obtaining these points, we varied parameters within a large range. For example, $\chi_{1,2}$ are varied from 0 to 2 while $\gamma_{1,2}$ are considered within their full range: 0-360°. Once we also incorporate the constraints following from the mass-squared differences as well as the one on the sum of the light neutrino masses, the entire allowed parameter space is reduced to a smaller region indicated by the dark blue patch on the left panel (in $\chi_1 - \chi_2$ plane) and four cornered patches (red, magenta, brown and purple) on the right panel (in $\gamma_1 - \gamma_2$ plane).

From Fig. 2.1, we find $0.584 \lesssim \chi_1 \lesssim 1.462$ whereas the ratio of the magnitudes of the antisymmetric contribution to the diagonal one (in view of Eq. (2.6)) falls in a range: $0.470 \gtrsim \chi_2 \gtrsim 0.145$. Turning into the right panel, we find that γ_1 and γ_2 both are pushed toward four cornered regions represented by red, magenta, brown and purple patches respectively. Here we find that for $0° \leq \gamma_1 \leq 69°$ the allowed regions for γ_2 are $(57° - 152°)$ and $(200° - 282°)$. Whereas for $291° \leq \gamma_1 \leq 360°$, the allowed regions for γ_2 are limited within $(78° - 161°)$ and $(206° - 287°)$. Here we also note that, in the right panel of Fig. 2.1, ★, ▲, ■ and ♦ represent four unique benchmark points in the parameter space $\{\chi_1, \chi_2, \gamma_1, \gamma_2\}$ given by BP1 = $(1.37, 0.399, 21.53°, 135.59°)$, BP2 = $(0.978, 0.235, 301.81°, 119.1°)$, BP3 = $(1.417, 0.372, 341.6°, 260.83°)$ and BP4 = $(0.707, 0.209, 68.62°, 231.15°)$. It is important to note that so far the analysis presented here is applicable only for normal hierarchy of light neutrino mass. In the present setup, due to the special flavor structure of the model an inverted hierarchy of light neutrino mass spectrum however can not be accommodated. This is an interesting prediction that will undergo tests in several ongoing and near-future experiments.

2.3.2 Implications for light neutrino masses and low energy phase

From the previous part of the analysis, we have an understanding on the allowed regions for the χ_1, χ_2, γ_1 and γ_2 which satisfy all the constrains in the form of mass square differences, mixing angles and sum of the light neutrino masses. Hence, we are now in a position to study the implications of this allowed parameter space toward the predictions involving sum of the light neutrino masses, and phases. We already have correlation between the Dirac CP phase δ and the atmospheric mixing angle θ_{23} as seen from Eqs. (2.38) and (2.39), both of which are functions of $\chi_{1,2}, \gamma_{1,2}$ as evident from Eqs. (2.24), (2.25). In left panel of Fig. 2.2,

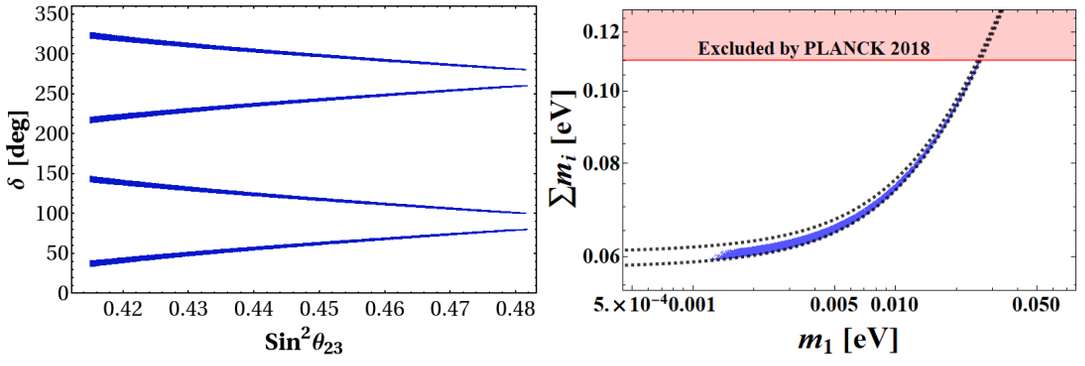

Figure 2.2: Correlations within $\delta - \theta_{23}$ (left panel) and $\sum_i m_i - m_1$ (right panel) are presented while allowed ranges for χ_1, χ_2, γ_1 and γ_2 are used from Fig. 2.1.

we have plotted this correlation in $\delta - \theta_{23}$ plane where only the allowed set of points for χ_1, χ_2, γ_1 and γ_2 are employed (as in Fig. 2.1). The model seems to predict δ to be in the range $33^\circ(213^\circ) \lesssim \delta \lesssim 80^\circ(260^\circ)$ and $100^\circ(280^\circ) \lesssim \delta \lesssim 147^\circ(327^\circ)$ which correspond to the atmospheric mixing angle θ_{23} in the lower octant. Similarly, in the right panel of Fig. 2.2, we use Eqs. (2.28), (2.29), (2.30) along with Eq. (2.41) to indicate the predictions related to the sum of the light neutrino masses against m_1, the lightest neutrino mass, indicated by the blue patch. The region between the black dotted lines represents 3σ allowed range for $\sum_i m_i$ and the blue patch within it represents the predicted region in our framework. The red shaded region with $\sum_i m_i \leq 0.11$ eV is disallowed by cosmological observation mentioned earlier. This plot shows that the lightest neutrino mass is $\mathcal{O}(10^{-3})$ eV whereas the sum of the light neutrino masses is around $\mathcal{O}(0.06)$ eV. On top of this, the present set up excludes the possibility of having maximum CP violation ($\delta = 90^\circ/270^\circ$) and at the same time favors θ_{23} to be below maximal mixing, *i.e.* $\theta_{23} < 45^\circ$. These are the salient features of our proposal.

2.3.3 Neutrinoless Double beta decay

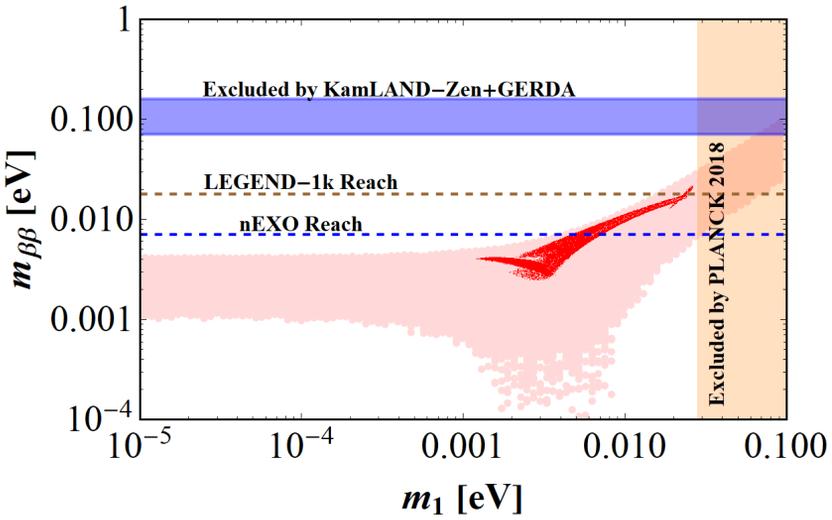

Figure 2.3: Correlation between $m_{\beta\beta}$ and lightest neutrino mass m_1 (for NH) with allowed ranges for χ_1, χ_2, γ_1 and γ_2 obtained from Fig. 2.1. Here the light blue shaded region represents the combined upper limit of GERDA and KamLAND-Zen experiments whereas the brown and blue dashed lines stand for future sensitivities of the LEGEND and nEXO experiments respectively.

It is pertinent to also shed light on the effective neutrino mass parameter, $m_{\beta\beta}$, involved in the half life of neutrinoless double beta decay in our set-up, which is given by [168]

$$m_{\beta\beta} = |m_1 c_{12}^2 c_{13}^2 + m_2 s_{12}^2 c_{13}^2 e^{i\alpha_{21}} + m_3 s_{13}^2 e^{i(\alpha_{31} - 2\delta)}|. \tag{2.42}$$

Note that for the normal hierarchy of light neutrino masses, one can write $m_2 = \sqrt{(m_1^2 + \Delta m_{21}^2)}$, and $m_3 = \sqrt{(m_1^2 + \Delta m_{31}^2)}$. Recall also that we have already elaborated on our finding for lightest neutrino masses m_1 (see right panel of Fig. 2.2), and δ (see left panel of Fig. 2.2) in the last subsections corresponding to the allowed parameter space of $\{\chi_1, \chi_2, \gamma_1, \gamma_2\}$ from Fig. 2.1. Using the same, we could also estimate the respective allowed ranges of Majo-

rana phases α_{21} and α_{31} via Eq. (2.36) (as $\alpha_{21} = \beta_{21}$ and $\alpha_{31} = \beta_{31}$) and in turn we can evaluate $m_{\beta\beta}$ as function of m_1 (substituting m_2 and m_3 in Eq. (2.42)). With the allowed ranges for χ_1, χ_2, γ_1 and γ_2 satisfying all the neutrino data inclusive of the cosmological mass bounds ($i.e.$ corresponding to the dark blue patch of left panel, and four cornered patches of right panel of Fig. 2.1), we therefore plot $m_{\beta\beta}$ as a function of lightest neutrino masses m_1 for normal hierarchy as presented in Fig. 2.3 by the red patch. The background light red patch indicates the allowed region in general when mixing angles, mass squared differences along with δ are allowed to vary within their 3σ range. Hence from this $m_{\beta\beta}$ vs m_1 plot (red patch), we notice that for m_1 within the range (0.001-0.027) eV (allowed in our set-up as per Fig. 2.2), the effective mass parameter is predicted to be: $0.002 \lesssim m_{\beta\beta} \lesssim 0.021$ eV. This prediction lies well within the limits on $m_{\beta\beta}$ by combined analysis of GERDA and KamLAND-Zen experiments denoted by the light blue shade. The horizontal brown and blue dashed lines stand for future sensitivity by the LEGEND and nEXO experiments.

2.3.4 Lepton flavor violation

Due to the existence of active-sterile neutrino mixing, the possibility of rare lepton flavor violating processes should arise in our framework. Out of all the processes, contribution to $\mu \to e\gamma$ is the most important one as it is significantly constrained. In the weak basis, $i.e.$ where charged and RHN mass matrix is diagonal, the branching ratio of the same process can be written as [169, 170]:

$$B(\mu \to e\gamma) = \frac{3\alpha}{8\pi}\left|\sum_i V_{ei}V^{\dagger}_{i\mu}\mathcal{F}\Big(\frac{M_i^2}{M_W^2}\Big)\right|^2, \tag{2.43}$$

where $\alpha = e^2/4\pi$ is the fine structure constant, M_W stands for $W^{\pm}$ mass, $V = m_D M_R^{-1}$ is the mixing matrix representing active-sterile mixing, M_i is the mass of RHN mass eigenstates N_i and $\mathcal{F}(x) = \frac{x(1-6x+3x^2+2x^3-6x^2\ln x)}{2(1-x)^4}$, with $x = M_i/M_W$. The current upper bound on the branching ratio of the $\mu \to e\gamma$ is found to be $\mathrm{BR}(\mu \to e\gamma) \lesssim 4.2 \times 10^{-13}$ (at 90% C.L.)[168]. In our analysis, with the allowed ranges for χ_1, χ_2, γ_1 and γ_2 (obtained from Fig. 2.1) and M_i in the TeV scale, the contribution towards the branching ratio for $\mu \to e\gamma$ turns out to be insignificant ($\mathcal{O}(10^{-35})$) compared to the experimental limit.

2.4 Leptogenesis

The presence of RHNs in the seesaw realization of light neutrino mass provides an opportunity to study leptogenesis from the CP-violating out-of-equilibrium decay of RHNs into lepton and Higgs doublets in the early universe[95, 152, 171]. The lepton asymmetry created is expected to be converted to a baryon asymmetry via the sphaleron process[172, 173]. In the previous part of our analysis, we have found that the phenomenology of the neutrino sector is mainly dictated by four parameters $i.e$ χ_1, χ_2, γ_1, and γ_2 which in turn determine most of the observables in the neutrino sector. However we also notice the presence of the prefactor $|f_3^{\nu^2}|v'^2/M$ associated to the light neutrino mass eigenvalues as given in Eq. (2.28)-(2.30). Using Eq. (2.41), though this prefactor can be evaluated, we can't have specific estimate for

the degenerate mass of the RHNs (M) as f_3^ν remains undetermined. To have a more concrete picture, we provide a plot for $|f_3^{\nu^2}|v'^2/M$ against one of the parameters, χ_1, in Fig. 2.4 obtained using the correlation with other parameters fixed by neutrino oscillation and cosmological data. Hence barring the ambiguity in determining f_3^ν apart from a conservative limit $|f_3^\nu| < \mathcal{O}(1)$, M is seen to be anywhere from a very large value (say 10^{14-15} GeV) to a low one (say TeV). Furthermore, the RHNs are exactly degenerate in our framework. Hence

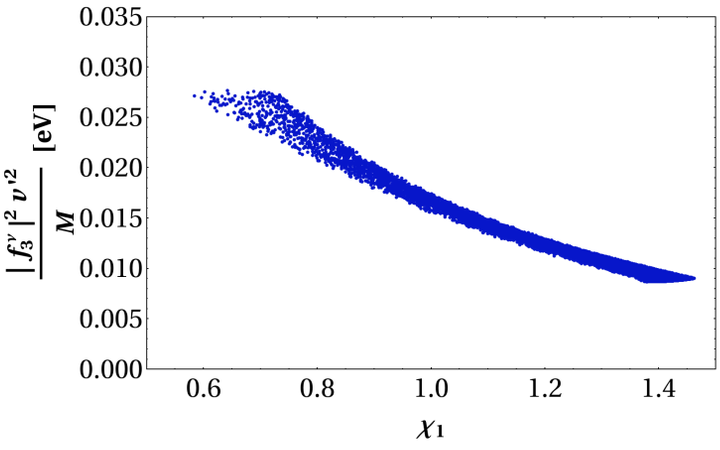

Figure 2.4: Correlation between $(|f_3^\nu|^2 v'^2)/M$ and χ_1 for NH.

unless we break this exact degeneracy, no CP asymmetry can be generated [97] . Below we proceed to discuss leptogenesis mechanism in the present framework keeping in mind that we need to remove the exact degeneracy of RHN masses and study of flavored leptogenesis becomes essential (as M can be below 10^{12} GeV).

2.4.1 Generation of mass splitting and CP asymmetry

As discussed in subsection 1.6, the CP asymmetry parameter generated as a result of the interference between the tree and one loop level decay amplitudes of RHN N_i decaying into a lepton doublet with specific flavor l_{L_α} and Higgs (H) is defined by :

$$\epsilon_i^\alpha = \frac{\Gamma(N_i \to \ell_{L_\alpha} H) - \Gamma(N_i \to \bar{\ell}_{L_\alpha} \bar{H})}{\Gamma(N_i \to \ell_{L_\alpha} H) + \Gamma(N_i \to \bar{\ell}_{L_\alpha} \bar{H})}. \tag{2.44}$$

Considering the exact mass degeneracy is lifted by some mechanism (will be discussed soon), the general expression for such asymmetry can be written as [174, 175] :

$$\begin{aligned}\epsilon_i^\alpha =& \frac{1}{8\pi \mathrm{H}_{ii}} \sum_{j\neq i} \mathrm{Im}[\mathrm{H}_{ij}(\mathcal{Y}_\nu^\dagger)_{i\alpha}(\mathcal{Y}_\nu)_{\alpha j}] \Big[f(x_{ij}) + \frac{\sqrt{x_{ij}}(1-x_{ij})}{(1-x_{ij})^2 + \frac{\mathrm{H}_{jj}^2}{64\pi^2}} \Big] \\ &+ \frac{1}{8\pi \mathrm{H}_{ii}} \sum_{j\neq i} \mathrm{Im}[\mathrm{H}_{ji}(\mathcal{Y}_\nu^\dagger)_{i\alpha}(\mathcal{Y}_\nu)_{\alpha j}] \Big[\frac{(1-x_{ij})}{(1-x_{ij})^2 + \frac{\mathrm{H}_{jj}^2}{64\pi^2}} \Big],\end{aligned} \tag{2.45}$$

where $\mathcal{Y}_\nu$ ($\equiv \mathcal{V}^\dagger Y_\nu$ in our case, see Eq. (2.11)) is the neutrino Yukawa matrix in charge lepton diagonal basis, H and the loop factor $f(x_{ij})$ are given by

$$\mathrm{H} = \mathcal{Y}_\nu^\dagger \mathcal{Y}_\nu = \; Y_\nu^\dagger Y_\nu; \tag{2.46}$$

$$f(x_{ij}) = \sqrt{x_{ij}}\Big[1 - (1+x_{ij})\ln\left(\frac{1+x_{ij}}{x_i j}\right)\Big], \tag{2.47}$$

with $x_{ij} = \frac{M_j^2}{M_i^2}$ where M_i are the masses of the RHNs after the degeneracy is removed. This is applicable for both hierarchical as well as quasi-degenerate mass spectrum of RHNs [174]. For the hierarchical RHNs, one neglects $\frac{\mathrm{H}_{jj}^2}{64\pi^2}$ compared to $(1-x_{ij})^2$ while the entire expression of Eq. (2.45) can be used for quasi-degenerate case inclusive of resonance situation for which $(1-x_{ij})^2 \simeq \frac{\mathrm{H}_{jj}^2}{64\pi^2}$ [175, 176]. Below we discuss the mass splittings induced by the running of the heavy RHNs.

2.4.1.1 Lifting the mass degeneracy

The exact mass degeneracy of heavy Majorana neutrinos is the result of the flavor symmetry imposed in our construction. To remove this degeneracy, here we adopt the renormalization group effects into consideration [177, 178]. Considering the discrete $A_4 \times Z_3 \times Z_2$ symmetry breaking scale close to the GUT scale $\sim \Lambda$ (the cut-off scale introduced in Eq. (2.1)), we determine the running of the RHN mass matrix M_R and Dirac neutrino Yukawa matrix $\mathcal{Y}_\nu$ from GUT scale to seesaw scale M (assuming $M < \Lambda$). Using renormalisation group equations, the evolution of the RHN mass matrix M (= diag(M_1, M_2, M_3)) and Dirac neutrino Yukawa matrix $\mathcal{Y}_\nu$ (in charged lepton Y_ℓ diagonal basis) at one-loop can be written as [177–179]

$$\frac{dM_i}{dt'} = 2M_i\,\mathrm{H}_{ii}\,, \tag{2.48}$$

$$\frac{d\mathcal{Y}_\nu}{dt'} = \left[\{\mathcal{T} - \frac{3}{4}g_2^2 - \frac{9}{4}g_3^2\}\mathbb{I}_3 - \frac{3}{2}\left(Y^\ell Y^{\ell\dagger} - \mathcal{Y}_\nu\mathcal{Y}_\nu^\dagger\right)\right]\mathcal{Y}_\nu + \mathcal{Y}_\nu \mathrm{R}\,, \tag{2.49}$$

with

$$\mathcal{T} = 3\mathrm{Tr}(Y_u Y_u^\dagger) + 3\mathrm{Tr}(Y_d Y_d^\dagger) + \mathrm{Tr}(Y_\ell Y_\ell^\dagger) + \mathrm{Tr}(\mathcal{Y}_\nu\mathcal{Y}_\nu^\dagger), \tag{2.50}$$

where $Y_{u,d}$ are the up-quark and down-quark Yukawa matrices respectively, and $\mathbb{I}_3$ is the identity matrix of order 3×3. Here the matrix R is anti-hermitian defined by [178]

$$\mathrm{R}_{11} = \mathrm{R}_{22} = \mathrm{R}_{33} = 0, \quad \mathrm{R}_{ji} = -\,\mathrm{R}_{ij}^*\,(i \neq j),$$
$$\mathrm{R}_{ij} = \frac{2+\delta_{ij}}{\delta_{ij}}\,\mathrm{Re}\,(\mathrm{H}_{ij}) + i\frac{\delta_{ij}}{2+\delta_{ij}}\,\mathrm{Im}\,(\mathrm{H}_{ij})\,, \tag{2.51}$$

$\delta_{ij} = \frac{M_j}{M_i} - 1$ is the degeneracy parameter for the RHN masses and $t' = \frac{1}{16\pi^2}\ln\left(\frac{\Lambda}{M}\right)$.

Now as the RHNs are exactly degenerate at scale Λ, the right hand side (first term) of Eq. (2.51) becomes singular unless we impose $\mathrm{Re}(\mathrm{H}_{ij}) = 0$. Note that, in our construction, H_{12} and H_{23} are already zero due to the flavor symmetry imposed. Hence the above condition

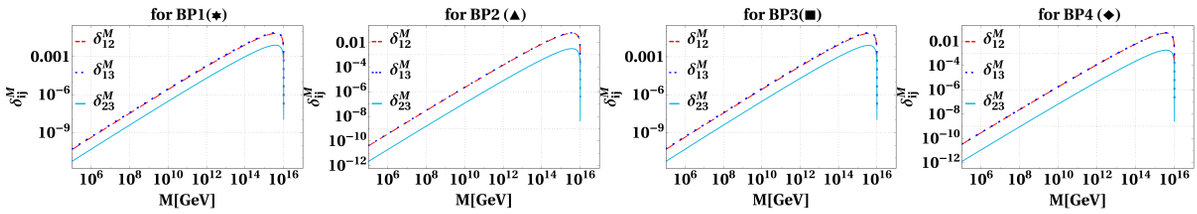

Figure 2.5: Variation of mass splitting δ^M_{ij} *w.r.t.* scale M for the benchmark points BP1, BP2, BP3 and BP4 respectively.

should be exercised only to realize $\mathrm{Re}(\mathrm{H}_{13}) = 0$ in our case which can be materialized if we choose to use $\widetilde{\mathcal{Y}}_\nu$, obtained by performing an orthogonal rotation (by a matrix O say) on Dirac Yukawa matrix $\mathcal{Y}_\nu$ as,

$$\widetilde{\mathcal{Y}}_\nu = \mathcal{Y}_\nu O\,, \text{ with } \quad O = \begin{pmatrix} \cos\Theta & 0 & \sin\Theta \\ 0 & 1 & 0 \\ -\sin\Theta & 0 & \cos\Theta \end{pmatrix}, \tag{2.52}$$

having the rotation angle Θ determined by the relation

$$\tan 2\Theta = \frac{2\mathrm{Re}\,(\mathrm{H}_{13})}{\mathrm{H}_{33} - \mathrm{H}_{11}} = \frac{-\cos\gamma_1}{\chi_2 \cos(\gamma_1 - \gamma_2)}. \tag{2.53}$$

In obtaining the rightmost expression above, we employ Eqs. (2.6), (2.22), (2.23) in Eq. (2.46). This flexibility in using $\widetilde{\mathcal{Y}}_\nu$ prevails due the following reason. Note that, if we rotate the $\mathcal{Y}_\nu$ in this manner, the neutrino Yukawa Lagrangian gets modified to:

$$\bar{\ell_L}\mathcal{Y}_\nu \tilde{H} N_R = \bar{\ell_L}\widetilde{\mathcal{Y}}_\nu O^T \tilde{H} N_R. \tag{2.54}$$

We can now redefine N_R by: $\widetilde{N}_R = O^T N_R$, *i.e.* if we rotate RHN fields by O^T, RHN mass term will not change as $\overline{N_R^C} M_R N_R = \overline{\widetilde{N}_R^C} M_R \widetilde{N}_R$ due to the orthogonal property of O matrix.

The Eqs. (2.48) and (2.49) can now be rewritten in terms of $\widetilde{\mathrm{H}} = O^T \mathrm{H} O$ and $\widetilde{\mathcal{Y}}_\nu$ by using the above relations. The form of $\widetilde{\mathrm{H}}$ can be obtained by

$$\widetilde{\mathrm{H}} = \widetilde{\mathcal{Y}}_\nu^\dagger \widetilde{\mathcal{Y}}_\nu = O^T \mathrm{H} O = \begin{pmatrix} \mathrm{H}_{11} - \Delta & 0 & i\,\mathrm{Im}\,(\mathrm{H}_{13}) \\ 0 & \mathrm{H}_{22} & 0 \\ -i\,\mathrm{Im}\,(\mathrm{H}_{13}) & 0 & \mathrm{H}_{33} + \Delta \end{pmatrix}, \tag{2.55}$$

where $\Delta \equiv \tan\Theta\,\mathrm{Re}\,(\mathrm{H}_{13})$. As seen from the Eq. (2.48) (with right hand side written in terms of $\widetilde{\mathrm{H}}$ now), we find that a mass splitting generated at a scale (M) as

$$\delta^M_{ij} = 2(\widetilde{\mathrm{H}}_{ii} - \widetilde{\mathrm{H}}_{jj})t'\,, \tag{2.56}$$

thanks to the effect of running. Using Eq. (2.49), we also get a off-diagonal contribution

$(\mathrm{H}^R_{ij}, i \neq j)$ to $\widetilde{\mathrm{H}}$ [178],

$$\widetilde{\mathrm{H}}^M_{ij} = \widetilde{\mathrm{H}}_{ij} + \mathrm{H}^R_{ij}; \;\; \mathrm{H}^R_{ij} \simeq 3y_\tau^2\,(\widetilde{\mathcal{Y}}^*_\nu)_{3i}(\widetilde{\mathcal{Y}}_\nu)_{3j}\,t'; \quad (i \neq j) \tag{2.57}$$

while $\widetilde{\mathrm{H}}^M_{ii} = \widetilde{\mathrm{H}}_{ii}$. As mentioned earlier, the seesaw scale M remains undetermined even after applying neutrino mass and mixing constraints, we have shown in Fig. 2.5 how such splitting δ^M_{12} varies with the degenerate RHN mass M due to running corresponding to benchmark points: BP1, BP2, BP3 and BP4 allowed by the neutrino data. We find that below $M \simeq 10^{12}$ GeV, δ^M_{ij} become smaller than $\mathcal{O}(10^{-4})$ implying that the masses of the three RHNs fall in the quasi-degenerate category [174]. Such a a small splitting, although crucial for generation of CP asymmetry, won't alter our findings of the neutrino section. Note that the estimated splitting does not correspond to the requirement of resonant leptogenesis. We are now in a position to evaluate the CP asymmetry generated at scale M, as discussed below.

2.4.1.2 Estimating CP asymmetry

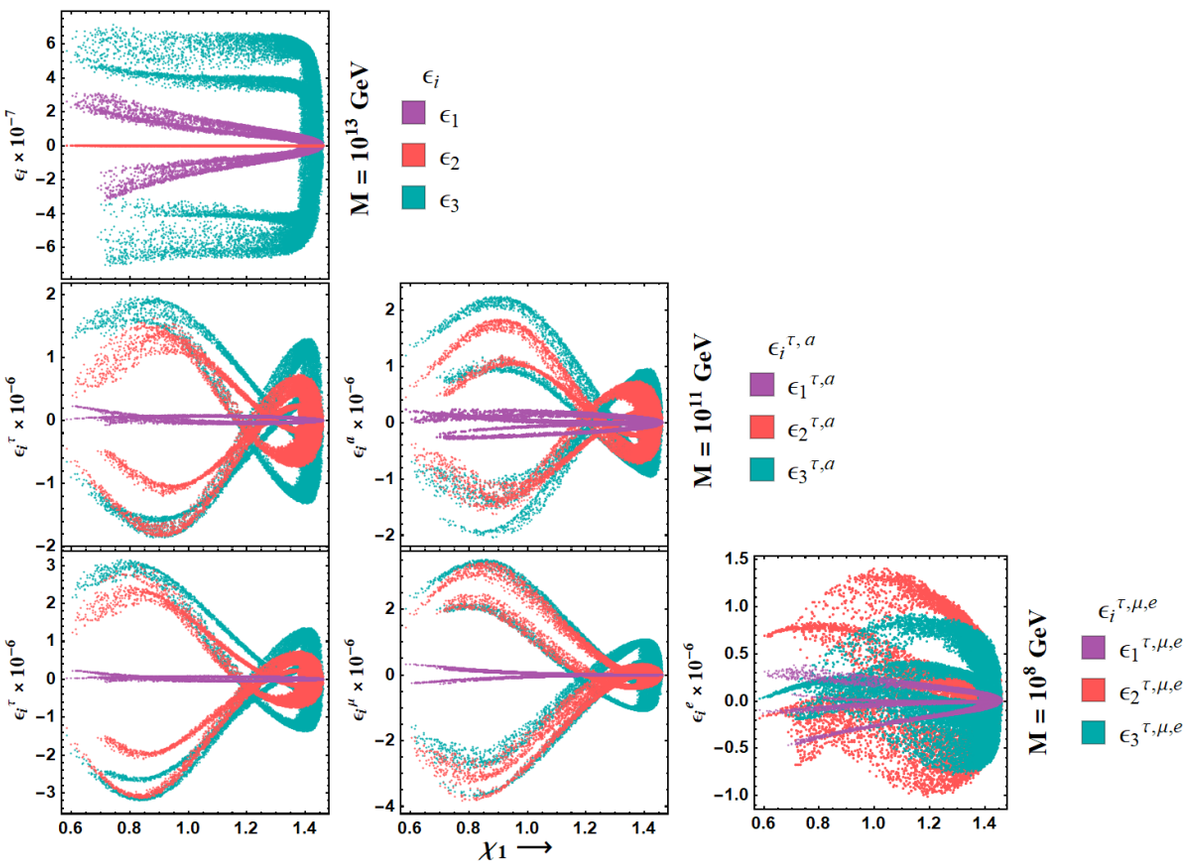

Figure 2.6: Variation of individual components of CP asymmetry $w.r.t.$ model parameter χ_1 for three different scales $M = 10^{13}$ GeV (top most plot), $M = 10^{11}$ GeV (plots from second row) and $M = 10^8$ GeV (plots from third row).

Starting with exact degeneracy of RHN masses, we have shown that the running of involved parameters from a typical high scale to the scale of the heavy neutrino masses leads to a quasi-degenerate spectrum of RHNs. Hence we can now estimate the CP asymmetry created at a scale M by using Eq. (2.45) while replacing H by $\widetilde{\mathrm{H}}^M$ and δ_{ij} by δ^M_{ij} in view of our

discussion above. Furthermore, it can be shown that maximum contribution to CP asymmetry comes from self energy diagram [99, 180, 181]. Therefore, the asymmetry expression of Eq. (2.45) gets modified to

$$\epsilon_i^{\alpha} \simeq -\frac{1}{16\pi \widetilde{\mathrm{H}}_{ii}^{M}} \sum_{j\neq i} \frac{\delta_{ij}^{M}}{(\delta_{ij}^{M})^2 + \left(\frac{\widetilde{\mathrm{H}}_{jj}^{M}}{16\pi}\right)^2} \Big\{ \mathrm{Im}[\widetilde{\mathrm{H}}_{ij}^{M} (\widetilde{\mathcal{Y}}_{\nu}^{*})_{\alpha i} (\widetilde{\mathcal{Y}}_{\nu})_{\alpha j}] + \mathrm{Im}[\widetilde{\mathrm{H}}_{ji}^{M} (\widetilde{\mathcal{Y}}_{\nu}^{*})_{\alpha i} (\widetilde{\mathcal{Y}}_{\nu})_{\alpha j}] \Big\}. \tag{2.58}$$

Now, using Eqs. (2.55) to (2.57) and employing them in Eq. (2.58), we estimate for the cp asymmetry parameter for the heavy RHNs decaying into various flavors which will be useful to evaluate the final lepton asymmetry taking the flavor effects into account. Since all the entities of Eq. (2.58) are function of set of parameters $\{\chi_1, \chi_2, \gamma_1, \gamma_2\}$ and M, we can make use of the allowed parameter space from neutrino phenomenology (refer to Fig. 2.1) and finally calculate the CP asymmetries produced from all three RHN decays ($i = 1, 2, 3$) to different flavors of lepton doublets and Higgs.

For representation purpose, in Fig. 2.6, we depict the variation of individual flavor components of CP asymmetry $w.r.t.$ χ_1 at three different RHN mass scales: $M = 10^{13}$ (top panel), 10^{11} (middle panel), 10^{8} (bottom panel) GeV respectively. Since the flavor effects are known not to be important beyond $T \sim M \simeq 10^{12}$ GeV, we estimate asymmetries produced by individual RHNs only for top panel. It is found that maximum asymmetry falls in the ballpark of $|\epsilon_{i=1,3}|_{\max} \sim 6\times10^{-7}$ whereas $(|\epsilon_2|)_{\max}$ remains subdominant. At $T = 5\times10^{11}$ GeV, tau Yukawa comes to equilibrium, so effectively the scenario with $M = 10^{11}$ GeV becomes a two flavor scenario (τ and another orthogonal direction, say a) and the corresponding CP asymmetries are marked by: $\{\epsilon_i^{\tau}, \epsilon_i^{a=\mu+e}\}$. At this scale, $|\epsilon_{i=2,3}^{\tau,a}|_{max} \sim 2\times10^{-6}$ (middle panel of Fig. 2.6) and $|\epsilon_1^{\tau,a}|_{\max}$ becomes relatively small. We also estimate CP asymmetry at $M = 10^{8}$ GeV (bottom panel of Fig. 2.6). At this temperature (or scale), all Yukawa couplings except e are in equilibrium and hence contributions to CP asymmetries from all the three flavors, $\{\epsilon_i^{e}, \epsilon_i^{\mu}, \epsilon_i^{\tau}\}$, become important. We find $|\epsilon_{i=2,3}^{\tau}|_{max} \sim 3\times10^{-6}$ and $|\epsilon_1^{\tau}|_{max} < |\epsilon_{i=2,3}^{\tau}|_{max}$. An analogous pattern is observed for ϵ_i^{μ}. CP asymmetry along electron flavor is shown in the third plot of the bottom panel of Fig. 2.6 and is found to be $|(\epsilon_{i=2,3}^{e})_{max}| \sim 1.5\times10^{-6}$, $|(\epsilon_1^{e})_{max}| \sim 5\times10^{-7}$. With these various flavor dependent CP asymmetries, we can now proceed for evaluation of baryon asymmetry by solving the Boltzmann equations as illustrated below.

2.4.2 Solution of Boltzmann equation

It is worth mentioning that while estimating the final lepton asymmetry, one needs to take care of decays and inverse decays of heavy RHNs as well as various scattering processes. As stated earlier, we consider the contributions of all three RHNs having $M_i \lesssim 10^{12}$ GeV. Hence flavor effects have to be considered [105] as discussed in subsection 1.6.2 of previous chapter.

In our analysis, therefore, we include these flavor effects into consideration while constructing the Boltzmann equations. We work in a most general setup for leptogenesis, where

all three RHNs are contributing to the asymmetry due to their quasi degenerate spectrum of masses. As standard, the produced lepton doublets from the RHN decay needs to be appropriately projected to flavor states in the three previously mentioned temperature regimes differently. Below we write down the relevant Boltzmann equations to study the time evolution of the lepton-number asymmetries (for a system of three RHNs) as [100, 104, 182]

$$s\mathcal{H}z\frac{dY_{N_i}}{dz} = -\left\{\left(\frac{Y_{N_i}}{Y^{\rm eq}_{N_i}}-1\right)\left(\gamma_{D_i}+2\gamma_{H^i_s}+4\gamma_{H^i_t}\right)+\sum_{j\neq i}\left(\frac{Y_{N_i}}{Y^{\rm eq}_{N_i}}\frac{Y_{N_j}}{Y^{\rm eq}_{N_j}}-1\right)\left(\gamma^{(1)}_{N_iN_j}+\gamma^{(2)}_{N_iN_j}\right)\right\}, \tag{2.59}$$

$$\begin{aligned} s\mathcal{H}z\frac{dY_{\Delta_\alpha}}{dz} = -\Bigg\{&\sum_i\left(\frac{Y_{N_i}}{Y^{\rm eq}_{N_i}}-1\right)\epsilon^\alpha_i\gamma_{D_i}+K^0_\alpha\sum_\beta\Bigg[\sum_i\Bigg(\frac{1}{2}\left(C^\ell_{\alpha\beta}+C^H_\beta\right)\gamma_{D_i}\\ &+\left(\frac{Y_{N_i}}{Y^{\rm eq}_{N_i}}-1\right)\left(C^\ell_{\alpha\beta}\gamma_{H^i_s}+\frac{C^H_\beta}{2}\gamma_{H^i_t}\right)+\left(2C^\ell_{\alpha\beta}+C^H_\beta\right)\left(\gamma_{H^i_t}+\frac{1}{2}\gamma_{H^i_s}\right)\Bigg)\\ &+\sum_\sigma\left(\left(C^\ell_{\alpha\beta}+C^\ell_{\sigma\beta}+2C^H_\beta\right)\left(\gamma^\sigma_{N_s}+\gamma^\sigma_{N_t}\right)+\sum_{i,j}\left(C^\ell_{\alpha\beta}+C^\ell_{\sigma\beta}\right)\gamma^{(1)\sigma}_{N_iN_j}\right)\Bigg]\frac{Y_{\Delta_\beta}}{Y^{\rm eq}}\Bigg\}, \end{aligned} \tag{2.60}$$

where $z = M/T$ and $i = 1, 2, 3$ for all three RHNs. Note that these equations are more general compared to Eq. (1.83) and (1.94) due to the following reasons:

- First of all, Eq. (2.59) now represents BE for all the three RHNs contrary to the Eq. (1.83), where only lightest RHN was considered. As a result, one now needs to incorporate the coannihilation channels of RHNs: $\gamma^{(1)\alpha\beta}_{N_iN_j} \equiv [N_i+N_j \leftrightarrow \ell_\alpha+\bar{\ell}_\beta]$, $\gamma^{(2)}_{N_iN_j} \equiv [N_i+N_j \leftrightarrow H+\bar{H}]$, which can change the number density of RHNs (last two terms of Eq. (2.59)).
- Secondly, since now all the RHNs are contributing to CP asymmetry generation and eventually to lepton asymmetry production, a sum over the generation of RHN is introduced in Eq. (2.60).
- Coannihilation channel $\gamma^{(1)\alpha\beta}_{N_iN_j} \equiv K^0_\alpha\gamma^{(1)\beta}_{N_iN_j}$ can have finite impact on lepton asymmetry generation. Hence, it is also incorporated in the last term of Eq. (2.60).
- Finally, $\Delta L = 2$ processes were neglected in eq. (1.94), which we have now introduced in the second last term of Eq. (2.60)[6].

With all the ingredients at hand, we first substitute the evaluated CP asymmetry (from Eq. (2.58)) in Eq. (2.60) and proceed for solving the coupled Boltzmann equations in order to find out the final lepton asymmetry as well as final baryon asymmetry. In doing so, we divide the temperature range into three zones so as to take care of the flavor effects as discussed before while taking into account the $\Delta L = 1$ interactions and coannihilation processes (and ignoring $\Delta L = 2$ processes). We have considered different benchmark values for RHN degenerate mass M (splittings are automatically taken cared by running in terms of other parameters): $M = 10^9, 10^6, 10^5$ GeV so that the effects of flavor can be visible. These

[6]The relevent interaction rate densities can be found in [151, 183].

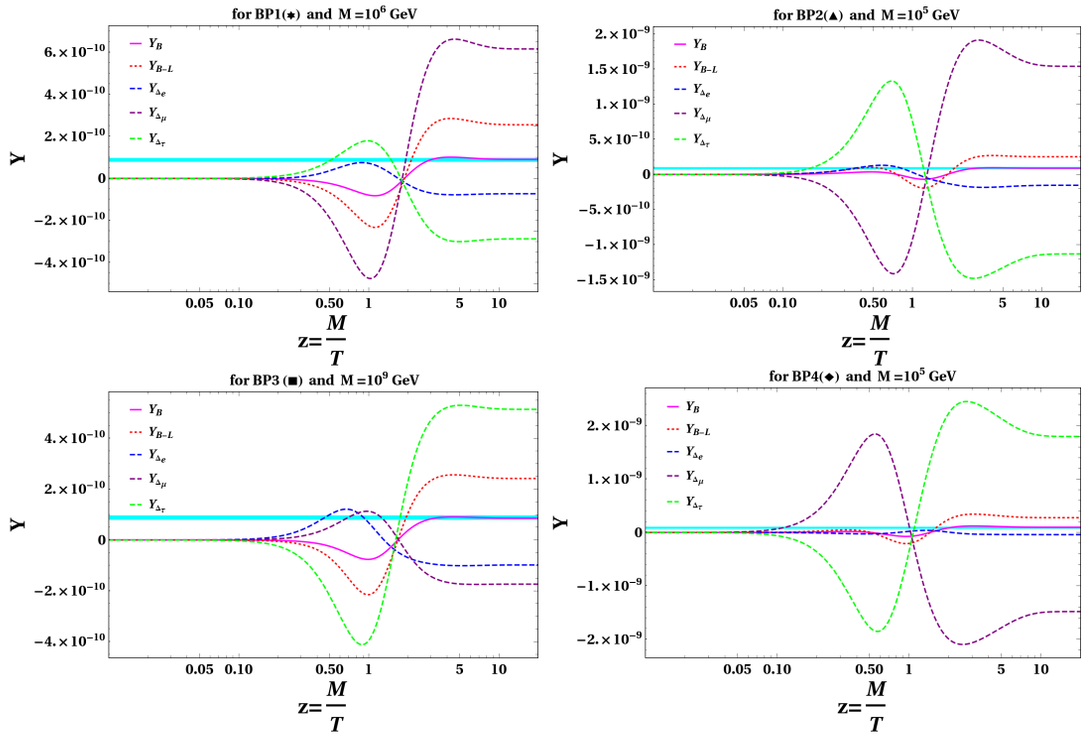

Figure 2.7: Variation of Y_B, Y_{B-L}, Y_{Δ_e}, Y_{Δ_μ}, $Y_{\Delta\tau}$ (denoted by solid magenta, dotted red, dashed blue, dashed pink and dashed green lines respectively) presented as function of $z = M/T$. Here we have considered one benchmark point from each of the four patches of γ_2 vs γ_1 plot for the light neutrino parameters of the model (from Fig. 2.1).

benchmark values of M are so chosen that they can produce requisite amount of baryon asymmetry corresponding to a specific choice of parameters: $\{\chi_1, \chi_2, \gamma_1, \gamma_2\}$.

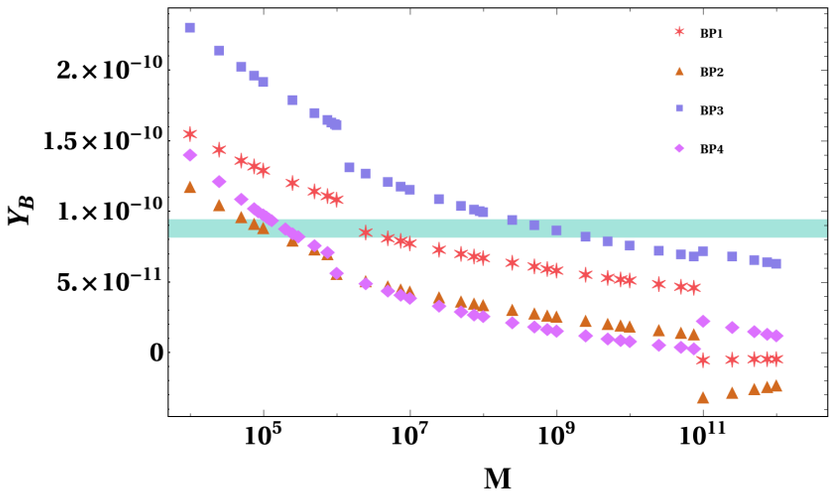

Figure 2.8: Variation of final Y_B $w.r.t.$ M (neglecting $\Delta L = 2$ processes) for four benchmark point BP1, BP2, BP3, BP4, from each of the four patches of γ_2 vs γ_1 plot for the light neutrino parameters of the model (from Fig. 2.1). Here the horizontal patch (light greenish-blue) indicates the observed value of baryon asymmetry [59].

In Fig. 2.7, we present our findings in terms of estimate of the evolution of the $B - L$ asymmetry (denoted by red dotted line) as well as B asymmetry (denoted by Magenta solid line) for specific choices of the parameters $\{\chi_1, \chi_2, \gamma_1, \gamma_2\}$ which correctly produce neutrino data as discussed in Section 2.3. Upper left, Upper right, lower left and lower right panel of Fig. 2.7 represent the benchmark points BP1, BP2, BP3, and BP4 respectively from the

allowed cornered patches of γ_1 and γ_2 plot of Fig. 2.1. Asymmetries of individual flavors are also drawn in these figures.

While solving the Boltzmann equations, we have assumed that initially there were no RHNs in the bath. Then due to annihilation of bath particles it gets produced and comes to equilibrium. Around $\frac{M}{T} \sim 1$, the production rate and decay rate of the RHN become almost equal and afterward the decay rate dominates over the production rate and hence it's abundance starts to fall. The correct baryon asymmetry can be produced with $M \sim 10^6$ GeV for BP1, $M \sim 10^5$ GeV for BP2 and BP4, $M \sim 10^9$ GeV for BP3 region respectively. For these individual sets of parameters, we have checked the variation of final baryon asymmetry, Y_B, $w.r.t.$ mass of M as shown in Fig. 2.8. From this Fig. 2.8, we also see that final Y_B is increasing with the decreasing of M. There seems to be two discontinuities for each such plot. For example, with blue-dotted line, these are observed at or around $M \sim 10^{11}$ GeV and at $M \sim 10^6$ GeV. These are indicative of the eras where different flavors of lepton doublets enter in (or exit from) equilibrium and the Boltzmann equations get modified.

2.5 Summary

In this analysis, we present an economical, predictive flavor symmetric setup based on $A_4 \times Z_3 \times Z_2$ discrete group to explain neutrino masses, mixing via type-I seesaw mechanism while matter-antimatter asymmetry is also addressed via leptogenesis. In the original AF model, TBM mixing scheme was realized introducing three flavon fields. With similar fields content, here we show that correct neutrino mixing and mass-squared differences are originated from non-trivial structure of the neutrino Dirac Yukawa coupling and diagonal RHN mass matrix, thanks to the contribution from the charged lepton sector too. In particular, the antisymmetric contribution in the Dirac Yukawa coupling plays an instrumental role in generating the non-zero θ_{13}. Using the current experimental observation on neutrino oscillation and other cosmological limits, we find the allowed parameter space for parameters $\chi_1, \chi_2, \gamma_1, \gamma_2$ which in turn not only restricts some of the observables associated to neutrinos like Dirac CP phase, neutrino-less double beta decay, lepton flavor violating decays, estimation of Majorana phases etc. but also are helpful in determining the matter-antimatter asymmetry of the universe. More specifically, we find that this model is highly predictive in nature. Only normal mass hierarchies are found to be allowed in the current setup. Interestingly the atmospheric mixing angle θ_{23} lies in the lower octant while the leptonic Dirac CP phase falls within the range $33°(213°) \lesssim \delta \lesssim 80°(260°)$ and $100°(280°) \lesssim \delta \lesssim 147°(327°)$. Apart from these predictions for absolute neutrino mass and effective mass parameter appearing the neutrino-less double beta decay have also been made. The model also predicts an interesting correlation between the atmospheric mixing angle θ_{23} and the Dirac CP phase which is a feature of the specific flavor symmetry considered here. At high scale, owing to the symmetry of the model, the heavy RHNs are found to be exactly degenerate apparently forbidding the generation of baryon asymmetry via leptogenesis. However, this is accomplished here elegantly by considering the renormalization group effects into the picture. A tiny mass splitting produced as a result of running from a high scale (GUT scale) to the scale of RHN mass opens the room for leptogenesis. We have incorporated the flavor effects in

leptogenesis as our working regime of RHN mass falls near or below 10^9 GeV. Finally, we figure out that the parameter space allowed by the neutrino data in fact is good enough to generate sufficient amount of baryon asymmetry of the universe with RHN mass as low as 10^5 GeV.

Chapter 3

Connecting Dark Matter with Flavor Leptogenesis

3.1 Introduction

The previous chapter discusses a scenario where high scale flavor symmetry breaking influences the lepton asymmetry production. More precisely, it provides one way to explain the special features of neutrino mixing angles and mass differences by supplying a uniqure structure of neutrino, charged lepton Yukawa and RHN mass matrices which eventually constraint the lepton asymmetry production. However, in modern particle physics and cosmology, another pressing issue which requires BSM explanations is the nature of DM. In this chapter, we provide two separate frameworks, where existance of DM can be connected to the problems associated to the neutrino mass and baryon asymmetry of the Universe. In order to achive this goal, we divide the chapter into two sections. In the section 3.2, we provide the most minimal model within the framework of the type-I seesaw mechanism where from a single structure of neutrino Yukawa matrix existence of DM and matter-antimatter asymmetry can be explained. In the section 3.3, we explore the type-II seesaw framework and find a direct influence of a different kind of DM on the production of CP asymmetry which eventually affects the flavor leptogenesis mechanism.

3.2 Imprint of Seesaw on FIMP Dark Matter and Flavor Leptogenesis

Among the various unresolved issues of present day particle physics and cosmology, perhaps the most pressing ones are the origin of tiny neutrino mass[33, 34, 116], nature of DM [15, 16] and observed matter-antimatter asymmetry of the universe [59]. In order to address these issues one has to anyway go beyond the SM of particle physics, hence it would be very pertinent to search for a single minimal framework that can accommodate all these three problems together. To start with, one notices that the type-I seesaw mechanism[40, 43–46] of neutrino mass generation provides a very promising platform for this. As discussed earlier, in this mechanism, three additional heavy SM singlet RHNs are added to the SM particle content. A handful of attempts has been made in identifying one of them as DM without including any further beyond the SM fields and symmetries. For example in the original

νMSM model[184, 185], the lightest RHN (say N_1) is shown to be the DM having mass $\sim \mathcal{O}$ (keV). While the production of DM proceeds via Dodelson-Widrow (DW) mechanism[186] incorporating the effective active-sterile neutrino mixing θ_1, the ARS mechanism[187] takes care of the observed baryon asymmetry via coherent oscillations of heavy RHNs. It turns out that the DW mechanism cannot make up the entire DM relic density taking into account the existing recent constraints on θ_1 [188–194]. However, a variant of this incorporating a resonant production of DM via Shi-Fuller mechanism[195] can still be operative [195, 196]. Though it bypasses the constraint on the mixing angle θ_1, the mechanism suffers from an un-natural level of degeneracy required between the two heavy RHNs $N_{2,3}$. Most of the other constructions with aim of identifying the RHN sector serving as the origin of DM and baryon asymmetry require additional fields and/or enhanced symmetry[197, 198].

In this section (based on [152]), we stick to the most minimal construction of type-I seesaw while identifying N_1 as the feebly interactive massive particle (FIMP)[73, 75] type of DM and rest of RHNs are mainly responsible for generating light neutrino mass and matter-antimatter asymmetry. Interestingly we find that a sufficient production of N_1 can be obtained from the decays of W, Z and SM Higgs h which are intricately related to the specific entries of neutrino Yukawa matrix, Y_ν and in turn depend on the lightest active neutrino mass (m_1). These entries, being involved in generating the respective active-sterile mixing θ_1 associated to N_1, also control possible decays of N_1. It turns out that an interplay between the production and decays of N_1 (such that it remains stable over the cosmological time scale) fixes the allowed range of DM mass (M_1) consistent with the stringent limits on θ_1.

The importance of this work lies in the fact that it provides perhaps the most minimal platform in the literature to address neutrino mass, DM and matter-antimatter asymmetry where the small coupling usually required for a FIMP realization is connected to the smallness of the lightest active neutrino mass m_1. Such a connection is presented here for the first time to the best of our knowledge. It indicates an upper limit on m_1 as $m_1 \lesssim \mathcal{O}(10^{-12})$ eV. Interestingly, we find the DM relic turns out to be effectively independent of the DM mass within its allowed range. This opens up the possibility that the scenario can be tested if the recent and future experiments can measure m_1. As masses of $N_{2,3}$ ($M_{2,3}$) are unconstrained at this stage, we find that imposing an additional constraint on Y_ν as $\text{Tr}[Y_\nu^\dagger Y_\nu] < \mathcal{O}(1)$ (justified later) restricts the production of N_1 from the decays of $N_{2,3}$. This ambiguity of fixing $M_{2,3}$ is resolved once we incorporate flavor leptogenesis[104–107].

3.2.1 Setup

We start with the conventional type-I seesaw Lagrangian (in charged lepton diagonal basis) involving SM lepton (l_L) and Higgs (H) doublets by

$$-\mathcal{L}_{\text{Int}} = (Y_\nu)_{\alpha i} \bar{l}_{L_\alpha} \widetilde{H} N_i + \frac{1}{2} M_i \overline{N_i^c} N_i + h.c., \tag{3.1}$$

with $i = 1, 2, 3$ and $\alpha = e, \mu, \tau$. We assume the RHN mass matrix M as diagonal with hierarchical masses. As a result of the electroweak (EW) symmetry breaking, the light neutrino mass matrix is given by the seesaw formula, $m_\nu = -m_D M^{-1} m_D^T$ which is diag-

onalized by $U^\dagger m_\nu U^* = \text{diag}\ (m_1, m_2, m_3) \equiv\ D_m$, where U is the PMNS matrix [165] and $(m_D)_{ij} = (Y_\nu)_{ij} v/\sqrt{2}$, where $v = 246$ GeV.

3.2.2 Production of DM

To begin with, we consider mass of the DM to be lighter than the W boson mass (m_W) so that possibility of its production from decays of the SM gauge bosons (via active-sterile neutrino mixing) and Higgs (via neutrino Yukawa interaction) remains plausible. On the other hand, masses of the remaining RHNs are assumed to be above the EW scale. Considering the fact that decay of N_1 can even proceed via the relevant active-sterile neutrino mixing $m_{Di1}/M_1 \equiv V_{i1}$, we propose the following structure of neutrino Yukawa matrix at the leading order

$$Y_\nu = \begin{pmatrix} \boxed{\begin{matrix} 0 \\ 0 \\ 0 \end{matrix}} & \boxed{\begin{matrix} y_{e2} & y_{e3} \\ y_{\mu 2} & y_{\mu 3} \\ y_{\tau 2} & y_{\tau 3} \end{matrix}} \end{pmatrix}. \tag{3.2}$$

As a result of the vanishing left block (L_B), N_1 remains completely decoupled and hence absolutely stable while $N_{2,3}$ along with the right block (R_B) entries of Y_ν generate light neutrino mass via seesaw. This also ensures that the lightest active neutrino mass m_1 becomes zero and a vanishing V_{i1} results. The entries of Y_ν can be written using the Casas-Ibarra (CI) parametrization [199]:

$$m_D = -i\, U D_{\sqrt{m}} \mathbb{R}^T D_{\sqrt{M}}, \tag{3.3}$$

where U is the PMNS [200] mixing matrix, D_m ($D_M = M$) is the diagonal active neutrino (RHN) mass matrix and $\mathbb{R}$ is a complex orthogonal matrix chosen to be of the form,

$$\mathbb{R} = \begin{pmatrix} 1 & 0 & 0 \\ 0 & \cos\theta_R & \sin\theta_R \\ 0 & -\sin\theta_R & \cos\theta_R \end{pmatrix}, \tag{3.4}$$

where θ_R is a complex angle in general. We employ the best fitted values [201] of mixing angles, CP phase as well as mass-square differences to define the U and $D_{\sqrt{m}}$.

Under such a situation, N_1 being completely segregated cannot be produced by any interaction (except gravitational one perhaps). This problem can be circumvented by perturbing m_D, *i.e.* introducing small but nonzero entries in $\text{L}_B = (\epsilon_1, \epsilon_2, \epsilon_3)^T$ with $\epsilon_{i=1,2,3} \ll 1$. The order of smallness will be determined from the relic satisfaction of DM as well as from the stability of N_1. Note that origin of these ϵ_i can be associated[1] to a tiny m_1 or an additional angle of rotation (say φ) over $\mathbb{R}$ or including both. In this work, without any loss of generality, we would like to pursue our analysis with small m_1 as the same result can be obtained from the use of φ. In this case, following Eq.(3.3), it is seen that ϵ_i turns out to be proportional to

[1] Alternatively, a tiny m_1 can be considered as an artifact of very small ϵ_i.

$\sqrt{m_1 M_1}$. The DM phenomenology is almost independent to R_B of Y_ν.

With such a scenario in mind, the active neutrinos and $N_{2,3}$ remain in thermal equilibrium with other SM fields while N_1 is expected to be in out-of-equilibrium (due to its small coupling proportional to ϵ_i) in the early universe having negligible abundance. Later, once the temperature goes down, the DM is expected to be produced non-thermally from decay of some massive particle or via annihilations. In this simplest seesaw set-up, we find subsequent to the EW symmetry breaking, the DM N_1 can be produced from the following dominant decays:

$$W^\pm \to N_1 \ell_i^\pm, \quad Z \to N_1 \nu_i, h \to N_1 \nu_i; \quad N_{i\neq 1} \to N_1 h(Z).$$

The relevant parts of the Lagrangian responsible for the above decays via the active sterile mixing $V = m_D M^{-1}$ are followed from the gauge interactions

$$-\mathcal{L}_{\mathcal{G}} \subset \frac{g}{\sqrt{2}} W_\mu^+ \sum_{i,j=1}^{3} \Big[\bar{N}_i^c (V^\dagger)_{ij} \gamma^\mu P_L \ell_j\Big] + \frac{g}{2C_{\theta_w}} Z_\mu \sum_{i,j=1}^{3} \Big[\bar{\nu}_i (U^\dagger V)_{ij} \gamma^\mu P_L N_j^c + \bar{N}_i^c (V^\dagger V)_{ij} \gamma^\mu P_L N_j^c\Big] + h.c., \tag{3.5}$$

and Yukawa interactions

$$-\mathcal{L}_{\mathcal{Y}} \subset \frac{\sqrt{2}}{v} h \sum_{i,j=1}^{3} \Big[\bar{\nu}_i (U^\dagger V)_{ij} M_j N_j + \bar{N}_i^c (V^\dagger U)_{ij} m_j \nu_j^c + \bar{N}_i^c (V^\dagger V)_{ij} M_j N_j\Big] + h.c., \tag{3.6}$$

where ν_i are active neutrino mass eigenstates. Origin of the most relevant mixing $V_{i1} = m_{Di1}/M_1$ ($\equiv \epsilon_i \frac{v}{\sqrt{2}M_1}$) is traced back to ϵ_i entries of Y_ν.

We then employ the coupled set of Boltzmann equations involving N_1 and $N_{2,3}$ separately to study the evolution of their abundance (Y_{N_i}) till the present time, as

$$\frac{dY_{N_1}}{dz} = \frac{2M_{pl} z}{1.66 m_h^2} \frac{g_\rho^{1/2}}{g_s} \Big[\sum_{i=2,3} \Big(Y_{N_i} \sum_{x=Z,W} \langle \Gamma_{N_i \to N_1 x}\rangle\Big) + \sum_{x=Z,h} Y_x^{eq} \langle \Gamma_{x\to N_1 \nu}\rangle + Y_W^{eq} \langle \Gamma_{W^\pm \to N_1 \ell^\pm}\rangle\Big], \tag{3.7}$$

$$\frac{dY_{N_i}}{dz} = -\frac{2M_{pl} z}{1.66 m_h^2} \frac{g_\rho^{1/2}}{g_s} \Big[(Y_{N_i} - Y_{N_i}^{eq}) \langle \Gamma_{N_i}\rangle + Y_{N_i} \sum_{x=h,Z} \langle \Gamma_{N_i \to N_1 x}\rangle\Big], \ (i = 2, 3), \tag{3.8}$$

with $z = m_h/T$. Here $\Gamma_{N_i} = \sum_\alpha \Gamma(N_i \to l_\alpha H) + \Gamma(N_i \to \bar{l}_\alpha \bar{H}) = \frac{M_i}{8\pi v^2} (m_D^\dagger m_D)_{ii}$ and $\langle \Gamma_{A\to BC}\rangle$ represents the thermally averaged decay width[74]. All relevant decay widths are obtained from Eqs. (3.5)-(3.6). Note that the annihilations producing N_1 are very much suppressed ($\sim \epsilon_i^4$) compared to decay ($\sim \epsilon_i^2$) and hence are not included. At this stage, we presume N_1 to be stable over the cosmological time scale which will be justified in a while. Back reactions involving N_1 are not included as N_1 number density is vanishingly small to start with and for the same reason, terms proportional to Y_{N_1} are also dropped. Substituting

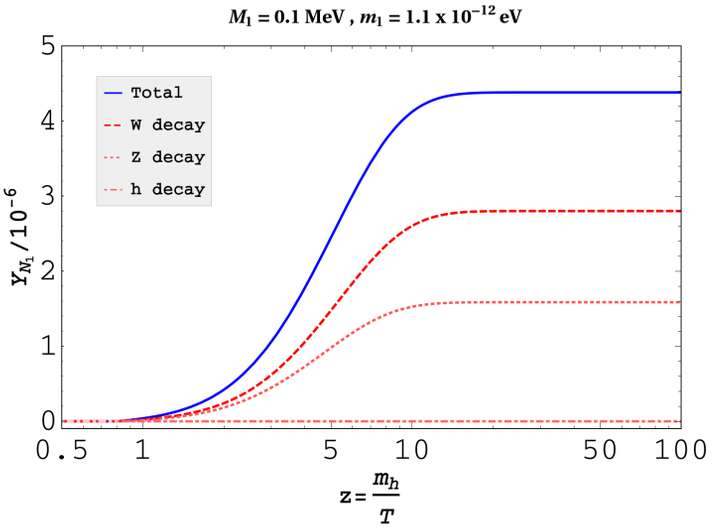

Figure 3.1: Abundance plot of N_1 with individual contributions (explained in inset) from different decays; final abundance (solid blue line) corresponds to the correct DM relic.

the abundance $Y_{N_1}(z_\infty)$ after freeze-in, the relic density is obtained from,

$$\Omega_{N_1}\mathrm{h}^2 \;=\; 2.755\times 10^5\left(\frac{M_1}{\mathrm{MeV}}\right)Y_{N_1}(z_\infty). \tag{3.9}$$

The variation of the DM abundance Y_{N_1} as function of z is shown in Fig.3.1 where Y_{N_1} (combined contribution as denoted by the solid blue line) reaches an asymptotic value, $Y_{N_1}(z_\infty)$, so as to obtain the correct relic, $\Omega_{N_1}\mathrm{h}^2 = 0.12$ [17] via Eq. (3.9). Note that, we have parameters $m_1, M_{1,2,3}$ and θ_R. In generating this plot, we have fixed M_1 at 0.1 MeV while $M_{2(3)}$ are kept at 3.5 (75) $\times 10^9$ GeV as deemed fit for generating correct baryon asymmetry via leptogenesis (discussed later). With such a choice of M_1, $m_1 \sim 1.1\times 10^{-12}$ eV is found to satisfy the relic implying $|\epsilon_i| \sim 10^{-15}$. We find that the production of N_1 is dominated by the decay of gauge bosons, in particular by $W^\pm$ decay[2], as emphasized in Fig.3.1. The reason is the following. The production of N_1 from gauge and Higgs bosons depends on ϵ_i elements of Y_ν only (via V) whereas N_1 production[3] from decay of $N_{2,3}$ involves a product of ϵ_i of L_B and elements of R_B (via $V^\dagger V$) as seen from Eqs. (3.5)-(3.6). While entries of L_B are generated from m_1, elements of R_B are controlled by the magnitude of θ_R, mostly by $\mathrm{Im}[\theta_R]$. We find that any value of $\mathrm{Im}[\theta_R] \lesssim 5$ keeps R_B entries (or more precisely $\mathrm{Tr}[Y_\nu^\dagger Y_\nu]$) below $\mathcal{O}(1)$. We also notice that with larger $\mathrm{Im}[\theta_R]$, entries of R_B would increase significantly. Such a large Y_ν would be problematic not only from perturbativity but also due to the fact that EW vacuum becomes unstable [204]. Since DM production except from $N_{2,3}$ decays are anyway independent to entries of R_B, we refrain from quoting specific value for $\mathrm{Re}[\theta_R]$ at this moment and reserve the related discussion for the leptogenesis part.

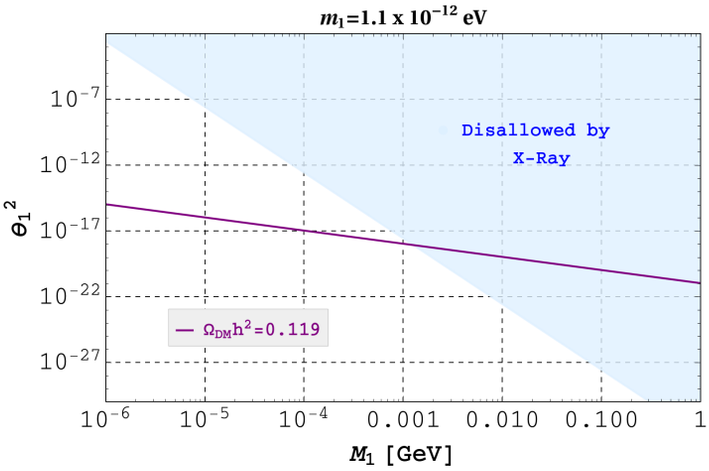

Figure 3.2: Relic satisfaction contour (solid purple line) in $\theta_1^2 - M_1$ plane. Constraint on θ_1^2 from X-ray observation due to $N_1 \to \gamma\nu$ decay excludes the blue shaded region.

3.2.3 Decay of dark matter

As the DM N_1 mixes with the SM fields via the active-sterile mixing angle V_{i1}, we need to look for the all possible decay channels of it. There are following decay channels:

(a) [via off shell W/Z]: $N_1 \to l_1^- l_2^+ \nu_{l_2}$, $N_1 \to l^- q_1 \bar{q}_2$, $N_1 \to l^- l^+ \nu_l$, $N_1 \to \nu_l \bar{l}' l'$, $N_1 \to \nu_l q\bar{q}$, $N_1 \to \nu_l \nu_{l'} \bar{\nu}_{l'}$, $N_1 \to \nu_l \nu_l \bar{\nu}_l$,

(b) [via off-shell Higgs]: $N_1 \to \nu_\ell \bar{\ell}\ell$,

(c) [radiative decay of N_1]: $N_1 \to \gamma\nu$.

Keeping in mind that the expected lifetime of N_1 must be greater than the age of the universe, it turns out that the most stringent constraint is obtained from (c), which can be translated on the active-sterile neutrino mixing V_{i1} as [205–207],

$$\theta_1^2 \;=\; \sum_{i=1,2,3} |V_{i1}|^2 \leq 2.8 \times 10^{-18} \left(\frac{\text{MeV}}{M_1}\right)^5, \tag{3.10}$$

Below in Fig.3.2, we generate the relic contour plot in the $\theta_1^2 - M_1$ plane drawn as the solid purple line, while the region in light blue is excluded from the above constraint. So at this point, we find N_1 as a successful FIMP type DM having mass below MeV. It is also interesting to note that the final DM relic density is independent to the mass of N_1. This observation stems from the fact that (a) the crucial parameter responsible for generating the DM abundance is $\epsilon_i \propto \sqrt{m_1 M_1}$ and (b) the dominant production of N_1 is from W and Z decays. The corresponding decay width (and hence Y_{N_1} also) turns out to be proportional to m_1/M_1 (see Eq. (3.5)). Then the final relic density $\Omega_{N_1}h^2$ being related to $M_1 Y_{N_1}$, the M_1 dependence is cancelled out and m_1 is uniquely fixed to satisfy the relic. This leads to an interesting prediction for lightest active neutrino mass $\sim (1.07-1.12)\times 10^{-12}$ eV (considering the 3σ range of DM relic density) so that the model remains falsifiable in nature. Off course

[2] In [74, 202], contributions of $W^\pm$ in N_1 production are estimated in the context of different extensions (gauge and/or fields) of the minimal set-up with SM and three RHNs.

[3] In a recent study [203], it is shown that production of N_1 having mass in 1-80 keV range from $N_{2,3}$ can satisfy the relic.

if one incorporates effect of both m_1 and the extra rotation φ, this value of m_1 serves as the upper limit of lightest neutrino mass.

We have verified that the non-thermality condition $\Gamma/\mathcal{H} < 1$ at $T \sim m$ is satisfied where Γ corresponds to the relevant decay width for a particular production channel of N_1 and m is mass of the decaying particle. Hence the DM particles produced (having mass range 1 keV - 1 MeV) cannot have sufficient energy to be associated with large free streaming length, thereby treated as cold DM, in contrary to the DW mechanism associated to warm DM ($\sim$ 2-10 keV). The lower limit on M_1 is considered as 1 keV to be in consistent with Tremaine–Gunn bound [208] on sterile neutrino mass. A detailed study on the nature of DM in this range is beyond the scope of the letter. Finally, considering all these constraints, the range of DM mass turns out to be restricted within 1 keV-1 MeV.

3.2.4 Lepton asymmetry generation

We now proceed to discuss the role of two other heavier RHNs, $N_{2,3}$ and their cosmological evolution. While they help in realizing the correct order of light neutrino mass and mixing, we find their contribution to DM production is almost negligible. That being said, their masses can be anywhere between a few hundred GeV to a very large scale. However, considering the fact that their decay can explain baryon asymmetry of the universe via leptogenesis, we can now have a complete picture including neutrino mass, DM and lepton asymmetry which will also tell us about these otherwise unspecified mass scales.

Being heavier than the Higgs mass, $N_{2,3}$ are expected to decay into lepton doublet and Higgs via the Yukawa interaction of Eq.(3.1). This out of equilibrium decay along with the CP violation present in Y_ν will be crucial in leptogenesis. Note that Im$[\theta_R]$ serving as the source of CP violation via Eq. (3.3), apart for a subdominant contribution from Dirac CP phase in U, is the same one which mostly restricts the production of DM from the decay of $N_{2,3}$ while in tension with the EW vacuum stability.

It is preferable to keep the heavy neutrino masses as low as possible in view of naturalness of hierarchy within RHNs, and hence we opt for flavor leptogenesis here. As $M_2 < M_3$, the CP asymmetry ε_2^α is effectively generated from the decay of N_2 to a specific flavor l_α. Using the standard expression presented in Eq. 1.79, we evaluate ϵ_2^α first and then proceed for estimating the final lepton asymmetry employing the set of Boltzmann equations similar to Eq. (1.83) and Eq. (1.94)[4]:

$$sHz'\frac{dY_{N_2}}{dz'} = -\left\{\left(\frac{Y_{N_2}}{Y_{N_2}^{\rm eq}}-1\right)(\gamma_{D_2}+2\gamma_{H_s^2}+4\gamma_{H_t^2})\right\}, \tag{3.11}$$

$$\begin{aligned} sHz'\frac{dY_{\Delta_\alpha}}{dz'} = -\Bigg\{&\left(\frac{Y_{N_2}}{Y_{N_2}^{\rm eq}}-1\right)\varepsilon_2^\alpha\gamma_{D_2} + K_\alpha^{0,2}\sum_\beta\left[\frac{1}{2}(C_{\alpha\beta}^\ell + C_\beta^H)\gamma_{D_2} + \left(\frac{Y_{N_2}}{Y_{N_2}^{\rm eq}}-1\right)\right. \\ &\left.\times\left(C_{\alpha\beta}^\ell\gamma_{H_s^2} + \frac{C_\beta^H}{2}\gamma_{H_t^2}\right) + \left(2C_{\alpha\beta}^\ell + C_\beta^H\right)\left(\gamma_{H_t^2}+\frac{1}{2}\gamma_{H_s^2}\right)\right]\frac{Y_{\Delta_\beta}}{Y^{\rm eq}}\Bigg\} \end{aligned} \tag{3.12}$$

where $K_\alpha^{0,2} = \frac{(Y_\nu^*)_{\alpha 2}(Y_\nu)_{\alpha 2}}{(Y_\nu^\dagger Y_\nu)_{22}}$ is the same flavor projector presented below Eq. (1.94), how-

[4]However, now all the relevant interactions will be associated with N_2.

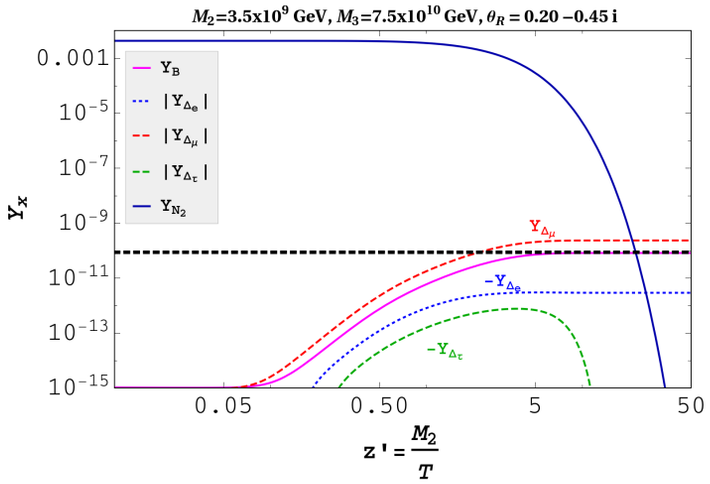

Figure 3.3: Evolution of individual flavor asymmetries as well as baryon asymmetry $w.r.t.\ z' = M_2/T$. Black dashed lines: range of observed baryon asymmetry of the universe.

ever now represents for N_2 decay processes. The final baryon asymmetry is obtained as $Y_B = (28/79)\sum_\alpha Y_{\Delta_\alpha}$.

Fig.3.3 depicts the variation of individual components of lepton asymmetry Y_{Δ_α} as well as the total baryon asymmetry Y_B $w.r.t.$ $z' = M_2/T$. It turns out that the observed baryon asymmetry results for the lowest possible value of $M_2 = 3.5(5) \times 10^9$ GeV with Re$[\theta_R]$ = 0.2(0) and Im$[\theta_R]$ = -0.45 (-0.4). The corresponding value of M_3 is found to be 7.5 (15) $\times 10^{10}$ GeV. At this temperature range $\sim M_2$ value, muon and tau Yukawa interactions come to equilibrium and hence lepton asymmetries along all the flavor directions become relevant (see Fig.3.3). We also infer from Fig.3.3 that the abundance of Y_{N_2} with such a large M_2 is falling sharply as temperature decreases and hence is expected to be vanishingly small in the EW broken phase where N_1 production is mainly taking place from the decay of the SM gauge bosons. This along with the fact that production of N_1 from N_2 decay is also suppressed (via $V^\dagger V$ as stated earlier) eventually indicate that N_2 contributes effectively nothing to N_1 production as seen from the right hand side of Eq. 3.7 (first term). The same conclusion holds for N_3 as well.

3.2.5 Summary

In summary, we have shown that the conventional type-I seesaw scenario itself has the potential to offer a FIMP type of DM in the form of lightest RHN, the relic density of which is mainly governed by decay of the SM gauge bosons in the electroweak symmetry broken phase. With the hypothesis that in the limit of zero lightest active neutrino mass the DM is absolutely stable, implies that production and stability of the DM both are effectively controlled by the tiny active neutrino mass. The proposal predicts an upper bound on this lightest neutrino mass as $m_1 \lesssim \mathcal{O}(10^{-12})$ eV which makes it falsifiable if ongoing (or future) experiments such as KATRIN [209] and PROJECT-8 collaboration [210] succeed to probe it. In this way, the smallness of couplings involved in a generic FIMP type model, related to DM production, can now be connected with the lightness of active neutrino mass m_1. While we find the DM mass $\sim$ 1 keV- 1 MeV satisfies the correct relic density as well as the stringent limits from X-ray observation, the DM phenomenology does not restrict the

mass scales of two other heavy RHNs. Then we incorporate the flavor leptogenesis scenario to show that they can be $\sim 10^{9-10}$ GeV to explain the baryon asymmetry of the universe. So the minimal set-up of type-I seesaw can simultaneously address the origin of neutrino mass, non-thermal production of DM and matter-antimatter asymmetry without any additional fields.The presence of active-sterile neutrino mixing in the set-up is suggestive of the rare lepton flavor violating decays. The most relevant branching ratio in this context is related to $\mu \to e\gamma$ which turns out to be function of active-sterile neutrino mixing V as well as RHN masses M_i. Employing values of M_i (used in producing Fig.3.1 or Fig. 3.3) and corresponding V elements, the branching ratio of $\mu \to e\gamma$ is found to be negligibly small compared to the present experimental limit [211]. We also evaluate the effective neutrino mass parameter involved in the half-life of neutrinoless double beta decay (function of m_i, lepton mixing angles and phases) and find it to be insignificant.

3.3 Scalar triplet flavor leptogenesis with dark matter

As discussed above and earlier chapters, in case of type-I seesaw framework, [40, 43–45] presence of SM singlet RHNs not only helps in generating tiny neutrino mass but they can also be responsible for explaining the observed matter-antimatter asymmetry via leptogenesis [77, 95, 171, 212–220]. A variant of it, namely the type-II seesaw construction [46–50] also provides an equally lucrative resolution by introducing a $SU(2)_L$ scalar triplet to the SM field content whose tiny vev takes care of the small neutrino mass. However, to generate the baryon asymmetry of the Universe via leptogenesis, this minimal type-II framework needs to be extended either with another triplet [221–224] or by a singlet right-handed neutrino [225–230]. In the latter possibility, the role of the single RHN is to contribute to CP asymmetry generation via the vertex correction (in the triplet decay) provided it carries a Yukawa interaction with the SM Higgs and lepton doublets.

Additionally, several astrophysical and cosmological observations indicate that energy budget of our Universe requires around 26% of non-baryonic matter, known as the DM [14–16, 231]. To explain such DM, an extension of the SM is required as otherwise it fails to accommodate any such candidate from its own particle content. Since all these unresolved issues (tiny neutrino mass, matter-antimatter asymmetry and nature of DM) point out toward extension(s) of the SM, it is intriguing to establish a common platform for them. With this goal in mind, we focus on the SM extended with a scalar triplet and a fermion singlet (like one RHN). While this can explain the neutrino mass and matter-antimatter asymmetry as stated above, accommodating a DM in it is not that obvious. One simplest possibility emerges if that singlet fermion (the RHN) can be considered as the DM candidate. However, as pointed out above, this fermion taking part in the CP asymmetry generation has to carry an Yukawa interaction (of sizable strength) and hence can't be stable provided its mass remains above the electroweak (EW) scale. On the other hand, if it happens to be lighter than the SM Higgs (or gauge bosons), it might be a freeze in type of DM [152]. In this case also, the small Yukawa coupling, as required by the freeze-in generation of DM relic, makes the CP asymmetry negligible and therefore such a possibility needs to be left out.

We thereby plan to extend this framework by including an inert Higgs doublet (IHD)

[232–248] such that its lightest neutral component results in DM while the IHD too contributes to CP asymmetry generation via its Yukawa interaction involving the SM lepton doublet and the sole RHN. Involvement of the DM in generating the CP asymmetry required for explaining the matter-antimatter asymmetry of the Universe is an important aspect of our work. Note that the inert doublet DM phenomenology is mostly governed by the gauge interactions and the mass-splitting among the inert Higgs doublet components, but not on the Yukawa interaction [242] (contrary to the case of freeze-in RHN as DM) and hence it is not expected to be in conflict with sufficient production of CP asymmetry. Furthermore, search for doubly and singly charged particles involved in the triplet can be quite interesting from collider aspects. Keeping that in mind, we plan to keep the mass of the triplet not very heavy. It is further supported by the finding that the mass splitting among the IHD components (for DM relic satisfaction) along with the neutrino mass generation dominantly by the type-II mechanism keeps the triplet mass below 10^{12} GeV. Note that it becomes essential to incorporate the flavor effects in leptogenesis [104–107, 145, 152, 228] which come in to effect below the mass equivalent temperature $\sim 10^{12}$ GeV. This observation, importance of including flavor effects in triplet leptogenesis, is another salient feature of our analysis.

This section is organized in the following manner. We introduce the structure of the model in subsection 3.3.1 where the particle content with their respective charges under different symmetry group have been discussed. In subsection 3.3.2, we discuss the mechanism to generate the neutrino mass and how to get a complex structure of the Yukawa coupling matrix responsible for generating the matter-antimatter asymmetry. In subsection 3.3.3, we briefly summarize the inert doublet DM phenomenology and move on to discuss generation of matter-antimatter asymmetry in the Universe via flavor leptogenesis in subection 3.3.4. Finally in subection 3.3.5, we conclude.

3.3.1 The Model

The SM is extended with a $SU(2)_L$ scalar triplet Δ, a scalar doublet Φ and a fermionic SM singlet field N_R. The corresponding charge assignments of the relevant fields are provided in Table 3.1. The Lagrangian involving the new fields is then given by

$$-\mathcal{L}_{new} = Y_\alpha \bar{\ell}_{L_\alpha} \widetilde{\Phi}\, N_R + Y_{\Delta\alpha\beta} \ell^T_{L\alpha} C i\tau_2 \Delta \ell_{L\beta} + \frac{1}{2} M_N \bar{N}^c_R N_R + h.c., \tag{3.13}$$

where α, β correspond to three flavor indices. Note that N_R and Φ are odd under an additional discrete symmetry Z_2, thereby making Φ as inert. This also forbids the Yukawa coupling of the SM Higgs with the RHN, however allows similar interaction with the inert Higgs doublet Φ. The lightest neutral component of this Φ field plays the role of the DM while decay of the triplet into lepton doublets generates the lepton asymmetry which will further be converted into baryon asymmetry by the sphaleron process. Here both the inert Higgs doublet and the RHN take part in producing the CP asymmetry.

	ℓ_L	e_R	H	N_R	Δ	Φ
$SU(2)_L$	2	1	2	1	3	2
$U(1)_Y$	$-\frac{1}{2}$	-1	$\frac{1}{2}$	0	1	$\frac{1}{2}$
Z_2	$+$	$+$	$+$	$-$	$+$	$-$

Table 3.1: Particles and their charges under different symmetries.

The scalar sector of our model consists of the interaction involving the inert Higgs doublet Φ, Higgs triplet Δ and the SM Higgs H. The most general scalar potential for the present scenario can be written as:

$$V(H,\Delta,\Phi) = V_H + V_\Delta + V_\Phi + V_{\rm int}, \tag{3.14}$$

where

$$\begin{aligned}
V_H &= \mu^2(H^\dagger H) + \lambda(H^\dagger H)^2, && \text{(3.15a)}\\
V_\Delta &= M_\Delta^2 \mathbf{Tr}(\Delta^\dagger\Delta) + \lambda_{\Delta 1}\mathbf{Tr}(\Delta^\dagger\Delta)^2 + \lambda_{\Delta 2}[\mathbf{Tr}(\Delta^\dagger\Delta)]^2, && \text{(3.15b)}\\
V_\Phi &= \mu_\Phi^2(\Phi^\dagger\Phi) + \lambda_\Phi(\Phi^\dagger\Phi)^2, && \text{(3.15c)}\\
V_{\rm int} &= -\mu_1(H^T i\tau_2\Delta^\dagger H + h.c) + \lambda_1 H^\dagger H\mathbf{Tr}(\Delta^\dagger\Delta) + \lambda_2 H^\dagger\Delta\Delta^\dagger H + \lambda_3 H^\dagger\Delta^\dagger\Delta H\\
&+ \lambda_4(H^\dagger H)(\Phi^\dagger\Phi) + \lambda_5(H^\dagger\Phi)(\Phi^\dagger H) + [\frac{\lambda_6}{2}(H^\dagger\Phi)^2 + h.c] - \mu_2(\Phi^T i\tau_2\Delta^\dagger\Phi + h.c)\\
&+ \lambda_7\Phi^\dagger\Phi\mathbf{Tr}(\Delta^\dagger\Delta) + \lambda_8\Phi^\dagger\Delta\Delta^\dagger\Phi + \lambda_9\Phi^\dagger\Delta^\dagger\Delta\Phi. && \text{(3.15d)}
\end{aligned}$$

Here we consider all the parameters appearing in the scalar potential to be real. We also consider $\mu^2 < 0$ as that would be crucial for electroweak symmetry breaking (EWSB). On the other hand, remaining mass parameters such as μ_Φ^2, M_Δ^2 are taken as positive. Denoting the vev of H and Δ by v (= 246 GeV) and v_Δ respectively, the multiplets after the EWSB can be expressed as

$$\Phi = \begin{bmatrix} \Phi^+ \\ \frac{H_0+iA_0}{\sqrt{2}} \end{bmatrix}, H = \begin{bmatrix} 0 \\ \frac{v+h}{\sqrt{2}} \end{bmatrix}, \Delta = \begin{bmatrix} \frac{\Delta^+}{\sqrt{2}} & \Delta^{++} \\ v_\Delta + \Delta^0 & -\frac{\Delta^+}{\sqrt{2}} \end{bmatrix}, \tag{3.16}$$

where h is the SM physical Higgs boson with mass 125.09 GeV [249] and the induced vev of the triplet is found to be related by [225]

$$v_\Delta \simeq \frac{v^2\mu_1}{2M_\Delta^2}, \tag{3.17}$$

considering $M_\Delta \gg v$. Interestingly, the constraint on ρ-parameter ($\rho = 1.00038 \pm 0.00020$) [250] restricts $v_\Delta \lesssim 4.8$ GeV. Note that v_Δ needs to be small enough to accommodate the tiny neutrino mass via $\Delta\ell_L\ell_L$ coupling and hence we fix it at 1 eV. Then depending on the mass of the Δ particle, μ_1 can be obtained by the use of Eq. (3.17). On the contrary, the analogous

coupling μ_2 remains unrestricted and hence can have a sizable value. This therefore will be treated as independent parameter for generating sufficient CP asymmetry as we see in the leptogenesis section.

The masses of the different physical scalars of IHD are given (unaffected by the presence of the triplet scalar) as

$$\begin{aligned} m^2_{\Phi^\pm} &= \mu^2_\Phi + \lambda_1 \frac{v^2}{2}, \\ m^2_{H_0} &= \mu^2_\Phi + (\lambda_4+\lambda_5+\lambda_6)\frac{v^2}{2}, \\ m^2_{A_0} &= \mu^2_\Phi + (\lambda_4+\lambda_5-\lambda_6)\frac{v^2}{2}. \end{aligned} \tag{3.18}$$

with $\lambda_L = \frac{\lambda_4+\lambda_5+\lambda_6}{2} > 0$. Without any loss of generality, we consider $\lambda_6 < 0$, $\lambda_5 + \lambda_6 < 0$ so that the CP even scalar (H_0) is the lightest Z_2 odd particle and hence the stable DM candidate. Due to the presence of the term proportional to μ_1, there will be a mixing between the SM Higgs and the triplet. However, the mixing being of order v_Δ (taken to be ~ 1 eV, responsible to generate light neutrino mass), this can safely be ignored. We set $\lambda_1, \lambda_2, \lambda_3 = 0$ for simplicity and then find masses of the physical triplet components as $M_{\Delta^{\pm\pm}} \simeq M_{\Delta^\pm} \simeq M_{\Delta^0} \simeq M_\Delta$. One should note that LHC puts a strong constraint on mass of $\Delta^{\pm\pm}$ as $M_{\Delta^{\pm\pm}} > 820$ GeV (870 GeV) at 95% C.L. from CMS [89] (ATLAS [88]) for $v_\Delta \lesssim 10^{-4}$ GeV. LHC also set a constraints on $M_{\Delta^\pm} > 350$ GeV.

3.3.2 Neutrino Mass

We now proceed to discuss the neutrino mass generation in the present model. As mentioned before, the neutrino mass is expected to be generated via the triplet interaction with the SM lepton doublets resulting the type-II contribution as

$$m_\nu^{\rm II} = 2 Y_\Delta v_\Delta. \tag{3.19}$$

With a choice of v_Δ as 1 eV, the coupling matrix Y_Δ can be accordingly adjusted to produce the light neutrino matrix (m_ν) consistent with the oscillation data. To make it more specific, we consider,

$$m_\nu = m_\nu^{\rm II} = U^* m_\nu^d U^\dagger, \tag{3.20}$$

with $m_\nu^d = {\rm diag}(m_1, m_2, m_3)$ and U is the PMNS mixing matrix (in the charged lepton diagonal basis) of the form:

$$U = \begin{pmatrix} c_{12}c_{13} & c_{13}s_{12} & e^{-i\delta}s_{13} \\ -c_{23}s_{12} - e^{i\delta}c_{12}s_{13}s_{23} & c_{12}c_{23} - e^{i\delta}s_{12}s_{13}s_{23} & c_{13}s_{23} \\ s_{12}s_{23} - e^{i\delta}c_{12}c_{23}s_{13} & -e^{i\delta}c_{23}s_{12}s_{13} - c_{12}s_{23} & c_{13}c_{23} \end{pmatrix} \times {\rm diag}(e^{i\alpha_1/2}, e^{i\alpha_2/2}, 1), \tag{3.21}$$

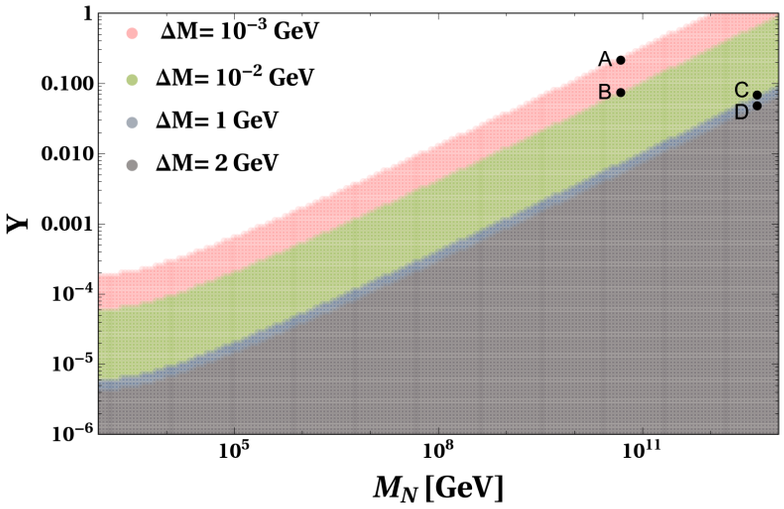

Figure 3.4: Allowed range of Y against M_N to keep $m_\nu^{\rm R}$ subdominant compared to $m_\nu^{\rm II}$.

parametrized by three mixing angles $\theta_{12}, \theta_{23}, \theta_{13}$ (denoted by $c_{ij} = \cos\theta_{ij}, s_{ij} = \sin\theta_{ij}$), the Dirac CP phase δ and Majorana CP phases (α_1, α_2).

For simplicity, we now consider Majorana phases and the lightest neutrino mass to be zero. Thereby, using the best-fit values of the mixing angles and δ [251] as in Table 2.2, we obtain the following structure of the coupling matrix (using Eq. (3.19)) in case of normal hierarchy (NH) of neutrinos,

$$Y_\Delta = \left(\frac{1eV}{v_\Delta}\right) \times 10^{-3} \times \begin{pmatrix} 1.84 + 0.27i & -1.31 - 0.75i & -3.76 - 0.64i \\ -1.31 - 0.75i & 15.94 - 0.08i & 10.90 + 0.0038i \\ -3.76 - 0.64i & 10.90 + 0.0038i & 12.09 + 0.07i \end{pmatrix} \tag{3.22}$$

We will make use of this Y_Δ in the rest of our analysis wherever appropriate.

Note that in our model, due to the presence of one RHN having Yukawa coupling Y, a radiative contribution to the light neutrino mass [252] is expected to be present which is given by

$$(m_\nu^{\rm R})_{\alpha\beta} = \frac{Y_\alpha Y_\beta M_N}{32\pi^2}\left[\frac{m_{H_0}^2}{m_{H_0}^2 - M_N^2}\ln\frac{m_{H_0}^2}{M_N^2} - \frac{m_{A_0}^2}{m_{A_0}^2 - M_N^2}\ln\frac{m_{A_0}^2}{M_N^2}\right]. \tag{3.23}$$

It is then understood that for a specific value of the DM mass, m_{H_0}, along with the mass splitting $\Delta M = m_{\Phi^\pm} - m_{H_0} = m_{A_0} - m_{H_0}$, and mass of the RHN, there is a contribution[5] to the light neutrino mass matrix which depends on the magnitude of Y_α coupling. Since we plan to investigate the scenario where the light neutrino mass is mainly contributed by the type-II contribution, we determine here the limits on Y_α for which $m_\nu^{\rm R}$ remains insignificant.

For this purpose, first we assume all Y_α to be same given by Y. Secondly, we impose a restriction that the contribution to m_2 (as m_2 is the second lightest eigenvalue of m_ν) coming

[5]Using the fact that M_N is very heavy compared to all IHD components, the radiative contribution can be approximated by $(m_\nu^R)_{\alpha\beta} \simeq \frac{Y_\alpha Y_\beta}{32\pi^2}\frac{(m_{H_0}+m_{A_0})}{M_N}\Delta M[1 + \ln(\frac{m_{H_0}^2+m_{A_0}^2}{2M_N^2})]$.

from $m_\nu^{\rm R}$ remains below 10% contribution followed from type-II seesaw estimate $m_\nu^{\rm II}$ (henceforth called type-II dominance). Using this ansatz, we provide Y versus M_N plot in Fig. 3.4 indicating an upper limit on Y value corresponding to a specific RHN mass. In making this plot, we consider DM mass $m_{H_0} = 535$ GeV with different ΔM indicated by different colors. This limit on Y will be useful in estimating the CP asymmetry. As the lightest neutrino is taken to be massless in type-II contribution, it is clear that with the appropriate Y value (consistent with the Fig. 3.4 and leptogenesis), m_1 will defer from zero value as it obtains a tiny correction from $m_\nu^{\rm R}$.

3.3.3 Dark Matter Phenomenology

The present setup shelters two particles N_R and Φ non-trivially charged under Z_2. Hence, being stable either of them can play the role of the DM. The phenomenology of a singlet fermions like N_R as a WIMP DM candidate with renormalisable interactions remain uninteresting as it predicts overabundant relic density due to the lack of their annihilation channels. On the other hand, as is well known, the study of an IHD provides several interesting prospects both in DM phenomenology as well as in collider searches and hence here we primarily stick to the IHD as DM by considering $M_N > m_{H_0}$. An unbroken Z_2 symmetry in the current scenario guarantees the stability of the scalar DM. Since it is a well studied framework, in this section, we briefly focus on the parts of DM phenomenology relevant for our analysis extended to leptogenesis section.

3.3.3.1 Relic Density

The inert Higgs doublet [232–241, 243–245] extension of the SM is one of the simplest extension where a scalar multiplet can accommodate a DM candidate. Before going into the details of the DM phenomenology of IHD, we first briefly discuss the Boltzmann equation required to study the evolution of the DM in the Universe. DM (H_0) being a part of a $SU(2)_L$ doublet always remains in thermal equilibrium in early Universe due to its gauge and quartic interactions. The relic density of such a DM can be calculated by solving the Boltzmann equation

$$\frac{dY_{H_0}}{dz'} = -\frac{1}{z'^2}\langle\sigma v_{H_0H_0\to XX}\rangle\left(Y_{H_0}^2 - (Y_{H_0}^{eq})^2\right), \tag{3.24}$$

where $z' = m_{H_0}/T$ and $Y_{H_0}^{eq}$ denotes equilibrium number density of H_0 whereas $\langle\sigma v_{H_0H_0\to XX}\rangle$ represents the thermally averaged annihilation cross-section [70] of the DM annihilating into the SM particles denoted by X. The relic density of the inert scalar H_0 is then expressed as

$$\Omega_{H_0}{\rm h}^2 = 2.755\times10^8\left(\frac{m_{H_0}}{\rm GeV}\right)Y_{H_0}^0, \tag{3.25}$$

with $Y_{H_0}^0$ denoting the asymptotic abundance of the DM particle after freeze out. In order to calculate the relic density and study the DM phenomenology of the IHD DM we use the package micrOMEGAs4.3.5 [253].

As stated before, the case of an IHD DM is well studied and hence, we only summarise the results (in terms of relevant parameters) crucial for our analysis of baryon asymmetry of the Universe in the setup. To facilitate our discussion on DM, we provide a variation of the relic density of H_0 ($\Omega_{H_0}\mathrm{h}^2$) with the DM mass (m_{H_0}) for three different choices of mass splitting in Fig. 3.5. Here, one notices that in the mass range $M_W \leq m_{H_0} < 500$ GeV (popularly known as the intermediate region), a typical feature of the IHD is observed where the relic abundance remains under-abundant. The DM being a part of $SU(2)_L$ doublet, it does annihilate and co-annihilate to the SM gauge bosons with a large effective annihilation cross-section resulting this under-abundance in general. However, the correct relic density can still be produced for $m_{H_0} \geq 535$ GeV with an appropriate choice of mass splitting ΔM and Higgs portal coupling (λ_L) as this leads to the cancellations among the $s-$channel, $t-$channel and the contact interaction involved in the scattering amplitude of the DM annihilating into the SM gauge bosons. In Fig. 3.5, one also notices that changing ΔM from 1 GeV

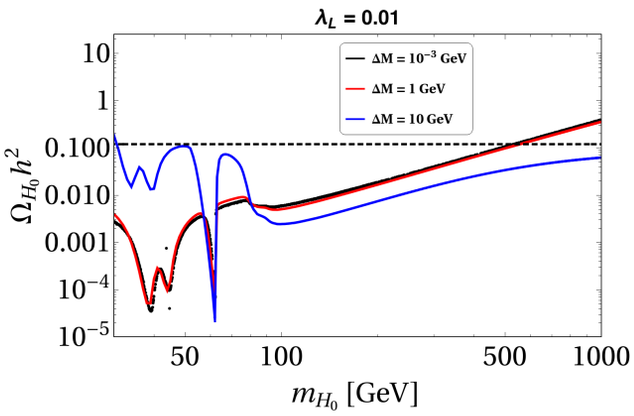

Figure 3.5: Variation of the DM relic density ($\Omega_{H_0}\mathrm{h}^2$) with its mass (m_{H_0}) for three different values of ΔM while keeping $\lambda_L = 0.01$.

to 10^{-3} GeV does not alter the relic result significantly. However, pushing ΔM to a relatively larger value such as 10 GeV keeps the entire mass range of IHD as under-abundant (except the Higgs resonance region). On the other hand, such a variation in ΔM carries significant impact on the DM direct detection experiments as we see in the sub-section 3.3.3.2 below. Aside such dependence, ΔM is also found to be restricted from the perturbativity point of view. As shown in [254], for $\Delta M \gtrsim 20$ GeV, the IHD-Higgs coupling along with the Higgs quartic coupling become non-perturbative much before the Planck scale.

At this stage it is important to point out that the Yukawa interaction of the IHD with the SM leptons and the singlet fermion N_R (see Eq. (3.13)) does not alter the DM phenomenology of the IHD. Although it introduces an extra annihilation channel for IHD ($t-$channels mediated via N_R of SM leptons), its contribution remains suppressed due to the p-wave suppression. Even though, if this additional annihilation channel has a sizeable contribution to DM abundance compared to other channels, it does not help generate new allowed DM masses in the intermediate mass regime of the IHD and hence remains uninteresting from the DM point of view.

3.3.3.2 Direct and Indirect Detection

The null detection of the DM in direct search experiments like LUX [255], PandaX-II [256, 257] and Xenon1T [258, 259] puts a severe constraints on the DM parameter space. There exists two different possiblities for the DM to interact with nuclei at tree level in the scenario under consideration: (a) elastic scattering mediated by SM Higgs boson and (b) inelastic one mediated by electroweak gauge bosons. The spin independent elastic scattering cross section mediated by SM Higgs is given as [260]

$$\sigma^{\rm SI} = \frac{\lambda_L^2 f_n^2}{4\pi} \frac{\mu_n^2 m_{\mathcal{N}}^2}{m_h^2 m_{H_0}^2} \tag{3.26}$$

where $\mu_n = m_{\mathcal{N}} m_{H_0}/(m_{\mathcal{N}}+m_{H_0})$ is the DM-nucleon reduced mass and λ_L is the quartic coupling involved in DM-Higgs interaction. A recent estimate of the Higgs-nucleon coupling f gives $f = 0.32$ [261]. On the other hand, the inelastic scattering cross-section mediated by a gauge boson is expressed as [262],

$$\sigma_{\rm IE}^{\rm SI} = c\frac{G_F^2 m_N^2}{2\pi} Y^2 (\mathcal{N} - (1-4s_W^2)\mathcal{Z})^2 \tag{3.27}$$

with c = 1 for fermions and c = 4 for scalars. Here the hypercharge of the DM is 1/2. Finally, $\mathcal{N}$ and $\mathcal{Z}$ represents the number of neutrons and protons respectively in the target nucleus with mass $m_{\mathcal{N}}$. With $\Delta M > 100$ keV [263], the inelastic scattering of DM with the nuclei is kinematically forbidden as the corresponding cross-section becomes larger than the average kinetic energy of the DM. While $\Delta M \leq 100$ keV can rule out the entire sub-TeV mass regime of the DM even though allowed by the relic density as $\sigma_{\rm IE}^{\rm SI} \simeq 4.9 \times 10^{-8}$ pb which is much larger than the constrained imposed by the Xenon1T experiment in a sub-TeV mass regime of the IHD DM.

Finally, one should also consider the indirect search experiments like Fermi-LAT [264], MAGIC [265] etc., which also provide promising detection prospects of the WIMP type DM. These experiments look for an excess of SM particles like photons and neutrinos in the Universe which can be produced from the annihilation or the decay of the DM. The present setup accommodates an IHD DM that can also produce such signals which can be detected in the indirect search experiments. The null detection of such signals so far can also constrain the DM parameter space. In a recent study [242], it has been shown that the IHD mass regime below 400 GeV is strictly ruled out by Fermi-LAT.

3.3.4 Leptogenesis

In this section, we aim to study the leptogenesis scenario resulting from the CP violating out of equilibrium decay of the triplet carrying lepton number of two units in the model. As advocated, this will happen due to the presence of the sole RHN of the setup contributing to the one-loop vertex correction to the tree level triplet decay into leptons as shown in Fig. 3.6. It is interesting to note that with one triplet, the generated CP asymmetry can't be of purely flavored one [228] in contrast to the presence of this possibility in standard triplet leptogenesis involving two scalar triplets. We first discuss the generation of CP asymmetry

from the triplet decay and then talk about the evolution of the lepton $(B-L)$ asymmetry using Boltzmann equations. In doing so, our plan is to keep the triplet mass as light as possible as that would be interesting from the point of view of collider search for triplet states. In turn, this indicates that flavor effects of the charged lepton Yukawa couplings need to be incorporated provided leptogenesis takes place below temperature $\sim 10^{12}$ GeV.

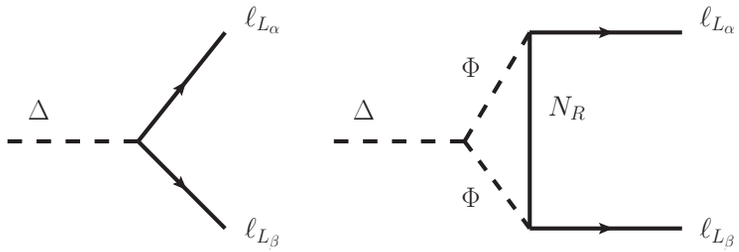

Figure 3.6: The tree level and the vertex digram required for the generation of CP asymmetry.

3.3.4.1 CP asymmetry generation

The flavored CP asymmetry produced as a result of the interference between the tree level and the loop level diagram shown in Fig. 3.6 can be defined and evaluated as [225, 226]

$$\epsilon_\Delta^{\ell_\alpha} = 2\frac{\sum_\beta \Gamma(\bar{\Delta} \to \ell_{L_\alpha} + \ell_{L_\beta}) - \Gamma(\Delta \to \bar{\ell}_{L_\alpha} + \bar{\ell}_{L_\beta})}{\Gamma_\Delta^{\rm tot} + \Gamma_{\bar{\Delta}}^{\rm tot}}, \tag{3.28}$$

$$= \frac{1}{4\pi} M_N \frac{\sum_j \mathbf{Im}\left[\mu_2 Y_i Y_j (Y_\Delta)_{ij}\right]}{\mathbf{Tr}(Y_\Delta^\dagger Y_\Delta) M_\Delta^2 + |\mu_1|^2 + |\mu_2|^2} \log\left(1 + \frac{M_\Delta^2}{M_N^2}\right), \tag{3.29}$$

where, $\Gamma_\Delta^{\rm tot}$ is the total decay width of Δ:

$$\Gamma_\Delta^{\rm tot} = \sum_{\alpha,\beta} \Gamma(\Delta \to \bar{\ell}_{L_\alpha} \bar{\ell}_{L_\beta}) + \Gamma(\Delta \to HH) + \Gamma(\Delta \to \Phi\Phi), \tag{3.30}$$

$$= \frac{M_\Delta}{8\pi}\left[\mathbf{Tr}(Y_\Delta^\dagger Y_\Delta) + \frac{|\mu_1|^2 + |\mu_2|^2}{M_\Delta^2}\right]. \tag{3.31}$$

Similarly, the anti-triplet decay $\Gamma_{\bar{\Delta}}^{\rm tot}$ also contributes to the total decay width in the denominator. It would be useful to define the branching ratios B_ℓ, B_H and B_Φ at this stage, representative of the Δ triplet decay to lepton and scalar final states as:

$$B_\ell = \sum_{\alpha=e,\mu,\tau} B_{\ell_\alpha} = \sum_{\alpha,\beta=e,\mu,\tau} B_{\ell_{\alpha\beta}} = \sum_{\alpha,\beta=e,\mu,\tau} \frac{M_\Delta}{8\pi\Gamma_\Delta^{\rm Tot}} |(Y_\Delta)_{\alpha\beta}|^2 ,$$
$$B_H = \frac{|\mu_1|^2}{8\pi M_\Delta \Gamma_{\Delta_\alpha}^{\rm Tot}} , \qquad B_\Phi = \frac{|\mu_2|^2}{8\pi M_\Delta \Gamma_{\Delta_\alpha}^{\rm Tot}} ; \qquad B_\ell + B_H + B_\Phi = 1 \tag{3.32}$$

We notice now that among the various parameters involved in the expression of flavored CP asymmetry $\epsilon_\Delta^{\ell_\alpha}$ in Eq. (3.29), Y_Δ is obtained from Eq. (3.22) while μ_1 becomes function of M_Δ via Eq. (3.17) with the choice $v_\Delta = 1$ eV. Finally, to maximize the CP asymmetry, we fix Y to its largest allowed value corresponding to a specific choice of M_N (and ΔM) from Fig. 3.4 so as to restrict the radiative contribution negligible (keeping it below 10%) compared to the

type-II one toward light neutrino mass. Although there is no direct correlation between CP asymmetry and the mass splitting ΔM among IHD components, it can be noted that ΔM being involved in restricting the maximum value of Y for the type-II dominance of neutrino mass (see Fig. 3.4), plays an important role here. Hence, $\epsilon_{\Delta}^{\ell_\alpha}$ effectively remains function of three independent parameters μ_2, M_Δ and M_N. It is interesting to note that in this case, there exists a coupling μ_2 in the CP asymmetry expression which does not participate in the neutrino mass generation unlike conventional type-(I+II) scenario where all the couplings involved in CP asymmetry also take part in the neutrino mass [225, 226, 230]. As a result, in the latter case (*i.e.* in type-(I+II)) with type-II dominance, the relevant parameter space is restricted leading to M_Δ quite heavy. For example, it was shown in [230], in the context of type-II-dominated left-right seesaw model, that M_Δ turns out to be 10^{12} GeV or beyond. On the other hand, involvement of otherwise free parameter μ_2 may open up a relatively wider parameter space in our case. Below we proceed to get some idea on the CP asymmetry generation by scanning over the parameters for our work.

Fig. 3.7 shows the density contour plot for the absolute value of individual components of CP asymmetry in the $M_\Delta - \mu_2$ plane while keeping M_N fixed at a specific value 5×10^{10} GeV. In producing these plots, we also consider two specific choices of $\Delta M = 10^{-3}$ GeV (top panel) and $\Delta M = 10^{-2}$ GeV (bottom panel). Benchmark Points (BP) [A] and [B] are used to specify the values of Yukawa coupling Y for these mass splittings respectively (see Fig. 3.4). For M_Δ below 10^{12} GeV (though larger than 10^9 GeV), tau-Yukawa interaction comes to equilibrium making the asymmetries along a (a coherent superposition of e and μ lepton flavors) and τ flavor distinguishable. We elaborate on it latter. Hence in this region, we study $\epsilon_{\Delta}^{\ell_{a,\tau}}$ separately in Fig. 3.7(a) and (b) respectively. In the plot, the red (blue) region indicates the highest (lowest) absolute value of CP asymmetry while the green and the yellow regions indicate intermediate values of it. Maximum CP asymmetry[6] (value of which is indicated in the top bar) results around the central region. Comparing the top and bottom panels of plots, we find that it is possible to generate relatively larger CP asymmetry once we lower ΔM. However, we can not keep on lowering ΔM indefinitely (ΔM below 100 keV is not feasible as we have discussed it in the DM section).

3.3.4.2 Evolution of $B - L$ asymmetry

With the above estimates of the CP asymmetries in different flavor directions, we study here the evolution of $B - L$ asymmetry via Boltzmann equations. It naturally involves all possible interactions with the thermal bath in the early Universe. As we aim here to bring down the leptogenesis scale (*i.e.* as low M_Δ as possible), as stated earlier in subsection 1.6.2.3 the situation becomes more involved. Below the energy scale $M_\Delta \lesssim 10^{12}$ GeV, particularly in the temperature regime 10^9 GeV $\lesssim T \lesssim 10^{12}$ GeV, along with bottom and charm quarks, tau Yukawa related interactions come to thermal equilibrium because of which the quantum coherence of lepton doublets is lost. As a result, in this regime, two orthogonal directions denoted by $\alpha = a$ (coherent superposition of e and μ lepton flavors) and τ survive. On the other hand, QCD instanton and EW sphaleron reactions also reach equilibrium at this

[6] For the present analysis, it turns out $B_l >> B_\Phi$.

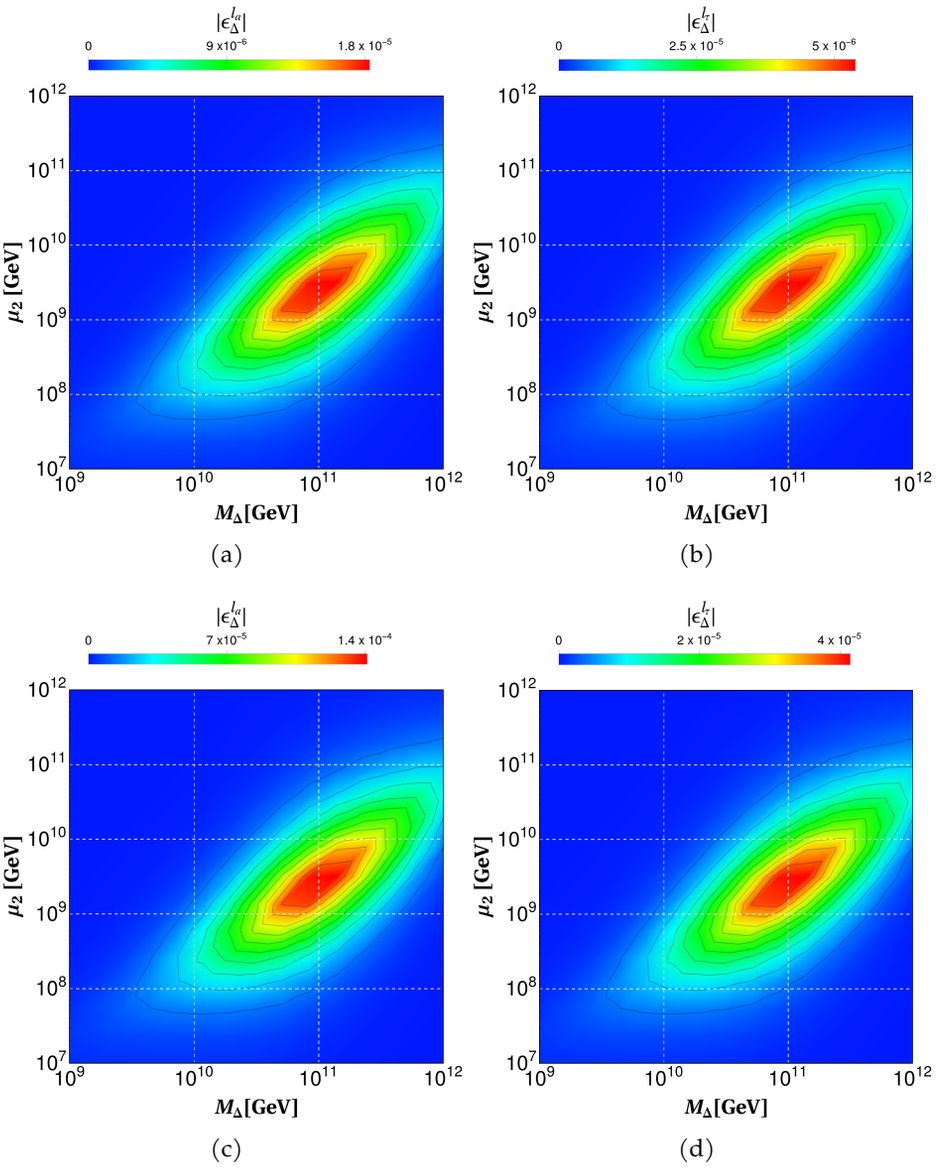

Figure 3.7: Density contour of individual CP asymmetry in $\mu_2 - M_\Delta$ plane with $M_N = 5 \times 10^{10}$ GeV. Top panel: $\Delta M = 10^{-3}$ GeV (using BP [A] from Fig. 3.4) ; Bottom panel: $\Delta M = 10^{-2}$ GeV (using BP [B] from Fig. 3.4).

temperature range making the baryon number as a non-conserved quantity, though it conserves the individual $B/3 - L_\alpha$ charges. So, an appropriate study of the evolution of the lepton asymmetry should be performed by knowing the evolution of the $B/3 - L_\alpha$ charges with $\alpha = a$ and τ. Further below region of 10^5 GeV $\lesssim T \lesssim 10^9$ GeV, strange quark and muon Yukawa interactions achieve thermal equilibrium indicating that the lepton doublets completely lose their quantum coherence. Hence, lepton asymmetry becomes distinguishable along all three flavors e, μ and τ. Below $T < 10^5$ GeV, electron Yukawa reaches the equilibrium.

In order to study the evolution of the $B - L$ asymmetry, we need to employ a set of coupled Boltzmann equations following the analysis of [228]. This set includes differential equations for triplet density $\Sigma = \Delta + \bar{\Delta}$, triplet asymmetry $\Delta_\Delta = \Delta - \bar{\Delta}$ and $B/3 - L_\alpha$ asymmetries considering flavor effects as we have considered a specific hierarchy $M_\Delta < M_N$ in our analysis. Assuming the triplet scalar was at thermal equilibrium with plasma in the

early Universe, below are the specified interactions which have the potential to change its number density as well as produce or washout the effective $B-L$ charge asymmetry:

- Decay [$\Delta \to \bar{\ell}_{L_\alpha}\bar{\ell}_{L_\beta}$, $\Delta \to HH$ and $\Delta \to \Phi\Phi$] and inverse decay: The total decay rate density is then represented by: $\gamma_D = \gamma_D^\ell + \gamma_D^H + \gamma_D^\Phi$, with $\gamma_D = \frac{K_1(z)}{K_2(z)}\, n_\Sigma^{\rm Eq}\, \Gamma_\Delta^{\rm Tot}$, $K_1(z), K_2(z)$ are the modifed Bessel functions. Here $n_\Sigma^{\rm Eq}$ is the equilibrium number desity of Σ_Δ and z is defined as M_Δ/T.
- Gauge induced scatterings $\Delta\Delta \leftrightarrow f\ f$, $\Delta\Delta \leftrightarrow XX$ (s-channel), $\Delta\Delta \leftrightarrow GG$ (triplet mediated t,u-channel and four point vertex contrubutions), where f stands for SM fermions, G are SM Gauge bosons, $X = H, \Phi$. Altogether the reaction densities are characterized by γ_A, where $\gamma_A = \frac{m_\Delta^4}{64\,\pi^4}\int_{x_{\rm min}}^\infty dx\sqrt{x}\,\frac{K_1(z\sqrt{x})\,\widehat{\sigma}_A}{z}$, $x = s/M_\Delta^2$ (s is the centre of mass energy). Here $\widehat{\sigma}_A$ is the reduced cross section inclusive of all gauge induced processes, where $\widehat{\sigma}$ is related to the usual cross section σ for a process $[1+2 \to 3+4+...]$ by: $\widehat{\sigma} = \frac{8}{s}[(p_1.p_2)^2 - m_1^2 m_2^2]\sigma$ with p_1, p_2 be the four momentum of initial particles having mass m_1, m_2.
- Lepton number ($\Delta L = 2$) and Lepton flavor violating s and t channel scatterings (mediated by the triplet/anti-triplet): $XX \leftrightarrow \bar{\ell}_{L_\alpha}\bar{\ell}_{L_\beta}$, $X\ell_{L_\beta} \leftrightarrow \bar{X}\bar{\ell}_{L_\alpha}$ having reaction densities $\gamma_{\ell_\alpha\ell_\beta}^{XX}$ and $\gamma_{X\ell_\alpha}^{X\ell_\beta}$ respectively.
- Lepton flavor violating triplet mediated s and t channel scattering: $(\ell_{L_m}\ell_{L_n} \leftrightarrow \ell_{L_\alpha}\ell_{L_\beta})_s$, $(\ell_{L_m}\ell_{L_n} \leftrightarrow \ell_{L_\alpha}\ell_{L_\beta})_t$ with reaction densities given by $(\gamma_{\ell_\alpha\ell_\beta}^{\ell_m\ell_n})_s$ and $(\gamma_{\ell_\alpha\ell_\beta}^{\ell_m\ell_n})_t$.

Keeping in mind the above discussion, the following Boltzmann equations are constructed,

$$s\mathcal{H}z\frac{dY_\Sigma}{dz} = -\left(\frac{Y_\Sigma}{Y_\Sigma^{\rm Eq}} - 1\right)\gamma_D - 2\left[\left(\frac{Y_\Sigma}{Y_\Sigma^{\rm Eq}}\right)^2 - 1\right]\gamma_A\,, \tag{3.33}$$

$$s\mathcal{H}z\frac{dY_{\Delta_\Delta}}{dz} = -\left[\frac{Y_{\Delta_\Delta}}{Y_\Sigma^{\rm eq}} - \sum_\sigma\left(\sum_\alpha B_{\ell_\alpha}C_{\alpha\sigma}^\ell - B_H C_\sigma^H\right)\frac{Y_{X_\sigma}}{Y_\ell^{\rm eq}}\right]\gamma_D\,, \tag{3.34}$$

$$\begin{aligned} s\mathcal{H}z\frac{dY_{B/3-L_\alpha}}{dz} =& -\left(\frac{Y_\Sigma}{Y_\Sigma^{\rm eq}} - 1\right)\epsilon_\Delta^{\ell_\alpha}\gamma_D + 2\sum_\beta\left(\frac{Y_{\Delta_\Delta}}{Y_\Sigma^{\rm eq}} - \frac{1}{2}\sum_\sigma C_{\alpha\beta\sigma}^\ell\frac{Y_{X_\sigma}}{Y_\ell^{\rm eq}}\right)B_{\ell_{\alpha\beta}}\gamma_D \\ & - \sum_{\beta,\sigma}\left\{2\left(C_\sigma^H + \frac{1}{2}C_{\alpha\beta\sigma}^\ell\right)\left(\gamma_{\ell_\alpha\ell_\beta}^{HH} + \gamma_{H\ell_\alpha}^{H\ell_\beta}\right) + C_{\alpha\beta\sigma}^\ell\left(\gamma_{\ell_\alpha\ell_\beta}^{\Phi\Phi} + \gamma_{\Phi\ell_\alpha}^{\Phi\ell_\beta}\right)\right\}\frac{Y_{X_\sigma}}{Y_\ell^{\rm eq}} \\ & - \sum_{\beta,m,n,\sigma} C_{\alpha\beta mn\sigma}^\ell\left((\gamma_{\ell_\alpha\ell_\beta}^{\ell_m\ell_n})_s + (\gamma_{\ell_\alpha\ell_\beta}^{\ell_m\ell_n})_t\right)\frac{Y_{X_\sigma}}{Y_\ell^{\rm eq}}, \end{aligned} \tag{3.35}$$

where $z = M_\Delta/T$ and Y_{Δ_X} is defined as the ratio between particle and antiparticle number densities difference to entropy: $Y_{\Delta_X} = (n_X - n_{\bar{X}})/s$, where $n_X(n_{\bar{X}})$ is number density of a particular species $X(\bar{X})$.

Depending on the temperature range, the index i in the RHS of Eq. (3.35) will run differently, *e.g.* for 10^9 GeV $\lesssim T \lesssim 10^{12}$ GeV, $\alpha = a, \tau$ as done in Fig. 3.7, while for $T < 10^9$ GeV, $\alpha = e, \mu, \tau$ need to be included. The generated asymmetry in number densities involving lepton doublets of a specific flavor $Y_{\Delta\ell_\alpha}$ as well as that of the Higgs (originated from the inverse decay and subtraction of the on-shell contribution for $\Delta L = 2$ processes) can be related to the fundamental asymmetries Δ_Δ and $B/3 - L_\alpha$ with the help of the equilibrium

conditions applicable. The corresponding conversion factors[7] are defined in terms of C^{ℓ} and C^{H} matrices as below (similar to type-I setup as presented in subsection 1.6.2.3) [104, 228]:

$$Y_{\Delta_{\ell_\alpha}} = -\sum_{\sigma} C^{\ell}_{\alpha\sigma}\, Y_{X_\sigma} \qquad \text{and} \qquad Y_{\Delta_H} = -\sum_{\sigma} C^{H}_{\sigma}\, Y_{X_\sigma}, \tag{3.36}$$

where Y_{X_σ} are the elements[8] of $Y_X^T = \left(Y_{\Delta_\Delta}, Y_{B/3-L_\sigma}\right)$ and $C^{\ell}_{\alpha\beta\sigma}$ and $C^{\ell}_{\alpha\beta mn\sigma}$ are given by:

$$C^{\ell}_{\alpha\beta\sigma} = C^{\ell}_{\alpha\sigma} + C^{\ell}_{\beta\sigma}\ , \quad C^{\ell}_{\alpha\beta mn\sigma} = C^{\ell}_{\alpha\sigma} + C^{\ell}_{\beta\sigma} - C^{\ell}_{m\sigma} - C^{\ell}_{n\sigma}. \tag{3.37}$$

Then the final lepton asymmetry is converted to Baryon asymmetry via sphaleron processes as given by :

$$Y_{\Delta B} = 3 \times \frac{12}{37} \sum_{\alpha} Y_{B/3-L_\alpha}, \tag{3.38}$$

where the factor 3 is due to the degrees of freedoms associated to the $SU(2)_L$ scalar triplet. Here we also assumed that the sphalerons have decoupled below SSB.

3.3.4.3 Results

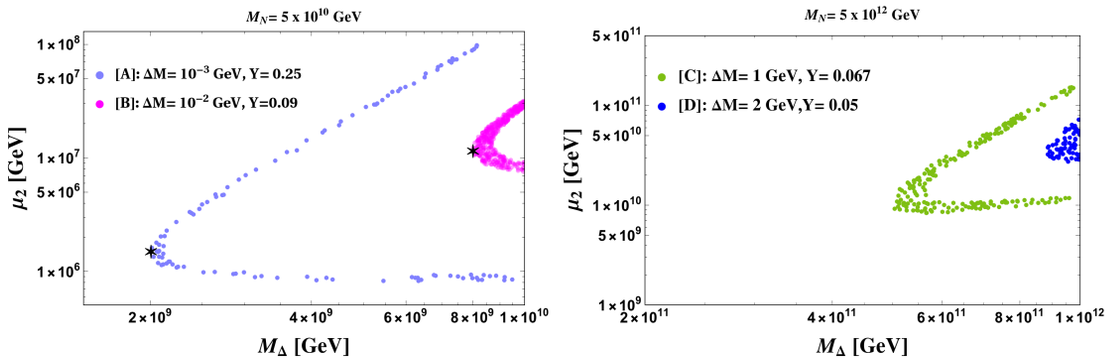

Figure 3.8: Contour plots for final baryon asymmetry ($Y_B = (8.7 \pm 0.06) \times 10^{-11}$) in $\mu_2 - M_\Delta$ plane. Left panel: $M_N = 5 \times 10^{10}$ GeV while $\Delta M = 10^{-3}$ GeV (light blue) and $\Delta M = 10^{-2}$ GeV (magenta), Right panel: $M_N = 5 \times 10^{12}$ GeV while $\Delta M = 1$ GeV (light green) and $\Delta M = 2$ GeV (blue).

In order to explore the parameter space of our model so as to produce the observed baryon asymmetry $Y_B = (8.7 \pm 0.06) \times 10^{-11}$ [17, 266], first we choose a specific value of $M_N = 5 \times 10^{10}$ GeV. Then based on our previous discussion we infer that lepton asymmetry with 10^9 GeV$< M_\Delta < M_N$ will be produced along two orthogonal directions, *i.e.* a and τ while below 10^9 GeV, all three flavor directions have to be taken into account. With the help of chemical equilibrium constraint equations (coming from relevant Yukawa and EW Sphaleron related reactions that are in equilibrium) as well as other constraints such as hypercharge conservation (applicable in this energy range) lead to the following structure of

[7] We simplify the situation by considering the chemical potential of the Φ field to be zero and hence corresponding C^{Φ} does not appear.

[8] Here we take $Y_{\Delta_\Delta} \equiv Y_{\Delta_{\Delta^0}} = Y_{\Delta_{\Delta^+}} = Y_{\Delta_{\Delta^{++}}}$ and $Y_{\Delta_H} \equiv Y_{\Delta_{H^0}} = Y_{\Delta_{H^+}}$.

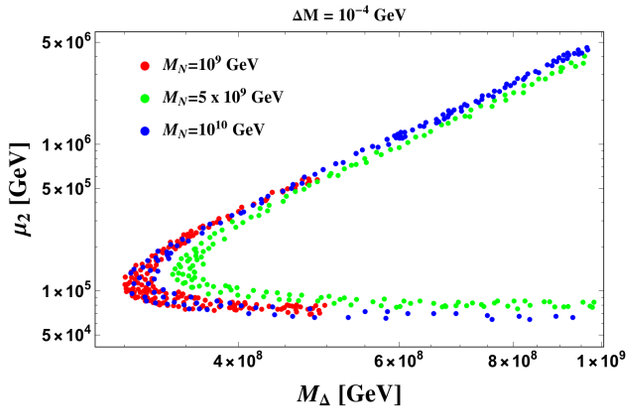

Figure 3.9: Contour plots for final baryon asymmetry ($Y_B = (8.7 \pm 0.06) \times 10^{-11}$) in $\mu_2 - M_\Delta$ plane for $\Delta M = 10^{-4}$ while $M_N = 10^{10}$ GeV (blue), $M_N = 5 \times 10^9$ GeV (green) and $M_N = 10^9$ GeV (red).

C^ℓ and C^H matrices (for 10^9 GeV$< M_\Delta < M_N$) [104, 228]:

$$C^\ell = \frac{1}{718}\begin{pmatrix} -12 & 307 & -36 \\ 78 & -21 & 234 \end{pmatrix}, \; C^H = \frac{1}{359}\begin{pmatrix} 258 & 41 & 56 \end{pmatrix}. \tag{3.39}$$

For M_Δ below 10^9 GeV, C^ℓ and C^H become 3×4 and 1×4 matrices.

Using the input on the flavored CP asymmetries along a and τ directions from Fig. 3.7, obtained as a function of μ_2 and M_Δ for a specific ΔM value, we employ the set of Boltzmann equations Eq. (3.33-3.35) while ignoring the last two terms of Eq. (3.35) to draw a contour plot for the correct final baryon asymmetry (via Eq. (3.38)) as shown in Fig. 3.8. The two contour plots, one in magenta and other in light blue patches, correspond to $\Delta M = 10^{-2}$ GeV and 10^{-3} GeV respectively. We therefore infer that the triplet can be as light as $\sim 10^9$ GeV, contrary to the type-(I+II) case, which can successfully generate the required amount of baryon asymmetry, thanks to the flexibility involved due to the presence of parameter μ_2.

We also notice that with the increase in ΔM value, the baryon asymmetry satisfying contour gets shifted toward heavier mass range of the triplet. This observation is interesting as it is correlated to the DM phenomenology. We recall that even though a smaller ΔM is not in conflict with the relic contribution to DM (in fact a relic satisfaction requires ΔM below $\mathcal{O}(1)$ GeV), it is actually restricted from below by the inelastic scattering of DM direct searches ($\Delta M \gtrsim 10^{-4}$ GeV). On the other hand, the upper bound on ΔM follows from the relic density satisfaction by the DM as can be seen from the Fig. 3.5. We find that with $\Delta M = 1$ GeV (light green), M_Δ can be as low as 5×10^{11} GeV, while a further increase in ΔM such as 2 GeV (blue)[9] pushes the lightest possible M_Δ value to 9×10^{11} GeV (while maintaining $M_\Delta < M_N$) (see right panel of Fig. 3.8). As a result, we can work in the two flavor regime of leptogenesis with such ΔM values. A further increase in ΔM will take us to unflavored regime of leptogenesis. However, we refrain from considering a further larger values of ΔM mainly because in that case, the relic density of the DM becomes under-abundant. In Fig. 3.9, a similar contour plots are presented, but for fixed $\Delta M = 10^{-4}$ GeV with different

[9]With such mass splitting, the DM having mass $m_{H^0} = 535$ GeV can constitute $\sim 83\%$ of the observed relic abundance.

M_N values. As can be seen, the allowed mass of the triplet comes down to an even lower mass close to 10^8 GeV. It is perhaps pertinent here to mention that our entire parameter space corresponds to the Yukawa regime [227, 228] where the Yukawa induced inverse decay processes (characterised by $B_{\ell_{\alpha\beta}}\gamma_D$) play important role and hence flavor effects become crucial.

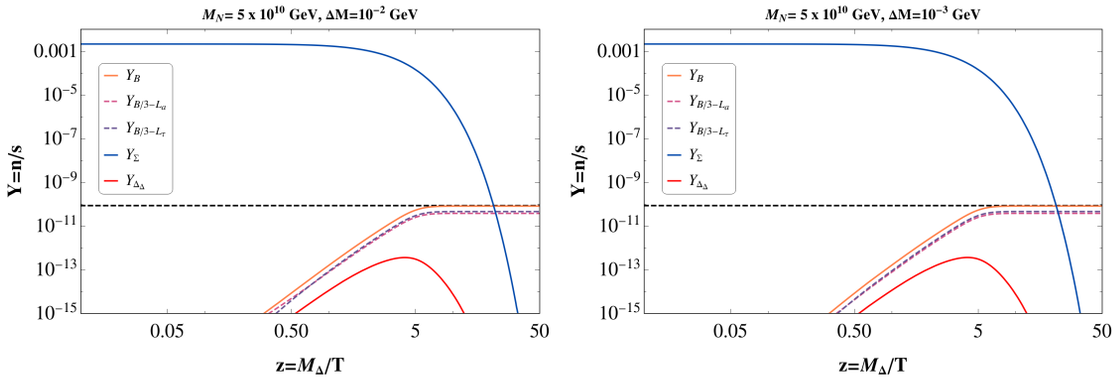

(a) (b)

Figure 3.10: Left panel depicts the evolution of the comoving number density of individual components of lepton asymmetry together with the overall baryon asymmetry for $M_\Delta = 8.02 \times 10^9$ GeV and $\mu_2 = 1.14 \times 10^7$ GeV. Right panel displays the same but for $M_\Delta = 2.01 \times 10^9$ GeV and $\mu_2 = 1.48 \times 10^6$ GeV. Evolution of comoving number density of Σ, Δ_Δ are also shown on both the plots. The values of M_Δ and μ_2 are obatined from the lowest allowed points for left panel of Fig. 3.8 (indicating by ★).

Hereafter, to show explicitly the various contributions of flavor in the evolution of $Y_{B/3-L_\alpha}$ ($\alpha = a, \tau$), we pick up the lowest possible values of M_Δ and corresponding μ_2 (for a fixed value of $\Delta M = 10^{-2}$ GeV and $M_N = 5 \times 10^{10}$ GeV) from left panel of Fig. 3.8. Then in Fig. 3.10(a), we show the evolution of number density to entropy ratio ($Y = n/s$) for individual component of lepton asymmetries as well as the total baryon asymmetry $w.r.t.$ $z = M_\Delta/T$. While plotting, we have assumed that initially $\Delta(\bar{\Delta})$ were in equilibrium so $\Delta_\Delta = 0$ and there were no lepton asymmetry. While the dark blue curve shows the evolution of Σ, abundances of $B/3-L_\alpha$ asymmetries along individual flavor directions are shown in purple (a direction) and violet (τ direction) dashed lines. The orange line stands for the evolution of the baryon asymmetry which asymptotically merges with the black dashed horizontal line indicative of the correct baryon asymmetry of the Universe. In a recent work [224], authors have shown the importance of incorporating density matrix formalism to evaluate the baryon asymmetry for triplet leptogenesis, even beyond $T \gtrsim 10^{12}$ GeV. In this formalism, diagonal entries of the density matrix indicate asymmetry along each lepton flavor direction while off-diagonal entries represent quantum correlations between different flavors. Though this is the most general approach, we have found that inclusion of the off-diagonal entries can only change the final result by 20% or less (corresponding to the values of parameters involved in producing the plots of Fig. 3.10) and hence neglected here. Note that the dark blue curve starts to fall around $z = 1$ due to the out of equilibrium decay of the triplet(anti-triplet) to different channels which in turn is reflected in the increase of lepton asymmetry (purple and violet-dashed lines). Around $z = 5$, the number density of the lepton asymmetry (in all directions) starts to saturate. The red curve shows the evolution

of asymmetry generated in Δ and $\bar{\Delta}$ particles. Next in Fig. 3.10(b), the similar evolution of flavors ($\alpha = a, \tau$) becomes prominent once we choose the lowest possible value of M_Δ corresponding to $\Delta M = 10^{-3}$ GeV from left panel of Fig. 3.8.

Finally, we elaborate on how the mass-splitting ΔM intervenes in different parts of the present work. Obviously, ΔM has its most important role in DM phenomenology. As shown in Fig. 3.5, a value of $\Delta M \sim \mathcal{O}(1)$ GeV or less is appropriate for having DM relic satisfaction having mass below TeV. Such a value therefore serves as the upper limit of ΔM while it is bounded from below by $\sim 10^{-4}$ GeV from the constraint on inelastic scattering amplitude of DM with detector nuclei. Turning into the neutrino part, we notice from Fig. 3.4 that in order to maintain the type-II dominance toward the neutrino mass, the maximum allowed value of neutrino Yukawa coupling Y has to be reduced with the increase of ΔM for a specific choice of RHN mass M_N. On the other hand, a larger Y (and hence smaller ΔM) is favored from the point of view of enhancing the CP asymmetry with a specific M_N. Therefore a judicious choice has to be made for choosing ΔM which not only be responsible for type-II dominance but also remains small enough so as to allow sufficient CP asymmetry. Such a choice has to be further guided by its upper ($\sim \mathcal{O}(1)$ GeV) and lower (10^{-4} GeV) limits. With this entire viable range of ΔM, masses of the RHNs are found to be in the regime $\sim 10^{(9-12)}$ GeV.

3.3.5 Summary

In this work, we present a simple extension of the basic type-II seesaw ($i.e.$ with one $SU(2)_L$ triplet in addition to SM) scenario including an additional RHN and one IHD, which can accommodate neutrino mass, DM as well as capable of explaining the baryon asymmetry of the Universe via leptogenesis mechanism. The interesting part of the study is the involvement of the DM multiplet, along with the RHN, in the vertex correction of the triplet's decay to two leptons which can successfully produce the required amount of CP asymmetry in order to address the baryon asymmetry of the Universe. Although the decay of RHN can also produce lepton asymmetry in the present setup, we assume a specific mass hierarchy $M_\Delta < M_N$ and hence the asymmetry generated by the decay of the triplet is the effective one. We incorporate the flavor effects in this triplet leptogenesis study as we aim to lower the triplet mass as much as possible in view of its accessibility at the collider. We find it is possible to generate sufficient lepton asymmetry with M_Δ as low as $\sim 10^8$ GeV.

Turning to the neutrino side, where the dominant contribution to the light neutrino mass follows from the tiny vev of the triplet, there exists a radiative contribution too which we restrict to be negligible by choosing the associated Yukawa to be small enough. This consideration is related to the mass splitting involved in the IHD which plays a twofold role here. Firstly, the IHD as a DM results with a specific range of this mass splitting ($10^{-4} - \mathcal{O}(1)$ GeV). Secondly, a smaller mass splitting (hence a larger neutrino Yukawa) turns out to be preferable for generating sufficient CP asymmetry in this flavored leptogenesis framework. Since the lower limit of ΔM is somewhat governed by the inelastic direct detection bound, in a way it restricts the mass of the triplet within a certain range.

On the other hand, due to the involvement of particles like $\Delta^\pm$, $\Delta^{\pm\pm}$, $\Phi^\pm$ and N_R, the present setup is also subjected to the constraints coming from the lepton flavor violating decays like $\mu \to e\gamma$. Keeping this in our mind, we calculate the $Br(\mu \to e\gamma)$ and found it to be

many orders of magnitude smaller than that of the present upper bound on it ($< 4.2 \times 10^{-13}$ at 90% C.L [267]).

Chapter 4

Effect of Post-inflationary epoch in Flavor Leptogenesis

4.1 Introduction

Till now, the discussion we had in the previous chapters, we mainly followed the standard prescription of *thermal* leptogenesis, where it is considered that after the Universe enters in the RD era (the beginning of which is marked by reheating temperature $T_{\rm RH}$), the RHNs can be created by thermal scattering more specifically via inverse decays and 2-2 scattering mediated by SM fields. Subsequently, considering a hierarchical RHN masses, the lightest among the three RHNs (say N_1 with mass M_1) starts to contribute to lepton asymmetry production via its out-of-equilibrium decay to the SM lepton (l_{L_α}) and Higgs (H) doublets around a temperature $T \lesssim M_1$. The reheating temperature obviously satisfies the condition $T_{\rm RH} > M_1$. The abundance of the RHNs (Y_{N_1}) and the produced lepton asymmetry in a specific flavor direction (Δ_{L_α}) in this RD epoch are connected by the BE where apart from production, one needs to incorporate all the lepton-number violating processes that can potentially erase such asymmetry.

Provided that such decay happens at sufficiently high temperature (at or above 5×10^{11} GeV), where all the right-handed charged leptons of different flavors are in out of equilibrium, one can safely use the unflavored approximation [95–97]. This is because the rate of charged lepton Yukawa interactions remains weaker compared to that of RHN Yukawa interactions. On the other hand, if the leptogenesis happens at a temperature (T) below 5×10^{11} GeV, the right-handed tau leptons equilibrate with the thermal bath and flavor effects [100, 102–107, 268] are inevitable. Once this tau lepton Yukawa interaction is equilibrated, it tends to destroy the lepton asymmetry carried by the tau leptons generated from the decay of RHNs. For the muon and electron Yukawa interactions, this happens below 10^9 GeV and 5×10^4 GeV respectively.

There exists a lower limit on the mass of the RHNs as $M_1 \gtrsim 10^9$ GeV (known as Davidson-Ibarra bound [269]) in order to satisfy the correct baryon asymmetry of the Universe via leptogenesis which in turn indicates that reheating temperature should be higher than this value for standard *thermal* leptogenesis. Although it is feasible to have such a high $T_{\rm RH}$,

there is no such concrete evidence in support of it too. On the contrary, it can be as low as few MeV [270–273]. In this context, it is interesting to investigate the possibility of having reheating temperature smaller than the mass of the RHNs in view of leptogenesis. While one such possibility is to have *non-thermal* leptogenesis [77, 274–297], a different possibility opens up where a non-instantaneous reheating period[270, 270, 298–302] (extended from $T_{\rm Max}$ to $T_{\rm RH}$) can be brought into the picture. In that case, a maximum temperature $T_{\rm Max}$ after inflation can be realized followed by the onset of RD era indicated by reheating temperature $T_{\rm RH}$ with $T_{\rm Max} > T_{\rm RH}$. In this chapter, we will show that the process of such non-instantaneous reheating during the post-inflationary period can have a sizable impact on the charged lepton Yukawa ET in the early Universe. The perturbative variant of reheating is intricately related with the coupling between the inflaton field and the decaying particles which produce the radiation bath.

Keeping this in mind, in section 4.2, we will couple inflaton with only SM fermion fields. As a result of which, the decay of inflaton to SM fermions will produce a prolonged reheating period. Then we will study its effect on the charged lepton Yukawa ET and, subsequently on the flavor lepton asymmetry generation.

In section 4.3, we will focus on a more general picture by allowing an additional interaction between the inflaton and the RHN fields on top of the existing effective coupling between the inflaton and SM fermion fields and observe its impact on flavor leptogenesis mechanism.

4.2 Setup a: inflaton couples to SM fermions

As previously discussed, a *thermal* leptogenesis scenario with N_1 mass $M_1 \lesssim 5 \times 10^{11}$ GeV experiences flavor effects since the charged lepton Yukawa interactions start to enter equilibrium below this temperature. An estimate of such ETs for different flavors is provided in Fig. 1.4. Note that the ETs of these Yukawa interactions (associated to different flavors of right handed charged leptons) are calculated assuming that the Universe is already in a RD era followed by an instantaneous reheating after inflation. Obviously, such consideration leads to $T_{\rm RH} > M_1$ indicating the presence of high reheating temperature. Now, it is also known that the reheating might not be an instantaneous process [270, 298, 301, 302]. On top of that, the reheating temperature can be low enough (though larger than a few MeV from BBN limit [270–273]).

The era of reheating begins when after inflation, the inflaton field ϕ starts to decay. Neglecting the possibility via preheating [303–305], as this field ϕ starts to decay to the lighter SM degrees of freedoms, the thermalization of these light decay products helps the Universe to attain a maximum temperature $T_{\rm Max}$. Subsequently, the temperature of the Universe falls at a rate much slower than the standard scaling $T \sim a^{-1}$ (a is the Friedmann–Robertson–Walker scale factor). This continues till a point (defining $T_{\rm RH}$) where the radiation component becomes the dominating one in the Universe. This nontrivial behavior of the temperature as a function of scale factor a results due to the faster expansion rate compared to the standard scenario (quantified by Hubble $\mathcal{H}$) during the lifetime of the inflaton.

As a result of this modified $\mathcal{H}$, a change in the behavior of $\langle\Gamma_\alpha\rangle/\mathcal{H}$ is also expected in the

period in between $T_{\rm Max}$ and $T_{\rm RH}$, compared to the standard scenario represented in subsection 1.6.2.1. This would be particularly prominent provided $T_{\rm RH}$ falls below the standard right handed charged lepton ET $T^*_{0(\alpha)}$ (for a specific flavor α) and $T_{\rm Max}$ maintains a relation $T_{\rm Max} > T^*_{0(\alpha)}$. In fact, as a result of such a delayed entry (due to the modified $\mathcal{H}$ for $T_{\rm Max} > T > T_{\rm RH}$) of the charged lepton Yukawa interactions into the equilibrium, a shift of the flavor regime(s) of leptogenesis compared to the standard scenario is expected in this case of extended reheating period. We begin the discussion on reheating below to estimate the modified temperature regimes where the right-handed charged leptons enter equilibrium, first without introducing any RHNs and later we incorporate RHNs so as to discuss their influence on flavored leptogenesis.

4.2.1 Reheating Process

As the era of reheating starts following the inflationary epoch, the discussion of reheating is somewhat connected to the form of inflaton potential near its minimum. Hence, to be specific, following [301] we consider a generic power-law form of the inflaton potential near the minimum,[301]:

$$V(\phi) = \lambda \frac{|\phi|^n}{M_P^{n-4}}\,, \tag{4.1}$$

where M_P is the reduced Planck mass. The magnitude of the coupling λ can be estimated from the CMB observables such as spectral index and tensor-to-scalar ratio and depends on the order of the polynomial n. The origin of such choice of potential can be traced back to T-attractor models in no-scale supergravity [306]. In such setups, the effective inflaton mass m_ϕ is a function of inflaton field. In the adiabatic approximation, it can be written as:

$$\begin{aligned} m_\phi^2 \;&\equiv\; \partial_\phi^2 V(\phi) = \;\lambda\, n(n-1)\phi^{n-2} M_P^{4-n} \\ &=\; n(n-1) M_P^{\frac{2(4-n)}{n}} \lambda^{\frac{2}{n}} \rho_\phi^{\frac{n-2}{n}}\,. \end{aligned} \tag{4.2}$$

where ρ_ϕ is the energy density of the inflaton field ϕ. For simplicity, we confine ourselves to a $n = 2$ case resembling the Starobinsky type of inflationary potential [307–309] (in the large field limit). As a result of which, from the Planck+BICEP2/Keck (PBK) constraints [310] on spectral index and tensor-to-scalar ratio, the magnitude of the parameter λ is found to be $\sim 2\times10^{-11}$. This leads to the effective mass of the inflaton as $m_\phi = (\partial_\phi^2 V(\phi))^{1/2} \simeq 1.5\times10^{13}$ GeV. For a more detailed discussion, see [272, 273, 301, 311].

Furthermore, we introduce an effective coupling between the inflaton and the SM fields as $y_{\phi ff}\phi f \bar{f}$ which will initiate the decay of the inflaton to radiation (composed of SM fields) having a width $\Gamma_\phi = \frac{y^2_{\phi ff}}{8\pi} m_\phi$. Then the energy densities of the inflaton field (ρ_ϕ) and radiation (ρ_R) satisfy the evolution equations:

$$\frac{d(\rho_\phi a^3)}{da} = -\frac{\Gamma_\phi}{\mathcal{H}}\rho_\phi a^2; \;\text{ and }\; \frac{d\left(\rho_R a^4\right)}{da} = \frac{a^3}{\mathcal{H}}\Gamma_\phi \rho_\phi, \tag{4.3}$$

where $\mathcal{H}^2 = (\dot{a}/a)^2 = (\rho_\phi + \rho_R)/3M_P^2$. At this moment, it is pertinent to define the temper-

ature $T(a)$ connected to the ρ_R by the relation

$$T(a) = \left[\frac{30}{g_*(a)\pi^2}\right]^{1/4} \rho_R^{1/4}(a). \tag{4.4}$$

T can therefore be estimated as a solution to the coupled Eqs. (4.3) whose variation with the relative scale factor (a_{end} is the scale factor at the end of inflation, considered as a mere reference point and is set to unity) is presented in the top panel of Fig. 4.1. Note that during the onset of reheating, $\mathcal{H}$ has the sole contribution from ρ_ϕ. However, as soon as the light decay products of ϕ thermalizes[1], ρ_R gets growing sharply and correspondingly a maximum temperature $T_{\rm Max}$ is attained. After this, ρ_R decreases slowly (as ϕ being decayed, ρ_ϕ diminishes) and finally a stage is reached where ρ_R eventually becomes equal to ρ_ϕ and starts dominating thereafter. This boundary is marked as the reheating temperature $T_{\rm RH}$.

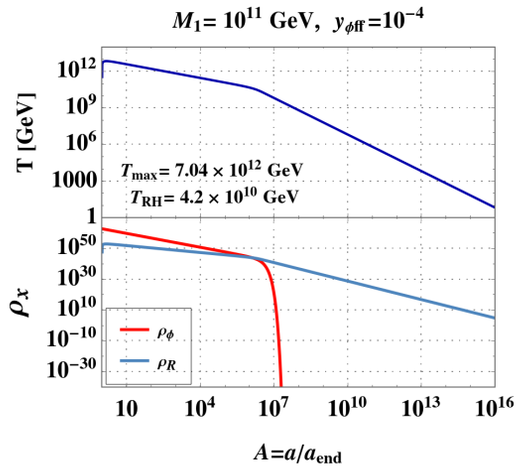

Figure 4.1: Top panel indicates T variation with the relative scale factor while the bottom panel illustrates evolution of various components of total energy density (explained in inset).

4.2.2 Change in equilibration temperature of charged Yukawa interactions

We now infer that provided the reheating temperature is smaller $T^*_{0(\alpha)}$, the epoch in which this equilibration (by equating $\langle\Gamma_\alpha\rangle$ with $\mathcal{H}$) happens may actually experience the era between $T_{\rm Max}$ and $T_{\rm RH}$. The relatively fast expansion of the Universe in this era will obviously affect the relation $\langle\Gamma_\alpha\rangle = \mathcal{H}$ (with $\langle\Gamma_\alpha\rangle \simeq 5\times10^{-3}Y^2_{\ell_\alpha}T(a)$ as presented in Eq. (1.93)) where the $r.h.s$ needs to be replaced with $\mathcal{H}(T)$ that depends on both ρ_ϕ and ρ_R. The modified $\langle\Gamma_\alpha\rangle/\mathcal{H}$ is therefore plotted against T in Fig. 4.2 indicated by the dashed lines. As expected, prior to entering into the RD phase, it depicts a non-standard behavior (slope is different within $T_{\rm Max}$ and $T_{\rm RH}$) as shown in Fig. 4.2, separately for three flavors of charged leptons. This is a new observation in our work.

We note that Y_{L_τ} comes to equilibrium around $T^*_\tau \sim 7.5\times10^{10}$ GeV (compared to $T^*_{0(\tau)} \simeq 5\times10^{11}$ GeV in standard scenario) while μ_R and e_R attain equilibriums at their standard temperatures $T^*_{0(\mu)}$ and $T^*_{0(e)}$ respectively in this case. This is because with the choice of $y_{\phi ff}$ coupling, $T_{\rm RH}$ is found to be 4.2×10^{10} GeV which falls below $T^*_{0(\tau)}$. Hence the non-standard

[1]We presume Higgs and left handed fermions (members of $SU(2)_L$ doublets) are in equilibrium (also the SM gauge bosons) immediately after production.

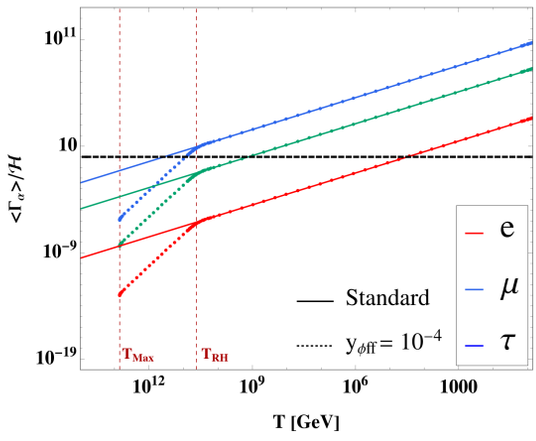

Figure 4.2: Variation of $\langle\Gamma_\alpha\rangle/\mathcal{H}$ $w.r.t.$ T is plotted for standard (solid lines) and modified (dotted) scenarios.

effect on Y_{L_μ} and Y_{L_e} interactions do not appear in this particular example. With the change of $y_{\phi ff}$, this particular situation is going to be altered of course. For further smaller $y_{\phi ff}$, $T_{\rm RH}$ may fall below $T^*_{0(\mu)}$ and correspondingly we would get a modified Y_μ ET. On the other hand, for sufficiently large $y_{\phi ff}$, the temperature regime between $T_{\rm Max}$ and $T_{\rm RH}$ is getting shortened and hence such departure in evaluating the charged lepton ET, even if it is present, becomes less prominent. At this stage, one may wonder what happens to the other SM interactions like the top, bottom, charm Yukawa interactions, EW sphaleron interactions, etc. In this regard, the point is to note that the source of the modified ET related to any interaction is related to $\mathcal{H}$ and hence all these other interactions should also be affected similarly. So overall a scaling effect $w.r.t.$ the charged lepton ET should be observed. As the strength of these interactions is more compared to Y_{L_τ}, it is natural to expect these interactions to be in equilibrium by the time T^*_τ has reached.

4.2.3 Lepton asymmetry generation

Equipped with this basic understanding behind such a non-standard situation in case of a prolonged reheating period, we now turn our attention to the realm of flavor leptogenesis. The lepton asymmetry being generated from the out-of-equilibrium decay of the lightest RHN N_1, its mass M_1 is at the center of interest. This is because, in standard thermal leptogenesis, N_1 starts to decay at a temperature $T \sim M_1$ when the Universe is radiation dominated and N_1 is present in equilibrium within the thermal bath. Contrary to this, in case of non-instantaneous reheating under study, in general there can be three possibilities: (a) $M_1 < T_{\rm RH}$, (b) $T_{\rm RH} < M_1 < T_{\rm Max}$ and (c) $M_1 > T_{\rm Max}$. While case (a) is a scenario close to standard thermal leptogenesis (and we refrain from discussing it here), case (c) stands for a situation where N_1 can not be thermally produced. Since in this case no inverse decay is possible, no washout of produced lepton asymmetry would happen. Consequently, no flavor effect would be expected in this case. So, in this work we focus on the case (b), where production of N_1 from thermal bath seems to be a possibility and it will also decay within the reheating epoch too.

To start, we need to introduce the energy density associated to N_1 (ρ_{N_1}) in the discus-

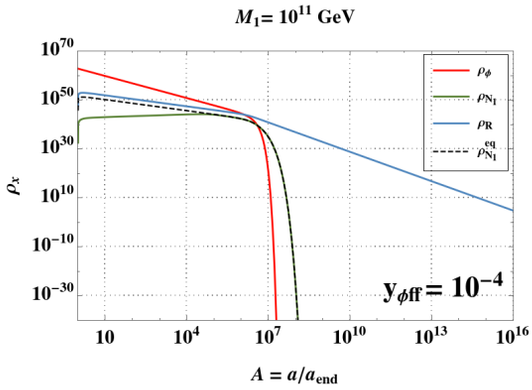

Figure 4.3: Evolution of various components of total energy density are displayed. The $*$ corresponds to the $T_{\rm RH}$.

sion as $T_{\rm Max}$ being greater than M_1, N_1 can be produced from the inverse decay[2]. For this purpose, we incorporate the type-I Lagrangian (as presented in Eq. (1.50)) into the system. The modified Hubble parameter is given by

$$\mathcal{H}^2 = \frac{\rho_\phi + \rho_R + \rho_{N_1}}{3M_P^2}. \tag{4.5}$$

Alongside, the ρ_R equation in Eq. 4.3 has an additional term $\frac{a^3}{\mathcal{H}}\langle\Gamma_{N_1}\rangle(\rho_{N_1} - \rho_{N_1}^{\rm eq})$ on the $r.h.s.$, the presence of which is to represent the dilution of ρ_R due to production of N_1 from it (via inverse decays). The decay rate of N_1 is given by $\langle\Gamma_{N_1}\rangle$ [212] and ρ_{N_1} satisfies the other equation

$$\frac{d(\rho_{N_1}a^3)}{da} = -\frac{\langle\Gamma_{N_1}\rangle a^2}{\mathcal{H}}(\rho_{N_1} - \rho_{N_1}^{\rm eq}). \tag{4.6}$$

Regarding initial conditions, in order to solve the coupled equations for ρ_ϕ, ρ_R and ρ_{N_1}, we employ $\rho_{N_1} = \rho_R = 0$ whereas energy density at the end of inflation is taken to be $\rho_{\phi_{end}} = 3V(\phi_{end})/2$. The value of ϕ_{end} for the class of models under consideration is $0.78M_P$ [301]. All the three components of the energy densities are now plotted against the relative scale factor in Fig. 4.3. For this plot, we keep the parameter $y_{\phi ff}$ same as in Fig. 4.1 and consider a specific $M_1 = 10^{11}$ GeV. We consider $M_{2(3)}$ as 100 times heavier than $M_{1(2)}$ for discussion and hence thermal generation of $N_{2(3)}$ is not possible. The neutrino Yukawa Y_ν appearing in $\langle\Gamma_{N_1}\rangle$ is evaluated with the help of Casas-Ibarra formalism [199],

$$Y_\nu = -i\frac{\sqrt{2}}{v}UD_{\sqrt{m}}\mathbb{R}^T D_{\sqrt{M}}, \tag{4.7}$$

where U is the PMNS [165, 200, 210] mixing matrix diagonalizing $m_\nu = -Y_\nu M_R^{-1}Y_\nu^T v^2/2$ ($v = 246$ GeV is the EW vev), $D_m(D_M)$ is the diagonal active neutrino (RHN) mass matrix and $\mathbb{R}$ is a complex orthogonal matrix of the form as in [312] parametrized by complex mixing angle θ_R. The values of $\mathrm{Re}[\theta_R], \mathrm{Im}[\theta_R]$ are so chosen as to produce correct baryon asymmetry via leptogenesis and also to keep Y_ν entries perturbative. We incorporate the best fit values of mixing angles and mass-squared differences [165] to define U and light neutrino mass eigenvalues (with $m_1 = 0$).

[2]For simplicity, we do not consider production via scattering.

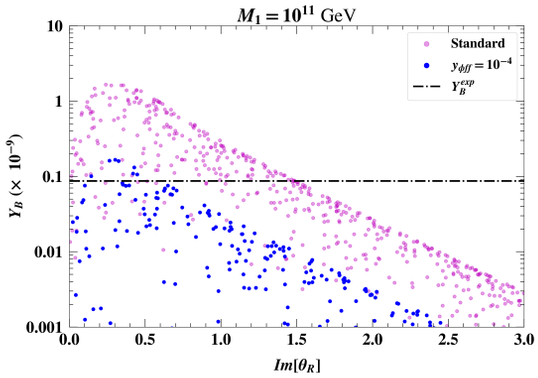

Figure 4.4: Amount of Y_B in case of (a) non-instantaneous reheating (blue) and (b) standard RD phase (magenta): variation with $\mathrm{Im}[\theta_R]$ is displayed.

As can be seen from Fig. 4.3, N_1 gradually increases, however, always remain subdominant compared to ρ_R. This is because it also decays out of equilibrium within the same period. As a result, the reheating temperature $T_{\rm RH}$ is essentially unchanged even in presence of this new component, ρ_{N_1}. From Fig. 4.2, we recall that Y_{L_τ} enters equilibrium below $T^*_\tau = 7.5 \times 10^{10}$ GeV in this modified scenario. Therefore, by the time N_1 starts to decay around $T \lesssim M_1 (= 10^{11}$ GeV), all the charged lepton Yukawa couplings are already out of equilibrium and hence, it falls in the unflavored regime. Note that for the same M_1 value, in standard thermal leptogenesis ($T^*_{0(\tau)} = 5 \times 10^{11}$ GeV), this belongs to the case of flavor leptogenesis where lepton asymmetries are produced in two orthogonal directions: τ and κ, κ forming the subspace of a coherent superposition of e and μ lepton flavors. The $B - L$ asymmetry in the unflavored regime can be studied by the following Boltzmann equation,

$$\frac{d(n_\Delta a^3)}{da} = -\frac{\langle\Gamma_{N_1}\rangle a^2}{\mathcal{H}} \left[\frac{\varepsilon_1}{M_1}(\rho_{N_1} - \rho^{\rm eq}_{N_1}) + \frac{n^{\rm eq}_{N_1}}{2n^{\rm eq}_\ell} n_\Delta \right], \tag{4.8}$$

with $n_\Delta = n_{B-L}$, while in the flavored regime, the corresponding equation would be

$$\frac{d(n_{\Delta_\alpha} a^3)}{da} = -\frac{\langle\Gamma_{N_1}\rangle a^2}{\mathcal{H}} \left[\frac{\varepsilon^\alpha_1}{M_1}(\rho_{N_1} - \rho^{\rm eq}_{N_1}) + \frac{1}{2} K^0_\alpha \sum_j (C^\ell_{\alpha\beta} + C^H_\beta) \frac{n^{\rm eq}_{N_1}}{n^{\rm eq}_\ell} n_{\Delta_j} \right]. \tag{4.9}$$

Here $K^0_\alpha = (Y^*_\nu)_{\alpha 1}(Y_\nu)_{\alpha 1}/(Y^\dagger_\nu Y_\nu)_{11}$ is flavor projector [104] and C^ℓ, C^H matrices connect the asymmetries in lepton and Higgs to asymmetries in $\Delta_\alpha = B/3 - L_\alpha$ (in terms of n_{Δ_τ} and n_{Δ_κ} here)[104]. The CP asymmetry ε^α_1 (for unflavored case, $\varepsilon_1 = \sum_\alpha \varepsilon^\alpha_1$) involved is obtained from the decay of N_1 to a specific flavor ℓ_{L_α} and estimated using standard expression [99, 104]. The final baryon asymmetry Y_B is related to n_{Δ_α} by [313]: $Y_B = \frac{28}{79} \sum_\alpha n_{\Delta_\alpha}/s$.

In Fig. 4.4, we compare the parameter space of Y_B against $\mathrm{Im}[\theta_R]$, for the choices of M_1 and $y_{\phi ff}$ discussed above, obtained in usual thermal leptogenesis (fall in two flavored regimes, shown in magenta) with that in case of prolonged reheating (unflavored regime, shown in blue). Here we scan over the range of θ_R as: $\mathrm{Re}[\theta_R]$ (0 - 2π) and $\mathrm{Im}[\theta_R]$ (0-3). We observe a clear shift in the asymmetry generation in these two cases, implying the effect of non-instantaneous reheating. Furthermore, in terms of the correct amount of baryon asymmetry, the situation becomes more restrictive as seen due to the presence of less number of

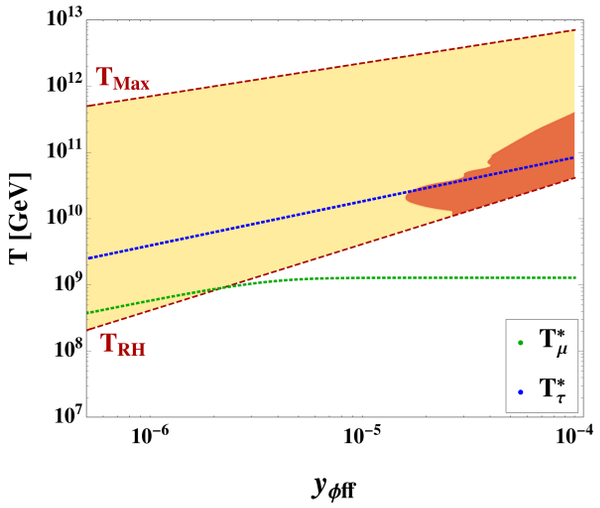

Figure 4.5: Important parameters related to temperature are plotted $w.r.t.$ inflaton-SM coupling $y_{\phi ff}$. Upper (lower) brown dashed line represents $T_{\rm Max}(T_{\rm RH}$), while blue (green) dotted line illustrates the equilibration temperature of tauon (muon) Yukawa interaction. The dark brown patch represents the allowed value of RHN mass M_1 and coupling $y_{\Phi ff}$, which can produce the correct baryon asymmetry.

blue points over magenta ones across the correct Y_B line (horizontal black dashed), when the asymmetry is generated within the reheating period.

With this understanding, we now aim to identify the region of parameter space in between $T_{\rm Max}$ and $T_{\rm RH}$, in which the observed baryon asymmetry via leptogenesis can be obtained from the decay of lightest RHN. However, in order to estimate the produced lepton asymmetry in this case, one also again needs to take into account the effect of individual lepton flavor interactions, which are non-negligible. As can be seen from the Fig. 4.5, both T^*_τ (blue dotted line) and T^*_μ (green dotted line) increase initially with the increase in $y_{\phi ff}$. Thereafter, T^*_μ saturates to a value $T^*_{0(\mu)}$ once it becomes comparable to T_{RH}. Contrary to this, T^*_τ increases monotonically with $y_{\phi ff}$. Due to such nontrivial dependance of $T^*_{0(\alpha)}$ on $y_{\phi ff}$, the flavor regimes also modify according to $y_{\phi ff}$. So, to see the effect of $y_{\phi ff}$ on the production of lepton asymmetry one needs to carefully take into account the change in the flavor regimes for each value of $y_{\phi ff}$. Dark brown patch of the Fig. 4.5 shows the region of parameter space where the correct amount of lepton asymmetry can be generated while taking into account the modified flavor regime. On the contrary, the light brown shaded region indicates the allowed parameter space when modification of flavor regimes has not been taken into account. It can be seen directly from these two patches that this modified scenario provides a more restrictive parameter space due to the modification of flavor regimes. Looking at this plot we find that successful leptogenesis can be achieved with a minimum value of $T \sim M_1 = 1.3 \times 10^{10}$ GeV and $T_{RH} = 1.1 \times 10^{10}$ GeV.

4.2.4 summary

To summarize, we have shown that the effect of a prolonged reheating period, starting from the maximum temperature of the Universe following inflation to the reheating, affects the equilibration of the charged lepton Yukawa interactions significantly. Due to the faster expansion of the Universe in this reheating period, the charged lepton Yukawa interactions enter equilibrium in a delayed fashion. This new observation depends on the effective cou-

pling of the inflaton field with SM fields. With low reheating temperature ($i.e.$ with a smaller effective coupling of the inflaton field with SM fields), the era of reheating becomes longer and hence the ET(s) can be significantly smaller. The effects of this observation should also be applicable to wider SM interactions and open a possibility for further investigation in different directions. As one such application, we proceed to study its effect on leptogenesis where the lightest RHN belonging to the type-I seesaw is being created and decayed out of equilibrium within $T_{\rm Max}$ and $T_{\rm RH}$. As expected, we find that the delayed entry of the charged lepton Yukawas in equilibrium can shift the flavor regimes of leptogenesis. Finally, taking into account such modified flavor regimes, a more restrictive parameter space for successful leptogenesis is observed.

4.3 Setup b: inflaton couples to lightest RHN and SM fermions

Motivated by the above result, in this work, we further consider an intriguing extension (in the context of case (B) itself) where in addition to the inflaton-SM fermion effective coupling ($y_{\phi ff}$) there exists a direct coupling ($y_{\phi NN}$) between the inflaton and N_1s. Introduction of such a coupling not only induces N_1s in the system from the decay of the inflaton (in addition to the thermally generated N_1), but also opens up the possibility of modifying the Hubble further, hence affecting $T_{\rm RH}$ as well as the ET depending on its relative coupling strength compared to inflaton-SM fermion coupling.

Hence, with a nonzero branching of the inflaton to N_1 in addition to the inflaton-SM fermion one, we expect to have N_1 production from inflaton decay as well as thermal production of it via inverse decay for a temperature range $T_{\rm Max} > T \gtrsim M_1$. These N_1 however find themselves in out of equilibrium as the Hubble $\mathcal{H}$ at this temperature regime remains large enough (ϕ dominates). Therefore, N_1 would decay and may contribute to lepton asymmetry generation even at temperature above M_1 unless it has been washed out by inverse decay. In case ρ_{N_1} dominates over ρ_R, the washout by inverse decay turns out to be weak so as not to erase the asymmetry. This particular era of leptogenesis turns out to be somewhat different from a purely thermal or non-thermal one since the lepton asymmetry here is generated from the decay of both the thermally produced N_1s and those produced from inflaton decays in this regime. We call it as *'quasi'*-thermal leptogenesis. Additionally for temperature below $T \sim M_1$, leptogenesis proceeds in the usual way. However, with a significantly dominant coupling of $y_{\phi NN}$ over $y_{\phi ff}$, N_1s can even be produced beyond $T = M_1$ point. In this case ($T < M_1$), such non-thermally produced N_1 would instantaneously decay and contribute to lepton asymmetry production similar to the usual *non-thermal* leptogenesis scenario.

4.3.1 Setup and Boltzmann equation

Following the above discussion, we now construct the relevant Lagrangian (apart from the SM one) as given by,

$$-\mathcal{L} = y_{\phi ff}\phi\overline{f}f + y_{\phi NN}\phi\overline{N_1}N_1 + V(\phi), \tag{4.10}$$

in addition to the Type-I seesaw Lagrangian of Eq. (1.50). Here, $y_{\phi ff}$ is only an effective coupling and $f(\overline{f})$ are the SM fermions. For simplicity, we only keep the coupling of inflaton with the lightest N_1.

After the end of the inflation, the inflaton starts to perform damped oscillations about the minima of the potential and eventually decays to the SM fermion-antifermion pair as well as to N_1 following Eq. (4.10). Here we ignore any potential contribution that may come from preheating [277, 305]. Consequently, the energy density of the inflaton field ρ_ϕ satisfies the equation:

$$\frac{d\rho_\phi}{dt} + 3\mathcal{H}\rho_\phi = -(\Gamma_{\phi ff} + \Gamma_{\phi NN})\rho_\phi, \tag{4.11}$$

where $\Gamma_{\phi ff}$ and $\Gamma_{\phi NN}$ are the decay widths of inflaton to SM fermions and N_1 respectively and expressed as

$$\Gamma_{\phi ff} = \frac{y^2_{\phi ff}}{8\pi} m_\phi\,, \quad \Gamma_{\phi NN} = \frac{y^2_{\phi NN}}{8\pi} m_\phi\,. \tag{4.12}$$

The term proportional to $\mathcal{H}$ indicates the dilution of energy density due to the expansion of the Universe while the term on the right hand side of the BE represents the dilution (hence comes with a negative sign) of the energy density of the ϕ as a result of its decay to N_1 and SM fermion/anti-fermions.

The produced fermion-antifermion pairs would interact quickly among themselves to produce other SM particles and rapidly thermalizes producing the radiation energy density component ρ_R. On the other hand, the N_1s produced from the inflaton decay further decays to the SM particles which will eventually contribute to ρ_R too. Additionally, as per our consideration in case (B), the thermal bath can also produce back N_1 particularly for the temperature of the Universe $T_{\rm Max} > T \gtrsim M_1$. The BEs for ρ_{N_1} and ρ_R can therefore be written as,

$$\frac{d\rho_{N_1}}{dt} + 3\mathcal{H}\rho_{N_1} = -(\rho_{N_1} - \rho^{eq}_{N_1})\langle\Gamma_{N_1}\rangle + \Gamma_{\phi NN}\rho_\phi\,, \tag{4.13}$$

$$\frac{d\rho_R}{dt} + 4\mathcal{H}\rho_R = (\rho_{N_1} - \rho^{eq}_{N_1})\langle\Gamma_{N_1}\rangle + \Gamma_{\phi ff}\rho_\phi. \tag{4.14}$$

In all the BEs above, $\mathcal{H}$ represents the Hubble expansion rate to be written as

$$\mathcal{H}^2 = \frac{\rho_\phi + \rho_{N_1} + \rho_R}{3M_P^2}, \tag{4.15}$$

since in this epoch $T_{\rm Max} > T > T_{\rm RH}$, the energy density of the Universe comprises of the components ρ_ϕ, ρ_{N_1} and ρ_R. The $\rho^{\rm eq}_{N_1}$ is the equilibrium energy density of N_1 as given by

$$\rho^{\rm eq}_{N_1} = \frac{M_1^4\left[\frac{3}{z^2}K_2(z) + \frac{1}{z}K_1(z)\right]}{\pi^2}, \tag{4.16}$$

where $z = M_1/T(a)$ and K_1, K_2 are the modified Bessel function. The presence of this term in the above BEs is related to the existence of the inverse decay from radiation bath to produce N_1. Eq.(4.11), (4.13)-(4.14) therefore together represent the most general set of

equations to study the scenario under consideration.

After discussing the N_1 production and the related BEs to study the respective components of the energy densities of the Universe, we now turn our attention to construct the BEs relevant for leptogenesis. As discussed earlier, being Majorana particle, the decay of the lightest RHN N_1 is a lepton number violating one and can produce CP asymmetry, which will eventually generate lepton asymmetry of the Universe. In order to take care effects of charged lepton Yukawa equilibration of different flavors, one needs to incorporate the BE presented in Eq. (4.9). Apart from the flavored setup, a situation may arise where flavor effects are not that important in discussing leptogenesis. In that case, an unflavored scenario exhibits where the evolution of the $B-L$ asymmetry is governed by the single BE given by Eq. (4.8).

Solving Eq. (4.11), (4.13), (4.14) and (4.9) or (4.8) simultaneously, will lead to the evolution of energy density of relevant elements of the Universe and produced lepton asymmetry from the time of the end of inflaton till today. However, while solving these BEs, it is convenient to use new variables [270, 287] for which we use the following transformations:

$$\begin{aligned} E_\phi = \rho_\phi a^3\,, \quad E_{N_1} = \rho_{N_1} a^3\,, \quad R = \rho_R a^4\,, \\ N_{B-L} = n_{B-L} a^3\,, \quad N_{\Delta_\alpha} = n_{\Delta_\alpha} a^3 \end{aligned} \tag{4.17}$$

Moreover, it is convenient to write the BEs as functions of the scale factor (a) rather than time (t). More precisely, we use the ratio of the scale factor to its value at the end of inflation,

$$A = \frac{a}{a_{\rm end}}. \tag{4.18}$$

We consider the initial value $a_{\rm end} = 1$ without loss of any generality. Using the newly introduced dimensionless variables, BEs in Eq. (4.11), (4.13), (4.14), (1.84) and (1.83) will look like:

$$\frac{dE_\phi}{dA} = -\frac{(\Gamma_{\phi ff} + \Gamma_{\phi NN})E_\phi}{A\mathcal{H}}\,, \tag{4.19}$$

$$\frac{dR}{dA} = \frac{\langle\Gamma_{N_1}\rangle a_{\rm end}}{\mathcal{H}}(E_{N_1} - E^{\rm eq}_{N_1}) + \frac{\Gamma_{\phi ff} E_\phi}{\mathcal{H}}\,, \tag{4.20}$$

$$\frac{dE_{N_1}}{dA} = \frac{\Gamma_{\phi NN} E_\phi}{A\mathcal{H}} - \frac{\langle\Gamma_{N_1}\rangle}{A\mathcal{H}}(E_{N_1} - E^{\rm eq}_{N_1})\,, \tag{4.21}$$

$$\frac{dN_{\Delta_\alpha}}{dA} = -\frac{\langle\Gamma_{N_1}\rangle}{A\mathcal{H}}\left[\frac{\varepsilon_{\ell_\alpha}}{M_1}(E_{N_1} - E^{\rm eq}_{N_1}) + \frac{1}{2}K^0_\alpha \sum_\beta (C^\ell_{\alpha\beta} + C^H_\beta)\frac{Y^{\rm eq}_{N_1}}{Y^{\rm eq}_\ell} N_{\Delta_\beta}\right], \tag{4.22}$$

$$\frac{dN_{B-L}}{dA} = -\frac{\langle\Gamma_{N_1}\rangle}{A\mathcal{H}}\left[\frac{\varepsilon_\ell}{M_1}(E_{N_1} - E^{\rm eq}_{N_1}) + \frac{Y^{\rm eq}_{N_1}}{2Y^{\rm eq}_\ell} N_{B-L}\right]. \tag{4.23}$$

Finally, the produced lepton asymmetry can be converted to baryon asymmetry using the relation:

$$Y_B = \frac{28}{79}\frac{1}{sA^3} N_{B-L} = \frac{28}{79}\frac{1}{sA^3}\sum_\alpha N_{\Delta_\alpha}. \tag{4.24}$$

4.3.2 Results

We now employ the set of BEs Eq. (4.19)-(4.21) simultaneously in order to estimate the individual components of energy densities such as ρ_ϕ, ρ_R and ρ_{N_1} which are connected to E_ϕ, E_R and E_{N_1} respectively via Eq. (4.17). By knowing ρ_R as a function of the scale factor a or the rescaled one A, the temperature can be defined by Eq. (4.4). Then, using Eq. (4.15), we estimate the shift of the ET if any from their standard estimate (see Fig. 1.4) by comparing the interaction rate of charged lepton Yukawa interaction of individual flavor $\langle\Gamma_\alpha\rangle$ with $\mathcal{H}$. Afterward, depending on the shift of ET of individual flavor, we proceed for evaluating the flavored (unflavored) $B-L$ asymmetries by solving Eq. (4.22) (Eq. (4.23)) where we also feed the solutions of other Eqs. (4.19)-(4.21).

In order to evaluate the BAU today following the above strategy, we notice that the mechanism is controlled by the following independent parameters (i) $y_{\phi ff}$ [inflaton-SM fermion effective coupling], (ii) $y_{\phi NN}$ [inflaton-RHN coupling], (iii) M_1 [the lightest RHN mass] and (iv) $\{Re[\theta_R],\ Im[\theta_R]\}$ [constituents of R matrix to estimate Y_ν]. We will maintain a typical hierarchy of RHN masses as: $M_3 = 10^2 M_2 = 10^4 M_1$. Furthermore, the value of $\lambda = 2\times10^{-11}$ is determined such that the inflationary observables like spectral index and tensor-to-scalar ratio are found to be within 95% C.L. of the Planck+BICEP2/Keck (PBK) constraints. Like the previous study [314], here also we confine ourselves by choosing $y_{\phi ff} \lesssim \mathcal{O}(10^{-5}-10^{-4})$ [301, 315] as above this value, non-perturbative production of fermions from inflaton decay may start to dominate. As a result, perturbative prescription for particle production would be invalid.

[In absence of inflaton-RHN coupling:] Note that the present scenario differs from the previous one due to the inclusion of $y_{\phi NN}$ coupling in this work. Hence, a choice of the parameter $y_{\phi NN} = 0$ should reproduce the outcome of our previous work. We therefore start studying the phenomenology by choosing $y_{\phi NN} = 0$ (case I) first and then turning on $y_{\phi NN}$ gradually to a value comparable to $y_{\phi ff}$. We choose $y_{\phi ff} = 4\times10^{-5}$ so as to be consistent with the perturbative limit on it. The Left plot of Fig. 4.6 shows the variation of temperature (along y axis) with the parametrized scale factor A (along x axis) where we use the solution for the radiation energy density of Eq. (4.20) (ignoring the first term in the right hand side as $y_{\phi NN}=0$) coupled with Eqs. (4.19) and put it back in Eq. (4.4). After inflation,

Case	$y_{\phi NN}$	$T_{\rm RH}$ (GeV)	T^*_τ (GeV)	Y_B
I	0	1.67×10^{10}	4.7×10^{10}	8.72×10^{-11}
II	10^{-7}	1.67×10^{10}	4.7×10^{10}	8.72×10^{-11}
III	10^{-5}	1.72×10^{10}	4.8×10^{10}	3.52×10^{-10}
IV	4×10^{-5}	2.37×10^{10}	5×10^{10}	4.29×10^{-10}

Table 4.1: Values of $T_{\rm RH}$, T^*_τ and final baryon asymmetry Y_B for different choices of $y_{\Phi NN}$. Here we have fixed $y_{\phi ff} = 4\times10^{-5}$ and $M_1 = 6\times10^{10}$ GeV. $T_{\rm Max} = 4.45\times10^{12}$ GeV is found to be constant for all four cases.

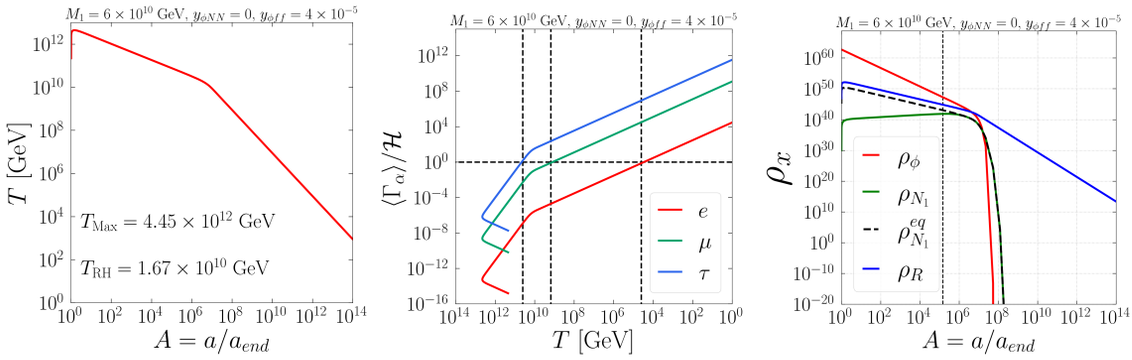

Figure 4.6: Evolution of temperature T (left panel) and various energy densities (right panel) $w.r.t.$ rescaled scale factor for $M_1 = 6 \times 10^{10}$ GeV and $y_{\phi NN} = 0$. In the middle plot we show the dependence of $\langle \Gamma_\alpha \rangle / \mathcal{H}$ on T for the same choice of M_1 and $y_{\phi NN}$.

the temperature of the Universe then attains a maximum value $\sim T_{\rm Max} = 4.45 \times 10^{12}$ GeV and thereafter falls (having a different slope compared to the RD epoch) to a point where $\rho_\phi = \rho_R$ is reached which defined the end of reheating as $T_{\rm RH} = 1.67 \times 10^{10}$ GeV.

Due to such faster expansion and nontrivial scale factor dependence of temperature during this extended reheating period $T_{\rm Max} > T > T_{\rm RH}$, the charged lepton Yukawa interaction (particularly for τ_R in this case) will come to thermal equilibrium at a smaller temperature than the standard radiation-dominated case. To provide a concrete evaluation of the same, we include middle plot of Fig. 4.6 where $\langle \Gamma_\alpha \rangle / \mathcal{H}$ evolution ($\alpha = e, \mu, \tau$ with blue, green and red lines respectively) are plotted against temperature T variation. This shift in τ_R ET is depicted clearly by the intersection point of the blue line and the horizontal dashed line indicating $\langle \Gamma_\tau \rangle / \mathcal{H} = 1$ in middle plot of Fig. 4.6. The relevant ET in this extended period of reheating turn out to be $T_\tau^* = 4.7 \times 10^{10}$ GeV and is included in Table 4.1 along with values of other parameters. The reheating temperature being bounded by $\sim \mathcal{O}(10^{10})$ GeV, no change in μ_R or τ_R ET has been found as expected.

With such a shift in the ET of τ_R in this particular case (first row of Table 4.1), flavor leptogenesis would get affected. In order to have an impact of it on flavor leptogenesis, we choose a value of N_1 mass $M_1 = 6 \times 10^{10}$ GeV which falls intermediate between the associated $T_{\rm Max}$ and $T_{\rm RH}$. First we estimate the evolution of various energy densities ρ_ϕ, ρ_R, ρ_{N_1} in this scenario against A by solving Eqs. (4.19)-(4.21) simultaneously as shown in the rightmost plot of Fig. 4.6 indicated by red, blue and green solid lines respectively. In evaluating Y_ν, we consider $Re[\theta_R] = 6.03$, $Im[\theta_R] = 0.22$ (the reason behind such a choice is to have correct baryon asymmetry finally). Note that in absence of $y_{\phi NN}$ coupling, N_1s are thermally generated during $T_{\rm Max} > T > M_1$ from the thermal bath consisting of SM fields, thanks to radiation production from inflaton decay via $y_{\phi ff}$. As the Universe expands, the radiation energy density is being diluted non trivially till an equality with inflaton energy density defining $T_{\rm RH}$ (intersection of blue and red lines). Standard RD follows only beyond this point.

These N_1s would effectively decay around $T \sim M_1$ and produce the lepton asymmetry via leptogenesis. The N_1 being thermally produced, this scenario is similar to the standard flavored *thermal* leptogenesis scenario, though impacted by the shift in T_τ^* as seen above. We find $M_1 > T_\tau^*$, all the charged lepton Yukawa interactions remain out of equilibrium in

this phase. As a consequence, an unflavored leptogenesis prevails here in case of extended period of reheating. This is the main difference we experience while comparing it with standard flavored *thermal* leptogenesis scenario in which with leptogenesis scale $T \sim M_1$, τ lepton Yukawa interaction occurs rapidly following which a two-flavor setup must be incorporated (compared to the unflavored one in present case). The corresponding evolution of lepton asymmetry is shown by black line in bottom portion of Fig. 4.7 as a function of the modified scale factor A which saturates to a lepton asymmetry value that eventually converts to the observed baryon asymmetry value. To make the correspondence between ρ_{N_1} and the production of Y_{B-L}, we also incorporate the ρ_{N_1} evolution in the top portion of the figure.

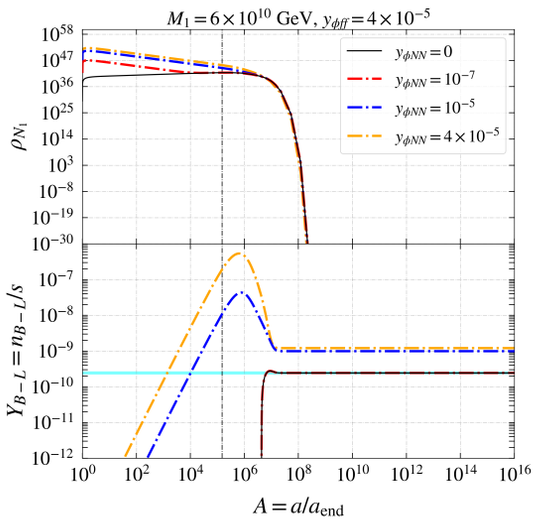

Figure 4.7: Evolution of energy density of N_1 (upper panel) and produced baryon asymmetry (lower panel) $w.r.t.$ rescaled scale factor for different values of $y_{\phi NN}$ for $M_1 = 6 \times 10^{10}$ GeV and $y_{\phi ff} = 4 \times 10^{-5}$.

[In presence of inflaton-RHN coupling:] We now turn on inflaton-RHN coupling and observe its impact on the charged lepton Yukawa equilibration and consequently on the produced baryon asymmetry during reheating era. Let us begin with a sufficiently small $y_{\phi NN} = 10^{-7}$ (tabulated in Table 4.1 as case II) as compared to $y_{\phi ff}$ chosen. As shown in the Fig. 4.8, switching on $y_{\phi NN}$ causes the inflaton to produce a large number of N_1s (indicated by green line) initially. This can be understood if we compare the ρ_{N_1} evolution (green line in Fig. 4.8) above temperature $T = M_1$ (indicated by the vertical black small dashed line) in this case versus the case with solely thermally produced N_1s (see Fig. 4.6). However, as the temperature drops, the production of N_1 from inflaton decay does not keep up with the Universe's expansion rate due to its feeble coupling chosen. As a result, the energy density of these N_1s (as decay products of inflaton) gets diluted and at some stage the production of N_1s from the inverse decay dominates over it. This is evident in the left plot of Fig. 4.8 by the sudden change of slope of ρ_{N_1} just before $T = M_1$ which coincides with the energy density of thermally produced N_1s of Fig. 4.6. This continues till a point beyond which N_1 decay starts to contribute to lepton asymmetry production.

We also notice that due to the dominant decay of ϕ into SM fermions, the ρ_ϕ and ρ_R (mainly contributed from $y_{\phi ff}$ coupling) do not alter by a noticeable amount and hence $\mathcal{H}$

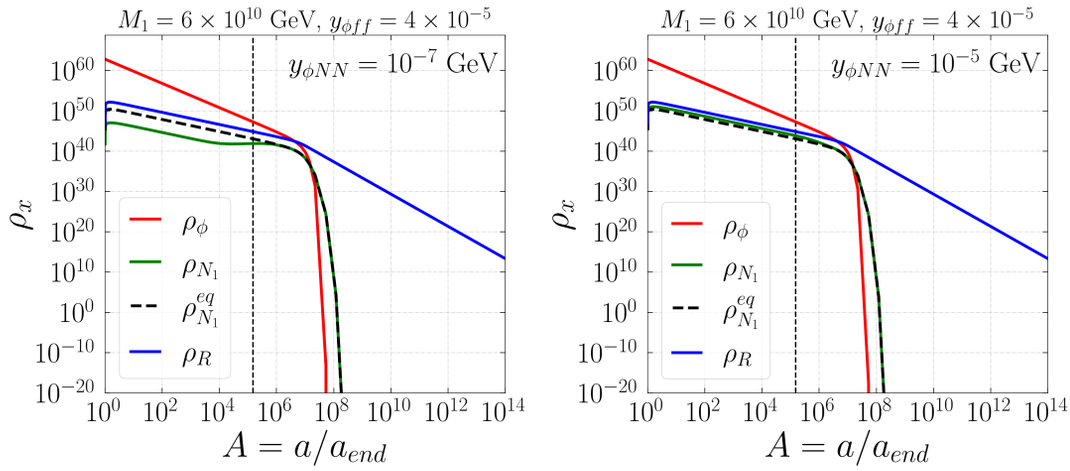

Figure 4.8: Evolution of different energy densities $w.r.t.$ rescaled scale factor for $y_{\phi NN} = 10^{-7}$(left panel) and $y_{\phi NN} = 10^{-5}$ (right panel). Here we set $M_1 = 6 \times 10^{10}$ GeV and $y_{\phi ff} = 4 \times 10^{-5}$.

remains essentially unchanged compared to the previous case with $y_{\phi NN}$ =0. As a result, together with $T_{\rm Max}$ and $T_{\rm RH}$, the τ_R ET T_τ^* remains identical with the *thermal* case (see second row of Table 4.1). Hence the present situation falls in the category of unflavored leptogenesis. The evolution of the $B-L$ asymmetry for $y_{\phi NN} = 10^{-7}$ scenario is presented by the red dash-dotted line in the bottom plot of Fig. 4.7 which overlaps with the $y_{\phi NN} = 0$ case (solid black line), thereby satisfying the observed baryon asymmetry of the Universe.

As we further increase the strength of the inflaton-N_1 coupling, $i.e.$ $y_{\phi NN} = 10^{-5}$ (as case III of Table 4.1 while keeping other parameters fixed at their previous values), a change in ρ_{N_1} becomes visible. The right plot of Fig. 4.8 shows the behavior of the energy densities of different components of the Universe in this case. Note that contrary to cases I and II, dominant contribution to ρ_{N_1} here follows from the N_1s being decay products of inflaton as it supersedes the thermally produced ones from inverse decay. The radiation component (blue line) however still remains dominant compared to ρ_{N_1} (green line). Note that $T_{\rm Max}$ remains unaffected as it is mainly controlled by $y_{\phi ff}$ coupling (fixed for cases I-IV) responsible for initial radiation production. However a small shift in the $T_{\rm RH}$ as compared to cases I and II, is observed and indicated in Table 4.1. This happens as a result of higher $y_{\phi NN}$ coupling which causes the inflaton to decay earlier than cases I and II so that $\rho_\phi = \rho_R$ defining the $T_{\rm RH}$ is realized at a slightly higher temperature. Due to the dominance of ρ_R (almost unchanged compared case I and II) over ρ_{N_1}, the temperature evolution above M_1 remains close to the two earlier cases. For the same reason, $\mathcal{H}$ is also almost unaffected and this is reflected in the evaluation of T_τ^* (only a slight change) as included in Table 4.1. As previously discussed, here also, even though we have a slightly higher value of T_τ^* than the previous cases, the leptogenesis scale however remains larger $w.r.t.$ T_τ^*. Hence, an unflavored prescription is still adequate for estimating the lepton asymmetry.

The evolution of produced lepton asymmetry in this case III is shown by the blue dash-dotted line in the bottom panel of Fig. 4.7. As seen in this plot, the lepton asymmetry starts to being produced at a stage above temperature $T \sim M_1$. This is related to the fact that N_1s produced during this era of reheating find themselves in out of equilibrium ($\mathcal{H}$ is larger than decay width of N_1) and would decay. Additionally, ρ_{N_1} being comparable to ρ_R, the inverse

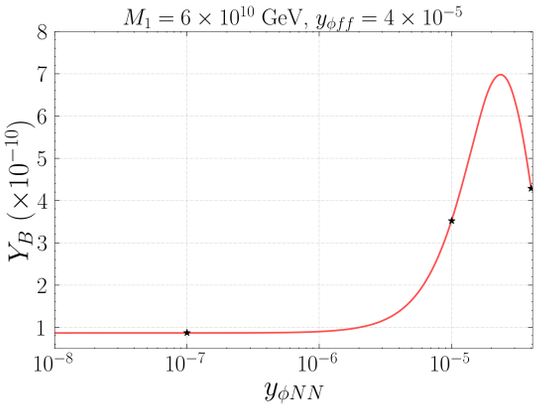

Figure 4.9: Variation of final baryon asymmetry Y_B *w.r.t.* $y_{\phi NN}$ for $M_1 = 6 \times 10^{10}$ GeV and $y_{\phi ff} = 4 \times 10^{-5}$. The points indicated by "star" represent the case-II-IV from Table 4.1.

decay process (related with neutrino Yukawa coupling) remains subdominant compared to the N_1 decay. As a result, lepton asymmetry (still unflavored though) produced from such decay of N_1 would not be washed out completely and a non-zero asymmetry survives. The amount of asymmetry production increases till a point where ρ_{N_1} ceases to exist. Beyond it, Y_{B-L} falls to some extent, before attaining its asymptotic value which is larger than the value of the lepton asymmetry necessary for the production of observed baryon asymmetry, as the produced asymmetry gets diluted due to the increase of entropy (N_1 decay produces a sizeable ρ_R and hence, entropy) in the Universe. Note that this phase of leptogenesis is different from *thermal* leptogenesis scenario as N_1s are never in thermal equilibrium. On the other hand, this is not purely the case of *non-thermal* leptogenesis which happens with N_1, as the decay product of inflaton, finding itself in an environment with $T \ll M_1$ (so, thermal generation is ruled out). So here with case (B), we find a nonstandard generation of lepton asymmetry as a consequence of extended reheating where the inflaton has a sizeable coupling with the lightest RHN. As discussed in the beginning of section, we call it a 'quasi'-thermal leptogenesis as neither it is the case of a purely thermal nor that of *non-thermal* leptogenesis. The value of Y_B can be brought down to the correct baryon asymmetry by decreasing $Im[\theta_R] = 0.031$, while all other parameters/outcomes are unaffected.

Finally, the above discussed effect becomes prominent if we choose to increase the $y_{\phi NN}$ coupling further, say $y_{\phi NN} = y_{\phi ff}$ as included in case IV of Table 4.1. In this case, we obtain $\rho_{N_1} = \rho_R$. As radiation and N_1s contribute equally to the energy density of the Universe during the reheating period, the expansion rate of the Universe gets modified in this scenario, affecting the $T_{\rm RH}$ as well as T_τ^*. In this case, we get a larger $T_{\rm RH}$ as inflaton decays earlier than the previous case owing to the larger $y_{\phi NN}$ coupling. The related numerical estimates for this case IV are listed in the fourth row of Table 4.1. In this case also, a larger baryon asymmetry of the Universe is created which can be settled to the observed Y_B value without altering any other parameter/predicted values once we reduce the value to $Im[\theta_R] = 0.02$.

In Table 4.1, we have listed a few specific values of $y_{\phi NN}$ coupling to describe the impact of reheating on leptogenesis. In Fig. 4.9, we provide the estimate of final baryon asymmetry (via unflavored leptogenesis) once the Yukawa coupling $y_{\phi NN}$ is varied ($y_{\phi NN} \leq y_{\phi ff}$). As already found in cases I-III, with tiny $y_{\phi NN}$ coupling ($y_{\phi NN} \lesssim 10^{-6}$), the final baryon asym-

Point	$y_{\phi NN}$	$y_{\phi ff}$	$T_{\rm Max}$ (GeV)	M_1 (GeV)	$T_{\rm RH}$ (GeV)	T^*_τ (GeV)	T^*_μ (GeV)	Y_B
BP1	10^{-6}	10^{-7}	2.23×10^{11}	5×10^9	4.2×10^8	2×10^9	7×10^8	5.67×10^{-9}
BP2	5×10^{-7}	5×10^{-8}	1.6×10^{11}	5×10^9	2.1×10^8	1.5×10^9	4×10^8	3.60×10^{-9}
BP3	10^{-7}	10^{-8}	7.04×10^{10}	5×10^9	4.2×10^7	6×10^8	1.3×10^8	7.28×10^{-10}

Table 4.2: We list three benchmark points (BP) where the leptogenesis scale falls in between $T_{\rm Max}$ and $T_{\rm RH}$. While BP1 represents the case where M_1 is closer to $T_{\rm RH}$, BP2 represents an intermediate scenario and BP3 indicates a scenario where M_1 lies closer to $T_{\rm Max}$.

metry Y_B almost remains independent of $y_{\phi NN}$. Thereafter, a rise in Y_B can be seen due to the fact that the production of RHN N_1 from the inflaton decay also becomes significant. This additional production channel causes a significant rise in the N_1's abundance ρ_{N_1} which further leads to a larger production of lepton asymmetry (also the baryon asymmetry). This behavior is also clear from Fig. 4.7. A peak in Y_B is observed when $y_{\phi NN} \simeq 2 \times 10^{-5}$ after which Y_B is reduced once the $y_{\phi NN}$ is further increased. This fall can be understood by looking at the third term of Eq. (4.23) where one notes that a larger production of asymmetry also results in a larger washout of the asymmetry.

[With dominant inflaton-RHN coupling:] So far the discussion we have, we find that the gradual increase of $y_{\phi NN}$ coupling not only affects the temperature behavior and expansion rate of the Universe during reheating period but also impacts the lepton asymmetry production in this *quasi*-thermal regime. However we have restricted ourselves with values of couplings associated to the inflaton below $\mathcal{O}(10^{-5} - 10^{-4})$ so as to keep the analysis consistent with perturbative reheating era [301, 315]. Alongside, we take $y_{\phi ff}$ at a borderline value 4×10^{-5} and hence we are unable to make $y_{\phi NN}$ larger than $y_{\phi ff}$ by order(s) of magnitude and discuss the impact of such consideration. Also, with such choice of $y_{\phi ff}$, the reheating temperature turns out to be high enough so as to keep M_1 accordingly large (to realize scenario [B]).

With an aim to observe the consequence of $y_{\phi NN} > y_{\phi ff}$ while keeping things more flexible such as lowering the scale of leptogenesis impacted by the extended period of reheating, we now consider three specific situations: (i) M_1 is close to $T_{\rm RH}$ [BP1], (ii) M_1 is intermediate between $T_{\rm Max}$ and $T_{\rm RH}$ [BP2], and (iii) M_1 is close to $T_{\rm Max}$ [BP3] where the mass of the lightest RHN is fixed at $M_1 = 5 \times 10^9$ GeV while $y_{\phi ff}$ and $y_{\phi NN}$ are floated to realize such considerations. We choose the values of $Re[\theta_R] = 2.83$ and $Im[\theta_R] = 0.24$ the result of which is consistent with correct baryon asymmetry. In the standard *thermal* framework, this choice of M_1 will lead to a two flavor leptongenesis scenario. The purpose of such a choice is to compare the outcome of the extended period of reheating on final baryon asymmetry generation with $y_{\phi NN} > y_{\phi ff}$.

Note that as inflaton-SM fermion coupling essentially define the $T_{\rm Max}$ while $y_{\phi NN}$ has some role to play in determining $T_{\rm RH}$, we first make some appropriate choices of these two parameters in defining the three benchmark cases BP-1,2,3. They are listed in Table 4.2. For all these sets, $y_{\phi NN}$ remains one order of magnitude larger than $y_{\phi ff}$ coupling. In evaluating the temperature evolution during the reheating, we solve Eqs. (4.19)-(4.21) as a function of the rescaled scale factor A simultaneously and using Eq. (4.4), temperature is evaluated.

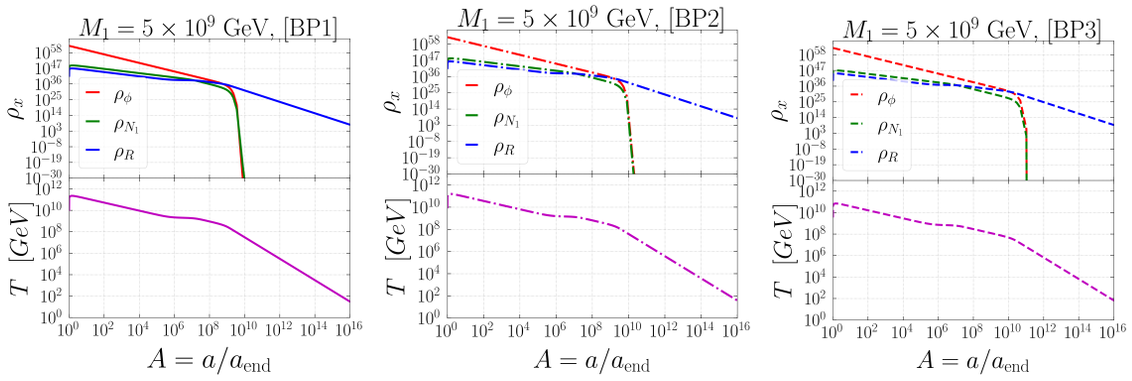

Figure 4.10: Evolution of different energy densities (upper panel) and temperature T (lower panel) $w.r.t.$ rescaled scale factor for BP1 (left panel), BP2 (middle panel), and BP3 (right panel). Here we fix $M_1 = 5 \times 10^9$ GeV and $\theta_R = 2.83 + 0.24i$.

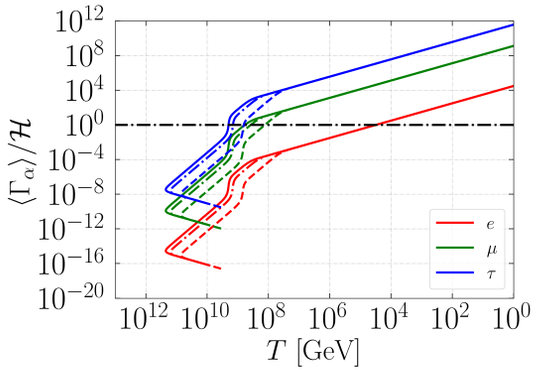

Figure 4.11: Variation of $\langle\Gamma_\alpha\rangle/\mathcal{H}$ $w.r.t.$ T for $M_1 = 5 \times 10^9$ GeV and $\theta_R = 2.83 + 0.24i$. Here solid lines indicate the BP1, dashed dotted line represents BP2, and BP3 is denoted by dashed lines.

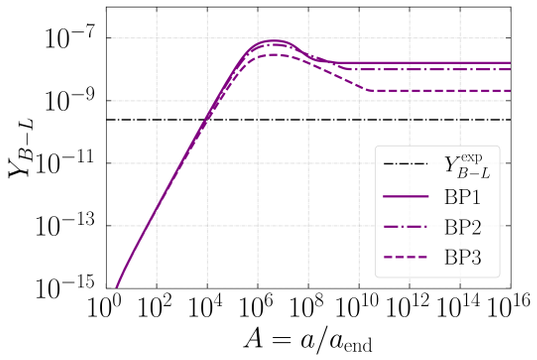

Figure 4.12: Evolution of produced lepton asymmetry $w.r.t.$ rescaled scale factor for all the three BPs for $M_1 = 5 \times 10^9$ GeV and $\theta_R = 2.83 + 0.24i$.

Bottom panels of all three plots of Fig. 4.10 represent the temperature variation with A and upper panels depict the same for energy densities of different components.

As seen from the plots, immediately after the end of inflation, the temperature reaches a maximum value $T_{\rm Max}$. Then it starts to decrease in accordance with our previous discussion due to faster expansion of the Universe during this period of extended reheating. However, an interesting departure of T from this fall is observed around $T \sim M_1$. This is related to the emergence of a new production channel, producing radiation from N_1 decay asa result of $y_{\phi NN}$ dominance. An interplay between such additional injection of radiation in the bath (which tries to increase ρ_R) and the depletion of ρ_R due to Hubble expansion, a plateau like region is formed in T evolution plot. This period however does not last long as eventually Hubble expansion rate overtakes this radiation production rate from N_1 decay (ρ_{N_1} decreases sharply beyond a point). Eventually, radiation dominates over matter beyond $T_{\rm RH}$ and temperature of the Universe drops as A^{-1}. In the upper panels of Fig. 4.10, we note that due to choice(s) of smaller coupling(s) $y_{\phi ff}$ ($y_{\phi NN}$) in going from BP1 to BP3, inflaton takes larger time to decay for BP3 (BP2)compared to BP1. As a result, matter radiation equality shifts at a later epoch resulting in lower reheating temperature for BP3 (BP2) relative to BP1.

This nontrivial behavior of temperature along with the larger expansion rate of the Universe during reheating period affects the ETs of charged lepton Yukawa interactions as can be seen from Fig. 4.11. For RHN mass $M_1 = 5 \times 10^9$ GeV, though there is no shift in ET for right-handed electron, ample amount of change can be seen for ET for μ_R and τ_R compared to the standard RD scenario for all three BPs. This change makes the charged Yukawa interactions come to equilibrium at a much lower temperature which are included in Table 4.2.

As a consequence of considerably lower values of T^*_μ and T^*_τ, we expect the quantum decoherence of the SM lepton doublet states to take place here at much lower temperatures (same as charged lepton ET) compared to the standard RD scenario. Hence, for all three BPs, lepton asymmetry generation process turns out to be not affected by individual charged lepton doublets at leptogenesis scale $M_1 = 5 \times 10^9$ GeV and an unflavored leptogenesis prevails here. This is a new result as compared with earlier standard analysis presented in subsection 1.6.2.1, where at this leptogenesis scale, τ_R was already in equilibrium affecting the lepton asymmetry generation along τ direction distinctively. Accordingly, a two flavor leptogenesis was incorporated for correct generation of lepton asymmetry. On the other hand, in this present case incorporating the effect extended reheating (with inflaton-RHN dominance), unflavor approach to evaluate the baryon asymmetry of the Universe would be enough.

For all three BPs, a different rate of washout during the reheating period accounts for the main difference in the produced final baryon asymmetry. Dashed purple line of Fig. 4.12 shows that as M_1 is closer to $T_{\rm Max}$ for BP3 as a result of which the produced asymmetry suffers a larger amount of washout (due to Hubble expansion) contrary to BP1 and BP2. Finally, even with a relatively low M_1 in this *quasi*-thermal regime, an overproduction of baryon asymmetry by one to two order(s) of magnitude is observed for these three BPs relaxing the parameter space even further $w.r.t.$ the modified thermal leptogenesis scenario studied in section 4.3.2. For completeness purpose, we notice that such final Y_B values can

be brought down to correct level of baryon asymmetry by changing θ_R without altering other parameter values or the outcomes such as $T_{\rm RH}$ and T^*_α. For example, for BP1 (BP2), one needs to set $Im[\theta_R] = 0.002\ (0.005)$, while for BP3, $Im[\theta_R]$ can be fixed at 0.02 so that observed baryon asymmetry can be generated.

4.3.3 Summary

In this section, we have shown that an extended period of reheating resulting from inflaton-decay into radiation together with the lightest RHN can significantly alter the ET of the charged lepton Yukawa interactions. Consequently, flavored leptogenesis mechanism gets affected. We start with a discussion on how the ET(s) of charged lepton Yukawa interaction(s) can be estimated in a RD Universe and its impact on lepton asymmetry generation known as flavored leptogenesis. In such a setup, the reheating process is generally assumed to be instantaneous and happens to be higher than the mass of the decaying RHN whose decay contributes to lepton asymmetry production. However, depending on the inflaton coupling to SM particles, the reheating process may survive a longer period creating a prolonged era of reheating, from $T_{\rm Max}$ to $T_{\rm RH}$. Motivated by our recent finding on the impact of this extended era of reheating on charged lepton ET and flavored leptogenesis, here we extend the setup by including additional inflaton-RHN coupling.

We find that with relatively large value of inflaton-RHN coupling compared to the inflaton-SM fermion effective coupling, the reheating period gets further modified. While the inflaton-SM fermion coupling mainly controls the maximum temperature of the Universe immediately after inflation, the inflaton-RHN coupling has the potential to impact the reheating temperature. The production of RHN and SM bath from the inflaton decay during this period of prolonged reheating helps the Universe to expand at a much faster rate (depending on the inflaton-RHN coupling though) in comparison to the scenario where inflaton decays directly to radiation solely. As a result of such faster expansion, along with the modified temperature behavior, the charged Yukawa interactions enter into equilibrium in a delayed fashion. We also observe that such a delayed equilibration of charged lepton Yukawa interactions can significantly modify the lepton asymmetry generation compared to what is observed in *thermal* leptogenesis. For example, a flavored leptogenesis scenario found to be in two flavor regime in standard *thermal* leptogenesis may emerge as an unflavored one here.

Another interesting outcome of the present scenario is revealed with a dominant inflaton-RHN coupling $w.r.t.$ inflaton-SM fermion effective coupling. Here we encounter an unusual situation where the lepton asymmetry starts to be produced at a temperature above the mass of the lightest RHN without being completely washed out. In fact, the reheating era produces an environment where the lightest RHN find itself in out-of-equilibrium in this regime and its decay therefore contributes to lepton asymmetry production. In a way, this helps to reduce the scale of leptogenesis since the inclusion of inflaton-RHN coupling may inject a large amount of RHN into the system on top of thermally produced ones (whose decay also contribute to produce lepton asymmetry) during reheating thereby resulting an enhanced lepton asymmetry. The framework however can be extended beyond our present consideration. In some of the low scale leptogenesis scenarios, the framework might alter the prediction as well as allowing the leptogenesis scale to drop even further opening the

possibility to explore leptogenesis in collider experiments. The related study is beyond the scope of this paper and we plan for some more work in these directions in future.

Chapter 5

Summary and conclusion

Various astrophysical and cosmological experiments continue to advocate a dynamical origin of the matter-antimatter asymmetry. Leptogenesis is an economical setup that can generate such baryon asymmetry dynamically. Due to its close relationship with the seesaw mechanism of neutrino mass generation, it is also arguably the most popular mechanism today. Furthermore, individual lepton flavors can play a nontrivial role during lepton asymmetry generation if their interaction strength becomes comparable to the decay rate of the heavy particle state responsible for asymmetry generation. This leads to a much richer dynamics involved in the production of lepton asymmetries. Keeping this in mind, the present thesis focuses on analyzing different scenarios that can impact the flavor leptogenesis mechanism or vice versa.

In chapter 1, we briefly introduce the SM of particle physics and standard big bang cosmology, together with the issues they fail to address. Next, we discuss in detail some of these issues which are relevant to the present thesis. Since the thesis revolves around the flavor leptogenesis mechanism, we provide an elaborate discussion on leptogenesis setup and subsequently discuss the importance of lepton flavor on leptogenesis.

In chapter 2, we provide a flavor symmetric origin of the unique mixing pattern observed in the lepton sector (compared to its quark-sector counterpart) as well as the matter-antimatter asymmetry of the Universe. To realize this scenario, we incorporate A_4 flavor symmetry and include three RHNs (for neutrino mass generation via type-I seesaw) and three flavons that transform nontrivially under A_4. The structure leads to a Dirac Yukawa mass matrix with both symmetric and anti-symmetric off-diagonal contributions along with a non-diagonal charged lepton mass matrix. The off-diagonal entries plays an important role in generating nonzero θ_{13}. The setup not only excludes maximum CP asymmetry in the leptonic sector but also favors mixing angle θ_{23} below 45°. The presence of RHNs provides an opportunity to study the generation of lepton asymmetry from their CP-violating decay. However, the degenerate mass spectrum generated due to imposed symmetry prevents us from going further, as the CP asymmetry generation mechanism fails at the exact degenerate limit. So, we adopt the renormalization group effects into consideration to create sufficient mass splitting among RHNs. We further aim to check what could be the lowest mass scale of RHN so as to produce the baryon asymmetry correctly. Hence, we consider the flavor ef-

fects in leptogenesis. Ultimately, we figure out that the parameter space satisfying neutrino oscillation data is good enough to produce a sufficient amount of lepton asymmetry with RHN having mass as low as 10^5 GeV.

Our goal in chapter 3 is to understand the interplay of dark matter and flavor leptogenesis and simultaneously explain neutrino mass and mixing. This chapter is divided into two parts. In the first part, we establish for the first time a novel connection between the smallness of the FIMP-type DM coupling with matters and the lightness of active neutrino mass within the context of the type-I seesaw mechanism. The SM is extended minimally by including three RHNs. The relic density of the non-thermal DM, in the form of the lightest RHN, was dictated by the decay of the SM gauge bosons along with the Higgs (in the electroweak symmetry broken phase) due to the presence of active-sterile mixing. Consequently, we find that the lightest neutrino mass should be of order $\mathcal{O}(10^{-12})$ eV to satisfy the correct relic density of DM. The same active-sterile mixing between the DM and SM neutrino fields makes it decay. Hence from DM's stability point of view over the age of the Universe and other constraints, the range of DM mass turns out to be restricted within 1 keV- 1 MeV. The dark matter phenomenology does not restrict the mass scales of two other heavy RHNs. Then we incorporate the flavor leptogenesis scenario to show that they can be of order 10^{9-10} GeV to explain the baryon asymmetry of the Universe. In the second part, we explore one of the alternative possibilities to the type-I seesaw framework, where dark matter can directly influence the baryon asymmetry generation process as well as neutrino mass generation. For that purpose, we start with a simple extension of the basic type-II seesaw ($i.e.$, with one $SU(2)_L$ triplet in addition to SM) scenario, including one additional RHN and one inert Higgs doublet. CP-even component of the IHD emerges as WIMP-type DM having mass $\mathcal{O}(500)$ GeV with a specific range of the mass splitting ($10^{-4} - \mathcal{O}(1)$ GeV) in this scenario. The most exciting feature of this work is the involvement of the same DM multiplet, along with the RHN, in the vertex correction diagram of the triplet's decay to two leptons for the successful production of CP asymmetry in order to address the baryon asymmetry of the Universe. We incorporate the flavor effects in this triplet leptogenesis study as we aim to lower the triplet mass as much as possible in view of its accessibility at the collider. Type-II dominance (compared to radiative correction) towards neutrino mass generation is assumed. Hence, a smaller mass splitting turns out to be preferable for generating sufficient CP asymmetry in this flavored leptogenesis framework if one tries to reduce the triplet mass. Additional coupling of triplet and IHD helps to reduce the scale of successful leptogenesis as low as $M_\Delta \sim 10^8$ GeV.

In chapter 4, we show how an extended reheating period after the end of inflation in the early Universe affects the equilibration temperature of the charged lepton Yukawa coupling having impact on lepton asymmetry production as well. During this extended period, the temperature of the Universe first reaches a maximum value ($T_{\rm Max}$) as then it decreases nontrivially until an early matter-radiation equality reaches (characterized by reheating temperature $T_{\rm RH}$). We construct two different setups to realize the extended reheating period. In the first analysis, the inflaton field effectively couples to the SM fermions only. As a result, the decay of the inflaton field to SM fermions reheats the Universe by producing the thermal bath. RHN is then produced from the thermal bath, and its decay generates the

lepton asymmetry during the process of reheating. The second scenario consists of inflaton-RHN coupling on top of the inflaton-SM fermion coupling. Depending on the effective coupling(s) of the inflaton field, a relatively lower reheating temperature is estimated while the reheating era can be extended enough. Consequently, a significantly smaller equilibration temperature(s) for right-handed charged leptons results shifting the flavor regime(s) of leptogenesis compared to the standard radiation-dominated era. In the first setup, we find a more restricted lower bound on RHN mass satisfying correct baryon asymmetry compared to the standard thermal scenario, as entropy injection during reheating process dilutes some amount of produced lepton asymmetry.However, due to the inflaton-RHN coupling in the second setup, a significant number of nonthermal RHNs can be produced from the inflaton decay, depending on the coupling value. As a result, one can easily evade the previous bound on RHN mass established in the first setup.

To sum up, in this thesis, we have shown that beyond the SM solutions required to explain problems such as neutrino mass, dark matter, horizon problem can also impact the result of flavor leptogenesis. To do that, firstly we have presented a scenario where degenerate RHNs, resulted from high scale flavor symmetry, can impact the leptogenesis mechanism. This led to some interesting results in the neutrino sector. Subsequently, a successful low-scale leptogenesis scenario emerged evading the important DI bound. Next, the role of early Universe evolution of DM on lepton asymmetry production was explored. In a minimal type-I seesaw framework, we found that the heavy RHN fields responsible for neutrino mass generation can explain DM abundance as well as baryon asymmetry of the Universe. On the other hand, in an alternative type-II seesaw framework, a direct influence of DM for the production of lepton asymmetry was observed. Then we moved on to construct the leptogenesis scenarios during the reheating period which originates from the decay of inflaton field and found that the prolonged reheating just after inflation would impact the flavor regimes of the leptogenesis framework by shifting the ET of the charged lepton Yukawa. Eventually, a change in allowed parameter space for successful leptogenesis was observed.

We conclude this chapter by pointing out some future possibilities which can be worked on as a continuation of this thesis. The effect of a prolonged reheating period should not be restricted to only the high scale leptogenesis framework. With a low enough reheating temperature, it can affect the low scale leptogenesis scenarios as well. In that case, it would be interesting to explore the experimental signatures of such impacts in colliders or as a form of gravitational wave detection. Investigating the production of DM during these modified cosmological periods would also be interesting to work on.

Appendix A

Appendix related to chapter 2

A.1 A_4 Multiplication Rules:

It has four irreducible representations: three one-dimensional and one three dimensional which are denoted by $\mathbf{1}, \mathbf{1'}, \mathbf{1''}$ and $\mathbf{3}$ respectively. The multiplication rules of the irreducible representations are given by [123]

$$\mathbf{1} \otimes \mathbf{1} = \mathbf{1}, \mathbf{1'} \otimes \mathbf{1'} = \mathbf{1''}, \mathbf{1'} \otimes \mathbf{1''} = \mathbf{1}, \mathbf{1''} \otimes \mathbf{1''} = \mathbf{1'}, \mathbf{3} \otimes \mathbf{3} = \mathbf{1} + \mathbf{1'} + \mathbf{1''} + \mathbf{3_a} + \mathbf{3_s} \quad \text{(A.1)}$$

where $\mathbf{a}$ and $\mathbf{s}$ in the subscript corresponds to anti-symmetric and symmetric parts respectively. Now, if we have two triplets as $A = (a_1, a_2, a_3)^T$ and $B = (b_1, b_2, b_3)^T$ respectively, their direct product can be decomposed into the direct sum mentioned above. The product rule for this two triplets in the S diagonal basis[1] can be written as

$$(A \times B)_{\mathbf{1}} \backsim a_1b_1 + a_2b_2 + a_3b_3, \quad \text{(A.2)}$$

$$(A \times B)_{\mathbf{1'}} \backsim a_1b_1 + \omega^2 a_2b_2 + \omega a_3b_3, \quad \text{(A.3)}$$

$$(A \times B)_{\mathbf{1''}} \backsim a_1b_1 + \omega a_2b_2 + \omega^2 a_3b_3, \quad \text{(A.4)}$$

$$(A \times B)_{\mathbf{3_s}} \backsim (a_2b_3 + a_3b_2, a_3b_1 + a_1b_3, a_1b_2 + a_2b_1), \quad \text{(A.5)}$$

$$(A \times B)_{\mathbf{3_a}} \backsim (a_2b_3 - a_3b_2, a_3b_1 - a_1b_3, a_1b_2 - a_2b_1), \quad \text{(A.6)}$$

here ω $(= e^{2i\pi/3})$ is the cube root of unity.

[1] Here S is a 3×3 diagonal generator of A_4.

Bibliography

[1] E. S. Abers and B. W. Lee, "Gauge Theories," *Phys. Rept.* **9** (1973) 1–141.

[2] J. E. Kim, P. Langacker, M. Levine, and H. H. Williams, "A Theoretical and Experimental Review of the Weak Neutral Current: A Determination of Its Structure and Limits on Deviations from the Minimal SU(2)-L x U(1) Electroweak Theory," *Rev. Mod. Phys.* **53** (1981) 211.

[3] P. Aurenche, "The Standard model of particle physics," in *Cinquieme Seminaire Rhodanien, Symetries en Physique*. 7, 1997. arXiv:hep-ph/9712342.

[4] M. K. Gaillard, P. D. Grannis, and F. J. Sciulli, "The Standard model of particle physics," *Rev. Mod. Phys.* **71** (1999) S96–S111, arXiv:hep-ph/9812285.

[5] M. Herrero, "The Standard model," *NATO Sci. Ser. C* **534** (1999) 1–59, arXiv:hep-ph/9812242.

[6] G. ALTARELLI, "The Standard model of particle physics," arXiv:hep-ph/0510281.

[7] J. Iliopoulos, "Introduction to the Standard Model of the Electro-Weak Interactions," in *8th CERN–Latin-American School of High-Energy Physics*. 5, 2013. arXiv:1305.6779 [hep-ph].

[8] F. Englert and R. Brout, "Broken Symmetry and the Mass of Gauge Vector Mesons," *Phys. Rev. Lett.* **13** (1964) 321–323.

[9] P. W. Higgs, "Broken Symmetries and the Masses of Gauge Bosons," *Phys. Rev. Lett.* **13** (1964) 508–509.

[10] G. S. Guralnik, C. R. Hagen, and T. W. B. Kibble, "Global Conservation Laws and Massless Particles," *Phys. Rev. Lett.* **13** (1964) 585–587.

[11] N. Cabibbo, "Unitary Symmetry and Leptonic Decays," *Phys. Rev. Lett.* **10** (1963) 531–533.

[12] M. Kobayashi and T. Maskawa, "CP Violation in the Renormalizable Theory of Weak Interaction," *Prog. Theor. Phys.* **49** (1973) 652–657.

[13] K. Begeman, A. Broeils, and R. Sanders, "Extended rotation curves of spiral galaxies: Dark haloes and modified dynamics," *Mon. Not. Roy. Astron. Soc.* **249** (1991) 523.

[14] D. Clowe, M. Bradac, A. H. Gonzalez, M. Markevitch, S. W. Randall, C. Jones, and D. Zaritsky, "A direct empirical proof of the existence of dark matter," *Astrophys. J. Lett.* **648** (2006) L109–L113, arXiv:astro-ph/0608407.

[15] W. H. Julian, "On the Effect of Interstellar Material on Stellar Non-Circular Velocities in Disk Galaxies," *Astrophys. J.* **148** (1967) 175.

[16] **SDSS** Collaboration, M. Tegmark *et al.*, "Cosmological parameters from SDSS and WMAP," *Phys. Rev. D* **69** (2004) 103501, arXiv:astro-ph/0310723.

[17] **Planck** Collaboration, N. Aghanim *et al.*, "Planck 2018 results. VI. Cosmological parameters," *Astron. Astrophys.* **641** (2020) A6, arXiv:1807.06209 [astro-ph.CO]. [Erratum: Astron.Astrophys. 652, C4 (2021)].

[18] B. D. Fields, K. A. Olive, T.-H. Yeh, and C. Young, "Big-Bang Nucleosynthesis after Planck," *JCAP* **03** (2020) 010, arXiv:1912.01132 [astro-ph.CO]. [Erratum: JCAP 11, E02 (2020)].

[19] J. A. Casas, J. R. Espinosa, and M. Quiros, "Improved Higgs mass stability bound in the standard model and implications for supersymmetry," *Phys. Lett. B* **342** (1995) 171–179, arXiv:hep-ph/9409458.

[20] G. Isidori, G. Ridolfi, and A. Strumia, "On the metastability of the standard model vacuum," *Nucl. Phys.* **B609** (2001) 387–409, arXiv:hep-ph/0104016 [hep-ph].

[21] G. 't Hooft, "Naturalness, chiral symmetry, and spontaneous chiral symmetry breaking," *NATO Sci. Ser. B* **59** (1980) 135–157.

[22] R. D. Peccei and H. R. Quinn, "CP Conservation in the Presence of Instantons," *Phys. Rev. Lett.* **38** (1977) 1440–1443.

[23] R. D. Peccei and H. R. Quinn, "Constraints Imposed by CP Conservation in the Presence of Instantons," *Phys. Rev. D* **16** (1977) 1791–1797.

[24] E. W. Kolb and M. S. Turner, *The Early Universe*, vol. 69. 1990.

[25] S. Dodelson, *Modern Cosmology*. Academic Press, Amsterdam, 2003.

[26] R. H. Brandenberger, "Introduction to Early Universe Cosmology," *PoS* **ICFI2010** (2010) 001, arXiv:1103.2271 [astro-ph.CO].

[27] D. Baumann, *Cosmology*. Cambridge University Press, 2022.

[28] G. Lazarides, "Introduction to inflationary cosmology," in *Corfu Summer Institute on Elementary Particle Physics (Corfu 2001)*. 2001. arXiv:hep-ph/0204294.

[29] A. H. Guth, "Inflationary universe: A possible solution to the horizon and flatness problems," *Phys. Rev. D* **23** (Jan, 1981) 347–356. https://link.aps.org/doi/10.1103/PhysRevD.23.347.

[30] A. D. Linde, "A New Inflationary Universe Scenario: A Possible Solution of the Horizon, Flatness, Homogeneity, Isotropy and Primordial Monopole Problems," *Phys. Lett. B* **108** (1982) 389–393.

[31] A. Riotto, "Inflation and the theory of cosmological perturbations," *ICTP Lect. Notes Ser.* **14** (2003) 317–413, arXiv:hep-ph/0210162.

[32] A. H. Guth, "The Inflationary Universe: A Possible Solution to the Horizon and Flatness Problems," *Phys. Rev.* **D23** (1981) 347–356.

[33] **Super-Kamiokande** Collaboration, Y. Fukuda *et al.*, "Evidence for oscillation of atmospheric neutrinos," *Phys. Rev. Lett.* **81** (1998) 1562–1567, arXiv:hep-ex/9807003.

[34] **K2K** Collaboration, M. H. Ahn *et al.*, "Indications of neutrino oscillation in a 250 km long baseline experiment," *Phys. Rev. Lett.* **90** (2003) 041801, arXiv:hep-ex/0212007.

[35] **KamLAND** Collaboration, S. Abe *et al.*, "Precision Measurement of Neutrino Oscillation Parameters with KamLAND," *Phys. Rev. Lett.* **100** (2008) 221803, arXiv:0801.4589 [hep-ex].

[36] **Super-Kamiokande Collaboration** Collaboration, Y. Ashie, J. Hosaka, K. Ishihara, Y. Itow, J. Kameda, Y. Koshio, A. Minamino, C. Mitsuda, M. Miura, S. Moriyama, M. Nakahata, T. Namba, R. Nambu, Y. Obayashi, M. Shiozawa, Y. Suzuki, Y. Takeuchi, K. Taki, S. Yamada, M. Ishitsuka, T. Kajita, K. Kaneyuki, S. Nakayama, A. Okada, K. Okumura, C. Saji, Y. Takenaga, S. T. Clark, S. Desai, E. Kearns, S. Likhoded, J. L. Stone, L. R. Sulak, W. Wang, M. Goldhaber, D. Casper, J. P. Cravens, W. Gajewski, W. R. Kropp, D. W. Liu, S. Mine, M. B. Smy, H. W. Sobel, C. W. Sterner, M. R. Vagins, K. S. Ganezer, J. Hill, W. E. Keig, J. S. Jang, J. Y. Kim, I. T. Lim, K. Scholberg, C. W. Walter, R. W. Ellsworth, S. Tasaka, G. Guillian, A. Kibayashi, J. G. Learned, S. Matsuno, D. Takemori, M. D. Messier, Y. Hayato, A. K. Ichikawa, T. Ishida, T. Ishii, T. Iwashita, T. Kobayashi, T. Maruyama, K. Nakamura, K. Nitta, Y. Oyama, M. Sakuda, Y. Totsuka, A. T. Suzuki, M. Hasegawa, K. Hayashi, I. Kato, H. Maesaka, T. Morita, T. Nakaya, K. Nishikawa, T. Sasaki, S. Ueda, S. Yamamoto, T. J. Haines, S. Dazeley, S. Hatakeyama, R. Svoboda, E. Blaufuss, J. A. Goodman, G. W. Sullivan, D. Turcan, A. Habig, Y. Fukuda, C. K. Jung, T. Kato, K. Kobayashi, M. Malek, C. Mauger, C. McGrew, A. Sarrat, E. Sharkey, C. Yanagisawa, T. Toshito, K. Miyano, N. Tamura, J. Ishii, Y. Kuno, M. Yoshida, S. B. Kim, J. Yoo, H. Okazawa, T. Ishizuka, Y. Choi, H. K. Seo, Y. Gando, T. Hasegawa, K. Inoue, J. Shirai, A. Suzuki, M. Koshiba, Y. Nakajima, K. Nishijima, T. Harada, H. Ishino, Y. Watanabe, D. Kielczewska, J. Zalipska, H. G. Berns, R. Gran, K. K. Shiraishi, A. Stachyra, K. Washburn, and R. J. Wilkes, "Measurement of atmospheric neutrino oscillation

parameters by super-kamiokande i," *Phys. Rev. D* **71** (Jun, 2005) 112005. https://link.aps.org/doi/10.1103/PhysRevD.71.112005.

[37] J. N. Bahcall, M. H. Pinsonneault, and S. Basu, "Solar models: Current epoch and time dependences, neutrinos, and helioseismological properties," *The Astrophysical Journal* **555** no. 2, (Jul, 2001) 990. https://dx.doi.org/10.1086/321493.

[38] **KATRIN** Collaboration, M. Aker *et al.*, "Improved Upper Limit on the Neutrino Mass from a Direct Kinematic Method by KATRIN," *Phys. Rev. Lett.* **123** no. 22, (2019) 221802, arXiv:1909.06048 [hep-ex].

[39] **CUPID** Collaboration, O. Azzolini *et al.*, "Final Result on the Neutrinoless Double Beta Decay of ^{82}Se with CUPID-0," *Phys. Rev. Lett.* **129** no. 11, (2022) 111801, arXiv:2206.05130 [nucl-ex].

[40] P. Minkowski, "$\mu \to e\gamma$ at a Rate of One Out of 10^9 Muon Decays?," *Phys. Lett. B* **67** (1977) 421–428.

[41] T. Yanagida, "HORIZONTAL SYMMETRY AND MASSES OF NEUTRINOS," *Conf. Proc.* **C7902131** (1979) 95–99.

[42] T. Yanagida, "Horizontal Symmetry and Mass of the Top Quark," *Phys. Rev. D* **20** (1979) 2986.

[43] M. Gell-Mann, P. Ramond, and R. Slansky, "Complex Spinors and Unified Theories," *Conf. Proc. C* **790927** (1979) 315–321, arXiv:1306.4669 [hep-th].

[44] R. N. Mohapatra and G. Senjanovic, "Neutrino Mass and Spontaneous Parity Nonconservation," *Phys. Rev. Lett.* **44** (1980) 912.

[45] J. Schechter and J. W. F. Valle, "Neutrino Masses in SU(2) x U(1) Theories," *Phys. Rev. D* **22** (1980) 2227.

[46] J. Schechter and J. W. F. Valle, "Neutrino Decay and Spontaneous Violation of Lepton Number," *Phys. Rev. D* **25** (1982) 774.

[47] R. N. Mohapatra and G. Senjanovic, "Neutrino Masses and Mixings in Gauge Models with Spontaneous Parity Violation," *Phys. Rev.* **D23** (1981) 165.

[48] G. Lazarides, Q. Shafi, and C. Wetterich, "Proton Lifetime and Fermion Masses in an SO(10) Model," *Nucl. Phys.* **B181** (1981) 287–300.

[49] C. Wetterich, "Neutrino Masses and the Scale of B-L Violation," *Nucl. Phys.* **B187** (1981) 343–375.

[50] B. Brahmachari and R. N. Mohapatra, "Unified explanation of the solar and atmospheric neutrino puzzles in a minimal supersymmetric SO(10) model," *Phys. Rev.* **D58** (1998) 015001, arXiv:hep-ph/9710371 [hep-ph].

[51] R. Foot, H. Lew, X. G. He, and G. C. Joshi, "Seesaw Neutrino Masses Induced by a Triplet of Leptons," *Z. Phys.* **C44** (1989) 441.

[52] R. N. Mohapatra and J. W. F. Valle, "Neutrino mass and baryon-number nonconservation in superstring models," *Phys. Rev. D* **34** (Sep, 1986) 1642–1645. https://link.aps.org/doi/10.1103/PhysRevD.34.1642.

[53] R. N. Mohapatra, "Mechanism for Understanding Small Neutrino Mass in Superstring Theories," *Phys. Rev. Lett.* **56** (1986) 561–563.

[54] A. Zee, "A Theory of Lepton Number Violation, Neutrino Majorana Mass, and Oscillation," *Phys. Lett. B* **93** (1980) 389. [Erratum: Phys.Lett.B 95, 461 (1980)].

[55] K. S. Babu, "Model of 'Calculable' Majorana Neutrino Masses," *Phys. Lett. B* **203** (1988) 132–136.

[56] A. Zee, "Quantum Numbers of Majorana Neutrino Masses," *Nucl. Phys. B* **264** (1986) 99–110.

[57] E. Ma, "Verifiable radiative seesaw mechanism of neutrino mass and dark matter," *Phys. Rev. D* **73** (2006) 077301, arXiv:hep-ph/0601225.

[58] **WMAP** Collaboration, E. Komatsu *et al.*, "Seven-Year Wilkinson Microwave Anisotropy Probe (WMAP) Observations: Cosmological Interpretation," *Astrophys. J. Suppl.* **192** (2011) 18, arXiv:1001.4538 [astro-ph.CO].

[59] **Planck** Collaboration, N. Aghanim *et al.*, "Planck 2018 results. VI. Cosmological parameters," arXiv:1807.06209 [astro-ph.CO].

[60] F. Zwicky, "Die Rotverschiebung von extragalaktischen Nebeln," *Helv. Phys. Acta* **6** (1933) 110–127. [Gen. Rel. Grav.41,207(2009)].

[61] V. C. Rubin and W. K. Ford, Jr., "Rotation of the Andromeda Nebula from a Spectroscopic Survey of Emission Regions," *Astrophys. J.* **159** (1970) 379–403.

[62] A. Bergmann, V. Petrosian, and R. Lynds, "Gravitational lens models of arcs in clusters," *ApJ* **350** (03, 1990) .

[63] G. Steigman and M. S. Turner, "Cosmological Constraints on the Properties of Weakly Interacting Massive Particles," *Nucl. Phys. B* **253** (1985) 375–386.

[64] K. A. Olive, "TASI lectures on dark matter," in *Theoretical Advanced Study Institute in Elementary Particle Physics (TASI 2002): Particle Physics and Cosmology: The Quest for Physics Beyond the Standard Model(s)*. 1, 2003. arXiv:astro-ph/0301505.

[65] D. Hooper, "Particle Dark Matter," in *Theoretical Advanced Study Institute in Elementary Particle Physics: The Dawn of the LHC Era*. 1, 2009. arXiv:0901.4090 [hep-ph].

[66] K. Garrett and G. Duda, "Dark Matter: A Primer," *Adv. Astron.* **2011** (2011) 968283, arXiv:1006.2483 [hep-ph].

[67] G. B. Gelmini, "The Hunt for Dark Matter," in *Theoretical Advanced Study Institute in Elementary Particle Physics: Journeys Through the Precision Frontier: Amplitudes for Colliders*. 2, 2015. arXiv:1502.01320 [hep-ph].

[68] M. Lisanti, "Lectures on Dark Matter Physics," in *Theoretical Advanced Study Institute in Elementary Particle Physics: New Frontiers in Fields and Strings*. 3, 2016. arXiv:1603.03797 [hep-ph].

[69] M. Bauer and T. Plehn, *Yet Another Introduction to Dark Matter: The Particle Physics Approach*, vol. 959 of *Lecture Notes in Physics*. Springer, 2019. arXiv:1705.01987 [hep-ph].

[70] P. Gondolo and G. Gelmini, "Cosmic abundances of stable particles: Improved analysis," *Nucl. Phys. B* **360** (1991) 145–179.

[71] J. Edsjo and P. Gondolo, "Neutralino relic density including coannihilations," *Phys. Rev. D* **56** (1997) 1879–1894, arXiv:hep-ph/9704361.

[72] F. Couchot, S. Henrot-Versillé, O. Perdereau, S. Plaszczynski, B. Rouillé d'Orfeuil, M. Spinelli, and M. Tristram, "Cosmological constraints on the neutrino mass including systematic uncertainties," *Astron. Astrophys.* **606** (2017) A104, arXiv:1703.10829 [astro-ph.CO].

[73] L. J. Hall, K. Jedamzik, J. March-Russell, and S. M. West, "Freeze-In Production of FIMP Dark Matter," *JHEP* **03** (2010) 080, arXiv:0911.1120 [hep-ph].

[74] A. Biswas and A. Gupta, "Freeze-in Production of Sterile Neutrino Dark Matter in $U(1)_{B-L}$ Model," *JCAP* **09** (2016) 044, arXiv:1607.01469 [hep-ph]. [Addendum: JCAP 05, A01 (2017)].

[75] N. Bernal, M. Heikinheimo, T. Tenkanen, K. Tuominen, and V. Vaskonen, "The Dawn of FIMP Dark Matter: A Review of Models and Constraints," *Int. J. Mod. Phys. A* **32** no. 27, (2017) 1730023, arXiv:1706.07442 [hep-ph].

[76] B. Barman, D. Borah, and R. Roshan, "Effective Theory of Freeze-in Dark Matter," *JCAP* **11** (2020) 021, arXiv:2007.08768 [hep-ph].

[77] B. Barman, D. Borah, and R. Roshan, "Non-thermal leptogenesis and UV freeze-in of dark matter: impact of inflationary reheating," arXiv:2103.01675 [hep-ph].

[78] G. Steigman, "Observational tests of antimatter cosmologies," *Ann. Rev. Astron. Astrophys.* **14** (1976) 339–372.

[79] **Particle Data Group** Collaboration, R. L. Workman *et al.*, "Review of Particle Physics," *PTEP* **2022** (2022) 083C01.

[80] G. Steigman, "When Clusters Collide: Constraints On Antimatter On The Largest Scales," *JCAP* **10** (2008) 001, arXiv:0808.1122 [astro-ph].

[81] O. Reimer, M. Pohl, P. Sreekumar, and J. R. Mattox, "Egret upper limits on the high-energy gamma-ray emission of galaxy clusters," *Astrophys. J.* **588** (2003) 155–164, arXiv:astro-ph/0301362.

[82] A. Edge, G. S. A. Fabian, and K. Arnaudº, "An x-ray flux-limited sample of clusters of galaxies: evidence for evolution of the luminosity function,".

[83] A. G. Cohen, A. De Rujula, and S. L. Glashow, "A Matter - antimatter universe?," *Astrophys. J.* **495** (1998) 539–549, arXiv:astro-ph/9707087.

[84] A. D. Sakharov, "Violation of CP Invariance, C asymmetry, and baryon asymmetry of the universe," *Pisma Zh. Eksp. Teor. Fiz.* **5** (1967) 32–35.

[85] V. A. Kuzmin, V. A. Rubakov, and M. E. Shaposhnikov, "On the Anomalous Electroweak Baryon Number Nonconservation in the Early Universe," *Phys. Lett. B* **155** (1985) 36.

[86] A. G. Cohen, D. B. Kaplan, and A. E. Nelson, "Progress in electroweak baryogenesis," *Annual Review of Nuclear and Particle Science* **43** no. 1, (1993) 27–70.

[87] **ATLAS** Collaboration, G. Aad *et al.*, "Observation of a new particle in the search for the Standard Model Higgs boson with the ATLAS detector at the LHC," *Phys. Lett. B* **716** (2012) 1–29, arXiv:1207.7214 [hep-ex].

[88] **ATLAS** Collaboration, M. Aaboud *et al.*, "Measurements of Higgs boson properties in the diphoton decay channel with 36 fb^{-1} of pp collision data at $\sqrt{s} = 13$ TeV with the ATLAS detector," *Phys. Rev.* **D98** (2018) 052005, arXiv:1802.04146 [hep-ex].

[89] **CMS** Collaboration, A. M. Sirunyan *et al.*, "Combined measurements of Higgs boson couplings in proton–proton collisions at $\sqrt{s} = 13$ TeV," *Eur. Phys. J.* **C79** no. 5, (2019) 421, arXiv:1809.10733 [hep-ex].

[90] S. Dimopoulos and L. Susskind, "On the Baryon Number of the Universe," *Phys. Rev. D* **18** (1978) 4500–4509.

[91] M. Yoshimura, "Unified Gauge Theories and the Baryon Number of the Universe," *Phys. Rev. Lett.* **41** (1978) 281–284. [Erratum: Phys.Rev.Lett. 42, 746 (1979)].

[92] S. Weinberg, "Cosmological Production of Baryons," *Phys. Rev. Lett.* **42** (1979) 850–853.

[93] I. Affleck and M. Dine, "A New Mechanism for Baryogenesis," *Nucl. Phys. B* **249** (1985) 361–380.

[94] M. Dine and A. Kusenko, "The Origin of the matter - antimatter asymmetry," *Rev. Mod. Phys.* **76** (2003) 1, arXiv:hep-ph/0303065.

[95] M. Fukugita and T. Yanagida, "Baryogenesis Without Grand Unification," *Phys. Lett. B* **174** (1986) 45–47.

[96] M. A. Luty, "Baryogenesis via leptogenesis," *Phys. Rev. D* **45** (1992) 455–465.

[97] A. Pilaftsis, "CP violation and baryogenesis due to heavy Majorana neutrinos," *Phys. Rev. D* **56** (1997) 5431–5451, arXiv:hep-ph/9707235.

[98] M. Flanz, E. A. Paschos, and U. Sarkar, "Baryogenesis from a lepton asymmetric universe," *Physics Letters B* **345** no. 3, (Feb, 1995) 248–252. https://doi.org/10.1016%2F0370-$\widetilde{\text{b}}$2693%2894%2901555-$\widetilde{\text{bq}}$.

[99] L. Covi, E. Roulet, and F. Vissani, "CP violating decays in leptogenesis scenarios," *Phys. Lett. B* **384** (1996) 169–174, arXiv:hep-ph/9605319.

[100] E. Nardi, Y. Nir, J. Racker, and E. Roulet, "On Higgs and sphaleron effects during the leptogenesis era," *JHEP* **01** (2006) 068, arXiv:hep-ph/0512052.

[101] J. A. Harvey and M. S. Turner, "Cosmological baryon and lepton number in the presence of electroweak fermion-number violation," *Phys. Rev. D* **42** (Nov, 1990) 3344–3349. https://link.aps.org/doi/10.1103/PhysRevD.42.3344.

[102] S. Blanchet, P. Di Bari, and G. Raffelt, "Quantum Zeno effect and the impact of flavor in leptogenesis," *JCAP* **03** (2007) 012, arXiv:hep-ph/0611337.

[103] R. Barbieri, P. Creminelli, A. Strumia, and N. Tetradis, "Baryogenesis through leptogenesis," *Nucl. Phys. B* **575** (2000) 61–77, arXiv:hep-ph/9911315.

[104] E. Nardi, Y. Nir, E. Roulet, and J. Racker, "The Importance of flavor in leptogenesis," *JHEP* **01** (2006) 164, arXiv:hep-ph/0601084.

[105] A. Abada, S. Davidson, F.-X. Josse-Michaux, M. Losada, and A. Riotto, "Flavor issues in leptogenesis," *JCAP* **04** (2006) 004, arXiv:hep-ph/0601083.

[106] S. Blanchet and P. Di Bari, "Flavor effects on leptogenesis predictions," *JCAP* **03** (2007) 018, arXiv:hep-ph/0607330.

[107] P. S. B. Dev, P. Di Bari, B. Garbrecht, S. Lavignac, P. Millington, and D. Teresi, "Flavor effects in leptogenesis," *Int. J. Mod. Phys. A* **33** (2018) 1842001, arXiv:1711.02861 [hep-ph].

[108] B. A. Campbell, S. Davidson, J. R. Ellis, and K. A. Olive, "On B+L violation in the laboratory in the light of cosmological and astrophysical constraints," *Astropart. Phys.* **1** (1992) 77–98.

[109] J. M. Cline, K. Kainulainen, and K. A. Olive, "Erasure and regeneration of the primordial baryon asymmetry by sphalerons," *Phys. Rev. Lett.* **71** (Oct, 1993) 2372–2375. https://link.aps.org/doi/10.1103/PhysRevLett.71.2372.

[110] J. M. Cline, K. Kainulainen, and K. A. Olive, "Protecting the primordial baryon asymmetry from erasure by sphalerons," *Phys. Rev. D* **49** (1994) 6394–6409, arXiv:hep-ph/9401208.

[111] A. Abada, S. Davidson, A. Ibarra, F.-X. Josse-Michaux, M. Losada, and A. Riotto, "Flavour Matters in Leptogenesis," *JHEP* **09** (2006) 010, arXiv:hep-ph/0605281.

[112] D. Bödeker and D. Schröder, "Equilibration of right-handed electrons," *JCAP* **05** (2019) 010, arXiv:1902.07220 [hep-ph].

[113] **Super-Kamiokande** Collaboration, S. Fukuda *et al.*, "Constraints on neutrino oscillations using 1258 days of Super-Kamiokande solar neutrino data," *Phys. Rev. Lett.* **86** (2001) 5656–5660, arXiv:hep-ex/0103033 [hep-ex].

[114] **Super-Kamiokande** Collaboration, S. Fukuda *et al.*, "Determination of solar neutrino oscillation parameters using 1496 days of Super-Kamiokande I data," *Phys. Lett. B* **539** (2002) 179–187, arXiv:hep-ex/0205075.

[115] **Super-Kamiokande** Collaboration, Y. Ashie *et al.*, "A Measurement of atmospheric neutrino oscillation parameters by SUPER-KAMIOKANDE I," *Phys. Rev. D* **71** (2005) 112005, arXiv:hep-ex/0501064.

[116] **SNO** Collaboration, Q. R. Ahmad *et al.*, "Direct evidence for neutrino flavor transformation from neutral current interactions in the Sudbury Neutrino Observatory," *Phys. Rev. Lett.* **89** (2002) 011301, arXiv:nucl-ex/0204008.

[117] **SNO** Collaboration, Q. R. Ahmad *et al.*, "Measurement of day and night neutrino energy spectra at SNO and constraints on neutrino mixing parameters," *Phys. Rev. Lett.* **89** (2002) 011302, arXiv:nucl-ex/0204009 [nucl-ex].

[118] **T2K** Collaboration, K. Abe *et al.*, "Indication of Electron Neutrino Appearance from an Accelerator-produced Off-axis Muon Neutrino Beam," *Phys. Rev. Lett.* **107** (2011) 041801, arXiv:1106.2822 [hep-ex].

[119] **Double Chooz** Collaboration, Y. Abe *et al.*, "Indication of Reactor $\bar{\nu}_e$ Disappearance in the Double Chooz Experiment," *Phys. Rev. Lett.* **108** (2012) 131801, arXiv:1112.6353 [hep-ex].

[120] **T2K** Collaboration, K. Abe *et al.*, "Observation of Electron Neutrino Appearance in a Muon Neutrino Beam," *Phys. Rev. Lett.* **112** (2014) 061802, arXiv:1311.4750 [hep-ex].

[121] M. Magg and C. Wetterich, "Neutrino Mass Problem and Gauge Hierarchy," *Phys. Lett. B* **94** (1980) 61–64.

[122] R. N. Mohapatra and J. W. F. Valle, "Neutrino Mass and Baryon Number Nonconservation in Superstring Models," *Phys. Rev. D* **34** (1986) 1642.

[123] G. Altarelli and F. Feruglio, "Discrete Flavor Symmetries and Models of Neutrino Mixing," *Rev. Mod. Phys.* **82** (2010) 2701–2729, arXiv:1002.0211 [hep-ph].

[124] Z.-z. Xing, "Flavor structures of charged fermions and massive neutrinos," *Phys. Rept.* **854** (2020) 1–147, arXiv:1909.09610 [hep-ph].

[125] S. F. King, "Models of Neutrino Mass, Mixing and CP Violation," *J. Phys. G* **42** (2015) 123001, arXiv:1510.02091 [hep-ph].

[126] W. Grimus and P. O. Ludl, "Finite flavour groups of fermions," *J. Phys. A* **45** (2012) 233001, arXiv:1110.6376 [hep-ph].

[127] S. F. King, "Unified Models of Neutrinos, Flavour and CP Violation," *Prog. Part. Nucl. Phys.* **94** (2017) 217–256, arXiv:1701.04413 [hep-ph].

[128] S. F. King and C. Luhn, "Trimaximal neutrino mixing from vacuum alignment in A4 and S4 models," *JHEP* **09** (2011) 042, arXiv:1107.5332 [hep-ph].

[129] S. F. King and C. Luhn, "Neutrino Mass and Mixing with Discrete Symmetry," *Rept. Prog. Phys.* **76** (2013) 056201, arXiv:1301.1340 [hep-ph].

[130] H. Ishimori, T. Kobayashi, H. Ohki, Y. Shimizu, H. Okada, and M. Tanimoto, "Non-Abelian Discrete Symmetries in Particle Physics," *Prog. Theor. Phys. Suppl.* **183** (2010) 1–163, arXiv:1003.3552 [hep-th].

[131] D. Wyler, "Discrete Symmetries in the Six Quark SU(2) X U(1) Model," *Phys. Rev. D* **19** (1979) 3369.

[132] G. C. Branco, H. P. Nilles, and V. Rittenberg, "Fermion Masses and Hierarchy of Symmetry Breaking," *Phys. Rev. D* **21** (1980) 3417.

[133] G. Altarelli and F. Feruglio, "Tri-bimaximal neutrino mixing, A(4) and the modular symmetry," *Nucl. Phys. B* **741** (2006) 215–235, arXiv:hep-ph/0512103.

[134] G. Altarelli and F. Feruglio, "Tri-bimaximal neutrino mixing from discrete symmetry in extra dimensions," *Nucl. Phys. B* **720** (2005) 64–88, arXiv:hep-ph/0504165.

[135] E. Ma and G. Rajasekaran, "Softly broken A(4) symmetry for nearly degenerate neutrino masses," *Phys. Rev.* **D64** (2001) 113012, arXiv:hep-ph/0106291 [hep-ph].

[136] E. Ma, "A(4) symmetry and neutrinos with very different masses," *Phys. Rev. D* **70** (2004) 031901, arXiv:hep-ph/0404199.

[137] G. Altarelli and D. Meloni, "A Simplest A4 Model for Tri-Bimaximal Neutrino Mixing," *J. Phys. G* **36** (2009) 085005, arXiv:0905.0620 [hep-ph].

[138] P. F. Harrison, D. H. Perkins, and W. G. Scott, "Tri-bimaximal mixing and the neutrino oscillation data," *Phys. Lett.* **B530** (2002) 167, arXiv:hep-ph/0202074 [hep-ph].

[139] P. F. Harrison and W. G. Scott, "Symmetries and generalizations of tri - bimaximal neutrino mixing," *Phys. Lett.* **B535** (2002) 163–169, arXiv:hep-ph/0203209 [hep-ph].

[140] **Daya Bay** Collaboration, F. P. An *et al.*, "Observation of electron-antineutrino disappearance at Daya Bay," *Phys. Rev. Lett.* **108** (2012) 171803, arXiv:1203.1669 [hep-ex].

[141] **RENO** Collaboration, J. K. Ahn *et al.*, "Observation of Reactor Electron Antineutrino Disappearance in the RENO Experiment," *Phys. Rev. Lett.* **108** (2012) 191802, arXiv:1204.0626 [hep-ex].

[142] G. C. Branco, R. Gonzalez Felipe, F. R. Joaquim, and H. Serodio, "Spontaneous leptonic CP violation and nonzero θ_{13}," *Phys. Rev. D* **86** (2012) 076008, arXiv:1203.2646 [hep-ph].

[143] C.-C. Li, J.-N. Lu, and G.-J. Ding, "A_4 and CP symmetry and a model with maximal CP violation," *Nucl. Phys. B* **913** (2016) 110–131, arXiv:1608.01860 [hep-ph].

[144] T. Araki, J. Mei, and Z.-z. Xing, "Intrinsic Deviation from the Tri-bimaximal Neutrino Mixing in a Class of A_4 Flavor Models," *Phys. Lett. B* **695** (2011) 165–168, arXiv:1010.3065 [hep-ph].

[145] A. Datta, B. Karmakar, and A. Sil, "Flavored leptogenesis and neutrino mass with A_4 symmetry," *JHEP* **12** (2021) 051, arXiv:2106.06773 [hep-ph].

[146] N. Memenga, W. Rodejohann, and H. Zhang, "A_4 flavor symmetry model for Dirac neutrinos and sizable U_{e3}," *Phys. Rev. D* **87** no. 5, (2013) 053021, arXiv:1301.2963 [hep-ph].

[147] D. Borah and B. Karmakar, "A_4 flavour model for Dirac neutrinos: Type I and inverse seesaw," *Phys. Lett.* **B780** (2018) 461–470, arXiv:1712.06407 [hep-ph].

[148] D. Borah, B. Karmakar, and D. Nanda, "Common Origin of Dirac Neutrino Mass and Freeze-in Massive Particle Dark Matter," *JCAP* **07** (2018) 039, arXiv:1805.11115 [hep-ph].

[149] D. Borah and B. Karmakar, "Linear seesaw for Dirac neutrinos with A_4 flavour symmetry," *Phys. Lett. B* **789** (2019) 59–70, arXiv:1806.10685 [hep-ph].

[150] G. Branco, R. Gonzalez Felipe, M. Rebelo, and H. Serodio, "Resonant leptogenesis and tribimaximal leptonic mixing with A(4) symmetry," *Phys. Rev. D* **79** (2009) 093008, arXiv:0904.3076 [hep-ph].

[151] M. Plumacher, "Baryogenesis and lepton number violation," *Z. Phys. C* **74** (1997) 549–559, arXiv:hep-ph/9604229.

[152] A. Datta, R. Roshan, and A. Sil, "Imprint of the Seesaw Mechanism on Feebly Interacting Dark Matter and the Baryon Asymmetry," *Phys. Rev. Lett.* **127** no. 23, (2021) 231801, arXiv:2104.02030 [hep-ph].

[153] D. Borah, M. K. Das, and A. Mukherjee, "Common origin of nonzero θ_{13} and baryon asymmetry of the Universe in a TeV scale seesaw model with A_4 flavor symmetry," *Phys. Rev.* **D97** no. 11, (2018) 115009, arXiv:1711.02445 [hep-ph].

[154] B. Karmakar and A. Sil, "Nonzero θ_{13} and leptogenesis in a type-I seesaw model with A_4 symmetry," *Phys. Rev.* **D91** (2015) 013004, arXiv:1407.5826 [hep-ph].

[155] B. Karmakar and A. Sil, "Spontaneous CP violation in lepton-sector: A common origin for θ_{13}, the Dirac CP phase, and leptogenesis," *Phys. Rev. D* **93** no. 1, (2016) 013006, arXiv:1509.07090 [hep-ph].

[156] S. Bhattacharya, B. Karmakar, N. Sahu, and A. Sil, "Unifying the flavor origin of dark matter with leptonic nonzero θ_{13}," *Phys. Rev.* **D93** no. 11, (2016) 115041, arXiv:1603.04776 [hep-ph].

[157] S. Bhattacharya, B. Karmakar, N. Sahu, and A. Sil, "Flavor origin of dark matter and its relation with leptonic nonzero θ_{13} and Dirac CP phase δ," *JHEP* **05** (2017) 068, arXiv:1611.07419 [hep-ph].

[158] C. Hagedorn, E. Molinaro, and S. T. Petcov, "Majorana Phases and Leptogenesis in See-Saw Models with A(4) Symmetry," *JHEP* **09** (2009) 115, arXiv:0908.0240 [hep-ph].

[159] E. E. Jenkins and A. V. Manohar, "Tribimaximal Mixing, Leptogenesis, and theta(13)," *Phys. Lett. B* **668** (2008) 210–215, arXiv:0807.4176 [hep-ph].

[160] P. Das, M. K. Das, and N. Khan, "Phenomenological study of neutrino mass, dark matter and baryogenesis within the framework of minimal extended seesaw," *JHEP* **03** (2020) 018, arXiv:1911.07243 [hep-ph].

[161] B. Karmakar and A. Sil, "An A_4 realization of inverse seesaw: neutrino masses, θ_{13} and leptonic non-unitarity," *Phys. Rev. D* **96** no. 1, (2017) 015007, arXiv:1610.01909 [hep-ph].

[162] X.-G. He, Y.-Y. Keum, and R. R. Volkas, "A(4) flavor symmetry breaking scheme for understanding quark and neutrino mixing angles," *JHEP* **04** (2006) 039, arXiv:hep-ph/0601001.

[163] Y. Lin, "A Predictive A(4) model, Charged Lepton Hierarchy and Tri-bimaximal Sum Rule," *Nucl. Phys. B* **813** (2009) 91–105, arXiv:0804.2867 [hep-ph].

[164] W. Rodejohann and X.-J. Xu, "A left–right symmetric flavor symmetry model," *Eur. Phys. J. C* **76** no. 3, (2016) 138, arXiv:1509.03265 [hep-ph].

[165] I. Esteban, M. C. Gonzalez-Garcia, M. Maltoni, T. Schwetz, and A. Zhou, "The fate of hints: updated global analysis of three-flavor neutrino oscillations," *JHEP* **09** (2020) 178, arXiv:2007.14792 [hep-ph].

[166] P. Langacker, S. T. Petcov, G. Steigman, and S. Toshev, "On the Mikheev-Smirnov-Wolfenstein (MSW) Mechanism of Amplification of Neutrino Oscillations in Matter," *Nucl. Phys. B* **282** (1987) 589–609.

[167] S. Vagnozzi, E. Giusarma, O. Mena, K. Freese, M. Gerbino, S. Ho, and M. Lattanzi, "Unveiling ν secrets with cosmological data: neutrino masses and mass hierarchy," *Phys. Rev. D* **96** no. 12, (2017) 123503, arXiv:1701.08172 [astro-ph.CO].

[168] **Particle Data Group** Collaboration, M. Tanabashi *et al.*, "Review of Particle Physics," *Phys. Rev.* **D98** no. 3, (2018) 030001.

[169] A. Ilakovac and A. Pilaftsis, "Flavor violating charged lepton decays in seesaw-type models," *Nucl. Phys. B* **437** (1995) 491, arXiv:hep-ph/9403398.

[170] D. Tommasini, G. Barenboim, J. Bernabeu, and C. Jarlskog, "Nondecoupling of heavy neutrinos and lepton flavor violation," *Nucl. Phys. B* **444** (1995) 451–467, arXiv:hep-ph/9503228.

[171] S. Bhattacharya, R. Roshan, A. Sil, and D. Vatsyayan, "Symmetry origin of Baryon Asymmetry, Dark Matter and Neutrino Mass," arXiv:2105.06189 [hep-ph].

[172] S. Y. Khlebnikov and M. E. Shaposhnikov, "The Statistical Theory of Anomalous Fermion Number Nonconservation," *Nucl. Phys. B* **308** (1988) 885–912.

[173] P. B. Arnold and L. D. McLerran, "The Sphaleron Strikes Back," *Phys. Rev. D* **37** (1988) 1020.

[174] B. Adhikary, M. Chakraborty, and A. Ghosal, "Flavored leptogenesis with quasidegenerate neutrinos in a broken cyclic symmetric model," *Phys. Rev. D* **93** no. 11, (2016) 113001, arXiv:1407.6173 [hep-ph].

[175] A. Pilaftsis and T. E. J. Underwood, "Resonant leptogenesis," *Nucl. Phys.* **B692** (2004) 303–345, arXiv:hep-ph/0309342 [hep-ph].

[176] P. S. B. Dev, M. Garny, J. Klaric, P. Millington, and D. Teresi, "Resonant enhancement in leptogenesis," *Int. J. Mod. Phys.* **A33** (2018) 1842003, arXiv:1711.02863 [hep-ph].

[177] J. Casas, J. Espinosa, A. Ibarra, and I. Navarro, "Naturalness of nearly degenerate neutrinos," *Nucl. Phys. B* **556** (1999) 3–22, arXiv:hep-ph/9904395.

[178] R. Gonzalez Felipe, F. Joaquim, and B. Nobre, "Radiatively induced leptogenesis in a minimal seesaw model," *Phys. Rev. D* **70** (2004) 085009, arXiv:hep-ph/0311029.

[179] P. H. Chankowski and S. Pokorski, "Quantum corrections to neutrino masses and mixing angles," *Int. J. Mod. Phys. A* **17** (2002) 575–614, arXiv:hep-ph/0110249.

[180] M. Flanz, E. A. Paschos, U. Sarkar, and J. Weiss, "Baryogenesis through mixing of heavy Majorana neutrinos," *Phys. Lett. B* **389** (1996) 693–699, arXiv:hep-ph/9607310.

[181] S. Pascoli, S. Petcov, and A. Riotto, "Leptogenesis and Low Energy CP Violation in Neutrino Physics," *Nucl. Phys. B* **774** (2007) 1–52, arXiv:hep-ph/0611338.

[182] T. Asaka and T. Yoshida, "Resonant leptogenesis at TeV-scale and neutrinoless double beta decay," *JHEP* **09** (2019) 089, arXiv:1812.11323 [hep-ph].

[183] M. Plümacher, *Baryon asymmetry, neutrino mixing and supersymmetric SO(10) unification*. PhD thesis, Hamburg U., 1998. arXiv:hep-ph/9807557.

[184] T. Asaka and M. Shaposhnikov, "The νMSM, dark matter and baryon asymmetry of the universe," *Phys. Lett. B* **620** (2005) 17–26, arXiv:hep-ph/0505013.

[185] T. Asaka, S. Blanchet, and M. Shaposhnikov, "The nuMSM, dark matter and neutrino masses," *Phys. Lett. B* **631** (2005) 151–156, arXiv:hep-ph/0503065.

[186] S. Dodelson and L. M. Widrow, "Sterile-neutrinos as dark matter," *Phys. Rev. Lett.* **72** (1994) 17–20, arXiv:hep-ph/9303287.

[187] E. K. Akhmedov, V. A. Rubakov, and A. Y. Smirnov, "Baryogenesis via neutrino oscillations," *Phys. Rev. Lett.* **81** (1998) 1359–1362, arXiv:hep-ph/9803255.

[188] L. Hui, N. Y. Gnedin, and Y. Zhang, "The Statistics of density peaks and the column density distribution of the Lyman-alpha forest," *Astrophys. J.* **486** (1997) 599, arXiv:astro-ph/9608157.

[189] N. Y. Gnedin and A. J. S. Hamilton, "Matter power spectrum from the Lyman-alpha forest: Myth or reality?," *Mon. Not. Roy. Astron. Soc.* **334** (2002) 107–116, arXiv:astro-ph/0111194.

[190] D. H. Weinberg, R. Dave, N. Katz, and J. A. Kollmeier, "The Lyman - alpha forest as a cosmological tool," *AIP Conf. Proc.* **666** no. 1, (2003) 157–169, arXiv:astro-ph/0301186.

[191] A. D. Dolgov and S. H. Hansen, "Massive sterile neutrinos as warm dark matter," *Astropart. Phys.* **16** (2002) 339–344, arXiv:hep-ph/0009083.

[192] K. Abazajian, G. M. Fuller, and W. H. Tucker, "Direct detection of warm dark matter in the X-ray," *Astrophys. J.* **562** (2001) 593–604, arXiv:astro-ph/0106002.

[193] C. R. Watson, J. F. Beacom, H. Yuksel, and T. P. Walker, "Direct X-ray Constraints on Sterile Neutrino Warm Dark Matter," *Phys. Rev. D* **74** (2006) 033009, arXiv:astro-ph/0605424.

[194] R. Essig, E. Kuflik, S. D. McDermott, T. Volansky, and K. M. Zurek, "Constraining Light Dark Matter with Diffuse X-Ray and Gamma-Ray Observations," *JHEP* **11** (2013) 193, arXiv:1309.4091 [hep-ph].

[195] X.-D. Shi and G. M. Fuller, "A New dark matter candidate: Nonthermal sterile neutrinos," *Phys. Rev. Lett.* **82** (1999) 2832–2835, arXiv:astro-ph/9810076.

[196] L. Canetti, M. Drewes, and M. Shaposhnikov, "Sterile Neutrinos as the Origin of Dark and Baryonic Matter," *Phys. Rev. Lett.* **110** no. 6, (2013) 061801, arXiv:1204.3902 [hep-ph].

[197] N. Okada and O. Seto, "Higgs portal dark matter in the minimal gauged $U(1)_{B-L}$ model," *Phys. Rev. D* **82** (2010) 023507, arXiv:1002.2525 [hep-ph].

[198] P. Di Bari, P. O. Ludl, and S. Palomares-Ruiz, "Unifying leptogenesis, dark matter and high-energy neutrinos with right-handed neutrino mixing via Higgs portal," *JCAP* **11** (2016) 044, arXiv:1606.06238 [hep-ph].

[199] J. A. Casas and A. Ibarra, "Oscillating neutrinos and muon —> e, gamma," *Nucl. Phys.* **B618** (2001) 171–204, arXiv:hep-ph/0103065 [hep-ph].

[200] **Particle Data Group** Collaboration, P. A. Zyla *et al.*, "Review of Particle Physics," *PTEP* **2020** no. 8, (2020) 083C01.

[201] G. L. Fogli, E. Lisi, A. Marrone, A. Palazzo, and A. M. Rotunno, "Neutrino masses and neutrino mixing," *Nucl. Phys. B Proc. Suppl.* **155** (2006) 5–9.

[202] R. Coy, A. Gupta, and T. Hambye, "Seesaw determination of the dark matter relic density," arXiv:2104.00042 [hep-ph].

[203] M. Lucente, "Freeze-In Dark Matter within the Seesaw mechanism," arXiv:2103.03253 [hep-ph].

[204] P. Ghosh, A. K. Saha, and A. Sil, "Study of Electroweak Vacuum Stability from Extended Higgs Portal of Dark Matter and Neutrinos," *Phys. Rev. D* **97** no. 7, (2018) 075034, arXiv:1706.04931 [hep-ph].

[205] P. B. Pal and L. Wolfenstein, "Radiative Decays of Massive Neutrinos," *Phys. Rev. D* **25** (1982) 766.

[206] V. D. Barger, R. J. N. Phillips, and S. Sarkar, "Remarks on the KARMEN anomaly," *Phys. Lett. B* **352** (1995) 365–371, arXiv:hep-ph/9503295. [Erratum: Phys.Lett.B 356, 617–617 (1995)].

[207] A. Boyarsky, O. Ruchayskiy, and M. Shaposhnikov, "The Role of sterile neutrinos in cosmology and astrophysics," *Ann. Rev. Nucl. Part. Sci.* **59** (2009) 191–214, arXiv:0901.0011 [hep-ph].

[208] S. Tremaine and J. E. Gunn, "Dynamical Role of Light Neutral Leptons in Cosmology," *Phys. Rev. Lett.* **42** (1979) 407–410.

[209] **KATRIN** Collaboration, M. Aker *et al.*, "The Design, Construction, and Commissioning of the KATRIN Experiment," arXiv:2103.04755 [physics.ins-det].

[210] **Project 8** Collaboration, A. Ashtari Esfahani *et al.*, "Determining the neutrino mass with cyclotron radiation emission spectroscopy—Project 8," *J. Phys. G* **44** no. 5, (2017) 054004, arXiv:1703.02037 [physics.ins-det].

[211] **MEG** Collaboration, A. M. Baldini *et al.*, "Search for the lepton flavour violating decay $\mu^+ \to e^+\gamma$ with the full dataset of the MEG experiment," *Eur. Phys. J. C* **76** no. 8, (2016) 434, arXiv:1605.05081 [hep-ex].

[212] W. Buchmuller, P. Di Bari, and M. Plumacher, "Leptogenesis for pedestrians," *Annals Phys.* **315** (2005) 305–351, arXiv:hep-ph/0401240.

[213] A. Anisimov, S. Blanchet, and P. Di Bari, "Viability of Dirac phase leptogenesis," *JCAP* **04** (2008) 033, arXiv:0707.3024 [hep-ph].

[214] S. Davidson, E. Nardi, and Y. Nir, "Leptogenesis," *Phys. Rept.* **466** (2008) 105–177, arXiv:0802.2962 [hep-ph].

[215] W. Buchmuller, R. Peccei, and T. Yanagida, "Leptogenesis as the origin of matter," *Ann. Rev. Nucl. Part. Sci.* **55** (2005) 311–355, arXiv:hep-ph/0502169.

[216] H. Davoudiasl and Y. Zhang, "Baryon Number Violation via Majorana Neutrinos in the Early Universe, at the LHC, and Deep Underground," *Phys. Rev. D* **92** no. 1, (2015) 016005, arXiv:1504.07244 [hep-ph].

[217] N. Narendra, N. Sahoo, and N. Sahu, "Dark matter assisted Dirac leptogenesis and neutrino mass," *Nucl. Phys. B* **936** (2018) 76–90, arXiv:1712.02960 [hep-ph].

[218] M. J. Dolan, T. P. Dutka, and R. R. Volkas, "Dirac-Phase Thermal Leptogenesis in the extended Type-I Seesaw Model," *JCAP* **06** (2018) 012, arXiv:1802.08373 [hep-ph].

[219] S. Kashiwase and D. Suematsu, "Baryon number asymmetry and dark matter in the neutrino mass model with an inert doublet," *Phys. Rev.* **D86** (2012) 053001, arXiv:1207.2594 [hep-ph].

[220] P. Konar, A. Mukherjee, A. K. Saha, and S. Show, "A dark clue to seesaw and leptogenesis in a pseudo-Dirac singlet doublet scenario with (non)standard cosmology," *JHEP* **03** (2021) 044, arXiv:2007.15608 [hep-ph].

[221] E. Ma and U. Sarkar, "Neutrino masses and leptogenesis with heavy Higgs triplets," *Phys. Rev. Lett.* **80** (1998) 5716–5719, arXiv:hep-ph/9802445.

[222] M. Senami and K. Yamamoto, "Leptogenesis with supersymmetric Higgs triplets in TeV region," *Int. J. Mod. Phys. A* **21** (2006) 1291–1306, arXiv:hep-ph/0305202.

[223] R. Gonzalez Felipe, F. R. Joaquim, and H. Serodio, "Flavoured CP asymmetries for type II seesaw leptogenesis," *Int. J. Mod. Phys. A* **28** (2013) 1350165, arXiv:1301.0288 [hep-ph].

[224] S. Lavignac and B. Schmauch, "Flavour always matters in scalar triplet leptogenesis," *JHEP* **05** (2015) 124, arXiv:1503.00629 [hep-ph].

[225] T. Hambye and G. Senjanovic, "Consequences of triplet seesaw for leptogenesis," *Phys. Lett. B* **582** (2004) 73–81, arXiv:hep-ph/0307237.

[226] T. Hambye, M. Raidal, and A. Strumia, "Efficiency and maximal CP-asymmetry of scalar triplet leptogenesis," *Phys. Lett. B* **632** (2006) 667–674, arXiv:hep-ph/0510008.

[227] T. Hambye, "Leptogenesis: beyond the minimal type I seesaw scenario," *New J. Phys.* **14** (2012) 125014, arXiv:1212.2888 [hep-ph].

[228] D. Aristizabal Sierra, M. Dhen, and T. Hambye, "Scalar triplet flavored leptogenesis: a systematic approach," *JCAP* **08** (2014) 003, arXiv:1401.4347 [hep-ph].

[229] S. Mishra and A. Giri, "Scalar triplet leptogenesis in the presence of right-handed neutrinos with S_3 symmetry," *J. Phys. G* **47** no. 5, (2020) 055008, arXiv:1909.12147 [hep-ph].

[230] T. Rink, W. Rodejohann, and K. Schmitz, "Leptogenesis and low-energy CP violation in a type-II-dominated left-right seesaw model," *Nucl. Phys. B* **972** (2021) 115552, arXiv:2006.03021 [hep-ph].

[231] **WMAP** Collaboration, C. L. Bennett *et al.*, "Nine-Year Wilkinson Microwave Anisotropy Probe (WMAP) Observations: Final Maps and Results," *Astrophys. J. Suppl.* **208** (2013) 20, arXiv:1212.5225 [astro-ph.CO].

[232] L. Lopez Honorez, E. Nezri, J. F. Oliver, and M. H. G. Tytgat, "The Inert Doublet Model: An Archetype for Dark Matter," *JCAP* **0702** (2007) 028, arXiv:hep-ph/0612275 [hep-ph].

[233] L. Lopez Honorez and C. E. Yaguna, "The inert doublet model of dark matter revisited," *JHEP* **09** (2010) 046, arXiv:1003.3125 [hep-ph].

[234] A. Belyaev, G. Cacciapaglia, I. P. Ivanov, F. Rojas-Abatte, and M. Thomas, "Anatomy of the Inert Two Higgs Doublet Model in the light of the LHC and non-LHC Dark Matter Searches," *Phys. Rev.* **D97** no. 3, (2018) 035011, arXiv:1612.00511 [hep-ph].

[235] S. Choubey and A. Kumar, "Inflation and Dark Matter in the Inert Doublet Model," *JHEP* **11** (2017) 080, arXiv:1707.06587 [hep-ph].

[236] L. Lopez Honorez and C. E. Yaguna, "A new viable region of the inert doublet model," *JCAP* **1101** (2011) 002, arXiv:1011.1411 [hep-ph].

[237] A. Ilnicka, M. Krawczyk, and T. Robens, "Inert Doublet Model in light of LHC Run I and astrophysical data," *Phys. Rev.* **D93** no. 5, (2016) 055026, arXiv:1508.01671 [hep-ph].

[238] A. Arhrib, Y.-L. S. Tsai, Q. Yuan, and T.-C. Yuan, "An Updated Analysis of Inert Higgs Doublet Model in light of the Recent Results from LUX, PLANCK, AMS-02 and LHC," *JCAP* **1406** (2014) 030, arXiv:1310.0358 [hep-ph].

[239] Q.-H. Cao, E. Ma, and G. Rajasekaran, "Observing the Dark Scalar Doublet and its Impact on the Standard-Model Higgs Boson at Colliders," *Phys. Rev.* **D76** (2007) 095011, arXiv:0708.2939 [hep-ph].

[240] E. Lundstrom, M. Gustafsson, and J. Edsjo, "The Inert Doublet Model and LEP II Limits," *Phys. Rev.* **D79** (2009) 035013, arXiv:0810.3924 [hep-ph].

[241] M. Gustafsson, S. Rydbeck, L. Lopez-Honorez, and E. Lundstrom, "Status of the Inert Doublet Model and the Role of multileptons at the LHC," *Phys. Rev.* **D86** (2012) 075019, arXiv:1206.6316 [hep-ph].

[242] D. Borah and A. Gupta, "New viable region of an inert Higgs doublet dark matter model with scotogenic extension," *Phys. Rev.* **D96** no. 11, (2017) 115012, arXiv:1706.05034 [hep-ph].

[243] J. Kalinowski, W. Kotlarski, T. Robens, D. Sokolowska, and A. F. Zarnecki, "Benchmarking the Inert Doublet Model for e^+e^- colliders," *JHEP* **12** (2018) 081, arXiv:1809.07712 [hep-ph].

[244] A. Bhardwaj, P. Konar, T. Mandal, and S. Sadhukhan, "Probing Inert Doublet Model using jet substructure with multivariate analysis," arXiv:1905.04195 [hep-ph].

[245] D. Borah, R. Roshan, and A. Sil, "Minimal two-component scalar doublet dark matter with radiative neutrino mass," *Phys. Rev. D* **100** no. 5, (2019) 055027, arXiv:1904.04837 [hep-ph].

[246] S. Bhattacharya, P. Ghosh, A. K. Saha, and A. Sil, "Two component dark matter with inert Higgs doublet: neutrino mass, high scale validity and collider searches," arXiv:1905.12583 [hep-ph].

[247] S. Bhattacharya, N. Chakrabarty, R. Roshan, and A. Sil, "Multicomponent dark matter in extended $U(1)_{B-L}$: neutrino mass and high scale validity," *JCAP* **04** (2020) 013, arXiv:1910.00612 [hep-ph].

[248] N. Chakrabarty, R. Roshan, and A. Sil, "Two Component Doublet-Triplet Scalar Dark Matter stabilising the Electroweak vacuum," arXiv:2102.06032 [hep-ph].

[249] **LHC Higgs Cross Section Working Group** Collaboration, D. de Florian *et al.*, "Handbook of LHC Higgs Cross Sections: 4. Deciphering the Nature of the Higgs Sector," arXiv:1610.07922 [hep-ph].

[250] **Particle Data Group** Collaboration, P. A. Zyla *et al.*, "Review of Particle Physics," *PTEP* **2020** no. 8, (2020) 083C01.

[251] P. F. de Salas, D. V. Forero, S. Gariazzo, P. Martínez-Miravé, O. Mena, C. A. Ternes, M. Tórtola, and J. W. F. Valle, "2020 global reassessment of the neutrino oscillation picture," *JHEP* **02** (2021) 071, arXiv:2006.11237 [hep-ph].

[252] A. Ahriche, A. Jueid, and S. Nasri, "Radiative neutrino mass and Majorana dark matter within an inert Higgs doublet model," *Phys. Rev. D* **97** no. 9, (2018) 095012, arXiv:1710.03824 [hep-ph].

[253] D. Barducci, G. Belanger, J. Bernon, F. Boudjema, J. Da Silva, S. Kraml, U. Laa, and A. Pukhov, "Collider limits on new physics within micrOMEGAs_4.3," *Comput. Phys. Commun.* **222** (2018) 327–338, arXiv:1606.03834 [hep-ph].

[254] A. Dutta Banik, R. Roshan, and A. Sil, "Neutrino mass and asymmetric dark matter: study with inert Higgs doublet and high scale validity," *JCAP* **03** (2021) 037, arXiv:2011.04371 [hep-ph].

[255] **LUX** Collaboration, D. S. Akerib *et al.*, "Results from a search for dark matter in the complete LUX exposure," *Phys. Rev. Lett.* **118** no. 2, (2017) 021303, arXiv:1608.07648 [astro-ph.CO].

[256] **PandaX-II** Collaboration, A. Tan *et al.*, "Dark Matter Results from First 98.7 Days of Data from the PandaX-II Experiment," *Phys. Rev. Lett.* **117** no. 12, (2016) 121303, arXiv:1607.07400 [hep-ex].

[257] **PandaX-II** Collaboration, X. Cui *et al.*, "Dark Matter Results From 54-Ton-Day Exposure of PandaX-II Experiment," arXiv:1708.06917 [astro-ph.CO].

[258] **XENON** Collaboration, E. Aprile *et al.*, "First Dark Matter Search Results from the XENON1T Experiment," arXiv:1705.06655 [astro-ph.CO].

[259] E. Aprile *et al.*, "Dark Matter Search Results from a One Tonne×Year Exposure of XENON1T," arXiv:1805.12562 [astro-ph.CO].

[260] R. Barbieri, L. J. Hall, and V. S. Rychkov, "Improved naturalness with a heavy Higgs: An Alternative road to LHC physics," *Phys. Rev.* **D74** (2006) 015007, arXiv:hep-ph/0603188 [hep-ph].

[261] J. Giedt, A. W. Thomas, and R. D. Young, "Dark matter, the CMSSM and lattice QCD," *Phys. Rev. Lett.* **103** (2009) 201802, arXiv:0907.4177 [hep-ph].

[262] M. Cirelli and A. Strumia, "Minimal Dark Matter: Model and results," *New J. Phys.* **11** (2009) 105005, arXiv:0903.3381 [hep-ph].

[263] C. Arina, F.-S. Ling, and M. H. G. Tytgat, "IDM and iDM or The Inert Doublet Model and Inelastic Dark Matter," *JCAP* **0910** (2009) 018, arXiv:0907.0430 [hep-ph].

[264] B. Eiteneuer, A. Goudelis, and J. Heisig, "The inert doublet model in the light of Fermi-LAT gamma-ray data – a global fit analysis," arXiv:1705.01458 [hep-ph].

[265] **MAGIC, Fermi-LAT** Collaboration, M. L. Ahnen *et al.*, "Limits to Dark Matter Annihilation Cross-Section from a Combined Analysis of MAGIC and Fermi-LAT Observations of Dwarf Satellite Galaxies," *JCAP* **02** (2016) 039, arXiv:1601.06590 [astro-ph.HE].

[266] R. H. Cyburt, B. D. Fields, K. A. Olive, and T.-H. Yeh, "Big Bang Nucleosynthesis: 2015," *Rev. Mod. Phys.* **88** (2016) 015004, arXiv:1505.01076 [astro-ph.CO].

[267] **MEG** Collaboration, A. M. Baldini *et al.*, "Search for the lepton flavour violating decay $\mu^+ \to e^+\gamma$ with the full dataset of the MEG experiment," *Eur. Phys. J. C* **76** no. 8, (2016) 434, arXiv:1605.05081 [hep-ex].

[268] A. Datta, R. Roshan, and A. Sil, "Scalar triplet flavor leptogenesis with dark matter," *Phys. Rev. D* **105** no. 9, (2022) 095032, arXiv:2110.03914 [hep-ph].

[269] S. Davidson and A. Ibarra, "A Lower bound on the right-handed neutrino mass from leptogenesis," *Phys. Lett.* **B535** (2002) 25–32, arXiv:hep-ph/0202239 [hep-ph].

[270] G. F. Giudice, E. W. Kolb, and A. Riotto, "Largest temperature of the radiation era and its cosmological implications," *Phys. Rev.* **D64** (2001) 023508, arXiv:hep-ph/0005123 [hep-ph].

[271] M. Kawasaki, K. Kohri, and N. Sugiyama, "MeV scale reheating temperature and thermalization of neutrino background," *Phys. Rev. D* **62** (2000) 023506, arXiv:astro-ph/0002127.

[272] J. Martin and C. Ringeval, "First CMB Constraints on the Inflationary Reheating Temperature," *Phys. Rev. D* **82** (2010) 023511, arXiv:1004.5525 [astro-ph.CO].

[273] L. Dai, M. Kamionkowski, and J. Wang, "Reheating constraints to inflationary models," *Phys. Rev. Lett.* **113** (2014) 041302, arXiv:1404.6704 [astro-ph.CO].

[274] G. Lazarides and Q. Shafi, "Origin of matter in the inflationary cosmology," *Phys. Lett. B* **258** (1991) 305–309.

[275] H. Murayama, H. Suzuki, T. Yanagida, and J. Yokoyama, "Chaotic inflation and baryogenesis by right-handed sneutrinos," *Phys. Rev. Lett.* **70** (1993) 1912–1915.

[276] E. W. Kolb, A. D. Linde, and A. Riotto, "GUT baryogenesis after preheating," *Phys. Rev. Lett.* **77** (1996) 4290–4293, arXiv:hep-ph/9606260.

[277] G. F. Giudice, M. Peloso, A. Riotto, and I. Tkachev, "Production of massive fermions at preheating and leptogenesis," *JHEP* **08** (1999) 014, arXiv:hep-ph/9905242.

[278] T. Asaka, K. Hamaguchi, M. Kawasaki, and T. Yanagida, "Leptogenesis in inflaton decay," *Phys. Lett. B* **464** (1999) 12–18, arXiv:hep-ph/9906366.

[279] T. Asaka, K. Hamaguchi, M. Kawasaki, and T. Yanagida, "Leptogenesis in inflationary universe," *Phys. Rev. D* **61** (2000) 083512, arXiv:hep-ph/9907559.

[280] K. Hamaguchi, H. Murayama, and T. Yanagida, "Leptogenesis from N dominated early universe," *Phys. Rev. D* **65** (2002) 043512, arXiv:hep-ph/0109030.

[281] R. Jeannerot, S. Khalil, and G. Lazarides, "Leptogenesis in smooth hybrid inflation," *Phys. Lett. B* **506** (2001) 344–350, arXiv:hep-ph/0103229.

[282] M. Fujii, K. Hamaguchi, and T. Yanagida, "Leptogenesis with almost degenerate majorana neutrinos," *Phys. Rev. D* **65** (2002) 115012, arXiv:hep-ph/0202210.

[283] G. Giudice, A. Notari, M. Raidal, A. Riotto, and A. Strumia, "Towards a complete theory of thermal leptogenesis in the SM and MSSM," *Nucl. Phys. B* **685** (2004) 89–149, arXiv:hep-ph/0310123.

[284] S. Pascoli, S. Petcov, and C. Yaguna, "Quasidegenerate neutrino mass spectrum, mu —> e + gamma decay and leptogenesis," *Phys. Lett. B* **564** (2003) 241–254, arXiv:hep-ph/0301095.

[285] T. Asaka, H. B. Nielsen, and Y. Takanishi, "Nonthermal leptogenesis from the heavier Majorana neutrinos," *Nucl. Phys. B* **647** (2002) 252–274, arXiv:hep-ph/0207023.

[286] G. Panotopoulos, "Non-thermal leptogenesis and baryon asymmetry in different neutrino mass models," *Phys. Lett. B* **643** (2006) 279–283, arXiv:hep-ph/0606127.

[287] F. Hahn-Woernle and M. Plumacher, "Effects of reheating on leptogenesis," *Nucl. Phys. B* **806** (2009) 68–83, arXiv:0801.3972 [hep-ph].

[288] Y. Hamada and K. Kawana, "Reheating-era leptogenesis," *Phys. Lett. B* **763** (2016) 388–392, arXiv:1510.05186 [hep-ph].

[289] D. Borah, S. Jyoti Das, and A. K. Saha, "Cosmic inflation in minimal $U(1)_{BL}$ model: implications for (non) thermal dark matter and leptogenesis," *Eur. Phys. J. C* **81** no. 2, (2021) 169, arXiv:2005.11328 [hep-ph].

[290] R. Samanta, A. Biswas, and S. Bhattacharya, "Non-thermal production of lepton asymmetry and dark matter in minimal seesaw with right handed neutrino induced Higgs potential," arXiv:2006.02960 [hep-ph].

[291] A. Azatov, M. Vanvlasselaer, and W. Yin, "Baryogenesis via relativistic bubble walls," *JHEP* **10** (2021) 043, arXiv:2106.14913 [hep-ph].

[292] B. Barman, D. Borah, S. J. Das, and R. Roshan, "Non-thermal origin of asymmetric dark matter from inflaton and primordial black holes," *JCAP* **03** no. 03, (2022) 031, arXiv:2111.08034 [hep-ph].

[293] B. Barman, D. Borah, S. Das Jyoti, and R. Roshan, "Cogenesis of Baryon Asymmetry and Gravitational Dark Matter from PBH," arXiv:2204.10339 [hep-ph].

[294] G. Lazarides, R. Maji, R. Roshan, and Q. Shafi, "Heavier W boson, dark matter, and gravitational waves from strings in an SO(10) axion model," *Phys. Rev. D* **106** no. 5, (2022) 055009, arXiv:2205.04824 [hep-ph].

[295] G. Lazarides, R. Maji, R. Roshan, and Q. Shafi, "A predictive SO(10) model," *JCAP* **12** (2022) 009, arXiv:2210.03710 [hep-ph].

[296] A. Ghoshal, D. Nanda, and A. K. Saha, "CMB footprints of high scale non-thermal leptogenesis," arXiv:2210.14176 [hep-ph].

[297] A. Ghoshal, R. Samanta, and G. White, "Bremsstrahlung High-frequency Gravitational Wave Signatures of High-scale Non-thermal Leptogenesis," arXiv:2211.10433 [hep-ph].

[298] D. J. H. Chung, E. W. Kolb, and A. Riotto, "Production of massive particles during reheating," *Phys. Rev.* **D60** (1999) 063504, arXiv:hep-ph/9809453 [hep-ph].

[299] K. Mukaida and M. Yamada, "Thermalization Process after Inflation and Effective Potential of Scalar Field," *JCAP* **02** (2016) 003, arXiv:1506.07661 [hep-ph].

[300] K. Harigaya, K. Mukaida, and M. Yamada, "Dark Matter Production during the Thermalization Era," *JHEP* **07** (2019) 059, arXiv:1901.11027 [hep-ph].

[301] M. A. G. Garcia, K. Kaneta, Y. Mambrini, and K. A. Olive, "Reheating and Post-inflationary Production of Dark Matter," *Phys. Rev. D* **101** no. 12, (2020) 123507, arXiv:2004.08404 [hep-ph].

[302] M. R. Haque, D. Maity, and P. Saha, "Two-phase reheating: CMB constraints on inflation and dark matter phenomenology," *Phys. Rev. D* **102** no. 8, (2020) 083534, arXiv:2009.02794 [hep-th].

[303] L. Kofman, A. D. Linde, and A. A. Starobinsky, "Reheating after inflation," *Phys. Rev. Lett.* **73** (1994) 3195–3198, arXiv:hep-th/9405187 [hep-th].

[304] L. Kofman, A. D. Linde, and A. A. Starobinsky, "Towards the theory of reheating after inflation," *Phys. Rev.* **D56** (1997) 3258–3295, arXiv:hep-ph/9704452 [hep-ph].

[305] P. B. Greene and L. Kofman, "Preheating of fermions," *Phys. Lett. B* **448** (1999) 6–12, arXiv:hep-ph/9807339.

[306] R. Kallosh and A. Linde, "Universality Class in Conformal Inflation," *JCAP* **07** (2013) 002, arXiv:1306.5220 [hep-th].

[307] A. A. Starobinsky, "A New Type of Isotropic Cosmological Models Without Singularity," *Phys. Lett. B* **91** (1980) 99–102.

[308] J. Ellis, D. V. Nanopoulos, and K. A. Olive, "No-Scale Supergravity Realization of the Starobinsky Model of Inflation," *Phys. Rev. Lett.* **111** (2013) 111301, arXiv:1305.1247 [hep-th]. [Erratum: Phys.Rev.Lett. 111, 129902 (2013)].

[309] S. Khalil, A. Moursy, A. K. Saha, and A. Sil, "U(1)R inspired inflation model in no-scale supergravity," *Phys. Rev. D* **99** no. 9, (2019) 095022, arXiv:1810.06408 [hep-ph].

[310] **BICEP2, Keck Array** Collaboration, P. A. R. Ade *et al.*, "BICEP2 / Keck Array x: Constraints on Primordial Gravitational Waves using Planck, WMAP, and New BICEP2/Keck Observations through the 2015 Season," *Phys. Rev. Lett.* **121** (2018) 221301, arXiv:1810.05216 [astro-ph.CO].

[311] Y. Ueno and K. Yamamoto, "Constraints on α-attractor inflation and reheating," *Phys. Rev. D* **93** no. 8, (2016) 083524, arXiv:1602.07427 [astro-ph.CO].

[312] S. Antusch, P. Di Bari, D. A. Jones, and S. F. King, "Leptogenesis in the Two Right-Handed Neutrino Model Revisited," *Phys. Rev.* **D86** (2012) 023516, arXiv:1107.6002 [hep-ph].

[313] J. A. Harvey and M. S. Turner, "Cosmological baryon and lepton number in the presence of electroweak fermion number violation," *Phys. Rev. D* **42** (1990) 3344–3349.

[314] A. Datta, R. Roshan, and A. Sil, "Effects of Reheating on Charged Lepton Yukawa Equilibration and Leptogenesis," arXiv:2206.10650 [hep-ph].

[315] M. Drewes, J. U. Kang, and U. R. Mun, "CMB constraints on the inflaton couplings and reheating temperature in α-attractor inflation," *JHEP* **11** (2017) 072, arXiv:1708.01197 [astro-ph.CO].